Numerical and Experimental Studies on Thin-Wall Machining of Aerospace Grade Aluminum Alloy

A Thesis

Submitted in Partial Fulfillment of the Requirement for the Degree of

Doctor of Philosophy

By

Gururaj Bolar

(Roll No. 126103020)

Department of Mechanical Engineering
Indian Institute of Technology Guwahati
Guwahati, Assam, India

2017

Indian Institute of Technology Guwahati
Department of Mechanical Engineering
Guwahati – 781 039

STATEMENT

The present thesis entitled, **"Numerical and Experimental Studies on Thin-Wall Machining of Aerospace Grade Aluminum Alloy"** has been carried out by me under the supervision of Dr. Shrikrishna N. Joshi, Department of Mechanical Engineering, Indian Institute of Technology Guwahati. This work has not been submitted elsewhere for the award of any degree.

Date: December, 2017

(**Gururaj Bolar**)
Roll No. 126103020
Department of Mechanical Engineering,
Indian Institute of Technology Guwahati,
Guwahati – 781 039

Indian Institute of Technology Guwahati
Department of Mechanical Engineering
Guwahati – 781 039

CERTIFICATE

It is certified that the work described in this thesis, entitled "**Numerical and Experimental Studies on Thin-Wall Machining of Aerospace Grade Aluminum Alloy**", done by **Mr. Gururaj Bolar** (Roll No. 126103020), a Ph.D. student in the Department of Mechanical Engineering, Indian Institute of Technology Guwahati, for the award of degree of **Doctor of Philosophy** has been carried out under my supervision. This work has not been submitted elsewhere for the award of any degree.

Date: December 2017

Dr. Shrikrishna N. Joshi
Associate Professor,
Department of Mechanical Engineering,
Indian Institute of Technology Guwahati,
Guwahati – 781 039

DEDICATION

I dedicate this study to my late father, Mr. Vasukumar, who throughout his lifetime etched in the walls of my heart the importance of education

Abstract

Due to homogeneity and excellent strength-to-weight ratio, monolithic thin-wall components are widely used in aerospace, marine, electronics and automobile industry. Machining of thin-wall parts eliminates the need for different set-ups and processes; however, it consumes a lot of power because of machining of about 90-95% bulk material. Today's manufacturing and tool room industry are striving to reduce the component cost and to improve the product quality in terms of surface finish and dimensional accuracy. To fulfill these requirements it is imperative to focus our research attention on improving the product quality and overall productivity during machining of thin-wall components. The thin-wall parts are always machined on computer numerically controlled (CNC) machines. In spite of using CNC technology, the process of thin-wall machining is not devoid of problems. This is because the process control by CNC is based on idealized geometry and does not take into account the deformation of the parts. As a result, there is a significant deviation between the desired part profile and the manufactured one. Another important aspect related to machining of aluminum thin-wall components is the surface roughness. Aluminum alloys possess a comparatively low modulus of elasticity, which causes the workpiece to spring back. This spring back action often results in deflection and chatter. Chatter affects the material removal (MRR) rate and leads to poor surface finish, part rejection and loss of productivity. Due to the poor stiffness, selecting the optimal machining conditions and parameters is crucial.

In this research work a realistic three-dimensional thermo-mechanical finite element method (FEM) based model was developed to simulate the complex physical interaction of helical cutting tool and workpiece during thin-wall milling of an aerospace grade aluminum alloy. Lagrangian formulation with explicit solution scheme was employed to simulate the interaction between helical milling cutter and the workpiece. The behavior of the material at high strain, strain rate and the temperature was defined by Johnson-Cook material constitutive model. Johnson-Cook damage law and friction law were used to account for chip separation and contact interaction. Experimental work was carried out to validate the results predicted by the developed 3-D numerical model. It was noted that the milling force component values predicted by the developed model match well with the values that are obtained by experiments. Mean prediction errors for F_x, F_y, F_z, wall deflection and workpiece temperature were found to be 11.61%, 16.38%, 26.1%, 10.02% and 15.61% respectively. Overall a very good agreement between the

simulated and experimentally measured responses has been noted which demonstrates the capability of the developed model to predict the process responses accurately.

In view of the requirement of huge computation time (in hundreds of hours) for a 3-D FEM based numerical simulation of thin-wall milling, in the present work, a simple and integrated force-deflection model was developed. The merits of this proposed approach lie in the utilization of unified mechanics based approach and three-dimensional finite element method based simulation together for quicker and accurate prediction the milling force and in-situ wall deflection. Unified mechanics based analytical equations have been thoroughly studied and employed to compute the milling force. Based on these forces, wall deflections have been computed using 3-D finite element method. In this work, the shearing force coefficients those take care of primary shear deformation were derived using established empirical relations. The edge force coefficients those consider the rubbing and ploughing effects were derived by using simple and computationally inexpensive 2-D FEM model. To examine the capability of the proposed approach, four case studies were carried out. Considering all test cases, the mean prediction errors for milling force components F_x, F_y and F_z were noted to be 9.56%, 7.44% and 21.48% respectively. The model was able to predict the wall deflection with a very good accuracy (mean prediction error of 9.3 %). The developed integrated model was found to be far more efficient than the 3-D FEM model. The time duration for prediction of the cutting force and magnitude of wall deflection using the developed integrated model was noted as 40 min in comparison of 344 hrs (average) consumed by the 3-D FEM based thermo-mechanical model. However, the proposed model does not provide the information about the quality of surface machined, chip morphology which is vital in deciding the milling parameters to obtain the desired process performance.

In this research work, systematic experiments have been carried out on thin-wall end milling operation. The experiments were conducted in three phases. Initially, the experiments were carried out to determine the most influential parameters among the milling parameters viz. feed per tooth, spindle speed, axial and radial depth. To carry out this exercise, the performance of milling process was measured in terms of milling force, surface roughness and wall deflection. Radial depth of cut, axial cut depth and feed rate were found to have a significant influence on the performance of thin-wall machining process. However, spindle speed was found to have comparatively less effect on the

responses. The levels of these milling parameters were finalized; and these levels were used to carry out further detail experimental investigations.

In the second phase of experiments, investigations into the influence of tool geometry parameters such as tool diameter, helix angle and number of flutes on the performance of the process were carried out. Grey relational analysis (GRA) methodology was utilized to obtain the optimal and influential tool geometry parameters. Based on the Grey relational rank, tool diameter was found be highly influencing on the process responses, viz. milling force, surface roughness and wall deflection. GRA suggested that an optimal combination of tool geometry parameters i.e. diameter 8 mm with a helix angle of 45° and 4 flutes achieves the desired process performance. This optimal combination was verified by conducting experiments and it was found that the suggested tool geometry parameters produce a significant improvement in the surface quality of the machined part. An excellent surface finish of 0.401 μm *Ra* value was obtained. It was also noted that the optimal tool geometry parameters significantly reduces the wall deflection by 6.33%.

In the third phase of work, full factorial experiments were carried out by varying feed per tooth, axial depth of cut, radial depth of cut and tool diameter at three levels. Total 81 experiments were conducted and the process performance in terms of milling force, surface roughness, wall deflection and material removal rate (MRR) were recorded for each experiment. Based on response surface methodology (RSM), systematic studies have been carried out on the perturbation and interaction effects of input milling parameters on the individual performance parameters. Results were studied and the findings were presented with suitable scientific justifications. Based on the RSM, mathematical models for the prediction of individual responses were derived. Further, the predictions by the models were verified by conducting confirmatory experiments. All the models were found to have good prediction capabilities. It was noted that the developed mathematical models predict the responses with good accuracy. The prediction errors (absolute) vary between 0.41 to 16.39%. The mean error for milling force, surface roughness, wall deflection and material removal rate were observed to be 5.9%, 5.5%, 7.9% and 7.8%. Extensive data was generated on the process performance for the chosen milling conditions by carrying out physical experiments. This data was used to derive optimum milling conditions by carrying out multi-objective optimization using the genetic algorithm (GA).

An integrated comprehensive approach for the selection of optimal milling parameters of the helical end milling process to manufacture thin-wall parts was carried out. The approach has the peculiar merit that it takes into account productivity, process efficiency (power consumption) and product quality together. The milling parameters viz. tool diameter, feed per tooth, axial and radial depth of cut were considered in the study. Based on a study of different GA based optimization strategies, non-dominated sorting GA - II (NSGA-II) was selected to solve our optimization problem. Independent objective sub-criteria were defined. Using NSGA-II, Pareto optimal fronts for the roughing and finishing operations were obtained. Exhaustive NSGA-II runs were carried out by varying the number of generations. The Pareto optimal fronts were studied and optimal milling parameters for roughing and finishing operations were suggested. These recommendations were further verified by conducting in-house experiments. The recommendations from the NSGA-II based optimization strategy were found to be very effective in producing quality thin-wall parts of straight as well as curvilinear shapes. It is concluded that good quality surface finish with minimal deflection can be obtained by using an end mill of diameter 8~9 mm and by maintaining the feed, axial and radial depth values at 0.02 mm/z, 8 mm and 0.3125 mm respectively.

The recommended optimum milling conditions were applied to manufacture a 700 µm ultra-thin-wall of curvilinear shape. It was observed that the suggested milling conditions produce an excellent surface finish of 0.25~0.32 µm (R_a values) and uniform thin-wall (deflection error of 32~41 µm). Thus it is felt that the approach developed in this work provided a very effective tool to the process engineers to choose optimum levels of end milling parameters for enhancing the product quality and process productivity.

Acknowledgements

Almost five years of hard work and the countless help and support from the people around me has made it possible to complete the thesis work.

I wish to express my sincere and deep appreciation to Dr. Shrikrishna N. Joshi for his encouragement, insightful guidance, all the patience, support, and enthusiastic support throughout my studies, including the writing of this dissertation. I must acknowledge him for providing the unconditional freedom to work, think and express on whatever I have done in my research work by having faith in my capabilities. I am also thankful to my supervisor for providing me the opportunity to work on this research project.

I am highly thankful to my doctoral committee members, Dr. S. Senthilvelan, Dr. Manas Das, Dr. Suresh Kartha and Dr. Ajay Kalamdhad for their continuous academic guidance and checking my work progress and seminars during my Ph.D. Their valuable discussions and suggestions were truly encouraging for me.

I would like to express my sincere gratitude to Prof. Anoop K. Dass and Prof. Pinakeswar Mahanta, present and former Heads, Department of Mechanical Engineering, Indian Institute of Technology Guwahati, for providing various laboratory facilities and sanctioning funds without which completion of the work would not have been possible. I am also grateful to all the faculty members of the Mechanical Engineering department.

I would also like to thank Ministry of Human Resource and Development (MHRD), Government of India and Science and Engineering Research Board (SERB), Government of India for providing financial support. I sincerely thank Indian Institute of Technology Guwahati for providing all sort of infrastructural facilities to carry out this doctoral research work. I would also like to acknowledge Advanced Manufacturing Laboratory, Material Science Laboratory, Central Workshop, and Central Instruments Facility of Indian Institute of Technology Guwahati and all scientific officers and staff members for providing instruments and helping me to carry out the research work.

I deeply acknowledge the unabated support and counselling provided by my colleagues and friends, Dr. Ravikant, Mr. Borad M. Barkachary, Mr. Sanasam Sunderlal Singh, Ms. Ngangkham Devarani, Ms. Sanghamitra Das and Ms. Upasana Sarma

throughout my studies. I also highly appreciate the technical cooperation given by Mr. Jiten Basumatary, Mr. Saiffuddin Ahmed and Mr. Argha Das. I am also grateful to my friends Mr. Anoop A.D, Mr. Surendra Bhakta and Mr. Vishal Kudva for their constant support.

My most sincere gratitude and appreciation go to my mother Mrs. Sundari Bolar, my sisters, Mrs. Vijayalaxmi and Mrs. Malathi, my niece Ms. Malavika, my nephew Mr. Mayur, my in-laws Mr. Ishwar and Mrs. Hema and finally my dear wife Dr. Shruthi for their patience, continuous encouragement and moral support over the past difficult years. I am deeply indebted to all the other members of my family who gave me continuous support and encouragement throughout my life.

Date: December 2017 Gururaj Bolar

(Roll No. 126103020)

Table of Contents

List of Figures

List of Tables

List of Abbreviations

2-D	Two-dimensional
3-D	Three-dimensional
ADOC	Axial depth of cut
ANOVA	Analysis of variance
ALE	Arbitrary Lagrangian-Eulerian
BUE	Built-up edge
CNC	Computer numerical control
CD	Crowding distance
DoE	Design of experiments
EA	Evolutionary Algorithm
FEA	Finite element analysis
FEM	Finite element method
GA	Genetic Algorithm
GRA	Grey relational analysis
GRG	Grey relational grade
J-C	Johnson-Cook
LB	Larger-the-Better
MRR	Material removal rate
MOGA	multi-objective genetic algorithm
NB	Nominal-is-better
SB	Smaller the better
S/N	signal-to-noise
SSI	Small scale industry
VEGA	Vector evaluated genetic algorithm
VMC	Vertical machining center
WC	Tungsten carbide

List of Symbols

a_d	Axial depth of cut
A, B, c, m, n	Johnson-Cook (J-C) material model coefficients
$[C]$	Viscous damping matrix
$[\bar{C}]$	Capacitance matrix
c	Damping coefficient
C_p	Specific heat
D	Scalar damage parameter
D_1-D_5	Johnson-Cook (J-C) damage constants
D_f	Wall deflection
D_{fmin} and D_{fmax}	Minimum and maximum values of deflection
d_i	End mill diameter
dz	elemental thickness
E	Elastic modulus
F	External force vector
F_C	Resultant milling force
f_f	Fraction of heat energy conducted into the chip
f_t	Feed per tooth
F_t, F_r and F_a	Three oblique force components
F_{tc}, F_{rc} and F_{ac}	Forces due to material shearing occurring in the primary shear zone
F_{te}, F_{re} and F_{ae}	Forces due to rubbing and ploughing at the flank face in the tertiary deformation zone
F_x	Milling force in X direction
F_y	Milling force in Y direction
F_z	Milling force in Z direction
G_f	Hillerborg's fracture energy
$h(\theta, z)$	Uncut chip thickness
h_c	Convection coefficient
k	Stiffness coefficient
$[K]$	Stiffness matrix
$[\bar{K}]$	Time-dependent conductivity matrix
K_c	Fracture toughness
k_{chip}	Shear flow stress
K_{tc}, K_{rc} and K_{ac}	Shearing force coefficients
K_{te}, K_{re} and K_{ae}	Edge force coefficients

k_t	Thermal conductivity
L	Characteristic length of the element
$[M]$	Mass matrix
n_s	Spindle speed
N_t	Number of teeth
P	Hydrostatic pressure
P_c	Milling power consumption
P_f	Power of feed motion
P_m	Machining power of spindle
P_u	Power consumed by auxiliary systems
P_y	Process productivity
$\dot{Q}$	Total heat generation rate
$\dot{q}_{conv}$	Convection coefficient
$\dot{Q}_f$	Volumetric heat flux due to friction
Q_1	Quality index
$\dot{Q}_{pl}$	Volumetric heat flux generated due to inelastic plastic deformation
R	End mill radius
R_a	Surface roughness
$R_{amin,}$ and R_{amax}	Minimum and maximum values of surface roughness
r_d	Radial depth of cut
R_T	Non-dimensional thermal number
T	Nodal temperature vector
$\dot{T}$	Derivative of the temperature with respect to time
T_c	Cutting temperature
T_{melt}	Melt temperature
T_{room}	Room temperature
$\ddot{u}$, $\dot{u}$, u	Nodal acceleration, velocity and displacement vectors
$\bar{u}$	Equivalent plastic displacement
$\bar{u}_f$	Equivalent plastic displacement at failure
V	Cutting speed
V_s	Shear velocity
Y_i	Mean grey relational grade at the preferred level
$Y_{predict}$	Predicted grey relational grade
Y_{mean}	Total mean of the grey relational grade

α	Thermal expansion
α_n	Normal rake angle
α_r	Radial rake angle
β	Mean friction angle
β_i	Grey relational grades
β_n	Normal friction angle
γ	Shearing strain
$\dot{\gamma}$	Shear stain rate
$\dot{\gamma}_s$	Slip rate
$\bar{\varepsilon}$	Equivalent plastic strain
$\dot{\varepsilon}$	Equivalent plastic strain rate
$\varepsilon_i(J)$	Grey relation co-efficient
$\bar{\varepsilon}_f$	Equivalent plastic strain at failure
ε_{fi}	Equivalent strain at fracture initiation
$\dot{\varepsilon}_o$	Reference plastic strain rate
$\bar{\varepsilon}_{0i}$	Plastic strain at damage initiation
η	S/N ratio
η_c	Chip flow angle
η_f	Frictional work conversion factor
η_p	Fraction of the mechanical work required for plastic deformation which is converted into thermal energy
η_{sh}	Shear flow angle
θ_{en}	Entry angle
θ_{ex}	Exit angle
$\theta_j(z)$	Cutter immersion angle
λ_h	Factor which considers plastic work done outside the thin shear zone
λ_s	Cutter helix angle
λ_w	Heat conducted into the work material
μ	Friction co-efficient
ν	Poisson ratio
ρ	Material mass
ρ_m	Material density
$\bar{\sigma}_{jc}$	Equivalent flow stress

σ_n	Normal stress
σ_y	Yield stress of the material
τ_{criti}	Critical frictional stress
τ_f	Frictional stress
τ_s	Shear stress
ω	Angular velocity
ω_s	Scalar stiffness degradation parameter
ϕ_n	Normal shear angle
Δy	Shear band spacing

Chapter 1

Introduction

Due to homogeneity and excellent strength-to-weight ratio, monolithic thin-wall components are widely used in aerospace, marine, electronics and automobile industry. Airframe structures of modern commercial and military aircraft contain hundreds of unitized monolithic metal structural components, which comprise of thinner ribs and webs. Figure 1.1 shows some applications of thin-wall structures used in real life. These are aerospace structural components such as ribs, stringers and spars. In aero-engine construction, about 90% parts are thin-walled. An impeller blade can be an example of thin-wall-asymmetric-open-component while engine-casing can be considered as thin-wall-axisymmetric-closed-components (Geng et al. (2011)). Panels or structural parts, heat sinks of processors of electronics products such as laptop computers are also made up of thin-wall parts. Thin-wall machining is essential in the manufacture of dies and molds required to produce thin-wall plastic parts. It is also used in power engineering applications such as turbine blades, housings and enclosures.

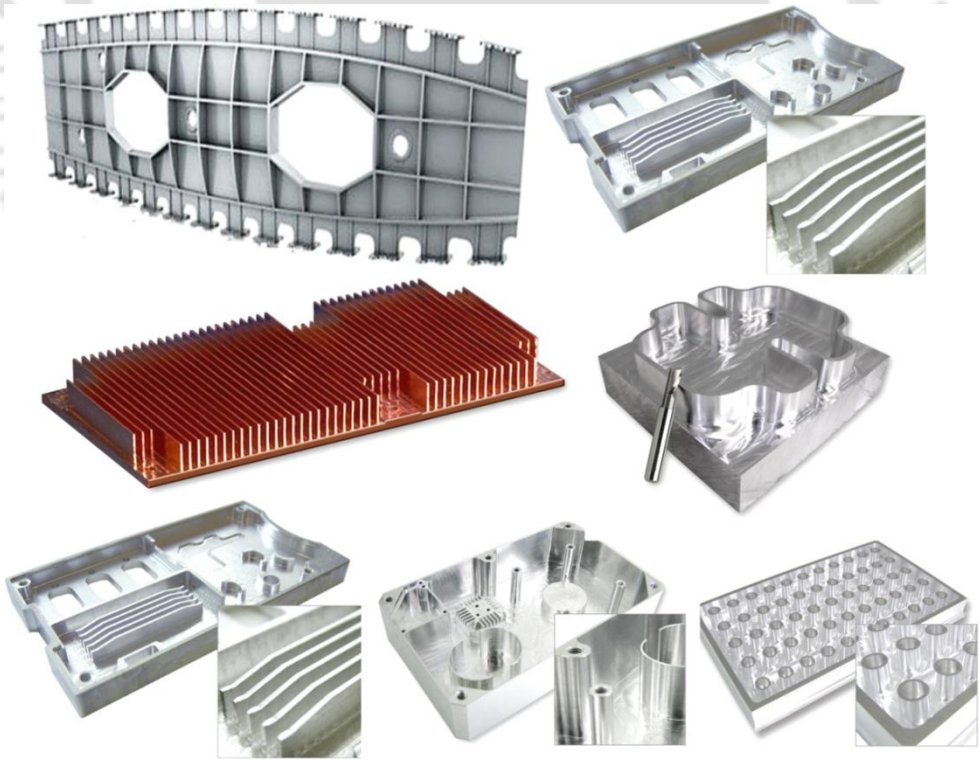

Figure 1.1 Thin-walled macro parts (Datron (2017), Sandvik Coromant (2017))

The conventional thin-wall structural components are manufactured in parts and then assembled together by using riveting or welding operations. The process involves

high part cost, and it is time-consuming and laborious (Campbell. 2006). Machining of thin-wall parts eliminates the need for different set-ups and processes; however, it consumes a lot of power because of machining of about 90-95% bulk material. Today's manufacturing and tool room industry are striving to reduce the component cost and to improve the product quality in terms of surface finish and dimensional accuracy. To fulfill these requirements it is imperative to focus our research attention on improving the product quality and overall productivity during machining of thin-wall components.

1.1 Thin-Wall Machining

In general, machining of parts having thin sections is called as thin-wall machining. Generally, peripheral milling is a commonly used in machining of thin-wall parts. During the machining process, low rigidity thin sections deflect under the influence of milling force and the heat generated by severe plastic deformation. Various milling parameters such as feed per tooth, axial depth of cut, radial depth of cut, tool diameter, spindle speed, tool angles influence the magnitude of the milling force, which in turn affects the accuracy of the machined component.

According to Kennedy (2007), a wall of thickness in the range of 1 mm to 2.5 mm can be considered as a thin-wall. Yang (1980) defined the thin plates and thick plates for plate bending theory as:

$$\left.\begin{aligned} \text{Thick plate} &= t/p > (1/5) \\ \text{Thin plate} &= (1/100) \le t/p \le (1/5) \end{aligned}\right\} \quad (1.1)$$

where p is the shorter length of two edges of the plate and t is the plate thickness.

The main difference between thin-wall machining and normal machining is that in thin-wall machining there is very less amount of material left to support against the milling force. This leads to lower stiffness of the workpiece and results in vibrations and deformation. Consequently, the effect of the milling parameters on thin-wall machining gets amplified compared to that of a normal machining operation.

1.2 Motivation for the Present Research Work

Most of the thin-wall components used in the industry are machined from aluminum and titanium blocks. Aluminum is widely used because of its low yield stress, good machinability rating. Moreover, good fatigue resistance makes it favorable in aerospace

and automobile applications. In the field of thin-wall machining, high-speed thin-wall machining is gaining popularity due to its merits such as low milling force, low cutting temperature, reduced machining time and generation of the better quality surface. High-speed machining utilizes machine tools having very high spindle power rating and thus it is very expensive. It requires high capital investment, which may not affordable by the small-scale industries. Therefore, it is essential to explore the employment of conventional low to medium duty computer numerical control (CNC) machining centers for manufacturing of quality thin-wall structures.

Generally, peripheral milling is a common process used in thin-wall component machining. During the peripheral milling operation, thin-walls deflect under the action of milling force which affects the surface quality and accuracy of the work-part. Figure 1.2 shows a schematic representation of thin-wall machining process.

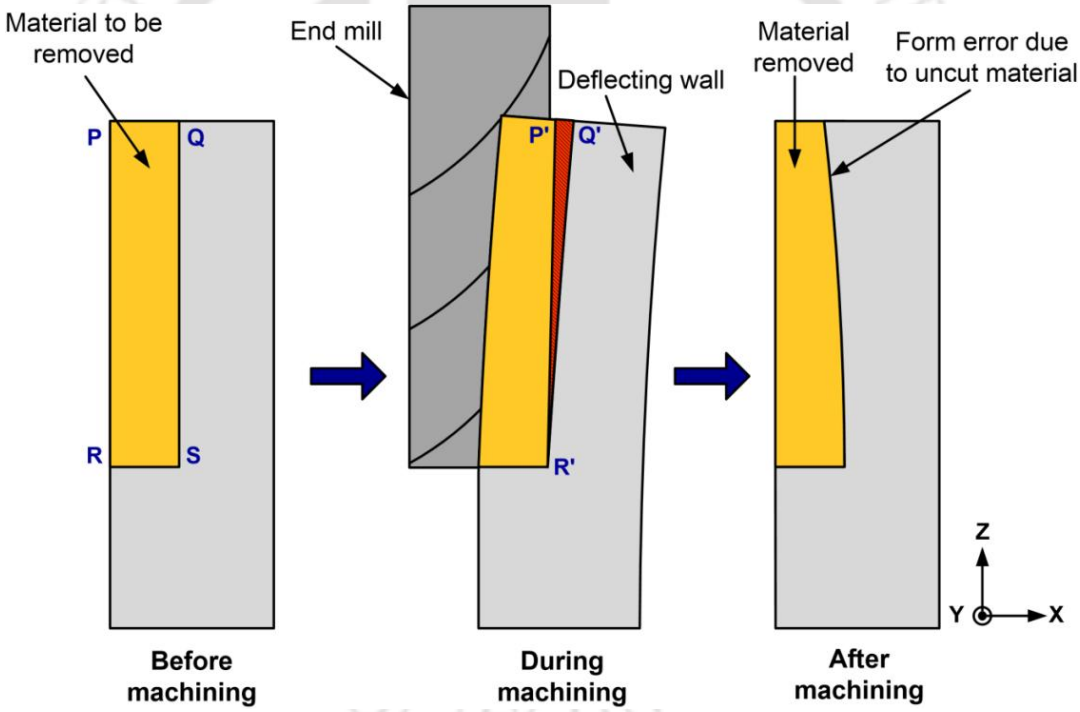

Figure 1.2 Wall deflection and form error produced in machining thin-wall feature

For the chosen milling parameters, the material to be cut is PQRS, however, under the action of milling force, the wall deflects causing the material P'Q'R' to remain uncut. As the cutter moves away in the feed direction (Y-direction), the wall recovers elastically and the material remains uncut which causes the shape of the wall to be thicker at its top and thinner at its base. The thin-wall parts are always machined on computer numerically controlled (CNC) machines. In spite of using CNC technology, the process of thin-wall

machining is not devoid of problems. This is because the process control by CNC is based on idealized geometry and does not take into account the deformation of the parts. As a result, there is a significant deviation between the desired part profile and the manufactured one. To reduce the form error generated due to the deflection and to improve the surface finish of work part, it is essential to set the milling parameters at their optimum levels. In view of this, if the deflection is predicted beforehand, effective countermeasures can be undertaken to obtain the desired process performance, that is, manufacturing of a dimensionally accurate finished component with good surface quality.

Another important aspect related to machining of aluminum thin-wall components is the surface roughness. Aluminum alloys possess a comparatively low modulus of elasticity, which causes the workpiece to spring back. This spring back action often results in deflection and chatter. Chatter affects the material removal (MRR) rate and leads to poor surface finish, part rejection and loss of productivity.

The optimum performance (efficiency) of the end milling of thin-wall parts aims to achieve high productivity (maximum MRR), low wall deflection (form accuracy), good surface finish (low surface roughness) and low power consumption (low milling force). These performance measures of end milling process are influenced by a large number of process and tool geometry parameters. Due to the complex and nonlinear relationship between the milling parameters and the performance measures, it is quite difficult to select the optimum milling parameters for specific (roughing or finishing) application of thin-wall end milling process. To improve process efficiency, thin-wall machining parameters are chosen based on shop floor experience, thumb rules and handbook values, which often lead to suboptimal and inconsistent machining process performance. In absence of a good process model, it is quite difficult to select the optimum milling parameters for specific application of thin-wall milling process such as roughing or finishing. It can be seen that no efficient and generalized approach to model the thin-wall milling process has so far been reported to predict the process performance (MRR, milling force, wall deflection and surface finish) accurately and use it further to derive the optimal milling parameters. Process models developed so far have either concentrated on developing analytical models for vibration analysis or alternatively experimental studies to support the outcomes of numerical or analytical models. A need was thus identified to develop an integrated numerical-analytical model for quicker and

accurate prediction of in-situ wall deflection and further to carry out systematic experimental studies to derive optimal process conditions for achieving the desired process performance in terms of high productivity, good product quality and low power consumption. This provided the motivation to carry out the present research work.

1.3 Scope of the Present Research

The present work primarily focuses on the development of an integrated analytical-numerical approach for three-dimensional thermo-mechanical modeling of end milling of thin-wall parts using unified mechanistic analytical equations and finite element method (FEM). Initially, a realistic three-dimensional thermo-mechanical FEM model is developed to simulate the complex physical interaction of helical cutting tool and workpiece during thin-wall milling of an aerospace grade aluminum alloy. Then an integrated force-deflection model for thin-wall milling was presented for quicker and accurate prediction of in-situ wall deflection. The results predicted by the numerical model and developed integrated approach were validated with our own experimental results.

Systematic experiments were carried out on thin-wall end milling operation to determine the influential milling parameters viz. feed per tooth, spindle speed, axial and radial depth of cut on the performance parameters such as milling force, surface roughness and wall deflection. Moreover, investigations into the influence of tool geometry parameters such as tool diameter, helix angle and number of flutes on the performance of the process were carried out. Grey relational analysis (GRA) methodology was used to obtain the optimal and influential tool geometry parameters.

Full factorial experiments were carried out on thin-wall machining of aluminum alloy 2024-T351 based on the recommended ranges of the milling parameters viz. axial depth of cut, radial depth of cut, feed per tooth, and tool diameter in the initial experiments. The influence of these milling parameters on the process performance measures such as machining power consumption (milling force), productivity (MRR) and product quality (uniform wall thickness and surface quality) was studied. Further, a study on the chip morphology has also been conducted.

Finally, optimum levels of end milling parameters were obtained for roughing and finishing operations using Non-Dominated Genetic Algorithm - II (NSGA-II). Case studies were conducted to examine the capability of employing the suggested optimum

levels of milling parameters in practice.

Study on the vibrations based static and dynamic lobes analysis is out of the scope of this study. It is primarily envisaged that the outcomes of present research work are applicable to small to medium duty CNC machining centers having a capacity to be operated at around 4000 to 5000 r/min, which generally available with small scale industry (SSI) or tool rooms.

1.4 Organization of the Thesis

The organization of chapters in this thesis in detail is as follows:

Chapter 1 presented an overview of the thin-wall machining process in terms of its definition, advantages and limitations, and applications. The motivation for carrying out research in the area of thin-wall machining of aluminum alloy has been brought out at the end of the chapter.

Chapter 2 presents a review of relevant literature for thin-wall machining process and outlines the objective. The status of research work on various aspects of thin-wall machining, such as experimental parametric investigations, development of analytical force and deflection prediction models, and process optimization models are presented. Aspects of analytical and FEM based machining modeling and simulation techniques are critically studied. The chapter concludes by summarizing important observations from the literature survey and stating the research objectives.

Chapter 3 presents, in detail, the development of a three-dimensional nonlinear thermo-structural numerical model of end milling of thin-wall parts using finite element method. The governing equation, boundary conditions and solution methodology for the analysis are explained at length. The model is validated by comparing the predicted results with our own experimental results. Case studies on the effect of input process conditions on the output performance parameters have been reported.

Chapter 4 presents, in detail, the development of an integrated numerical-analytical oblique cutting based force-deflection model. The developed approach in terms of unified mechanics based equations and the methodology of integration with three-dimensional FEM-based simulation model are presented at length. Cutting force coefficients determination based on an analytical and numerical hybrid principle has been presented. The proposed model has been validated by comparing the predicted

results with our own experimental results. At the end, the performance evaluation of proposed approach is discussed.

Chapter 5 reports, in detail, the experimental investigations that carried out to find out a set of initial process parameters. Experimental details in terms of the machine tool, fixtures, process responses measurement instruments, fixtures, and methodology are presented. Detailed discussions on the influence of process parameters such as spindle speed, radial depth of cut, axial depth of cut those affect the milling force, surface roughness and magnitude of wall deflection have been presented. Moreover, an investigation into the influence of tool geometry parameters on the process performance is carried out using Grey relation analysis (GRA).

Chapter 6 presents the results obtained during full factorial experiments carried out on thin-wall machining of aluminum alloy 2024-T351. A systematic study has been presented on the influence of milling parameters viz. axial depth of cut, radial depth of cut, feed per tooth, and tool diameter on the process performance measures such as machining power consumption (milling force), productivity (MRR) and product quality (uniform wall thickness and surface quality). Further, a study on the chip morphology has been presented. Based on the present study, recommendations for practical applications have been suggested.

Chapter 7 presents the methodology for optimum selection of end milling parameters using Non-Dominated Genetic Algorithm - II (NSGA-II). Details regarding the objective functions, variables and their constraints, methodology of optimization using NSGA-II algorithm are presented. By employing the algorithm, optimum milling parameters for roughing and finishing operations for end milling of thin-wall parts have been derived and verified by conducting experiments. Finally, few case studies are presented to demonstrate the capability of the suggested optimum levels of milling parameters in practice.

Chapter 8 presents the important observations and conclusions from the present research work. The scope for carrying out future work in this area is presented at the end of the chapter.

Chapter 2

Literature Review

2.0 Scope

This chapter presents a critical review of literature in the area of process modeling and optimization of the thin-wall end milling process. Initially, the details of end milling process in terms of milling parameters; and challenges in machining are presented. Various approaches of thin-wall milling process modeling such as analytical modeling, numerical modeling and mathematical modeling based on the design of experiments (DOE) techniques have been critically studied. Published literature on experimental investigations into the influence of process parameters, cutting tool geometry parameters, thin-wall manufacturing strategies and process planning are covered extensively. Process optimization approaches using the regression analysis, statistical techniques and genetic algorithm have been presented. The chapter concludes by summarizing important observations from the literature survey and stating the research objectives.

2.1 Machining of Thin-Wall Parts

The process of machining components having thin sections from a single, monolithic workpiece is known as thin-wall machining. Machining of thin-wall parts poses a challenge of maintaining tight dimensional tolerance. Peripheral milling is a common process used to machine thin-wall components. Manufacturing of these components using machining operation has low productivity because approximately 90-95 % of the material from the initial work material volume gets removed during the operation (Scippa et al. (2014)). Moreover, thin-wall structures possess low stiffness and often deflect and deform under the action of milling forces. Even in CNC milling, where the tools are controlled precisely according to the contour of the thin-wall component, the wall undergoes in-process deflection. In-process deflection and deformation of the work-parts result in form errors, which severely affect the accuracy and quality of the machined part.

Researchers worldwide are focusing their attention on thin-wall machining to manufacture structural components required for aerospace, automobile and electronics applications. Literature reports esteemed research articles and reports published by international universities, industry and research organizations. These are focused on various aspects of thin-wall machining such as analytical modeling, numerical modeling,

experimental investigations into vibrations, and influence of process parameters such as feed, depth of cut, tool geometry parameters, tool path planning strategies and optimization of process parameters. In this chapter published research work in the area of analytical, numerical modeling and experimental investigations have been critically reviewed and discussed at length. Initially, a section on milling parameters used in thin-wall machining is presented.

2.2 Thin-Wall Machining Parameters

There are many machining parameters that influence the geometric accuracy and precision of final component in the milling of thin-wall components. The selection of machining parameters becomes challenging due to the complexities associated with the thin-wall milling process. Figure 2.1 shows some of the factors that affect the machining precision of thin-wall components.

These parameters can broadly be divided into three groups namely process parameters, tool geometry parameters and workpiece attributes. An exhaustive literature review has been carried out to understand the effects of process parameters, tool geometry parameters and workpiece attributes on the performance parameters such as wall deflection, surface roughness, and material removal rate. Details about the reported experimental works are discussed in the following sections.

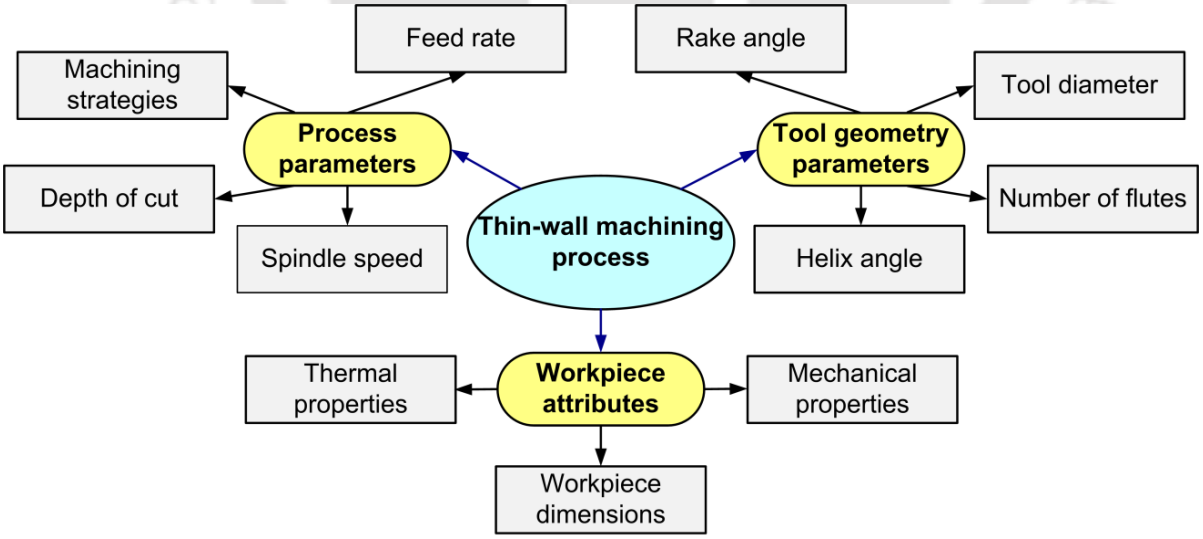

Figure 2.1 Thin-wall machining parameters

2.3 Experimental Studies into the Influence of Milling Parameters on Performance Parameters

2.3.1 Process Parameters

Figure 2.2 shows the various process parameters that are employed in the milling of thin-wall parts. The axial depth of cut (a_d) is the immersion length of the cutting tool inside the workpiece along the axial direction of the tool. The radial depth of cut (r_d) is the depth of the cutting tool along the radial direction. Feed rate (f_r) is the velocity at which the workpiece is fed to the tool. It is generally expressed in units of distance per unit time (typically inches per minute (inch/min) or millimeters per minute (mm/min)) with consideration of the number of teeth (or flutes) of the cutter. It is also expressed in terms of feed per tooth (f_z). Cutting speed also called surface speed or simply speed is the speed difference (relative velocity) between the cutting tool and the surface of the workpiece it is operating on. It is expressed in units of distance along the workpiece surface per unit of time, typically surface feet per minute (sfm) or meters per minute (m/min). Spindle speed (n_s) is the frequency of rotation of the spindle, measured in revolutions per minute (r/min).

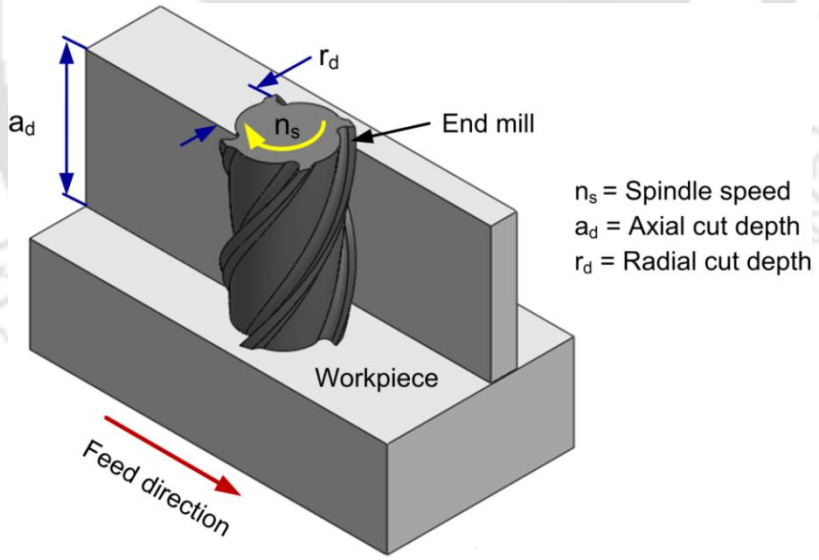

Figure 2.2 Process parameters in thin-wall milling operation

Researchers have extensively carried out experimental studies on the influence of process parameters on surface roughness and wall deflection. Kazemi et al. (2007) studied the surface integrity of thin-walled titanium parts by varying the cutting speeds and immersion angle. They also investigated the influence of radial depth of cut on cutting forces and microstructure. It was noted that cutting force increases with the

increase in radial depth of cut, while the variation in spindle speed was found to have a nonlinear effect on cutting force. The surface defects were found to increase with the spindle speed. During the hardness evaluation, it was noted that at high cutting speeds the hardness of machined surface increases. Cao et al. (2010) worked on machining of straight thin-walls of aluminum alloy LY12CZ. They studied the deformation characteristics of the thin-walled workpieces under different cutting conditions by varying process parameters viz. spindle speed, feed rate, axial and radial depth of cut. Moreover it was noted that the deformation of the free end of the wall was higher in comparison to the base. Since the workpiece was machined on a large block of aluminum, the deformation at the bottom section of the wall was very small.

Polishetty et al. (2014) assessed the machinability of titanium alloy Ti-6Al-4V and studied the influence of trochoidal tool path. Authors reported that cutting force was higher in the case of high cutting speed and it severely affects the tool life. Better dimensional accuracy was observed for lower cutting speeds. Similarly, Patil et al. (2014) also reported that trochoidal milling is a favorable milling technique to machine Ti-6Al-4V thin-wall parts as it helps in easier chip evolution. Moreover, the authors studied the influence of process parameters viz. cutting speed, feed/ tooth, axial and radial depth of cut on productivity, quality and machine tool dynamics. It was realized that low radial depth of cut produces low cutting force and temperature. Michalik et al. (2014) conducted experiments to determine the influence of up milling and down milling conditions on surface roughness (R_z) for the workpiece with variable geometry. Authors found that surface roughness was low when down milling condition was used.

Sonawane and Joshi (2015) analyzed the influence of workpiece thickness, workpiece inclination, and cutter orientation on surface quality and the workpiece deflection during ball end milling of thin cantilever parts model of Inconel-718. Authors reported that cutting force, feed rate, wall thickness and cutting orientation greatly influences the surface finish. Slusarczyk and Matras (2016) conducted milling tests of aluminum alloy with a sintered carbide tool using up and down milling conditions. They noted that down milling condition provided better results in terms of lower deformation as compared to that of up milling condition.

Literature reports few attempts on the study of variation in process parameters on the vibration behavior of thin-wall and cutting tool during the milling operation. Song et al. (2014) proposed a methodology to predict the dynamic stable lobe diagram of the

thin-walled component during the peripheral milling process. The model took into account the variations of dynamic characteristics of the workpiece with the tool position. It was noted that chatter plays an important part in the distortion. The cutting distortion was very little under unstable cutting conditions but the time-dependent distortion was very large and changed with time.

Huang et al. (2014) studied the machinability issues associated with tools having variable and uniform pitch during dry thin-wall milling of aeronautical material Ti6Al4V. The vibration minimizing characteristics of variable pitch tool was analyzed using Fast Fourier Transform (FFT) and wavelet analysis. Experimental results showed that tool vibration decreases when the variable pitch tool was employed. Authors observed that vibration energy was more disperse with uniform pitch tool. Later Huang et al. (2016) analyzed the cutting force and spindle acceleration signals obtained during machining of titanium thin-wall and non-thin-wall components. Frequency spectrum and wavelet analysis methods were used to illustrate the impact of tool wear on cutting force. The tool wear was also analyzed during the whole cutting process. The experimental results showed that cutting vibrations in the milling of thin-wall components were higher than those measured for non-thin-wall components. It was seen that due to tool wear, there was a change in cutting load acting on each cutting edge, which resulted in the reduction of cutting force frequency from the tooth passing frequency (TPF) to the spindle frequency (SF).

Recently, Guo et al. (2016) experimentally investigated the influence of flank milling of thin-wall components made of titanium alloy Ti6AL4V using carbide tools. The cutting force signals were analyzed in time and frequency domain. The influence of cutting parameters such as feed per tooth, the axial depth of cut, cutting width and cutting speed on cutting force was studied. Finally, the mathematical relationship between the cutting force and process parameters was established using regression analysis. Mundim et al. (2017) investigated the effect of variation in cutting speed on cutting force and excitation frequency. A methodology to predict the resonance based on frequency chart was proposed. The results indicated that frequency chart method can be used to predict and explain the occurrence of instability during thin-wall machining.

2.3.2 Cutting Tool Geometry Parameters

Tănase et al. (2010) measured the cutting forces and deformation of thin-wall parts by

varying the cutter diameter. Large diameter tools (25 mm and 80 mm) equipped with indexable inserts was used for roughing operation while 8 mm tool was used for finishing operation. It was observed that deformation and cutting forces reduce when a smaller diameter tool (8 mm) is used for finish machining condition. Similarly, Jiang et al. (2013) studied the effects of variation in tool diameter on the residual stress and distortion induced by milling of the thin-walled part. It was observed that the large tool diameter reduces the uncut chip thickness and produces more uniform residual stress distribution. Authors also reported that larger tool diameter improves the productivity and reduces the wall distortion. Izamshah et al. (2013) carried out an experimental investigation into the effects of end mill helix angle on the accuracy of machining thin-rib aerospace component. They reported that larger helix angle provides the least surface error. It was concluded that end mills with small helix angles cause high cutting forces which deflect the workpiece due to chatter.

2.3.3 Workpiece Attributes

The workpiece attributes such as dimension of the wall i.e. thickness, length and height, and its shape i.e. open straight wall, curvilinear are important aspects that to be considered in the study of thin-wall milling process. Literatures report few attempts on this aspect. Liu (1993) investigated the effects of wall thickness, wall length and wall height on elastic deformation of a rectangular plate. It was noted that the magnitude of deformation increases with reduction in wall thickness, and increase in wall height. Izamshah et al. (2011) carried out experimental work to determine the influence of spindle speed, feed rate, radial depth of cut, wall thickness, wall height and wall length on wall deflection. The experimental data was statistically analyzed and used to develop regression equations to determine the correlation between wall deflection and process parameters.

2.3.4 Machining Strategies

Selection of a proper tool path strategy is an important aspect in the process of milling. This provides substantial savings in machining time, improvement in workpiece surface quality and improvement in tool life. Literature reports various research works on the cutter path strategies employed in the milling of thin-walled parts. For high-speed milling of aluminum parts with large, thin, flexible webs, Smith and Dvorak (1998) suggested that it is desirable to choose the cutter paths that provide maximum work

material support and minimum and minimum wall deflection. Authors recommended the use of a tool with minimum possible corner radius as it helps in reduction of cutting forces. They also suggested that to machine a fillet, low spindle speed should be employed. Fry et al. (1999) observed that raster milling along the longest dimension of the workpiece generated the shortest cutting path and hence it can be used in practice. Gologlu and Sakarya (2008) conducted an experimental investigation on the effects of cutter path strategies on the surface roughness of pocket milling. Authors found that one direction followed back and forth cutter path strategy provides better surface roughness. Jabbaripour et al. (2010) also carried out experimental studies on the influence of cutter path strategies on cutting force and surface roughness during milling of thin-walls. The experiments were performed using four cutter directions viz. transversal outward, transversal inward, longitudinal outward and longitudinal inward directions. Best cutting condition was obtained with a transversal inward orientation, and the worst cutting condition was obtained with a longitudinal outward orientation. Later, Conradie et al. (2012) compared various milling strategies such as down milling and up milling, rolling-in and out, ramp and interpolate, drill and profile milling, drill and plunge, spiral milling, trochoidal machining. Smith et al. (2012) recommended the use sacrificial structures to improve the dimensional accuracy and surface quality during machining of thin-wall components. Figure 2.3 shows typical sacrificial structures in buttressed and corrugated geometries. Buttress type sacrificial structures were found to provide ample stiffness for stable machining of the thin-walls. However, it requires more lead time in designing the sacrificial structures.

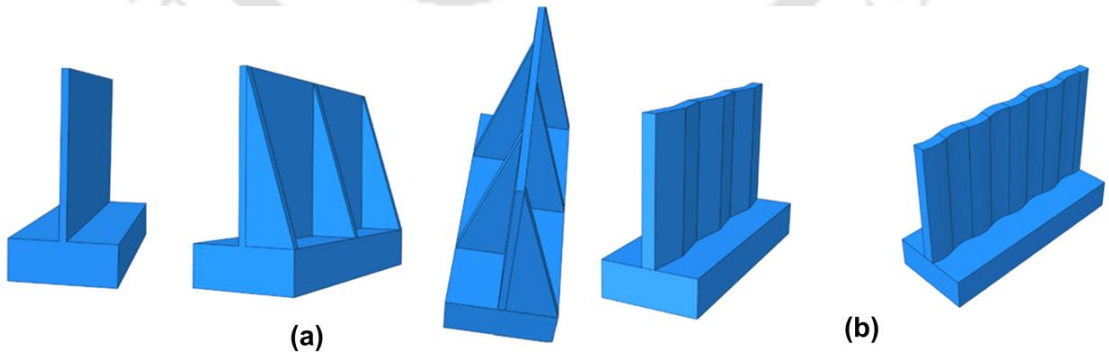

Figure 2.3 Typical sacrificial structures in buttressed and corrugated geometries (Smith et al. (2012))

Kadir et al. (2013) conducted experiments to compare various cutting path strategies for milling thin-walled aluminum alloys fabrication. It was found that true

spiral provides better dimensional accuracy while parallel spiral strategy generates quality surfaces. Authors reported that one-way cutting strategy consumes the lowest time whilst parallel spiral cutting strategy requires comparatively more time to complete the job. Izamshah et al. (2014) carried out experimental studies to compare the process performance by employing three cutter path strategies viz. waterline-step, overlapping-step and tree wise-steps. It was noted that use of overlapping steps resulted in overcut form errors whereas the tree-wise steps produced undercut form errors. Based on the observations, it was recommended that waterline cutter path produces the least surface error followed by overlapping and tree-wise steps. Recently Polishetty et al. (2014) and Patil et al. (2014) assessed the machinability of titanium alloy Ti-6Al-4V and reported that trochoidal tool path provides best results in terms of smoother cutting operation, good quality surface and minimum deflection. Trochoidal milling tool path is a combination of uniform circular motion that includes simultaneous forward movements. The simultaneous circular milling and slicing operation generate uniform forces on the tool. Recently, Li et al. (2015) developed an approach of optimizing the profile and magnitude of residual stress by analyzing the effects of depth of cut on the redistribution of residual stress. Experiments and simulations were conducted to compare the cutting forces, temperature and residual stress. The results showed that, in the roughing, by selection of a subsequent depth exceeding prior depth of maximum compressive residual stress, the material which contains the main machined residual stress can be removed in favor of the subsequent machining. Furthermore, in the finishing, different depths of cut were utilized in different cutting stages, resulting in smaller magnitude of maximum machined residual stress and depth of maximum compressive residual stress.

2.3.5 Experimental Setup and Process Monitoring

Literature depicts various experimental investigations on thin-wall machining process. To carry out these studies, researchers have developed various experimental setups. Ratchev et al. (2004) developed an experimental setup to measure instantaneous cutting forces and deflections during in machining of low-rigidity thin-wall parts. Figure 2.4 shows the typical arrangement developed.

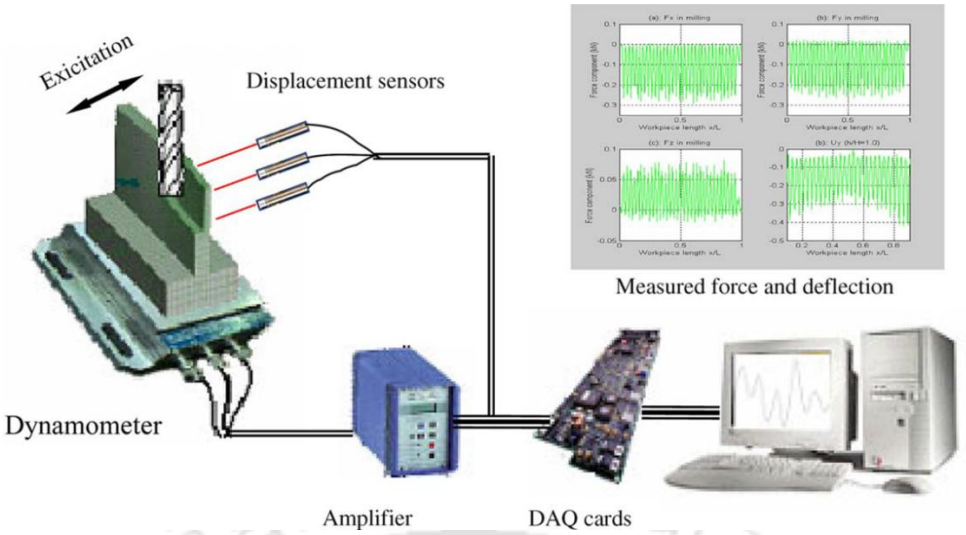

Figure 2.4 Thin-wall machining experimental set-up (Ratchev et al. (2004))

Online deflection of the part was measured by monitoring the displacement using three inductive displacement sensors mounted at the back of the workpiece. Recorded responses were used for validation of the developed numerical model.

Similarly, Rai and Xirouchakis (2009) developed an experimental set up to measure cutting force components, workpiece temperature distribution, part deflection, and stresses analyzed the errors induced during milling of thin-wall components by carrying milling experiments on aluminum alloy. Figure 2.5 shows the developed experimental arrangement to record the responses during milling of a vertical rib and horizontal web feature. The results were used to analyze the process performance and validate 3-D FEM based numerical model.

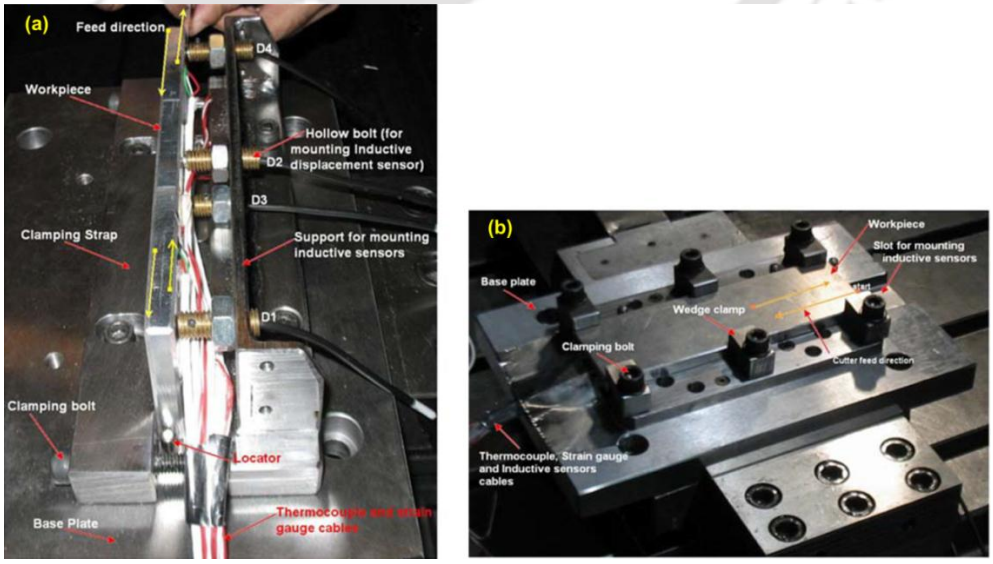

Figure 2.5 Thin-wall machining experimental set-up: **(a)** Vertical rib **(b)** Horizontal rib (Rai and Xirouchakis (2009))

Tănase et al. (2010) developed an integrated experimental arrangement for measurement and analysis of cutting forces and deformation during milling of thin parts. The set up was equipped with the required instrumentation such as three component piezoelectric dynamometer (*Type 9257 B Kistler make*) and inductive differential transducers. Research groups such as Seguy et al. (2008), Houjun et al. (2009), Cao et al. (2010), Jabbaripour et al. (2010), have developed simple experimental setups to measure cutting forces during the thin-wall machining. Most of them have employed piezoelectric based force dynamometers to record the responses. The responses were also recorded to analyze surface roughness (Seguy et al. (2008)) and online deflection of the work part (Houjun et al. (2009), Cao et al. (2010)).

Observations

In thin-wall machining, the influencing parameters can be classified into three groups namely process parameters, tool geometry parameters and workpiece attributes. Literature reports significant research on the effects of these parameters on the performance measures viz. milling forces, deflection, surface roughness, and material removal rate. However, it was noted that, in most of these studies, limited experiments have been conducted. The outcomes of these studies were mainly used to validate the numerical or analytical models developed. Very scant research is reported on comprehensive full factorial studies on the influence of process parameters viz. feed, speed, axial and radial depth of cut as well as tool geometry parameters viz. tool diameter, helix angle on all the performance parameters viz. deflection, material removal rate, surface roughness, power consumption in integrated and comprehensive manner. Literature also reports some experimental studies on the effect of tool path planning strategies and use of sacrificial structures to improve the process productivity. Literature depicts various experimental setups developed for measurement and analysis of milling forces and deformation during milling of thin parts.

2.4 Analytical Modeling of Cutting Forces and Wall deflection

Machining of thin-wall components is a complex operation as it involves removal of material from low rigidity parts. Thin-wall parts often defect during machining operation under the action of milling forces. Therefore it is essential to set parameters that evolve maximum possible material removal rate and minimum wall deflection. Wall deflection is dependent upon milling forces; hence prior prediction of milling forces certainly helps

in controlling the dimensional accuracy. Moreover milling forces are useful in analyzing the tool wear and tool breakage. It is thus, important to understand the relationship between the milling forces and wall deflection with the process parameters, tool geometry parameters and work material properties. Modeling of a metal cutting process using analytical methods has been effectively used to reduce the machining costs and analysis time. Over the years, intensive efforts have made by various researchers to develop cutting force models for end milling operation. Accordingly, mechanistic models and shear plane/zone models have been developed. These are discussed at length in the following sections.

2.4.1 Modeling of Milling Forces for End Milling Process

Since the early forties, researchers have been developing the analytical models of machining operations. In the work, only relevant papers to helical end milling and thin-wall operations have been studied. Initially, Martellotti (1941, 1945) worked on the kinematics of milling process and developed expressions for chip thickness considering trochoidal tool path. Comparison between up and down milling condition was carried out and it was found that power consumed by down milling was greater while the tool life improves with the use of down milling condition. Sabberwal (1961) developed a force model to predict the tangential cutting forces in helical milling. However, the authors did not consider normal and axial force in their analysis. The model was able to define the different tool engagement conditions for the helical milling process. In the start of eighties, DeVorr et al. (1980) improved the model of cutting geometry analysis given by Martellotti (1941, 1945). Authors added empirical force predicting equations to determine the instantaneous milling force. The cutting force coefficients called empirical constants were experimentally determined using the average forces. It was noted that the coefficients were mainly dependent on the chosen process parameters. Altintas and Montgomery (1991) developed a two-dimensional (2-D) model for helical end milling process to predict the forces under static or dynamic conditions. The geometry of the workpiece and cutting tool were considered in the model. Young et al. (1994) used orthogonal machining theory to predict the cutting forces during face milling operation.

In the late nineties, Armarego (1998, 2000) presented in detail a unified-generalized mechanics of cutting approach which can be used for a wide variety of machining operations. The model involved generalized mechanics of cutting analyses for single and multi-point cutting and a database was established for basic cutting quantities

and edge force coefficients. Later they developed a methodology for modeling machining operations based on the database. Zheng et al. (1999) developed a theoretical model for predicting the cutting forces during face milling. The milling cutter was discretized into several single point cutting tools to determine the forces acting on each tool. The model took into account the material properties, cutter parameters, tooth geometry, cutting conditions and types of milling. Li et al. (2001) developed a theoretical model for determination of cutting forces during helical end milling based on Oxley's model. For an oblique cutting process, the forces along the cutting, feed and radial directions (P_1, P_2 and P_3) were determined as follows. Figure 2.6 shows the schematic of the developed oblique cutting model.

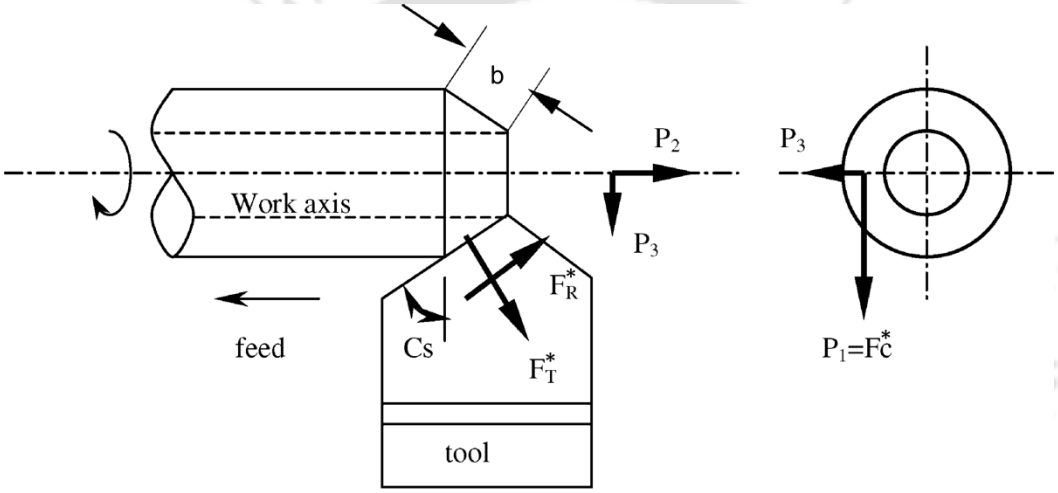

Figure 2.6 Model for simple oblique cutting (Li et al. (2001))

$$\begin{aligned} P_1 &= F_C^* \\ P_2 &= F_T^* \cdot \cos(C_s) + F_R^* \cdot \sin(C_s) \\ P_3 &= F_T^* \cdot \sin(C_s) - F_R^* \cdot \cos(C_s) \end{aligned} \tag{2.1}$$

where, C_S is the tool side cutting edge angle, F_C, F_T and F_R are the force components in the cutting, feed and radial directions, respectively, which were calculated as:

$$\begin{aligned} F_C^* &= R^* \cdot \cos(\beta - \alpha_n) \\ F_T^* &= R^* \cdot \sin(\beta - \alpha_n) \\ F_R^* &= \frac{F_C^*(\sin(\lambda_s) - \cos(\lambda_s)\sin(\alpha_n)\tan(\eta_c)) - F_T^*(\cos(\alpha_n)\tan(\eta_c))}{\sin(\lambda_s)\sin(\alpha_n)\tan(\eta_c) + \cos(\lambda_s)} \end{aligned} \tag{2.2}$$

where β is the mean angle of friction at the tool-chip interface, α_n is the tool normal rake angle, λ_s is the tool inclination angle, η_c is the chip flow angle calculated according to Stabler's chip flow law, and R^* is the resultant force at the shear plane and tool-chip

interface, and was calculated using the equation:

$$R^* = \frac{k_{AB} \cdot h \cdot b}{\sin(\phi)\cos(\theta)} \tag{2.3}$$

where k_{AB} is the shear flow stress along the shear plane, h is the undeformed chip thickness, b is the width of cut, ϕ is the shear angle and θ is the angle made by R^* with the shear plane.

Moufki et al. (2000, 2004, and 2015) presented visco-plastic models to predict the cutting forces in the oblique cutting mode of operation. These models were equipped with thermo-mechanical properties, inertia effects and friction at the chip-tool interface. The material characteristics such as strain rate sensitivity, strain hardening and thermal softening were considered in the model. The model could predict the cutting forces, chip flow direction, temperature distribution and the contact length between the chip and the tool. Authors carried out a study to understand the influence of the normal shear angle, the thickness of the primary shear zone and the pressure distribution at the tool–chip interface. Further, they developed a predictive machining theory for cutting force determination during peripheral end milling based on an analytical oblique cutting model for machining titanium alloy Ti6Al4V.

Becze and Elbestawi (2002) worked on the development of an oblique cutting based force model. The oblique cutting forces were based on the orthogonal cutting force. The shear stress during material deformation was modeled using a thermo-visco-plastic material constitutive law. In this model, the strains and strain rates those used to define the shear stress were obtained from chip formation and morphology derived from orthogonal cutting tests.

Palanisamy et al. (2006) developed a dynamic cutting force model for end milling operation. The model was developed to predict the tangential cutting force and thrust force during machining of AISI 1020 steel. The chip-tool interface temperature was determined using Oxley's energy partition function and Rapier's equation. Li et al. (2011) used oblique cutting analysis to develop an analytical end milling force model. In their work, the orthogonal cutting theory based on unequal division shear zone was extended to oblique cutting analysis. Chip flow through the primary shear zone was modeled using a piecewise power law distribution under the assumption of shear strain rate. The material flow stress was defined using Johnson-Cook (JC) constitutive model. Subsequently, Li and Wang (2012) proposed a cutting force model for milling of Inconel

718. Johnson and Cook material constitutive model was used to specify the material flow, whereas the shear angle was determined based on a shear plane model. Cutting temperature was defined based on the model developed by Kronenberg. Cutting forces acting on each tooth of the milling cutter was calculated from its chip load considering the oblique cutting effects.

Recently, Song et al. (2015) used vector transformation derived from orthogonal cutting process to determine oblique cutting forces. The model was based on the fundamental mechanics of the friction relationship between tool and material (chip) at the primary and secondary shear zones. Fu et al. (2015) proposed an analytical milling force model for helical end milling. It was based on predictive machining theory. The input data provided were the workpiece material properties, cutting conditions, cutting tool geometry and cutting conditions. The cutting edge was discretized into a series of infinitesimal elements and each element was equated to an oblique cutting edge. Cutting force components were predicted for the oblique edge and the forces were integrated to determine the global forces acting on the helical end mill. Lin et al. (2016) developed an oblique cutting based end milling based force model. The model considered the pitch angle and the helix angle of each flute.

2.4.2 Modeling of Force and Deflection during Thin-Wall End Milling Process

Literature reports important research works on the development of cutting force-deflection prediction models. In the early eighties, Kline et al. (1982) developed combined cutting force-deflection model to predict the workpiece and tool deflection. Altintas et al. (1992) developed a dynamic model for milling flexible thin-wall parts. The model provided details about the surface finish, form errors and cutting forces for dynamic end milling operations. In the model, the interaction between a flexible plate and rigid end mill during dynamic milling was considered. Also, the dynamics of tool-work contact zone was modeled. In 1994, Budak and Altintas modeled the peripheral milling operation by considering the workpiece and cutting tool as plate and elastic beam member, respectively. A mechanistic force model for end milling operation was developed. For an infinitesimal element thickness (dz) of the end mill, the tangential (dF_t), radial (dF_r), and axial (dF_a) differential milling forces were given by:

$$dF_t(\theta,z) = K_t \cdot h(\theta,z)] \cdot dz$$
$$dF_r(\theta,z) = K_r \cdot dF_t(\theta,z) \quad (2.4)$$
$$dF_a(\theta,z) = K_a \cdot dF_t(\theta,z)$$

where θ is the immersion angle. The tangential, radial and axial forces given by Equation (2.3) were resolved in the feed (x) normal (y) and the axial direction (z) and integrated within the immersed part of the tool to obtain the total milling force applied on each tooth. For the exponential force model, the force components obtained after the integration was given by:

$$F_x(\phi) = \frac{K_t \cdot f_t \cdot R}{4\tan\beta}\left[-2\cos(\phi) + K_r \cdot 2\phi(z) - \sin 2\phi(z)\right] K_t \cdot h(\theta,z)]_{z_l(\phi)}^{z_u(\phi)}$$
$$F_y(\phi) = \frac{K_t \cdot f_t \cdot R}{4\tan\beta}\left[(2\phi(z) - \sin 2\phi(z)) + K_r \cdot \cos 2\phi(z)\right]_{z_l(\phi)}^{z_u(\phi)} \quad (2.5)$$
$$F_z(\phi) = \frac{K_a \cdot K_t \cdot f_t \cdot R}{4\tan\beta}\left[\cos\phi(z)\right]_{z_l(\phi)}^{z_u(\phi)}$$

where $z_l(\phi)$ and $z_u(\phi)$ are the lower and upper axial engagement limits of the in cut portion of the flute. By using the model, authors investigated the workpiece dimensional errors generated during the process. Further, they developed an analytical cutting force and surface generation model which considered the partial separation of tool and plate structures due to static displacements. The model identified the feed variation required along the plate to keep the static form errors within the specified tolerance (Budak and Altintas (1995)). Finally, a model was developed that was capable of optimization of process variables such as feed, depth of cut and spindle speed was (Budak 2006).

Ratchev and his research group also developed a force-deflection model to simulate the cutting operation thin-wall machining (Ratchev et al. (2003)). They developed a flexible force model for end milling of low rigidity parts. The forces were computed by considering the changes in immersion angles of engaged teeth (Ratchev et al. (2004)). Further, an adaptive flexible theory was used to determine static deflection during thin-wall machining. Figure 2.7 outlines the developed force-deflection prediction model. The approach was based on an extended perfect plastic layer model which was integrated with a FEM model (Ratchev et al. (2004)). The material removal was simulated by considering the interaction of tool volume with deflected part (Ratchev et al. (2004, 2004)). Based on this simulation model, an error prediction and compensation model was developed and employed in practice ((Ratchev et al. (2004, 2006)).

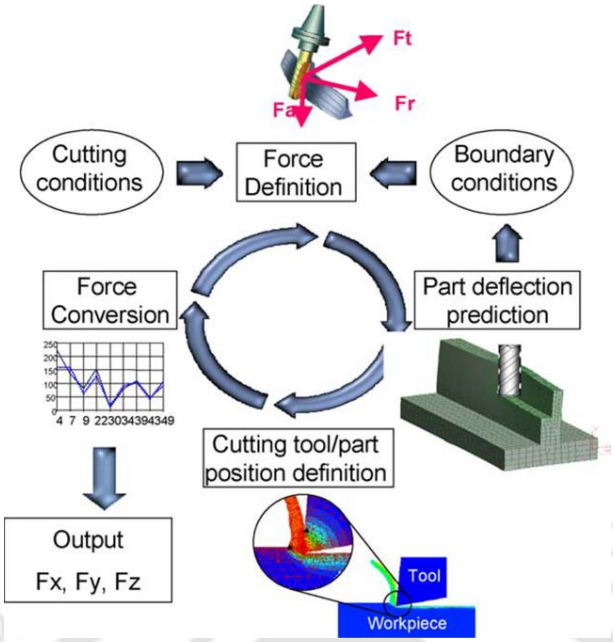

Figure 2.7 Force-deflection prediction model (Ratchev et al. (2004))

Herranz et al. (2005) proposed efficient process planning strategies by analyzing the static and dynamic phenomena that occur during high-speed cutting. They suggested useful guidelines to minimize part bending during machining of low rigidity parts. Aijun and Zhanqiang (2008) developed an analytical model to predict the static deformation during end milling of thin plates. The part deformations were predicted using a theoretical deformation equations model, which was established on the basis of reciprocal theorem when the linear load acts on thin-walled plates. The work considered the influence of radial cutting force on the deformations. Accordingly, the unit linear load was expressed as:

$$q = \frac{F_x}{a_d} = \frac{N_t \cdot f_z}{8\pi}\left[K_{tc}(2\phi - \sin 2\phi) + K_{rc}\cos(2\phi)\right]_{\phi_{en}}^{\phi_{ex}} \tag{2.6}$$

where N_t is the tooth number of cutter, f_z is the feed per tooth (mm/tooth), a_d is the axial depth of cutting (mm), ϕ is the immersion angle that varies with time, ϕ_{st} and ϕ_{ex} are the start and exit immersion angles of the cutter to and from the cutting zone, respectively. K_{tc} and K_{rc} are the milling force coefficients; F_x is the milling force in the radial direction. Later, they simulated the cutting process and obtained the instantaneous part deformations using FEM software ANSYS. In this study, the influence of linear loads, the location of the cutter, and thickness of work plates on the deformations of the thin-walled plates were analyzed.

Wan et al. (2008) developed an integrated model to predict the cutting force, uncut

chip thickness and instantaneous cutting force coefficients. Izamshah et al. (2011) developed a new methodology to predict the wall deflection during thin-wall machining by integrating the FEM based model and statistical analysis techniques. The cutting force was predicted using a mechanistic model.

Recently, Du et al. (2017) developed a precise and economical cutting force induced error compensation method for both low-rigidity parts and other complex components based on a generalized explicit analytical milling force model and a fast ANSYS parametric design language (APDL) deformation calculation procedure has been proposed for peripheral milling process. Authors demonstrated the great potential of analytical modeling in the compensation of errors induced due to real-time milling forces.

Observations

Researchers worldwide have developed various force models to obtain the cutting forces generated during end milling operation. Most of these models predict cutting forces while very few are capable of predicting cutting forces as well as deflections. Developed analytical models are based on the estimation of cutting force coefficients and important parameters such as chip thickness ratio and normal shear angle (empirical models). These coefficients and parameters, in general, need to be obtained by conducting experiments which are time-consuming and costly. Moreover, their values are applicable only to the chosen workpiece-tool material combinations. In most of the reported literatures, the thin-wall part deflection was predicted by using rigid or mechanistic cutting force models. Some of the deflection prediction models utilize experimentally determined cutting forces as input to calculate the magnitude of deflection. Some of the deflection models did not consider the influence of workpiece material properties and reduction in the rigidity due to material removal of work part, which are important to develop a realistic force-deflection prediction model.

2.5 Numerical Modeling and Simulation of Thin-Wall Milling Process

Literature depicts numerous attempts on modeling and simulation of the metal cutting process using numerical modeling techniques such as finite element method (FEM). Researchers have developed various models of material removal such as two-dimensional (2-D), three-dimensional (3-D) oblique cutting models and full 3-D models. Developed 2-D models were used to study the orthogonal mode of metal cutting,

whereas full 3-D models were employed to simulate the various machining processes such as turning, milling, drilling, tapping, etc. Most of these models have been developed by using finite element method (FEM). Application of FEM effectively reduced the cost associated with carrying out physical experiments. By using FEM, it is possible to incorporate the effects of large deformation; strain rate effect; tool-chip contacts and friction; local heating and temperature effect. FEM is also capable of handling different boundary and loading conditions such as thermal, structural, electrical, magnetic. Thus FEM is widely been used in modeling and simulation of the complex physical interaction of tool and workpiece during a typical metal cutting operation such as end milling. These models are discussed in the following sections.

2.5.1 Two-Dimensional Numerical Models for Metal Cutting Simulation

Several research works have been reported on the development of 2-D FEM models of metal cutting processes. Ceretti et al. (1996) used commercial FEM package DEFORM 2-D to simulate a 2-D plain strain cutting process. They used damage criteria to simulate segmented chip formation. Özel and his group have pioneered in numerical modeling and simulation of metal cutting operations. In 2000, Özel and Altan used finite element method to predict the cutting forces, tool stresses and temperatures during high-speed machining of P-20 mold steel using flat end mill. It was observed that maximum temperatures occur at the primary cutting edge of flat end mill inserts. Rech et al. (2005) investigated the influence of cutting edge wear behavior of powder metallurgical high-speed steel (PM-HSS) milling inserts experimentally. Simultaneously, Lagrangian thermo-visco-plastic based 2-D FE cutting simulations were carried out to analyze the tool-stress distributions within the tool coating and substrate. Predicted results were used to obtain optimum cutting edge radius for minimal stresses. Ec et al. (2005) determined residual stresses in a machined component by using a thermal elastic-visco-plastic finite element model. Johnson-Cook material model was used to describe the material behavior.

Literature reports some important research works on the study of friction behavior between the tool and the workpiece, cut chips and tools using FEM based numerical simulation methodology. Özel (2006) used orthogonal cutting process using finite element (FE) simulations to simulate the continuous chip formation process in orthogonal cutting of low carbon free-cutting steel. Five friction models viz. constant shear friction at the entire tool-chip interface, constant shear friction in sticking region

and Coulomb friction in sliding region, variable shear friction at the entire tool-chip interface, variable friction coefficient at the entire tool-chip interface, variable shear friction in sticking region and variable friction coefficient in sliding region were considered. These models were developed using the experimentally determined stress distributions on the tool rake face. Finally, the effects of tool-chip interfacial friction models on the FE simulations are investigated. Haglund et al. (2008) used Arbitrary Lagrangian Eulerian (ALE) approach to explore and evaluate various friction models such as constant friction coefficient model, two friction coefficients model, limited shear stress model, temperature-dependent friction coefficient model, temperature-dependent limited shear stress (with constant Coulomb friction in sliding region) model and constant limited shear stress in sticking region (with temperature-dependent Coulomb friction in sliding region) model in their numerical simulations. Maranhão and Davim (2010) developed a thermo-mechanical 2-D FEM model to study the influence the friction coefficient in the tool-chip interface on cutting and feed forces, cutting temperature, plastic strain, plastic strain rate, maximum shear stress and residual stresses during machining of stainless steel (AISI 316). Figure 2.8 shows a typical maximum shear stress in the tool, workpiece and chip at the end of the length of cut profiles observed during the simulations.

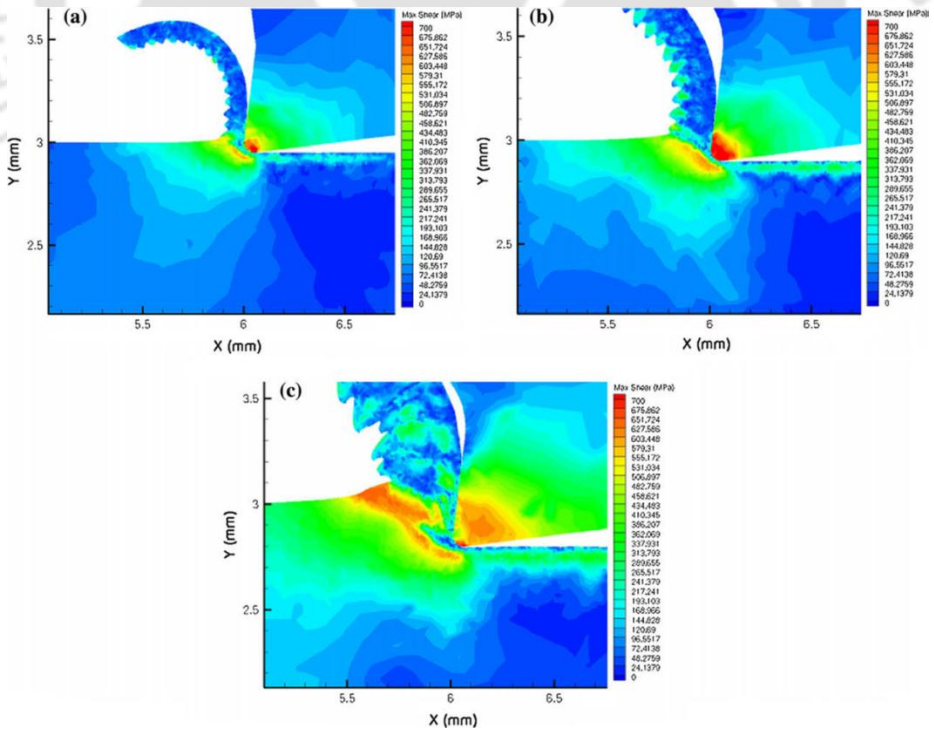

Figure 2.8 Detailed comparison of maximum shear stress in the tool, workpiece and chip at the end of length of cut in the machining of the stainless steel **(**Maranhão and Davim (2010))

It was concluded that friction coefficient at the tool-chip interface had a significant influence on the accuracy of prediction. Arrazola et al. (2008) proposed a variable friction coefficient approach to identify friction coefficient during machining process using finite element modeling. The developed approach reduced the differences between the experimental and FEM results in terms of feed force and cutting force. Arrazola and Özel (2010) investigated the effects of friction modeling at the tool-chip-workpiece interfaces during chip formation process. A systematic investigation has been carried out on predicting the cutting forces, temperatures (see Figure (2.9)), normal stresses and shear stress acting on the cutting tool. Authors employed Arbitrary Lagrangian Eulerian (ALE) method and a fully coupled thermal-stress analysis to study the effects of limiting shear stress at the tool-chip contact on frictional conditions. Moreover, more realistic friction modeling of the tool-chip and tool-work interfaces were carried on by coupling sticking and sliding frictions.

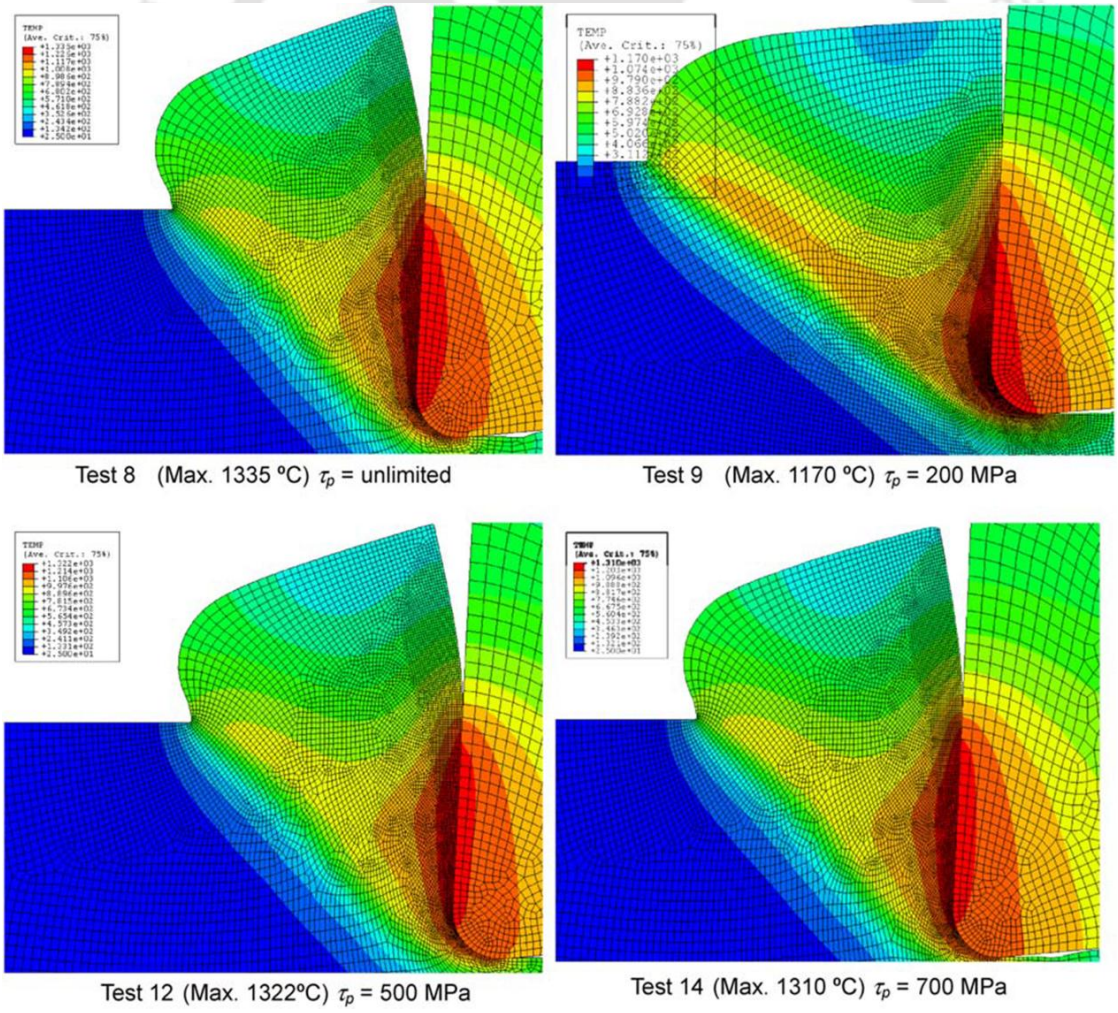

Figure 2.9 Simulated temperature fields during 2-D simulations **(**Arrazola and Özel (2010))

Some of the reported research efforts were focused upon deducing the relationship between machining parameters and various responses such as temperature, cutting forces, chip thickness ratio, residual stress, etc. by using 2-D FEM based models. Ginting and Nouari (2006, 2007) performed dry ball-end milling of aerospace titanium alloy Ti-6242S and investigated the suitability of uncoated cemented carbide tools. They obtained optimal cutting conditions by developing 2-D FEM model. Özel and Zeren (2007) studied the influence of edge roundness on stress and temperature fields induced during high-speed machining AISI 4340 steel by developing a fully coupled thermal-stress model. Davim et al. (2008) carried out a comparison study to analyze the performances of two different types of cutting tools viz. PCD (polycrystalline diamond) and K10 (cemented carbide) on the thermal and mechanical behavior of work material aluminum alloys (Al7075). It was noted that polycrystalline tool provides superior performance in terms of cutting, feed forces and cutting temperature in comparison to that of cemented carbide tool.

Li et al. (2009) studied residual stresses induced during high-speed end milling of hardened steel SKD11. A 2-D thermo-mechanical fully coupled FEM model was developed to determine the stresses generated in the machined component. The model considered the effective rake angle and variable undeformed chip layer. Similar to this, Agmell et al. (2011) developed a fully coupled thermo-mechanical 2-D numerical model to study the influence of process parameters such as feed force, cutting force, chip thickness ratio, relative deformation widths and temperature distribution. Adetoro and Wen (2010) utilized FE tool to simulate the cutting process and determined average as well as instantaneous cutting force coefficients. The model was found accurately predicting the cutting forces. Tang et al. (2011) carried out finite element simulation on dry hard orthogonal cutting AISI D2 tool steel with CBN cutting tool. Cutting temperature and stress were considered as most important aspects in hard dry machining. The influences of cutting speed and depth of cut on temperature fields and residual stress were studied. Recently Lu et al. (2016) developed 2-D coupled thermo-mechanical model to simulate orthogonal cutting of titanium alloy Ti6Al4V. Johnson-Cook material constitutive model and Cockroft-Latham damage criterion were utilized to simulate the plastic behavior and chips formation during the cutting process.

Some of the researchers investigated the microstructures of machined surfaces using FE based simulations. Pu et al. (2014) investigated the microstructural changes in

dry and cryogenic machining of AZ31B magnesium alloy. They also studied the influence of rake angle on microstructural changes after cryogenic machining. Similarly, Rotella and Umbrello (2014) studied the microstructural changes during dry and cryogenic cutting of titanium alloy Ti6Al4V. In the FE subroutine, Zener-Hollomon (Z-H) equation was used to predict the dynamic recrystallization (*DRX*), while the hardness variation has been predicted by using the Hall-Petch (*H-P*) equation. Furthermore, a modified flow stress model was used to incorporate the effects of new grain size on the material behavior.

2.5.2 Three-Dimensional Numerical Models for Cutting Simulation and Thin-wall Machining Process

Literature reports various research works on the development of 3-D FE-based numerical simulations for milling operation. Initially, Bacaria et al. (2001) developed a 3-D transient numerical model of metal cutting for milling operation by incorporating dynamic effects, thermo-mechanical coupling with damage criterion and contact with friction. Johnson-Cook material law was used to model the yield stress by taking into account the strain, the strain rate and the temperature in order to incorporate realistic behavior of the material in the metal cutting process simulation. The material damage was modeled using Johnson-Cook damage criterion. The model was able to predict the stress distributions, chip formation and tool forces during the milling process.

Soo et al. (2004, 2004) successfully simulated the high-speed ball nose end milling process using 3-D FEM. Formation of chips, cutting forces and temperature were studied during machining of Inconel 718 workpiece. The material yield stress behavior was determined experimentally by using an elevated strain rate and temperature compression test. The machining process was simulated for various cutting speeds. Later, Saffar et al. (2008) employed 3-D FE simulations to predict cutting forces and tool deflection during end milling operation. It was noted that the predicted results with Johnson-Cook (JC) theory were agreeing well with the experimental results in comparison to the results obtained based on the theoretical relationships, where the material properties were simply defined using the constant material coefficients.

Özel et al. (2010) investigated the performance of various multi-layered coated inserts in machining of titanium alloy Ti6Al4V by using 3-D simulations. In this study, uncoated, TiAlN coated, and TiAlN + cBN coated single and multi-layer coated tungsten

carbide inserts were considered and their influences on forces and tool wear were studied. It was noted that cBN and TiAlN + cBN coated inserts generate largest cutting forces at higher cutting speeds and cBN coatings reduce the tool wear in dry machining.

Soo et al. (2010) developed a Lagrangian-based, 3-D finite element (FE) model to simulate the high-speed ball nose end milling of Inconel 718 nickel-based superalloy using a commercial FE package Abaqus/Explicit. Cutting forces and chip formation during the machining process were studied. Pittalà and Monno (2010) carried out a FE-based simulation of face milling operations using a 3-D milling insert using commercial code DEFORM 3-D. Milling tests were conducted and the measured cutting forces were compared with finite element modeling results. Rao et al. (2011) carried out numerical simulations to study the tool performance and surface integrity during face milling of titanium alloy Ti6Al4V. During the course of work, tool wear patterns under various cutting conditions and the influence of tool wear on surface integrity were investigated. Özel et al. (2011) modeled the chip formation process for machining of Inconel 718. Results were obtained in terms of temperature, strain and stress distributions by using two different commercial finite element packages viz. Abaqus/Explicit and DEFORM 3-D. Maurel-Pantel et al. (2012) also conducted a 3-D FE simulation of shoulder milling operation by implementing the J-C plastic material model to study the cutting forces and chip formation during the process. Typical stress contours obtained during the simulation are shown in Figure 2.10.

Özel and Ulutan (2012) developed 3-D finite element model to study the residual stresses induced in turning of titanium and nickel based alloys. Authors used uncoated tools with various edge radii and TiAlN coated carbide tools during the study. Chen et al. (2012) developed a FEM model to simulate inclined ball-end milling. They utilized Cockcroft-Latham criterion for chip formation study. Asad et al. (2013) investigated the effects of cutting speed and depth of cut on chip morphology and surface finish for down-cut milling case. 3-D simulations were performed for roughing, semi-finishing and finish cutting operations of A2024-T351. Wang et al. (2013) worked on the development of 3-D finite element model to simulate the high-speed end milling of Ti-6Al-4V titanium alloy using commercial finite element package Abaqus/Explicit. Johnson-Cook material constitutive model was employed to model the flow stress behavior of the workpiece. Johnson-Cook shear failure criterion was used to model the chip separation and Zorev's friction model was used to determine the frictional behavior at the tool–chip

interface.

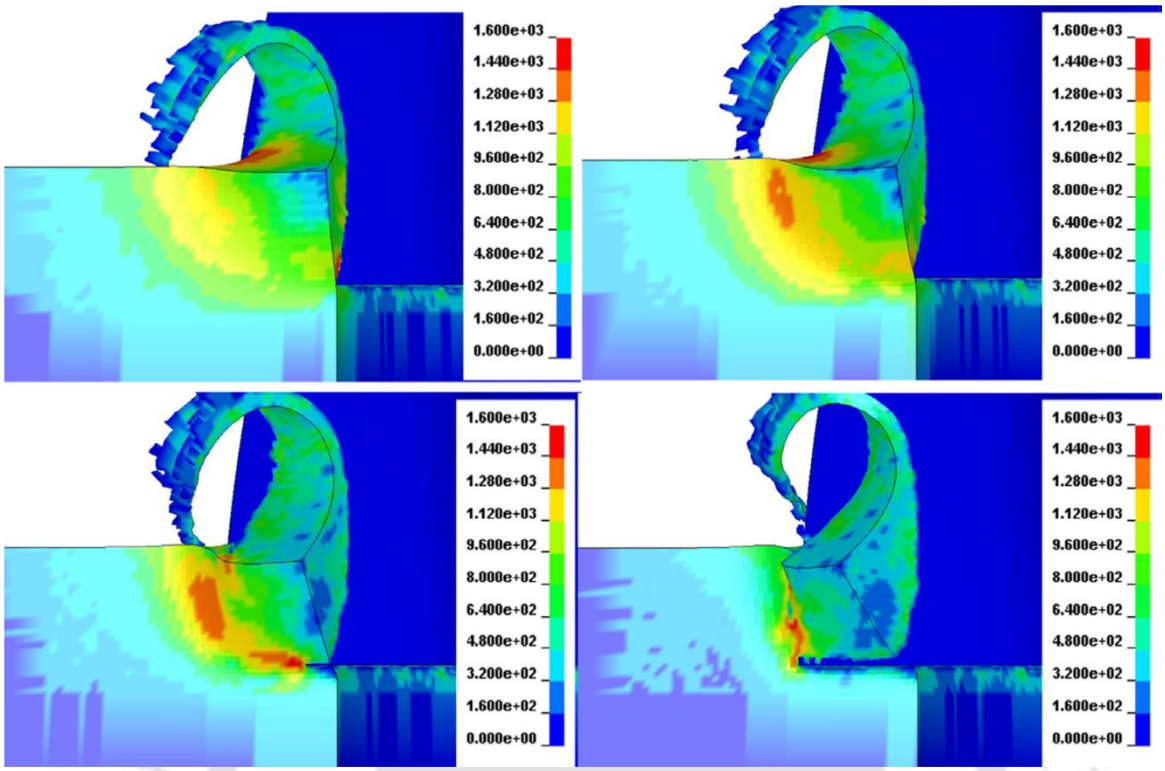

Figure 2.10 Von Mises stress contours during the chip separation (Maurel-Pantel et al. (2012))

Wu and Zhang (2014) developed an improved model by incorporating the damage constitutive law in addition to the material model to define the chip separation in the milling of titanium alloy Ti6Al4V. The milling force and cutting temperature (see Figure 2.11)) obtained by FEM simulations were experimentally validated. Liu et al. (2014) evaluated six ductile fracture models to identify their suitability to define fracture criterion for metal cutting processes. These models were: constant fracture strain, Johnson-Cook, Johnson-Cook coupling criterion, Wilkins, modified Cockcroft-Latham, and Bao-Wierzbicki fracture criterion. It was concluded that the Bao-Wierzbicki fracture model which considers rate dependency, temperature effect and damage evolution gives the best prediction of chip removal behavior of ductile metals. Ji et al. (2015) investigated the process of precision milling of a hole in a titanium alloy Ti-6Al-4V workpiece using a 3-D FEM. Jiao et al. (2015) carried out a transient 3-D simulation to predict the temperature field on the machined surface using single tooth and multi-tooth milling using the FE method. All of these works were focused on the end milling process.

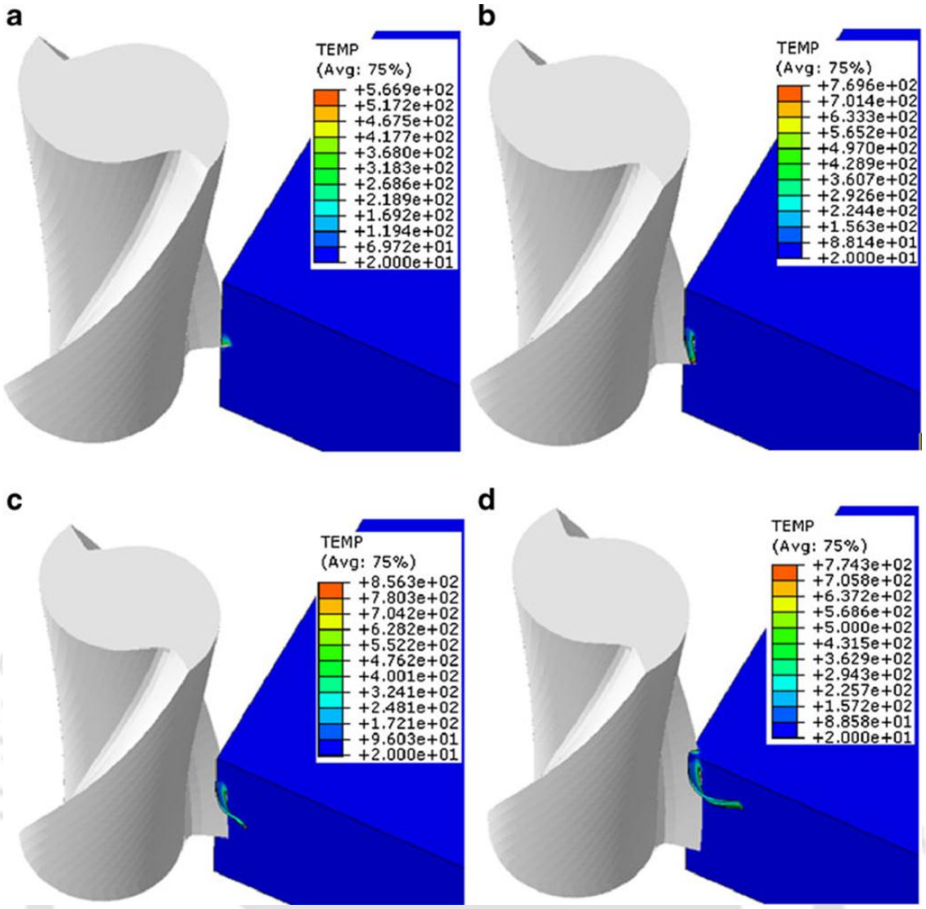

Figure 2.11 Temperature distribution of chip at different cutting times (Wu and Zhang (2014))

Literature also reports some dedicated research works on numerical modeling and simulation of thin-wall machining operations. Ning et al. (2003) applied finite element method (FEM) to analyze and calculate the deformation of thin-walled structures. They analyzed the influence of wall thickness on deformation. It was reported that the wall deformation during machining varies inversely with the wall thickness and the constraining walls had insignificant influence on the deformation. Moreover it was also noted that the deformation varies linearly with the load applied and the deformation along the wall height varies linearly.

Wan et al. (2005) developed a FE-based numerical model to simulate the flexible peripheral milling and predicted the static form errors in thin-wall workpieces. In this work, irregular FE meshes were used to enhance the flexibility and robustness of the simulation approach. Wan and Zhang (2006) developed an algorithm to predict the form errors during peripheral milling of the thin-wall workpiece. The algorithm considered the contact between the tool and workpiece, radial and axial depth of cut. It was reported that 3-D irregular volume elements such as tetrahedral elements, prismatic elements, and

hexahedral elements can be used to predict form errors. Denkena and Schmidt (2007) developed a numerical model to predict form deviation in end milling of thin-walled structures. The cutting force was also predicted using the developed model. Rai and Xirouchakis (2008, 2009) conducted numerical studies to analyze the cutting force components, workpiece temperature distribution, part deflection and stresses in the machining of thin-wall components. The model considered the effects of fixturing, operation sequence, tool path and cutting parameters. The geometric model of the workpiece comprised of machining features like steps, slots, pockets and nested features. An integrated analytical force model was incorporated into the finite element model. An attempt was made to predict transient temperature distributions and elastic-plastic deformations induced during milling of prismatic parts. It was found that cutting parameters like spindle speed and feed/ tooth, workpiece thermal properties, and coolant have significant influence on the heat dissipation rate.

Gang (2008) developed a three-dimensional (3-D) FEM model to simulate the chip separation during thin-wall machining of titanium alloy Ti6Al4V. Johnson-Cook flow model was used to define the material behavior. The work also incorporated the friction between cutter and chip. Similarly, Tănase et al. (2010) analyzed the influence of depth of cut, feed and spindle speed on cutting forces, elastic deformation and stress during thin-wall machining by conducting experiments and carrying out 3-D numerical simulations. Izamshah et al. (2011) developed a finite element analysis (FEA) model to predict the instantaneous deflection of a thin-wall part. Tool and workpiece were modeled using three-dimensional iso-parametric tetrahedron elements. A set of machining tests were carried out to validate the accuracy of the model.

Recently, Wang and Sun (2014) proposed a method to generate interference-free tool paths those were used to compensate the deformation error during spiral milling of blades. During the numerical simulations, it was noted that warping deformation occurs at the leading and trailing edge of the blade while bending and torsion deformation occur in the whole blade. Qasim et al. (2014) developed a methodology which combines the usefulness of the statistical analysis and finite element method to determine the correlation between form errors and process parameters. The mean cutting force was determined by using a mathematical model and it was further used to compute the wall deformation. Ślusarczyk (2015) compared the influence of conventional and climbing mode of milling operation on the deformation of thin-walled components during machining of ST3S steel. Wall deflection occurred while using climbing mode was

found to be lower during the study. Cheng et al. (2015) also developed 3-D FEM model to simulate the thin-wall machining of titanium alloy. Li et al. (2015) studied the machining of 45 steel thin-walled parts using a 3-D numerical model developed in Abaqus/Explicit. It was noted that trends of the simulated results were matching well with the experimental results.

Observations

From the literature, it was realized that a lot of research work have come up on the employment of finite element method to develop two-dimensional and three-dimensional model of the material removal process. Majority of the efforts have been focused on the prediction of cutting forces generated during bulk milling operation. In view of computational simplicity, researchers have developed 2-D orthogonal cutting models. Some of the research attempts have established 3-D numerical models for more realistic simulation of metal cutting operation. By using developed numerical models researchers have determined very useful information in terms of cutting forces, mechanism of chip formation, the evolution of cutting temperature, shear zone, contact length, chip thickness, cutting and residual stress distributions. 3-D models have incorporated realistic aspects such as tool-friction and material damage. In comparison to the significant efforts put on modeling and simulation of bulk milling, few attempts have been made on acquiring characteristics of thin-wall milling operation using FEM based simulations. In most of these models, the cutting forces were determined either experimentally or by using analytical force models and were provided as a process input to determine the deflection numerically. Some of these models took into account the material properties, tool-friction model and material damage model together. Scant research is reported on development of realistic 3-D thermo-mechanical models which take into account the material behavior, friction behavior, temperature generation and material damage model to study the cutting forces, wall deflection, chip morphology and cutting temperature during the thin-wall machining process.

2.6 Optimum Process Conditions for Thin-Wall Machining Process

Selection of optimal machining parameters and conditions is crucial to obtain desired performance during a machining process. Thus, determination of efficient machining parameters has attracted a wide international research. The main goal of thin-wall machining is to machine dimensionally accurate thin-wall components by an economical

and energy efficient process. Various process characteristic parameters such as spindle speed, feed rate, depth of cut, tool geometry, milling condition, tool path strategies, etc. play very important role in efficient and quality machining of thin-wall parts. Many research attempts have been made by researchers to optimize machining parameters during milling process using a variety of optimization techniques. Some of the works reported on optimization of bulk milling and end milling operations have been reviewed as follows.

Alauddin et al. (1996) presented an approach to optimize surface finish during end milling of Inconel 718 using uncoated carbide inserts under dry condition. The surface finish was analyzed by varying speed and feed values. Response surface method (RSM) was used to plot the surface contours and to determine optimum process parameters. Suresh et al. (2002) developed a surface roughness optimization model for machining of mild steel by using Response Surface Methodology (RSM) and Genetic Algorithms (GA). Öktem et al. (2005) also used RSM and GA to optimize cutting conditions for surface roughness during milling of mold surfaces. Process parameters viz. feed, cutting speed, axial depth of cut, radial depth of cut and machining tolerance were considered for the study. Further, they used coupled neural network (NN) with GA to obtain the optimum process parameters. Palanisamy et al. (2007) carried out optimization of milling process using GA. In their work, machining time was considered as the objective function and the constraints were tool life, feed rate, depth of cut, cutting speed, surface roughness, cutting force and amplitude of vibrations.

In 2010, Chandrasekaran et al. provided a comprehensive overview of various soft computing techniques used in evaluation and optimization of machining operations. Zain et al. (2010) used GA to optimize machining conditions for minimizing surface roughness during end milling process. Surface roughness was evaluated against radial rake angle of the tool, cutting speed and feed rate. It was concluded that GA technique was capable of estimating the optimal cutting conditions which resulted in minimum surface roughness. Yang et al. (2011) developed an efficient fuzzy global and personal best-mechanism-based multi-objective particle swarm method to obtain optimum machining parameters during face milling. Kondayyaa and Krishna (2012) used GA to optimize CNC end milling process in terms of spindle speed, feed and depth of cut on performance measures. Further, non-dominated sorting genetic algorithm-II (NSGA-II) was used to obtain Pareto optimal fronts. Yildiz (2013) presented an application of

Cuckoo search algorithm to find out the optimal machining parameters in the milling operation. Sivasakthivel and Sudhakaran (2013) focused on analyzing the effect of machining parameters such as helix angle of the cutter, spindle speed, feed rate, axial and radial depth of cut on temperature rise in end milling of Al 6063. Kuram et al. (2013) carried out an assessment of cutting fluids and cutting parameters during end milling by using a D-optimal design of experiments. The effects of cutting fluid types were investigated as a function of three milling factors viz. cutting speed, depth of cut and feed rate and optimal levels of setting were determined. Alrashdan et al. (2014) also used GA to optimize end milling of AISI D2 steel. The work was focused on minimizing the machining cost caused by poor surface roughness and energy consumption during machining. Campatelli and his group (2014) worked on optimizing the process parameters such as cutting speed, axial and radial depth of cut, and feed rate for minimum consumption of machining power using Response Surface Method (RSM). Li et al. (2015) worked on optimizing the production cost and surface quality during machining of titanium alloy Ti6Al4V. NSGA-II was adopted to solve the multi-objective optimization problem. Sarikaya et al. (2015) carried out multi-response optimization of milling of AISI 1050 steel using Taguchi based gray relational analysis. In their work, the effects of process parameters such as depth of cut, feed rate, cutting speed, and number of insert on vibration signals, cutting force and surface roughness were investigated.

Recently Masmiati et al. (2016) reported optimum levels of cutting conditions for minimum residual stress, cutting force and surface roughness in end milling of S50C medium carbon steel. Du et al. (2016) investigated multiple performance characteristics viz. surface roughness, surface micro-hardness, and surface residual stress during high-speed milling of titanium alloy TB17 using Taguchi-Grey relational analysis method. Saini et al. (2016) conducted multi-process parameter optimization in face milling of titanium alloy Ti6Al4V using RSM. This work was focused on developing mathematical relations between input factors and response parameters, namely, surface roughness, tool wear and tool vibration. Zhang et al. (2017) worked on optimization the multi-pass dry milling for high efficiency, low energy and low carbon emissions. The multi-objective optimization model was converted into a single goal problem using weight coefficients. Pereira et al. (2017) optimized helical milling of aluminum alloy Al7075 using Augmented-Enhanced Normalized Normal Constraint method. This multi-objective

problem dealt with optimization of axial cutting force component, total roundness and material removal rate. TOPSIS decision-making approach was used to determine the best solution among the obtained Pareto optimal solutions. Jomaa et al. (2017) attempted to optimize peripheral milling under dry machining condition with regard to the surface finish and residual stress during machining of aeronautical Al-Zn-Mg-Cu alloy. Grey relational analysis (GRA) was employed to obtain optimum levels of machining parameters viz. cutting tool geometry, milling mode, feed per tooth, cutting speed, and radial depth of cut.

In comparison to end milling process, very few attempts have been reported on obtaining the optimum process parameters for thin-wall milling process. Ghoddisian et al. (2011) worked on optimizing the surface roughness for peripheral milling of thin-walls. Authors used two different optimization techniques viz. genetic algorithm (GA) and Imperialist competitive algorithm (ICA). They reported that ICA method provides better results than that of GA method in the scope of their study. Songtao et al. (2012) used the genetic algorithm (GA) to optimize the thin-wall machining process for minimal milling force. Experiments were carried out on aluminum alloy 7475-T7351 by varying the cutting speed, feed rate, axial and radial depth of cut. Based on the work it was concluded that high spindle speed conditions (471 m/min) with large radial cutting depth (12 mm) and low axial cut (0.8 mm) reduce the deformation of thin-walls. Qu et al. (2016) worked on the selection of proper machining parameters for improving the quality and productivity of thin-wall parts. Machining parameters viz. spindle speed, axial and radial depths of cut were varied and their influence on cutting force, material removal rate and surface roughness were investigated. Multi-objective optimization using the non-dominated sorting genetic algorithm (NSGA-II) was employed to determine the optimum parameters. However, the work was limited to cutting force, surface roughness and material removal rate optimization. Authors did not consider the wall deflection in their objective function.

Observations

Literature reports significant research on optimization of bulk milling process; however scant work is available on obtaining optimum parameters for efficient and quality thin-wall machining. For bulk milling process, researchers have used various optimization techniques such as response surface methodology (RSM), Taguchi based gray relational analysis (GRA), Augmented-Enhanced Normalized Normal Constraint method, TOPSIS

decision-making approach and evolutionary optimization approaches such as genetic algorithms (GA), artificial neural network (ANN), non-dominated sorting genetic algorithm-II (NSGA-II) and Cuckoo search algorithm. Most of the researchers have worked on determining the optimal settings of feed, cutting speed, axial depth of cut, radial depth of cut, tool life, the radial rake angle of the tool, helix angle of the cutter, and cutting fluids. These studies were focused on achieving various objectives such as minimum surface roughness; cutting force and amplitude of vibrations and a maximum value of material removal rate (MRR).

As mentioned above very few researchers have worked on optimizing the thin-wall machining process. Their works are limited to optimizing either wall deflection or surface roughness. No work has been reported on optimization of thin-wall machining process for improving the overall productivity, product quality and energy consumption in an integrated and comprehensive manner.

2.7 Discussion

Thin-wall components possess low rigidity as they have a large surface area as compared to their thickness. During the machining operation, thin-walls deflect under the action of milling forces which in turn affects the quality and accuracy of the work-part. If the deflection is predicted beforehand, effective counter measures can be undertaken to obtain the desired process performance that is, manufacturing of a dimensionally accurate finished component with good surface quality. This requires developing a realistic numerical model to predict the process responses which will help for better control of the process parameters during the actual cutting operation.

From the reported literature, it was concluded that a significant amount of work is reported on 2-D as well as 3-D simulations of the bulk milling operation. Extensive research has been reported on simulation of orthogonal metal cutting process using 2-D FEM methods. These are based on plane stress, plane strain conditions and axisymmetric assumptions. In view of model development, they are simple and require lesser number of elements in comparison to that of a 3-D model. These 2-D models were basically used to evaluate cutting forces, contact length of the chip with the tool, chip thickness, cutting temperatures and residual stress distributions. In spite of providing computationally faster responses, 2-D models have a limitation during FEM simulation of thin-wall machining process that, these models are unable to simulate the deflection of a free wall

in 2-D. Thin-wall milling using a helical end milling cutter is a complex operation and is difficult to comprehend and analyze in a 2-D domain. Scant work is reported on 3-D thermo-structural modeling and simulation of machining of low rigidity thin-wall components. A realistic 3-D numerical model may provide milling forces, deflection, stresses, cutting temperature, chip morphology with fair and acceptable accuracy. Also, the model may also give very useful insights into the complex physical interaction of helical cutting tool and workpiece.

An extensive literature review has been reported on analytical modeling of milling process. Many research attempts have been reported on the computation of milling force and wall deflection. However, in most of these models, the forces have been determined by using chip load and force coefficients. The chip load and force coefficients are usually determined by orthogonal cutting experiments or slot milling experiments for chosen cutting tool geometry and tool-workpiece combination. These models predict the wall deflection quickly; however, physical experiments are needed to determine the milling force coefficients. Conducting experiments is costly and tedious. Moreover, these models do not take into account the thermo-mechanical aspects of machining. This limits their application in practice.

Some of the reported analytical works predict the wall deflection by using simple cantilever geometry of the workpiece without due consideration to the in-process change in workpiece geometry i.e. reduction in wall thickness during the milling process. This specifies a void to have efficient force-deflection prediction model for quicker and accurate prediction of the wall deflection for chosen process parameters conditions. The model should take into account the thermo-mechanical characteristic of the process and tool-workpiece geometries.

From the published esteemed literatures, it is realized that significant research has been reported on analytical and numerical investigations into bulk wall machining which certainly helped to understand the complex interaction between cutting tool and the workpiece. However mathematical modeling of uncontrollable parameters such as imperfections in machine tool and cutting tool structures, errors in the cutting tool settings, deformations in the critical machine tool such as spindle, workpiece fixtures and modeling of material inhomogeneity is difficult.

From the experimental investigations reported on end milling process, it is realized

that determination of optimum levels of parameters for efficient and quality bulk machining process has always been a key research problem and is still a subject of study for the manufacturing researchers and engineers. Literature reports significant work on optimization of bulk machining operations such as surface milling, end milling. However, few attempts have been reported on optimization of thin-wall machining process to improve its productivity and product quality. Most of these works have limited applicability as they consider either wall deflection or surface roughness or material removal rate. Moreover, there is hardly any comprehensive and systematic study reported on the influence of critical process parameters such as feed, depth of cut, tool geometry parameters viz. helix angle, tool diameter on the performance measures i.e. material removal rate, wall deflection, cutting forces, and surface roughness. Literature reports that GA is a better optimization methodology over the classical optimization techniques due to its robustness (Deb (2002)).

Nowadays researchers worldwide are focusing their attention on minimizing the carbon footprint of manufacturing processes. Energy saving has become a priority for the manufacturing industry. Therefore, reducing the energy consumption during machining process has become an integral part of sustainable manufacturing. Thus it is imperative to consider the requirement of low energy consumption in addition to the other objectives such as high surface quality and productivity. To the best of our knowledge, there is no published work that deals with the multi-objective optimization of thin-wall machining process for improving the productivity, product surface quality, dimensional accuracy and energy consumption.

2.8 Research Objectives

Based on the research gaps identified during the literature review on various aspects of thin-wall machining, the objectives of present research have been derived. The overall objective of the proposed research work is to enhance the productivity, product quality and energy efficiency during thin-wall machining of the aerospace grade aluminum alloy by carrying out systematic numerical, analytical and experimental investigations. The specific objectives of the proposed work are as follows:

- To study the complex physical interaction between the helical end mill cutter and low rigidity thin-wall by using a realistic three-dimensional, thermo-mechanical numerical model. To study the milling forces, stress distribution, cutting temperature,

part deflection and chip morphology during the thin-wall cutting operation.

- To develop an efficient force-deflection prediction model for quicker and accurate prediction of the wall deflection for chosen process parameters conditions. The model should take into account the thermo-mechanical characteristic of the process and tool-workpiece geometries.
- To carry out comprehensive experimental investigations into the influence of process parameters viz. feed per tooth, axial depth of cut, radial depth and tool geometry parameters viz. tool diameter, helix angle and number of flutes on the process responses viz. cutting force, wall deflection, surface integrity and material removal rate during thin-wall machining of aluminum alloy 2024-T351.
- To derive optimum levels of characteristic milling parameters viz. feed per tooth (f_z), axial depth of cut (a_d), radial depth of cut (r_d) and tool diameter (d_i) for obtaining desired process performance in terms of maximum productivity, superior surface quality, excellent dimensional accuracy and low power consumption during thin-wall milling process.

Figure 2.12 gives an overview of the research carried out in the present work. The various stages of the work are as follows.

- Stage 1: Development of a finite element based three-dimensional thermo-mechanical numerical model of thin-wall machining by considering realistic assumptions followed by the experimental validation of developed numerical model.
- Stage 2: Development of an integrated analytical-finite element based model for quicker prediction of milling force and wall deflection during thin-wall machining.
- Stage 3: Experimental investigations into the influence of cutting tool geometry parameters and process parameters on performance parameters such as milling force, surface roughness, wall deflection and material removal rate.
- Stage 4: Multi-objective optimization of thin-wall machining process to derive optimum levels of milling parameters for obtaining desired process performance.

The details of these stages are presented in the next chapters.

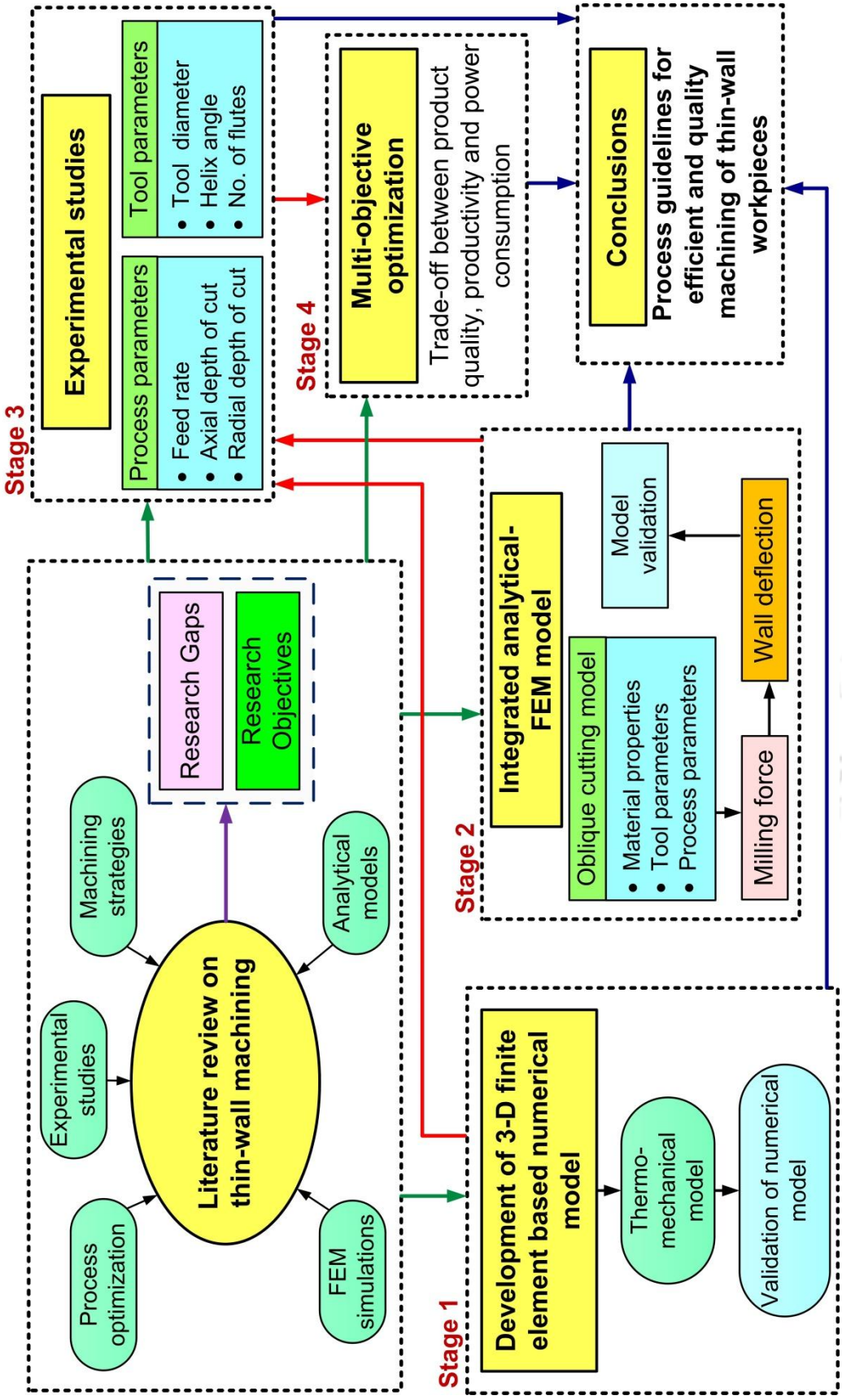

Figure 2.12 Overview of the present research work

CHAPTER 3

Three-Dimensional Thermo-Mechanical Modelling and Simulation of End Milling of Thin-Wall Parts using Finite Element Method (FEM)

3.0 Scope

This chapter presents the development of thermo–mechanical numerical model of end milling of thin-wall parts using finite element method (FEM). Initially, the need to carry out thermo-mechanical analysis of thin-wall machining process is defined. Then an overview of the proposed approach for modeling thin-wall milling using FEM is presented. Further, the numerical FEM model of the end milling process considering its thermo-mechanical characteristics is presented, in detail, in terms of its governing equation, boundary conditions, material model, damage model, contact modeling, and solution methodology. The predicted responses from the model are validated with the experimental results. This chapter concludes by reporting a study on the evaluation of the computational efficiency of the 3-D simulation process.

3.1 The Need

Thin-wall components possess low rigidity as they have a large surface area as compared to their thickness. During the machining operation, thin-walls deflect under the action of milling force which in turn affects the quality and accuracy of the work-part. If the deflection is predicted beforehand, effective counter measures can be undertaken to obtain the desired process performance that is, manufacturing of a dimensionally accurate finished component with good surface quality. A need was thus identified to develop a realistic numerical model to predict the process responses which will help for better control of the process parameters during the actual cutting operation.

From the reported literature, it was concluded that a significant amount of work is reported on two-dimensional (2-D) as well as three-dimensional (3-D) simulations of the bulk milling operation. Many researchers have reported the development of 2-D FEM model to simulate the metal cutting process (Ceretti et al. (1996), Shi et al., Barge et al. (2005), Özel (2006), Agmell et al. (2011)). Generally, the orthogonal metal cutting process is modeled and simulated using 2-D FEM methods. These are based on plane stress, plane strain conditions or axisymmetric assumptions. In view of model development, they are simple and require a much lesser number of elements in

comparison to that of a 3-D model. These 2-D models are basically used to evaluate cutting forces, contact length, chip thickness, cutting temperatures and residual stress distributions. Figure 3.1 shows the difference between the process continuums required for 2-D and 3-D mode of simulation of a typical end milling operation.

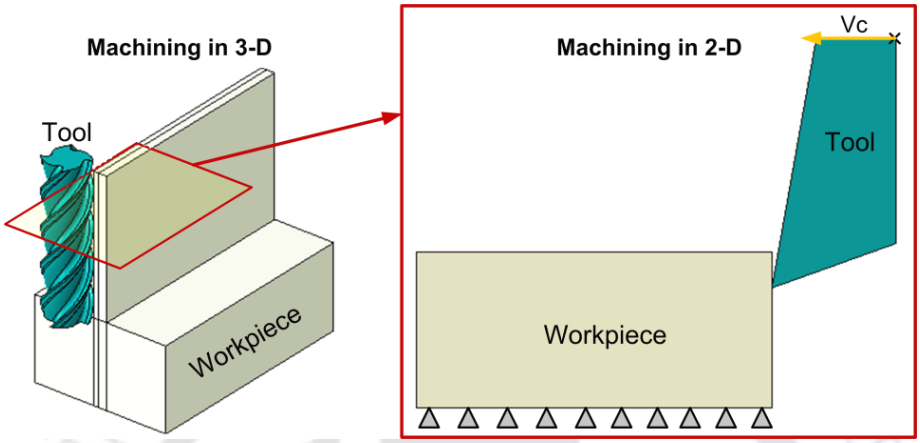

Figure 3.1 3-D and 2-D process continuums in numerical simulation of end milling operation

In spite of providing computationally faster responses, 2-D models have a limitation during FEM simulation of thin-wall machining process that, these models are unable to simulate the deflection of a free wall in 2-D. Thin-wall milling using a helical end milling tool is a complex operation and is difficult to comprehend and analyze in a 2-D domain. Scant work has been reported on 3-D thermo-structural modeling and simulation of machining of low rigidity thin-wall components.

In view of this, in this work, a Lagrangian-based 3-D FEM based numerical model has been developed to simulate the deflection of the workpiece during the thin-wall machining of aluminum 2024-T351 alloy. The developed model was aimed to predict the milling forces, temperature, stress distribution and chip formation in the workpiece for chosen process parameters by considering realistic material behavior, friction consideration, damage model, heat generation and by employing realistic geometry of the milling tool,. Subsequently, milling experiments were carried out to validate the developed model. Details of the model development are presented below.

3.2 Overview of the Process Model Development

To understand and improve the thin-wall machining process, it is important to develop a mathematical model to establish a realistic relationship between input and output process parameters. The aim of this work was to analyze the metal cutting phenomenon in the

thin-wall milling process by proposing a thermo-mechanical analysis. The work mainly includes the following steps. These steps are schematically depicted in Figure 3.2.

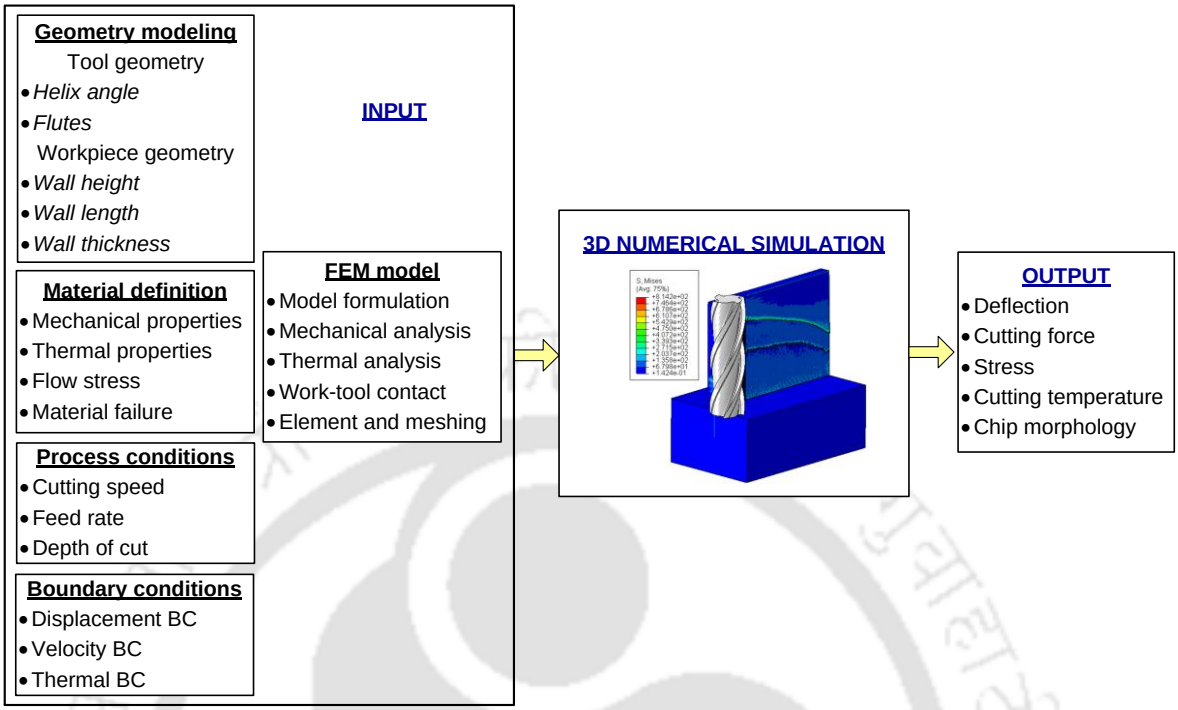

Figure 3.2 Overall approach and development of 3-D numerical model

- Design and development of geometric models of helical cutting tool and workpiece and selection of suitable mesh element
- Define the material models and material failure criteria
- Governing equation and boundary conditions
- Selection and application of required process conditions
- Solution of the problem using finite element analysis (FEA) tool Abaqus/Explicit in nonlinear mode
- Determination of stress-strain, temperature distribution in the workpiece and cutting tool, and computation of process performance parameters such as milling force, stress distribution, cutting temperature, part deflection and chip morphology.
- Validation of computed responses with the experimental results.
- Evaluation of computational efficiency of developed 3-D numerical simulation approach.

These steps are discussed at length in the following sections.

3.3 Thermo-Mechanical Modeling of End Milling Operation

During the milling process, the material is removed from the workpiece using a rotating tool. The most commonly used milling operations are peripheral (or end) milling and face (or plain) milling. Generally, peripheral milling is a common process used in aircraft thin-wall component machining. The thin-wall sections are deformed due to the influence of forces developed during tool-workpiece interaction and the heat generated during cutting. The milling force developed depends upon various process parameters; therefore, the accuracy of the component depends upon the proper selection of the process parameters during machining. In the machining process, heat is generated due to plastic deformation and frictional contact between the workpiece and the tool. The heat generated directly influences the material properties. Therefore, it is essential to couple the mechanical and thermal responses to obtain the solution for such a problem. In this work, a fully coupled thermo-mechanical analysis of thin-wall milling operation has been attempted.

3.4 Assumptions

In the present work, determination of the deflection of the workpiece under the action of milling force is considered to be the main objective. Numerical modeling and simulation of thin-wall machining involve complex interaction between the tool and the workpiece, contact modeling, material properties. Following assumptions were made in the present thermo-mechanical modeling.

- The helical milling cutter has sharp cutting edges.
- The rigidity of cutting tool is significantly larger than that of workpiece; therefore the tool is considered as rigid body. In the present work, tungsten carbide cutting tool is used. It has very high Young's modulus (about 7 times) as compared to that of the workpiece material.
- Workpiece material is deformable. It is isotropic and homogeneous in nature.
- The workpiece material is free of initial residual stresses.
- Initial temperatures for both workpiece and the tool are set at 25 ºC.
- Workpiece and tool surfaces lose the heat generated during the machining process to the environment by convection. The convection coefficient, h_c is assumed as 20 $W/m^{2o}C$ (Kiliçaslan (2009)).
- The workpiece has uniform thickness along the height and width. There are no

deformations present in the workpiece at the commencement of the machining simulation.

- Dynamic re-crystallization of the material and microstructure are not considered.
- 90 % of the energy due to plastic deformation process converted into heat (Li et al. (2002)).
- 100% of the dissipated energy caused by friction is transformed into heat and 50 % of the heat goes into the chip (Li et al. (2002), Haddag et al. (2010)).

3.5 Workpiece, Tool Geometry and Finite Element Meshing

Initially, the geometric models of cutting tool and workpiece have been developed. The thin-wall workpiece was modeled as an inverted cantilever structure with bottom portion being constrained, while the other three ends were free. The tool geometry influences the surface properties of the machined workpiece, so importance has been given to accurately model the cutting tool. A 3-D model of the end mill with actual tool geometry parameters was designed using a CAE tool and then imported in Abaqus/Explicit as a solid 3-D homogeneous part. Figure 3.3 shows the workpiece, cutting tool, and relevant geometric parameters. The influence of vibrations of thin-wall structure that occurs during the machining was not considered in this work. The cutting tool geometry parameters are listed in Table 3.1.

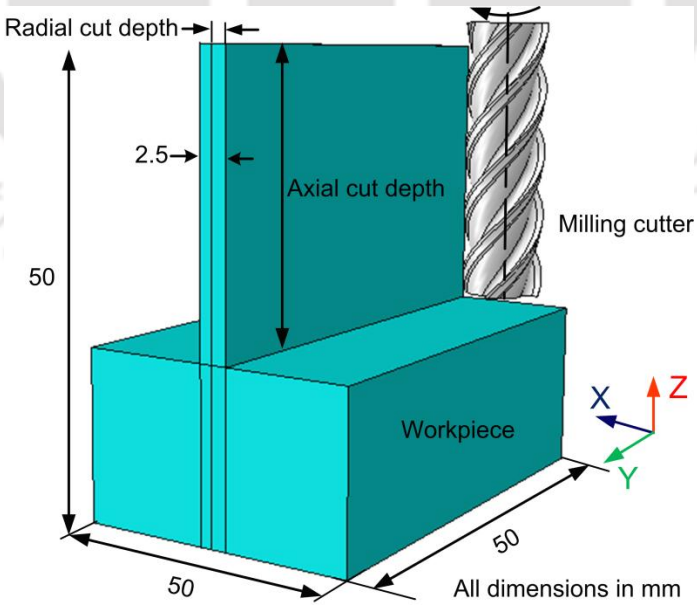

Figure 3.3 Workpice geometry and dimensions

Thin-wall machining process involves non-linear and complex interaction between the tool and workpiece. It also involves large deformations. It is thus essential to select the

right type of element to handle such complex thermo-mechanical interaction and large deformation. In the present work, hexahedral elements were chosen over the tetrahedral elements.

Table 3.1 Cutting tool geometry parameters

Tool diameter (mm)	8
Tool rake angle (º)	8
Tool helix angle (º)	45
Tool clearance angle (º)	15
Number of flutes	4

It was noted that tetrahedral elements perform poorly while solving problems involving plasticity and bending. Severe locking problem has been noted when solving FE problems using tetrahedral elements. Also, the tetrahedral elements are over stiff and extremely fine meshes are required to obtain accurate results (Puso and Solberg (2006)). In the recent years, researchers such as Soo et al. (2004), Gang (2009), Wang et al. (2013) and Ji et al. (2015) have used hexahedral elements C3D8RT to handle complex thermo-mechanical simulation problems and obtain fairly accurate and realistic results. Therefore, hexahedral C3D8RT elements were selected for meshing the workpiece and the tool. It is a 3-D displacement-temperature coupled 8-noded solid element with reduced integration and hourglass control.

Meshing of the workpiece is a problematic process as high resolution mesh is needed at the machining area of the workpiece. In the work, mesh was refined around some areas of interest such as tool-chip interface. To reduce the computational time, non-contact region was discretized with coarse mesh. However, refinement of mesh means increasing the number of elements number thereby the computational time. Therefore a tradeoff between the mesh refinement and the processing time should be taken into consideration. Hence mesh sensitivity analysis was carried out to mesh the workpiece for accurate prediction of performance parameters in an optimum time frame. The mesh sensitivity analysis was carried out for a typical process condition: Spindle speed = 3000 r/min, feed per tooth = 0.1 mm/z axial depth of cut= 8 mm and radial depth of cut = 1 mm. Figure A3.1 (Appendix A3.1) shows the various sizes of the element used to discretize the workpiece-tool contact domain. Table 3.2 presents the influence of mesh size on computational time and output response viz. milling force. A computer system of

3.9 GHz 4GB RAM processor was employed. The milling force components were affected by the mesh size. It was found that the change in resultant force (F_r) was lowest, when the element size reduced from 0.2 mm × 0.2 mm to 0.1 mm × 0.1 mm in comparison with those obtained in other cases. It was also noted that the minimum time was recorded for mesh size of 0.4 mm × 0.4 mm. As the element size reduced the computational time increased due to increase in the number of elements. But the time needed increased drastically when element size reduced from 0.2 mm × 0.2 mm to 0.1 mm × 0.1 mm. As computation time was equally important, based on the analysis, the mesh size of 0.2 mm × 0.2 mm in the work-tool contact region was considered.

Table 3.2 Mesh sensitivity analysis for fine mesh region

Mesh size (mm^2)	Average milling force			Change in force value ΔF_r (N)	CPU time (hrs)
	F_x (N)	F_y (N)	F_r (N)		
0.4*0.4	134.36	101.94	168.65	-	49.25
0.3*0.3	111.91	92.18	144.98	23.67	57
0.2*0.2	104.4	85.43	134.89	10.09	66
0.1*0.1	96.7	81.87	126.70	8.91	79.5

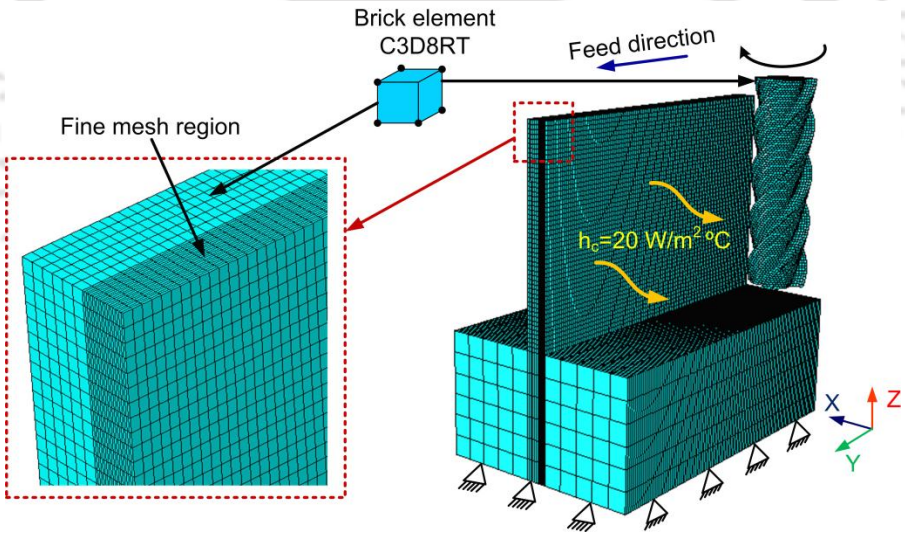

Figure 3.4 Workpiece-tool meshing and boundary conditions

As shown in Figure 3.4 the entire geometry is discretized into very small finite C3D8RT elements. For this particular case, the tool and the workpiece were discretized into 12650 and 293745 elements respectively. Figure 3.4 also depicts the boundary conditions applied on the workpiece and tool geometries. The workpiece was constrained at the bottom to imitate the clamping action during machining. The milling tool was provided

with two motions, namely linear motion along the feed direction and rotational motion about its own axis. The initial temperature of the tool and workpiece was set at room temperature. Heat loss to the environment from the tool and workpiece interface was considered primarily by convection.

3.6 Material Properties

The FE-simulation of thin-wall milling process has been carried out on the aluminum 2024-T351 aerospace grade commercial alloy. It possesses high strength and good fatigue resistance and is widely used in aircraft wings and fuselage structures. The workpiece material is considered to be an elastic-plastic type. The end mill is considered to be made of uncoated tungsten carbide (WC). Tungsten carbide otherwise known as cemented carbide composes of tungsten carbide powder (85-95%) cemented with a binder material namely cobalt or nickel. It has many desirable qualities such as high resistant to abrasion, erosion, wear, compression, and heat (Juneja (2003)). The effect of machining process parameters on the cutting tool wear is not considered of the present study; therefore the tool is to be a rigid body throughout the simulation. Table 3.3 lists the mechanical and thermal properties of the workpiece as well as the tool material (Mabrouki et al. (2008)).

Table 3.3 Workpiece and cutting tool material properties (Mabrouki et al. (2008))

Properties	Workpiece	Tool
Density, ρ_m (kg/m^3)	2700	11900
Elastic modulus, E (GPa)	73	534
Poisson ratio, ν	0.33	0.22
Fracture toughness, K_c(MPa$\sqrt{m}$)	37	-
Specific heat, C_p (J/kg°C)	= 0.557 T +877.6	400
Thermal expansion , α (10e-6/°C)	= 8.9*10^{-3}T+22.2	30
Thermal conductivity, k_t (W/m°C)	$25 \leq T \leq 300$ = 0.247 T+114.4 $300 \leq T \leq T_{melt}$ = 0.125T+ 226	50
Melt temperature, T_{melt} (°C)	520	-
Room temperature, T_{room}(°C)	25	-

3.7 Material Constitutive Model

During the metal cutting process, the material deforms plastically and is subjected to high strains, strain rates and temperature conditions. To describe the thermo-mechanical behavior of a material undergoing deformation at such high strains and strain rate conditions, Johnson and Cook developed a constitutive material model in 1983. As per their model, the equivalent flow stress $\bar{\sigma}_{jc}$ is expressed as:

$$\bar{\sigma}_{jc} = \left(A + B\bar{\varepsilon}^{n}\right)\left[1 - c\ln\left(\frac{\dot{\varepsilon}}{\dot{\varepsilon}_{o}}\right)\right]\left(1 - \left(\frac{T_c - T_{room}}{T_{melt} - T_{room}}\right)^{m}\right) \tag{3.1}$$

where, A(MPa) is the initial yield stress of the material, B(MPa) the hardening modulus, c the strain rate dependency coefficient, n the work-hardening exponent, m the thermal softening coefficient, $\bar{\varepsilon}$ is the equivalent plastic strain, $\dot{\varepsilon}$ is the equivalent plastic strain rate and $\dot{\varepsilon}_o$ is the reference plastic strain rate, T_{room} is the room temperature and T_{melt} is the workpiece melting temperature. Table 3.4 lists the J-C material model constants for aluminum 2024-T351 alloy (Mabrouki et al. (2008)).

Table 3.4 Johnson-Cook material parameters values for A2024-T351 (Mabrouki et al. (2008))

***A*(MPa)**	***B*(MPa)**	***n***	***c***	***m***
352	440	0.42	0.0083	1

3.8 Material Damage Model

In the metal cutting process, chips are formed as a result of excessive (large) material deformation at the cutting tool-work material interface under the action of applied force. The material is said to be failed when it loses its load carrying capacity. In machining processes, the prediction and control of the material failure is a critical issue. In order to investigate the surface finish and integrity of the produced parts, it is essential to simulate the damage and fracture of the material under the action of applied loads.

In this work, it was desired to simulate the material ductile failure with high strain, strain rate and temperature effects. Johnson & Cook (1985) shear failure criterion was used to model the chip detachment. Figure 3.5 shows the progressive damage degradation curve obtained from a uniaxial stress-strain response of a ductile metal. Chip formation due to the shear deformation occurs in two stages: first, the failure initiation and the second is the failure evolution. During the initial phase, material response is linear elastic (stages 1 and 2) which is followed by plastic yielding with strain hardening

(stages 2 and 3). Beyond point 3, the material loses its load carrying capacity until it undergoes the fracture (stages 3 and 4).

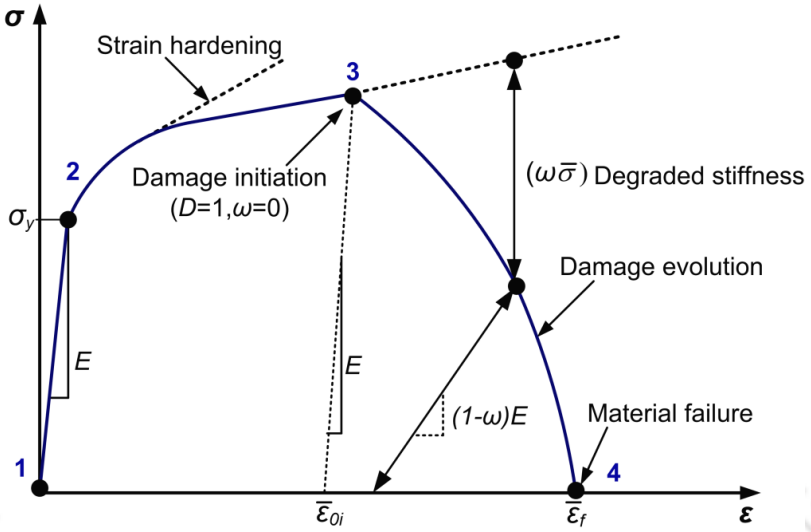

Figure 3.5 Stress-stain curve with progressive damage degradation

Point 3 represents the damage initiation point, which is referred to as damage initiation criterion. Complete failure of the material occurs at point 4. Deformation occurring in the final stage (3-4) is governed by evolution law which is based on fracture energy principle (Liu et al. (2014)). Damage in the element is initiated by scalar damage parameter D, which is defined as sum of ratio of the increments in the equivalent plastic strain $\Delta\bar{\varepsilon}$ to the equivalent strain at fracture initiation ε_{fi}. It is given by Equation 3.2. The damage initiation is said to have occurred when scalar damage parameter D exceeds unity.

$$D = \Sigma \frac{\Delta\bar{\varepsilon}}{\varepsilon_{fi}} \tag{3.2}$$

The equivalent strain at failure initiation ε_{fi} is determined as:

$$\varepsilon_{fi} = \left[D_1 + D_2 \exp\left(D_3 \frac{P}{\bar{\sigma}} \right) \right] \left[1 + D_4 \ln\left(\frac{\dot{\varepsilon}}{\dot{\varepsilon}_o} \right) \right] \left(1 + D_5 \left(\frac{T_c - T_{room}}{T_{melt} - T_{room}} \right) \right) \tag{3.3}$$

where P is the hydrostatic pressure and $\bar{\sigma}$ is the von Mises equivalent stress. The J-C damage constants ($D_1 - D_5$) are listed in Table 3.5. It can be noted that the value of coefficient D_5 is zero. This indicates that temperature has no effect on the damage initiation during machining of the aluminum alloy 2024-T351. Only, stress triaxiality and strain rate effects can induce damage initiation (Mabrouki et al. (2008)).When ductile material damage occurs, the stress-strain relationship no longer accurately represents the

material behavior.

Table 3.5 Johnson-Cook failure parameters for A2024-T351 (Mabrouki et al. (2008))

D_1	D_2	D_3	D_4	D_5
0.13	0.13	-1.5	0.011	0

After the damage initiation, the use of stress–strain relation causes strong mesh dependency which is based on strain localization. This reduces the energy dissipation as the mesh becomes smaller. Influence of mesh dependency on energy dissipation can be reduced by using the Hillerborg's fracture energy proposal. The damage evolution is based on Hillerborg's fracture energy G_f required to open a unit area of crack. It is defined as:

$$G_f = \int_{\bar{\varepsilon}_{0i}}^{\bar{\varepsilon}_f} L\bar{\sigma}_Y \mathrm{d}\bar{\varepsilon} = \int_0^{\bar{u}_f} \bar{\sigma}_Y \mathrm{d}\bar{u} \tag{3.4}$$

The damage evolution parameter is defined in the form of a scalar stiffness degradation parameter ω_s. It is given as:

$$\omega_s = \frac{L\bar{\varepsilon}}{\bar{u}_f} = \frac{\bar{u}}{\bar{u}_f} \tag{3.5}$$

where $\bar{\varepsilon}_{0i}$ plastic strain at damage initiation, $\bar{\varepsilon}_f$ equivalent plastic strain at failure, $\bar{\varepsilon}$ is the equivalent plastic strain, $\bar{u}$ is the equivalent plastic displacement, $\bar{u}_f$ is the equivalent plastic displacement at failure and L is the characteristic length of the element. The equivalent plastic displacement at failure can be expressed by:

$$\bar{u}_f = \frac{2G_f}{\sigma_y} \tag{3.6}$$

where σ_y is the yield stress of the material, G_f is the fracture energy dissipation. It can be determined by:

$$G_f = \left(\frac{1-\nu^2}{E}\right) K_c^2 \tag{3.7}$$

where K_c is the fracture toughness of the material.

3.9 Workpiece-Cutting Tool Contact Model

The friction condition at the tool and workpiece interface influences the milling forces,

temperature, machining quality and tool wear. The contact between the cutting tool and the workpiece was defined using modified Coulomb friction model. As per this model, contact between the chip and the rake surface region can be divided into two regions, namely the sliding region and the sticking region (see Figure 3.6).

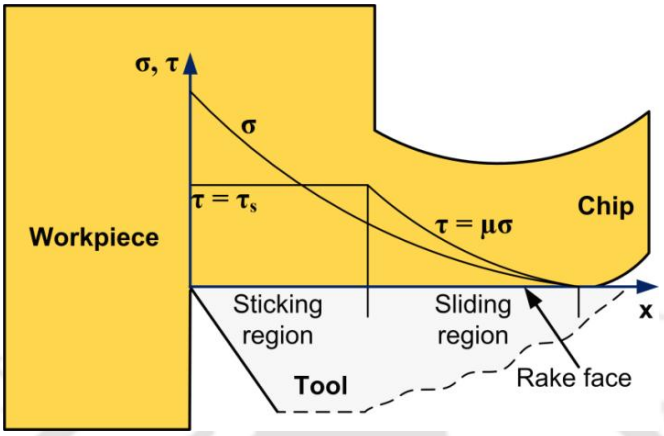

Figure 3.6 Schematic illustration of normal and shear stress distribution at chip-tool interface

Sticking friction occurs very near to the cutting edge which is in contact with the workpiece. Sliding friction occurs far away from the contact area. The sliding region obeys the Coulomb friction law. In the sticking region, the frictional stress τ_f is equal to the critical frictional stress. The model can be expressed by the following formulations:

$$\tau_f = k_{chip} \text{ when } \mu\sigma_n > k_{chip} \text{ (Sticking region)} \quad (3.8)$$

$$\tau_f = \mu\sigma \text{ when } \mu_n\sigma < k_{chip} \text{ (Sliding region)} \quad (3.9)$$

Where τ is the frictional stress, σ_n is the normal stress and k_{chip} is the shear flow stress of the material. In the present work, the coefficient of friction μ is considered as 0.17 (Liu et al. (2014)). The advantage of using the modified Coulomb friction model is that the solver determines the friction state automatically according to the contact stress value during the simulation process (Wu and Zhang (2014)).

3.10 Solution Methodology

After the development of geometric models of workpiece and tool, material properties, material damage law and friction law were applied and thermo-mechanical analysis of thin-wall end milling was carried out. The mathematical equations employed in the present work are given below.

3.10.1 Mechanical Analysis

The differential equation of motion governs the mechanical response and is given by:

$$\rho\ddot{u} + c\dot{u} + ku = F \tag{3.10}$$

Equation (3.10) is rewritten in matrix form as:

$$[M]\ddot{u} + [C]\dot{u} + [K]u = F \tag{3.11}$$

where ρ is the mass, c is the damping coefficient, k is the stiffness coefficient, *[M]* is the mass matrix, *[C]* is the viscous damping matrix, *[K]* is the stiffness matrix, F is the external force vector and $\ddot{u}$, $\dot{u}$ and u are the nodal acceleration, velocity and displacement vectors, respectively. Nodal acceleration at the beginning of time increment can be obtained by rewriting Equation (3.11) as:

$$\ddot{u}_i = M^{-1}\left(F - C\dot{u}_i - Ku_i\right) \tag{3.12}$$

In the present work, explicit formulation was employed which uses central difference scheme to discretize the equations. The acceleration equation can be written as:

$$\ddot{u}_i = \frac{\left(\dot{u}_{i+1/2+} - \dot{u}_{i-1/2}\right)}{(\Delta t_{i+1} + \Delta t_i)/2} \tag{3.13}$$

Velocity change is calculated by integrating acceleration term explicitly through time using central difference method. The change in velocity obtained is then added to velocity from the middle of the previous step and is used to calculate the velocities at the middle of the current step using:

$$\dot{u}_{i+1/2} = \left(\frac{\Delta t_{i+1} + \Delta t_i}{2}\right)\ddot{u}_i + \dot{u}_{i-1/2} \tag{3.14}$$

Displacement is calculated by integrating velocity through time, which is then used to update the displacements at the end of time step using:

$$u_{i+1} = u_i + \Delta t_{i+1}\dot{u}_{i+1/2} \tag{3.15}$$

3.10.2 Thermal Analysis

The governing equation which outlines the transient heat transfer process during machining process is written as:

$$\rho C_p \frac{\partial T}{\partial t} = \frac{\partial}{\partial x}\left[k_x \frac{\partial T}{\partial x}\right] + \frac{\partial}{\partial y}\left[k_y \frac{\partial T}{\partial y}\right] + \frac{\partial}{\partial z}\left[k_z \frac{\partial T}{\partial z}\right] + \dot{Q} \tag{3.16}$$

where C_p is the specific heat; k_x, k_y and k_z are the heat conductivity in x, y and z directions, respectively; T is the cutting temperature; and $\dot{Q}$ is the total heat generation rate. Equation (3.16) can be rewritten in matrix form as:

$$\left[\bar{C}\right]\dot{T}+\left[\bar{K}\right]T=\dot{Q} \tag{3.17}$$

Where $[\bar{C}]$ is the capacitance matrix, $[T]$ is the nodal temperature vector, $[\bar{K}]$ is the time-dependent conductivity matrix, $\dot{T}$ is the derivative of the temperature with respect to time and $\dot{Q}$ is the time-dependent heat vector. Solving the nodal temperature rate from the above equation yields:

$$\dot{T}_i = C^{-1}\left(\dot{Q}-KT_i\right) \tag{3.18}$$

After applying the forward difference integration scheme on Equation (3.18), the nodal temperature rate is given by:

$$\dot{T}_i = \frac{T_{i+1}-T_i}{\Delta t_{i+1}} \tag{3.19}$$

Equation (3.19) can be rewritten as:

$$T_{i+1} = (\Delta t_{i+1})\dot{T}_i + T_i \tag{3.20}$$

The explicit expression for nodal temperature rate can finally be written as:

$$T_{i+1} = (\Delta t_{i+1})C^{-1}\left(\dot{Q}-KT_i\right)+T_i \tag{3.21}$$

Total volumetric heat generation rate $\dot{Q}$ is due to the heat generated during plastic deformation and friction at the work-tool interface. Volumetric heat flux generated due to inelastic plastic deformation is expressed as:

$$\dot{Q}_{pl} = \eta_p \sigma \dot{\varepsilon}_p \tag{3.22}$$

where η_p is the fraction of the mechanical work required for plastic deformation which is converted into thermal energy, σ the stress and $\dot{\varepsilon}_p$ is the rate of plastic straining. Considering that most of the plastic work is converted into the heat, the value of η_p is taken as 0.9 (Li et al., (2002)). Friction at the work-tool interface is a potential heat source and the volumetric heat flux due to friction is given by:

$$\dot{Q}_f = f_f \cdot \eta_f \cdot \tau \cdot \dot{\gamma}_s \tag{3.23}$$

where $\dot{\gamma}_s$ is the slip rate, η_f is the frictional work conversion factor, f_f is the fraction of

heat energy conducted into the chip and τ_f the frictional stress. During the machining process, the tool and workpiece surfaces lose the heat to the environment. This phenomenon is described by Newton's law of convection as:

$$\dot{q}_{conv} = h_c(T_c - T_{room}) \tag{3.24}$$

The milling process involves large deformations and continuously changing contact between cutting and workpiece. With the above stated equations (3.10 to 3.24), Abaqus/Explicit, the FEA solver computed the responses such as milling force, wall deflection, cutting temperature. In the present analysis, explicit time integration scheme has been used to solve the transient problem. It was originally developed to solve high-speed dynamic problems those were difficult to simulate using the implicit method. This scheme is simple and can handle problems which involve high nonlinearity, large deformation, complex friction-contact conditions, thermo-mechanical coupling and fragmentation. The formulation using explicit solution can be of Eulerian, Lagrangian, or Adaptive-Lagrangian Eulerian (ALE) type. Figure 3.7 shows a comparison between Lagrangian, Eulerian and ALE formulations. In the Lagrangian formulation, the finite element mesh is attached to the material and follows the mesh deformation. The Lagrangian formulation is used to analyze transient problems which undergo large deformations. It is widely used due to its ability to form chips and to determine the chip geometry as a function of cutting parameters, plastic deformation process and material properties. This enables the evolution of the cut material from its nascent stage to a stable state without any predetermined material geometrical boundary conditions. The development of chip is entirely a function of physical deformation process, machining parameters and the input material properties.

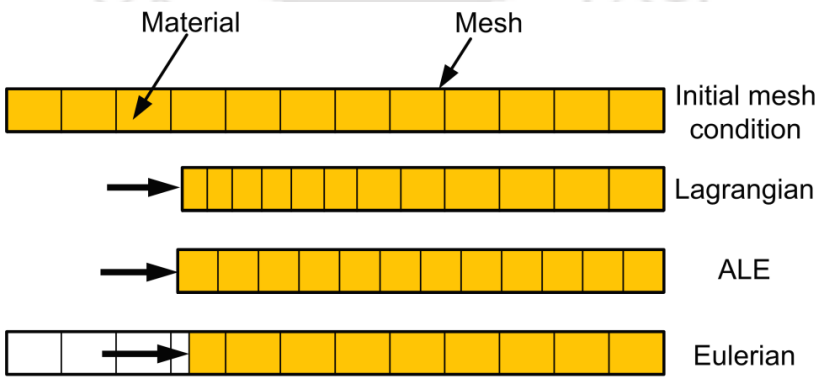

Figure 3.7 Comparison of motion of mesh and material with Lagrangian, Eulerian and ALE formulation

In the Eulerian formulation, the finite element mesh is fixed in the space and the material flows through the control volume that eliminates the possibility of element distortion during the process. It reduces the computation time as fewer elements required for the analysis. These models do not need separation criteria for simulating the material failure. The major drawback of the Eulerian formulation is that it needs prior knowledge of the chip geometry, chip-tool contact length, chip thickness, and contact conditions to simulate the chip formation. Also, the chip thickness, tool-chip contact length and contact conditions between tool-chip must be kept constant during analysis which makes Eulerian formulation not suitable for simulation of workpiece deformation that occurs during metal cutting. To overcome these drawbacks, researchers have developed a new iterative procedure which combines the best features of Lagrangian and Eulerian formulations. It is called arbitrary Lagrangian-Eulerian (ALE) approach. In this approach, the mesh follows the material flow and the problem is solved for displacements in Lagrangian steps, while for velocity the mesh is repositioned and the problem is solved in Eulerian step. The combined formulation avoids the severe element deformation which is a typical problem often associated with the Lagrangian approach. However, in view of simplicity and high computational efficiency, most of the 3-D FEM based simulations of metal cutting operations have used the Lagrangian formulation. Therefore in the present work, the same approach has been adopted.

In this work, Abaqus/Explicit, a commercial finite element solver has been used to carryout 3-D numerical simulations of machining of thin-walls. Extensive trials have been carried out to fine tune the FEM solver parameters. In general, a typical simulation of material removal during a complete pass of the milling tool along the wall length of 50 mm took about 340 to 350 hours.

3.11 Experimental Validation of FEM based Simulation of Thin-Wall Machining

After the development of numerical model, experimental validation of the responses predicted by the numerical model was carried out. For this purpose, an experimental setup was developed on a three-axis computer numerically controlled vertical machining center (CNC-VMC). Figure 3.8(a) depicts the details of the experimental setup developed. The workpiece was clamped in a workpiece holder, which was fixed firmly on a piezoelectric sensor based three-component dynamometer (make: Kistler 9272B). The dynamometer is capable of measuring three components of milling force (F_x, F_y and

F_z). The dynamometer was mounted firmly onto the base plate of the machine tool. For the data acquisition, the dynamometer was connected to a computer through a force measurement multi-channel charge amplifier (type 5070A). The data sampling rate was set to 500 Hz per channel.

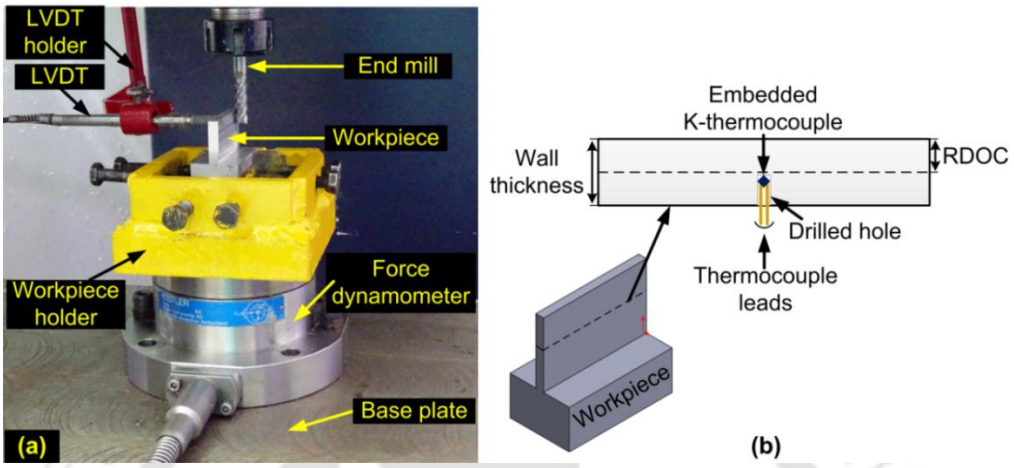

Figure 3.8 Experimental set-up: **(a)** Workpiece and force dynamometer, **(b)** Thermocouple placement for temperature measurement

The component F_x is normal to the machined wall surface. The component F_y is oriented along the direction of feed movement and the F_z component is along the tool's axis. The temperature was recorded by using a K-type thermocouple embedded in the workpiece. The thermocouple was connected to the Agilent-temperature DAQ system for the data acquisition (Figure 3.8(b)). The workpiece deflection was measured by Solartron linear variable differential transformer (LVDT) sensor. Experiments were repeated thrice for each set of process conditions.

3.11.1 Simulation of Process Conditions

The work was carried out to assess the capability of the developed numerical model to predict the responses such as milling force, wall deflection, chip morphology and workpiece temperature during thin-wall machining process. In addition, the efficiency of the developed model in terms of the computational time was also analyzed. Milling conditions used for simulation studies are listed in Table 3.6.The results obtained during the numerical simulation of machining thin-wall aluminum 2024-T351 alloy part are discussed in the following sections.

3.11.2 Milling Force

Using the developed experimental setup, force components, namely F_x, F_y and F_z, were

recorded for a typical process condition (Test case 1) as mentioned in Table 3.6. For the same process condition, a numerical simulation using the developed mathematical model was carried out.

Table 3.6 Milling conditions employed for thin-wall machining simulation

Test case	n_s (rev/min)	f_z (mm/z)	r_d (mm)	Workpiece length (mm)
1	4500	0.1	1	40
2	4500	0.1	1	50
3	3500	0.1	0.625	40
4	3500	0.1	0.625	50

Figure 3.9 shows the comparison between the simulation predictions and the experimental results. The dotted lines represent the milling forces in three directions which are obtained experimentally in the stable region, while the solid lines represent the respective simulation results.

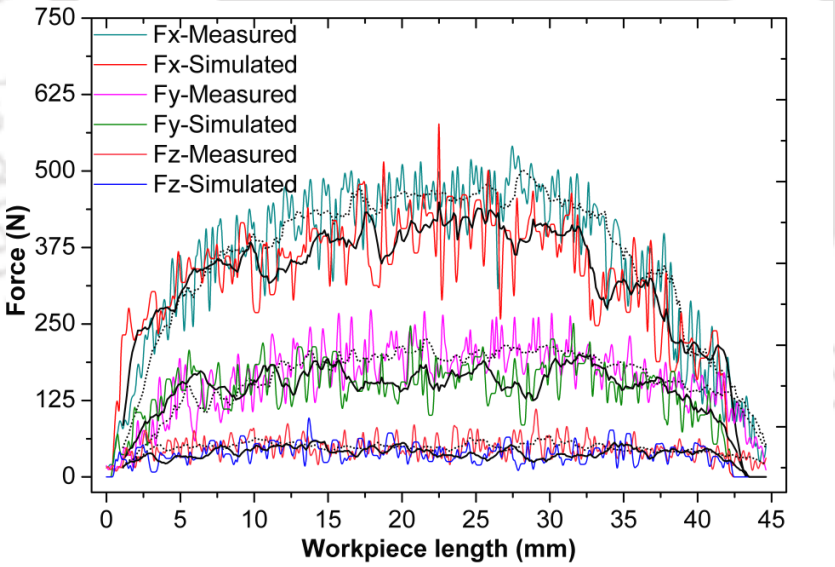

Figure 3.9 Comparison of simulated and measured milling force components F_x,F_y and F_z

From the plot, it is observed that the forces predicted by the numerical model are in good agreement with those obtained in the experimental study. The average prediction errors were noted to be 13.93%, 20.82% and 32.68% in F_x, F_y and F_z direction respectively. Lower values of force predicted by numerical simulation can be attributed to the factors such as consideration of isotropic nature of material properties, stress-free work material and absence of tool vibration and tool run-out. It was observed that the prediction error

of F_z is quite high in comparison with that of F_x and F_y. It is because the magnitude of F_z is smaller and it is more sensitive than the forces generated in the other directions.

It is difficult to analyze the cutting action occurring around the tool tip. Also, the factors such as re-cutting of chips and ploughing of cutting tool edges on the work surface result in the generation of fluctuating force values. However, the trends of variations of experimental and numerical forces are matching. It can be seen that the forces are fluctuating with the time. This is due to the fact that during the cutting process, the material softens due to the rise in temperature which reduces the force values. As the magnitude of force decreases, the heat production also reduces which in turn affects the metal softening effect that further leads to rise in the milling forces.

3.11.3 Wall Deflection and Form Error

During the machining process, the thin-wall part deflects due to low rigidity under the action of milling forces. Maximum deflection occurred at top edge of the wall in comparison to that of the wall base. It is due to the low rigidity of top edge of the workpiece. The base material has sufficient rigidity as it is firmly supported by the bulk material. Figure 3.10 shows the variation of deflection along the workpiece length measured perpendicular to the feed direction for the process condition mentioned in Table 3.6.

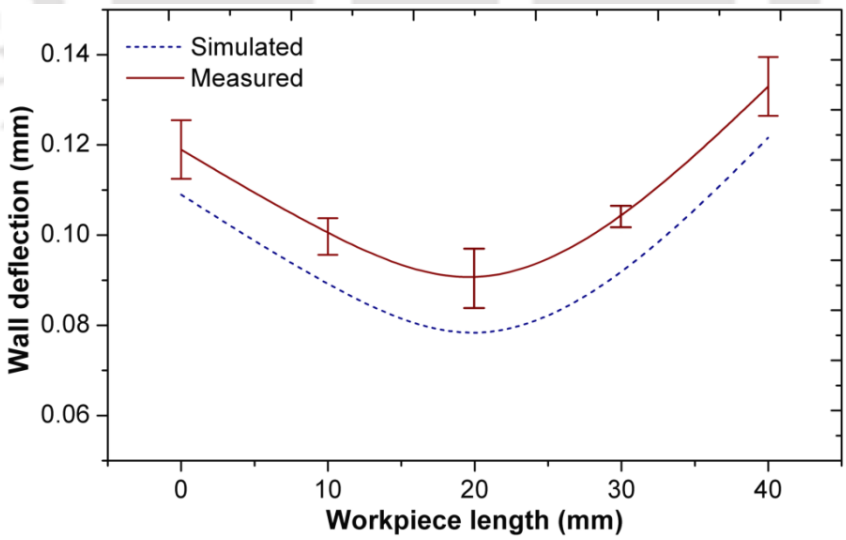

Figure 3.10 Comparison of numerical and experimental maximum deflection along the length of workpiece at top portion (2 mm below the top edge)

It is noted that the deflections at free ends of the workpiece are higher in comparison to that of the middle portion of the wall. The two ends are less stiff and deflect readily

under the action of milling force, whereas the center portion has sufficient rigidity as it is supported by the material all around. It can also be observed that experimentally obtained deflection values are slightly on the higher side than those obtained in the simulations. The absolute error between the experimental and numerically obtained results is noted to be 11%. The trends of variations are found to match well. Figure 3.11 shows the section view of the machined workpiece obtained during the numerical simulation and experimental work. It is noted that due to higher deflection occurring at top end during the milling process, material remains uncut leading to thicker top edge compared to the base of the workpiece. It can be seen that developed numerical model could successfully predict the form error that occurred during the machining process.

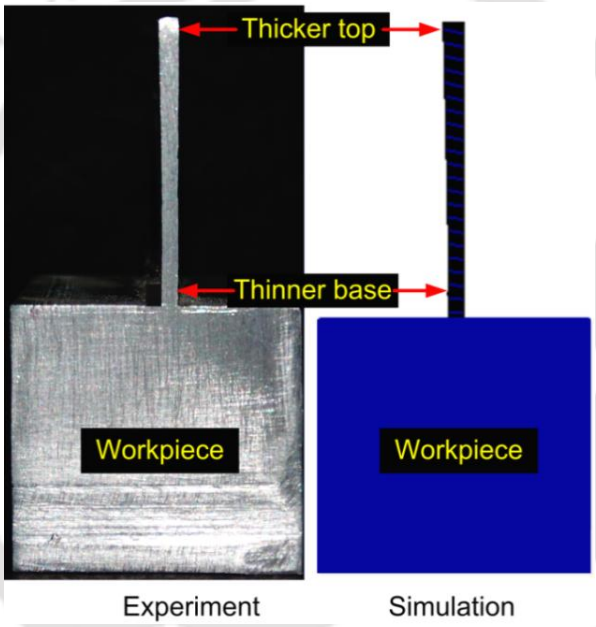

Figure 3.11 Comparison of form error obtained with experiment and numerical simulation

3.11.4 Stress Distribution

FEM-based simulation provides the prediction of stress distribution during the machining process. Figure 3.12 shows the stress distribution during end milling of the thin-wall part. During milling process, maximum stress occurs at the primary deformation zone, where the tool and workpiece are in contact. Figure 3.12(a) shows the stress developed during the process. It can be observed that the stress is highly localized at the work-tool contact region near to the cutting edge. The maximum induced stress at the milling area is around 700 MPa. Stress field gradually reduces away from the cutting zone. Also, the residual stress contour in the machined surface at the end of the process

is shown in Figure 3.12(b).

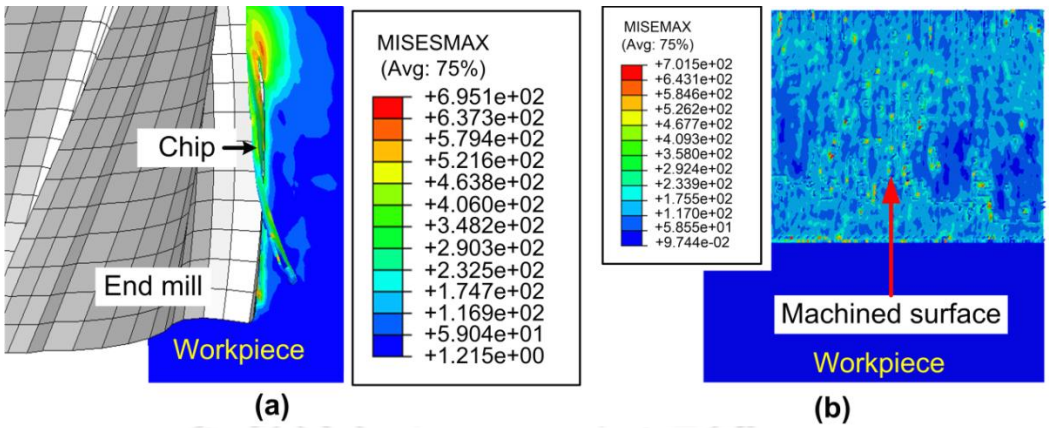

Figure 3.12 Stress distributions in thin-wall machining: **(a)** Stress at cutting zone, **(b)** Residual stress at the end of machining process

3.11.5 Chip Morphology

Generally, chips formed during aluminum machining are of continuous type. These long chips have a tendency to curl back into the work surface. Many a times, curled chips degrade the machined surface quality and damage the cutting tool (Songmene et al. (2011)). Another important characteristic is the formation of built-up-edges (BUE) during the machining operation. BUEs are harder than the work material, and act as temporary cutting edges which interrupt the smooth work-tool interaction and results in poor surface quality (Okonkwo et al. (2015)). During the machining process, periodic fractures of BUEs due to cyclic formation and disappearance lead to cutting instability which results in machining vibration (Ramaswami (1974)). Therefore it is very important to select proper cutting and tool related parameters that help in obtaining the desired chip morphology and surface finish during aluminum alloy machining. In the present work, formation of chips due to shear deformation is simulated by using Johnson-Cook damage model. Figure 3.13(a-d) illustrates the chip formation recorded at four different time intervals during the numerical simulation of helical end milling process. Figure 3.13(a) depicts the initial cut as the tool enters the workpiece. As the tool applies pressure over the workpiece, chip separation from the workpiece is initiated. In Figure 3.13(b) shows the flow of chip over the rake face. Figure 3.13(c) presents a curl of chip formed as it slides over the spiral tool flute. Figure 3.13(d) shows the chip about to detach from the workpiece.

Figure 3.14 shows a comparison between the morphology of chips obtained by using numerical simulation model and experiments. The shape and size of the simulated

chips are quite similar to that obtained during the experiments. Average values of chip width recorded during the experimental study and numerical simulation were around 680.52 µm and 773.8 µm respectively. The chip is curled due to the effect of helical shape associated with the flute over which the chip slides during its formation. Present 3-D numerical model successfully simulated this realistic phenomenon.

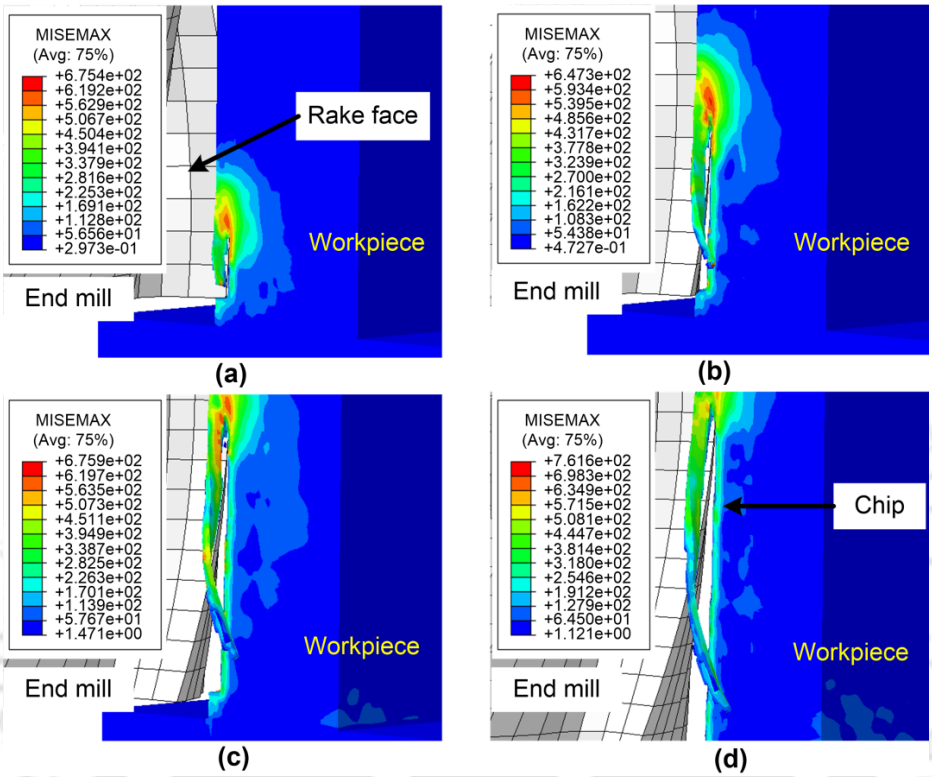

Figure 3.13 Chip evolution stages: **(a)** Initial chip cut, **(b)** Chip flow over rake face, **(c)** Chip curling, **(d)** Chip detachment

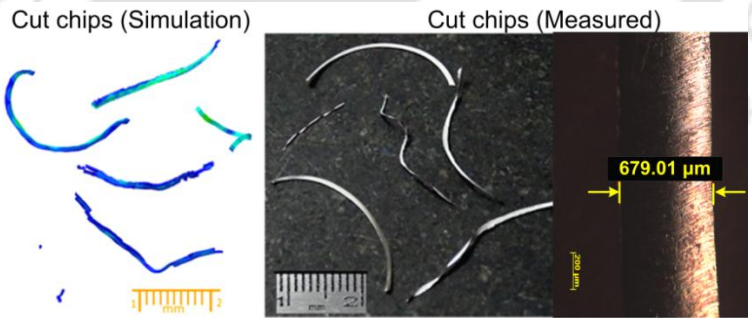

Figure 3.14 Comparison of chip morphology obtained by numerical simulation and experiments

3.11.6 Temperature Distribution

In the present work, the transient temperature distribution generated during the severe plastic deformation of the work material has been recorded. The cutting temperature affects tool wear and quality of finished surface. In a machining process, the temperature

rise is mainly attributed to the plastic deformation of work in the shear zone and frictional heat generated at the chip-tool interface. Out of the total heat generated, a portion of the heat dissipated into the surrounding environment by convection; however, the remaining portion gets transferred to the chip and tool through conduction mode of heat transfer. It is to be noted that during the machining of aluminum alloy, the heat dissipation to the environment is high due to high thermal conductivity of the work material. Figure 3.15 shows a plot of temperature rise during the milling process. It is observed that as the machining commences, the temperature rises gradually due to the generation of heat in the process of plastic deformation. It increases with the time, attains its peak during the chip separation and then reduces when the chip detaches from the parent material. In this work, it was found that the simulation results are very well matching with that of the experimental studies with an average error of 17%. The trends of variations are also agreeing well. This demonstrates the capability of 3-D thermo-mechanical numerical model to simulate the machining process in terms of machining temperature.

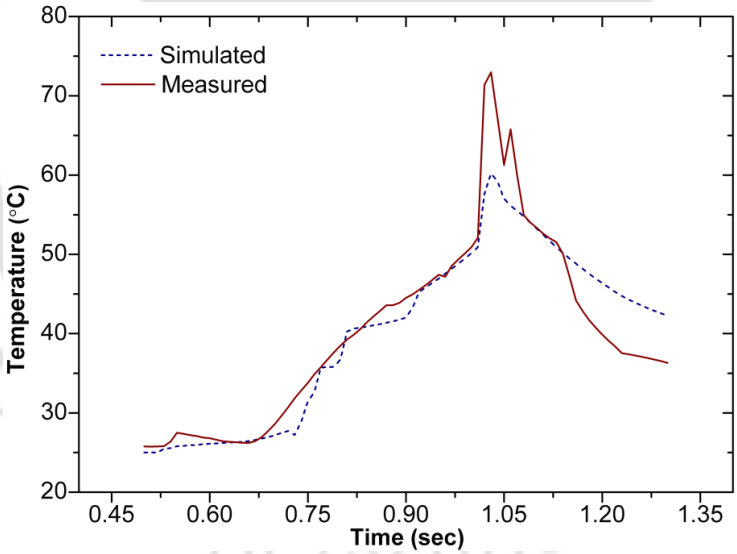

Figure 3.15 Comparison of temperature obtained by numerical simulation and experiments

Similar to test case 1, experiments were conducted for three other test cases. Table 3.7 summarizes the values of measured and simulated milling force components, wall deflection and workpiece temperature for all the four test cases. It can be seen that the milling force component values predicted by the developed model match well with the values that are obtained by experiments for all the test cases. Mean prediction errors for F_x, F_y, F_z wall deflection and workpiece temperature were noted to be 11.61%, 16.38%,

26.1%, 10.02% and 15.61% respectively. Overall a very good agreement between the simulated and experimentally measured responses has been noted which demonstrates the capability of the developed model to predict the process responses accurately.

Table 3.7 Comparison of the simulated and measured responses for test cases listed in Table 3.6

Test case		Milling force (N)			Wall deflection (mm)	Workpiece temperature (°C)
		Fx	Fy	Fz		
1	**Predicted**	294.3	132.44	37.04	0.096	60.21
	Measured	341.8	167.28	55.10	0.107	72.95
	Absolute error (%)	13.93	20.82	32.68	11.00	17.00
2	**Predicted**	289.6	127.11	38.31	0.133	62.67
	Measured	323.1	152.9	51.64	0.124	76.58
	Absolute error (%)	10.53	16.86	25.81	6.780	18.16
3	**Predicted**	252.74	175.02	38.49	0.091	59.30
	Measured	287.50	204.32	52.10	0.104	70.29
	Absolute error (%)	12.09	14.34	26.13	12.50	15.63
4	**Predicted**	246.98	168.16	36.67	0.0956	66.98
	Measured	274.40	194.37	45.72	0.106	75.84
	Absolute error (%)	9.9	13.5	19.79	9.81	11.68
	Mean Error (%)	**11.61**	**16.38**	**26.1**	**10.02**	**15.61**

3.12 Evaluation of Computational Performance of the Developed 3-D FEM Model

From the results obtained, it can be seen that the 3-D FEM model was able to simulate the complex interaction of helical milling cutter with the thin-walled work part. It could predict the process responses viz. milling forces, wall deflection and workpiece temperature with good accuracy. However, it was noticed that 3-D numerical simulation took hundreds of hours of time to simulate a single pass of cutting by using a computer system with 3.9 GHz, 4GB RAM processor. In view of this, the computational efficiency of the developed model was examined by conducting extensive trials. Table 3.8 provides the total time consumed by the FEM simulations for some of these trials. In a FEM based simulation model, the computational speed vastly depends on the model parameters such as material properties considered, geometric complexity and meshing and boundary conditions. It was noted that as the length of the workpiece increases the computation time increases. Also, the process parameters viz. feed rate and radial depth of cut greatly

influence the computation time. This is because as the depth of cut increases, fineness of mesh increases, thereby increasing the number of elements in the model.

Table 3.8 Computation time for 3-D thin-wall machining simulation

Test case	CPU time (hrs)
1	340
2	348
3	334
4	343

The observations made during the course of work are listed.

- FEM simulation can predict the deflection during thin-wall machining process with reasonable accuracy.
- Simulation needs very long computational time (several days).
- Computation times increases with increase in workpiece size and number of elements.
- Huge data storage spaces are required to store the output data files.
- The complex geometry of the helical tool needs to be modeled using a separate CAD package and transferred into the FE package which is time consuming.

From this work, it can be seen that a 3-D mathematical model and its successful simulation solves a quite complex problem of simulation of helical milling of thin-wall components. It helps in the prediction of important process performance parameters such as milling force, deformation, stresses, chip morphology and temperature quite accurately and easily. A prior knowledge about these parameters certainly helps the process engineers to tune up the process parameters to achieve the desired process performance. Predicted milling forces provide an approximate estimation of energy requirement. Deformation values forecast the quality of the product in terms of the dimensional accuracy. Stresses will help in the estimation of the strength of the machined workpiece, while the chip morphology predicts the surface quality of the machined workpiece. Thus, it can be said that numerical modeling and simulation provides a useful tool to the engineers and scientists to carry out a prior detail study of the cutting process. However the requirement of huge computation time beset the application of 3-D FEM based simulation in practice. A need was thus identified to develop a simple and quicker approach to predict the important process responses such

as part deflection and milling forces during thin-wall milling operation. It is envisaged that such an approach will provide comprehensive analysis of thin-wall milling operation for a wide range of process parameters.

3.13 Summary

This chapter presented, in details, the development of a numerical (FEM) model for the thin-wall machining process. A realistic three-dimensional thermo-mechanical finite element based FEM model is developed to simulate the complex physical interaction of helical cutting tool and workpiece during thin-wall milling of an aerospace grade aluminum alloy. Lagrangian formulation with explicit solution scheme was employed to simulate the interaction between helical milling cutter and the workpiece. The behavior of the material at high strain, strain rate and the temperature was defined by Johnson-Cook material constitutive model. Johnson-Cook damage law and friction law were used to account for chip separation and contact interaction. Experimental work was carried out to validate the results predicted by the mathematical model. The developed model predicted the forces in radial, feed and axial directions with errors of 11.61%, 16.38% and 26.1%, respectively. The prediction error for deflection at the top portion of thin-wall was 10.02%. It was noted that maximum deflections occur at the free ends of the wall as compared to that at the center. It was also observed that due to the deflection of the wall, some material at the base of the wall remained uncut that further leads to geometric form error in the workpiece. The simulated chip dimensions were in good agreement with experimental results while the computed cutting temperature varied by 17% with respect to the experimental value. The simulated cut-chip was noted to have a similar curl as that occurs in physical experiments. Overall, it was found that the developed model predicts the process responses with fair and acceptable prediction accuracy.

Although the developed model provides very useful insights into the complex physical interaction of helical cutting tool and workpiece such as milling forces, stress distribution, cutting temperature, part deflection and chip morphology, it has limited applications in practice due to the requirement of huge computation time. In view of this, in the present work, an integrated analytical-numerical approach has been developed to predict the process responses quickly with reasonable accuracy. The details of the same are provided in the next chapter.

Chapter 4

An Integrated Analytical-Numerical Modeling of Milling Force and Wall Deflection in Helical End Milling of Thin-Wall Parts

4.0 Scope

This chapter presents the development of an integrated analytical-numerical approach for three-dimensional thermo-mechanical modeling of end milling of thin-wall parts using unified mechanics of cutting approach and finite element method (FEM). Initially, the need to develop such an approach is defined. Then an overview of the proposed approach for modeling of thin-wall milling is presented. Further, the thermo-mechanical characteristics are presented in detail, in terms of shear flow stress, shearing temperature, tool-chip interface friction, and solution methodology. The model is validated in comparison with the experimental results. This chapter concludes by reporting a study on the evaluation of the computational efficiency of the developed force-deflection prediction process.

4.1 The Need

Wall deflection is an important aspect during thin-wall milling which influences the quality of the work part; therefore research on accurate prediction of in-situ deflection of thin-walls has attracted worldwide attention. The previous chapter presented a finite element based three-dimensional numerical model of the thin-wall milling operation. The model was developed by considering all realistic aspects such as material flow, material failure, tool-chip interface friction, and workpiece and tool geometries. It computed the process responses such as milling force, deflection, machining stresses, workpiece temperature and chip morphology with fair and acceptable accuracy. Also, the model provided very useful insights into the complex physical interaction of helical cutting tool and the workpiece. However, the requirement of huge computation time (approx. 340 hours) besets its application in practice. In view of this, a literature review was carried out to find out analytical alternatives for quicker and accurate predictions of wall deflection during the thin-wall milling operation. Few attempts on the computation of milling force and deflection prediction have been reported. In the reported models the workpiece was considered as rigid and the forces were determined using mechanistic force models (Kline et al. (1982), DeVor et al. (1983), Izamshah et al. (2012)). In most

of these models, the forces have been determined by using the chip load and force coefficients. The chip load and force coefficients are usually determined by orthogonal cutting experiments or slot milling experiments for the chosen cutting tool geometry and tool-workpiece combination. These models can compute the deflection quickly; however, experiments are needed to determine the milling force coefficients. Conducting experiments is costly and tedious. Moreover, these models do not take into account the thermo-mechanical aspects of machining. This limits their application in practice.

Some of the reported works predict the wall deflection by using simple cantilever geometry of the workpiece without due consideration to the in-process change in workpiece geometry i.e. reduction in wall thickness during the milling process (Altintas et al. (1992)). Thus a need was identified to develop an efficient force-deflection prediction model for quicker and accurate prediction of the wall deflection for chosen milling conditions. The model should take into account the thermo-mechanical characteristic of the process and tool-workpiece geometries. A research work in this direction has been carried out in the present work and its details are provided in the following sections.

4.2 Overview of the Development of an Integrated Force-Deflection Model

In the present work, an integrated model has been proposed by combining the merits of analytical unified mechanics based computation approach of milling force and finite element method. It quickly predicts the milling force and wall deflection during end milling of thin-wall parts. Figure 4.1 shows an overview of the proposed methodology.

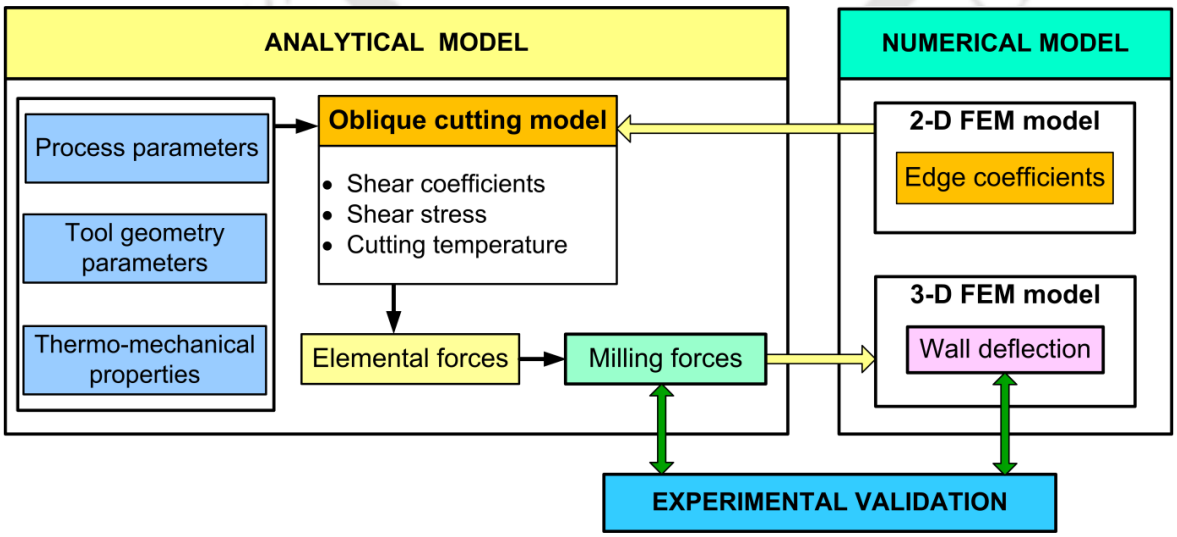

Figure 4.1 Overview of the integrated force-deflection prediction model

The stages of the model development are as follows.

- Development of an analytical model for computation of milling forces. It comprises of determination of milling forces by using the shear force coefficients, shear stress and shear temperature those obtained by using metal cutting theory. The peculiarity of the present work is that the edge force coefficients are computed by using simple 2-D finite element simulations which otherwise to be determined by conducting costly and tedious physical experiments. The computed milling force was validated by using experimental results. This experimentally validated approach can further be employed to predict wall deflection for given set of process conditions. No further experiments will be required for obtaining the force coefficients and validation of the predictions.
- Based on the computed milling forces, the in-situ wall deflection was predicted by developing a 3-D finite element based numerical model. The predicted response of the FEM model was also validated by using experimental results.

It is envisaged that the proposed approach saves the computation time and data storage space at a very large scale in comparison with that of 3-D FEM based numerical approach. The details of above-mentioned stages are presented in detail in the coming sections.

4.3 Development of an Analytical Model for Computation of Milling Force

In this work, to compute the milling forces, the unified mechanics of cutting approach proposed by Armarego (2000) has been used. Unified mechanics of cutting approach model is based on the concept of the shear plane. The calculation of milling forces are based on the shear stress and strains within the workpiece and are further dependent on the workpiece material properties and cutting tool configuration. The model is based on the classical orthogonal and oblique cutting operations. In addition to the shearing forces usually observed in the classical oblique cutting operations, the model incorporates an additional force component called edge forces which arise due to the rubbing and ploughing phenomena at the cutting edge.

Figure 4.2 depicts an overview of the analytical methodology used for modeling of milling forces. The inputs to the model were the milling parameters and the material properties. The milling parameters considered are spindle speed, feed per tooth, axial

depth of cut, radial depth of cut and tool diameter. The material properties in terms of mechanical, thermal and Johnson-Cook material model parameters have been applied. After that, the milling forces were computed by carrying out the following steps.

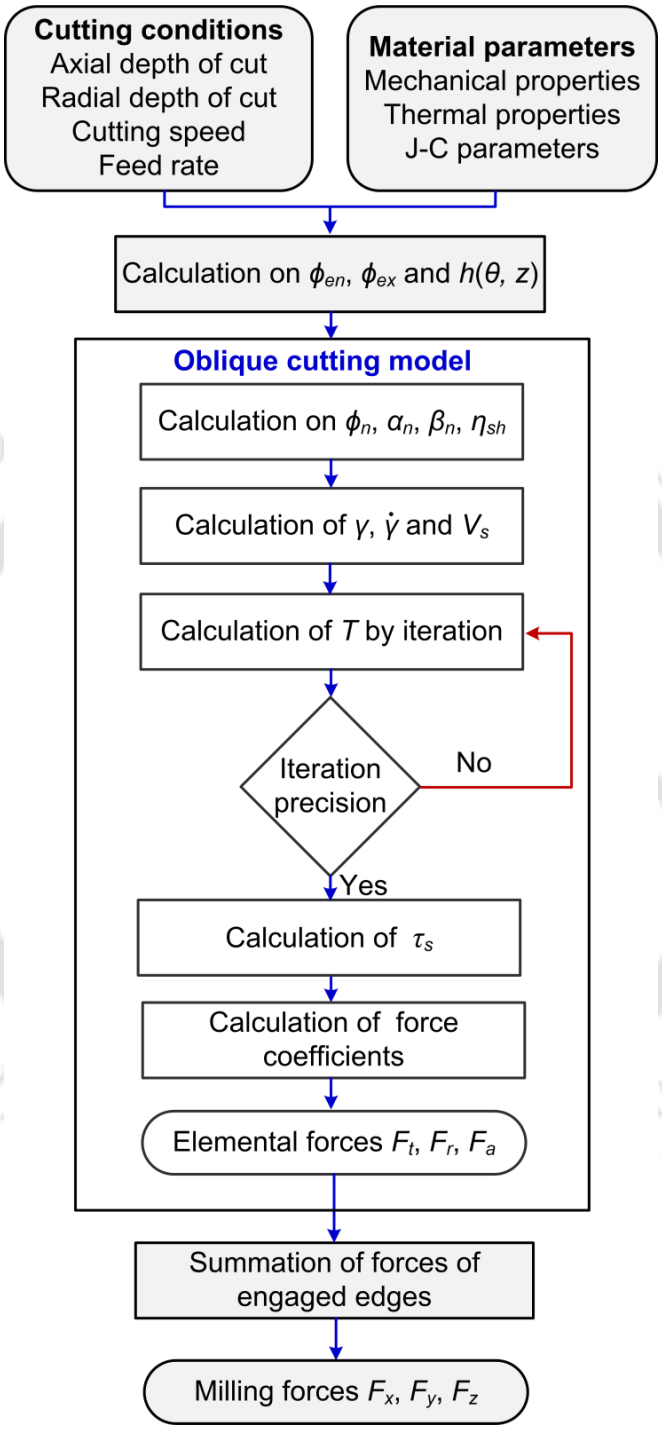

Figure 4.2 Flow chart for computation of milling force using unified mechanics approach

- Determination of uncut chip thickness, and cutting tool entry and exit angle.
- Determination of shear strain, strain rate, shear stress and shear temperature to

compute the shear force coefficients.

- Determination of edge force coefficients based on 2-D FEM simulations.
- Computation of elemental forces occurring at the cutting edge by using unified mechanics of cutting approach.
- Determination of end milling forces by summing up the elemental forces.

In the present work, the milling cutter geometry was discretized into a series of axial cutting elements as shown in Figure 4.3.

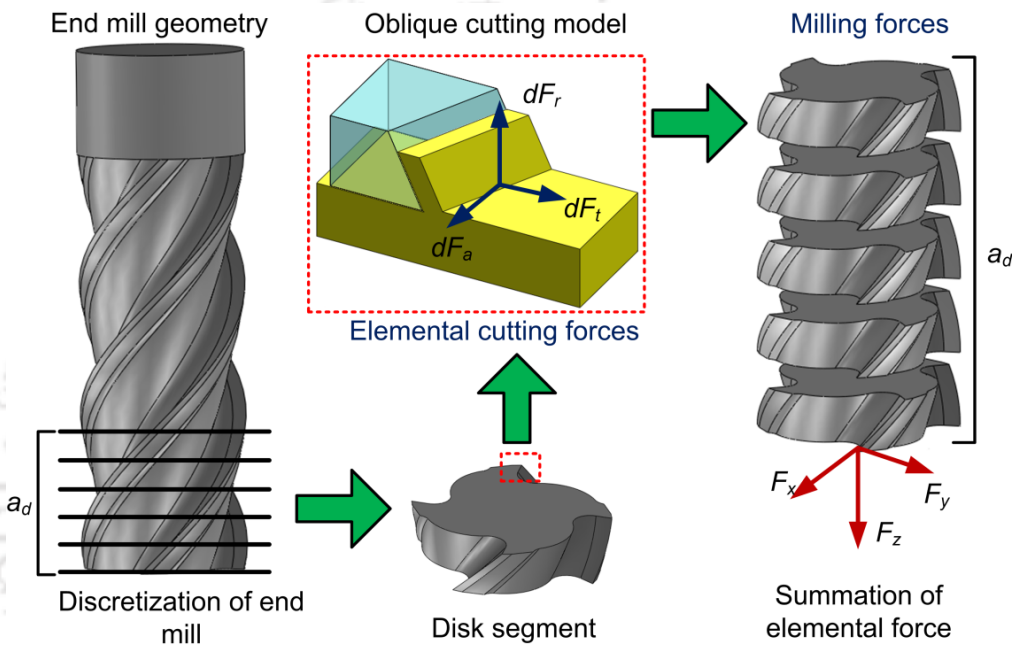

Figure 4.3 Determination of end milling force from the elemental forces

Based on the oblique cutting model, the elemental forces were computed on a small cutting section of the tool that represents a single point cutting tool. The forces acting on an oblique cutting element were resolved into tangential (F_t), radial (F_r) and axial (F_a) components in three mutually perpendicular directions. The three oblique force components (F_t, F_r and F_a) of the total forces can be expressed as:

$$\begin{aligned} F_t &= F_{tc} + F_{te} \\ F_r &= F_{rc} + F_{re} \\ F_a &= F_{ac} + F_{ae} \end{aligned} \tag{4.1}$$

In the above expressions, the first components (F_{tc}, F_{rc} and F_{ac}) represent the forces due to material shearing occurring in the primary shear zone while the second components (F_{te}, F_{re} and F_{ae}) account for the forces due to rubbing and ploughing at the flank face in the tertiary deformation zone. Equation 4.1 can be rewritten as:

$$F_t = K_{tc} bh + K_{te} b$$
$$F_r = K_{rc} bh + K_{re} b \quad (4.2)$$
$$F_a = K_{ac} bh + K_{ae} b$$

where K_{tc}, K_{rc} *and* K_{ac} are the shearing force coefficients and K_{te}, K_{re} *and* K_{ae} are the edge force coefficients.

As per Armarego (2000), the shearing coefficients can be determined by using the analytical expressions based on the theory of metal cutting. On the other hand, there is no single straightforward relationship to determine edge force coefficients. Some of the popular classical approaches to determine the six coefficients are by carrying orthogonal cutting experiments (Altintas and Armarego (1996)), conducting experiments to measure average forces per revolution in slot milling tests (Altintas (2000), Wang and Zheng (2002)) or arbitrary radial immersion tests (Gradisek et al. (2004)). As per these models, carrying out cutting experiments is a necessity to compute the edge coefficients; however experiments are costly and time consuming. To solve this problem, it was thought that use of finite element based simulation could be an economical, efficient and simple alternative. Therefore, in the present work, shearing coefficients have been computed by using the analytical expressions provided by Armarego (2000) while the edge force coefficients have been obtained by conducting FEM based simulation of metal cutting process. Further, in FEM based method, the coefficients can be obtained by conducting 2-D or 3-D simulations of metal cutting operation. In view of the computational simplicity and efficiency, simple 2-D FEM based approach was followed. The approach was duly validated by conducting experiments. It is envisaged that it provides a quicker and simpler way to determine the milling forces which can further be utilized to estimate the thin-wall deflection.

In the following section, the analytical procedure to determine the shearing coefficients is presented in detail. Initially, the geometric model and related terms are presented and then the computation of elemental forces based on the oblique model is presented. Finally, the procedure to determine the end milling force is described.

4.3.1 Geometric Analysis of the Helical End Mill

Figure 4.4 shows the geometry of a four-fluted helix end mill cutter. The end milling operation was analyzed with respect to the global Cartesian coordinate system (XYZ). In this system, X-axis has been defined perpendicular to the machined surface, while Y-axis and Z-axis were considered along the feed direction and tool axis direction respectively.

The end milling cutter was discretized into a stack of disk elements along the cutter length. Each disk is of thickness *dz*.

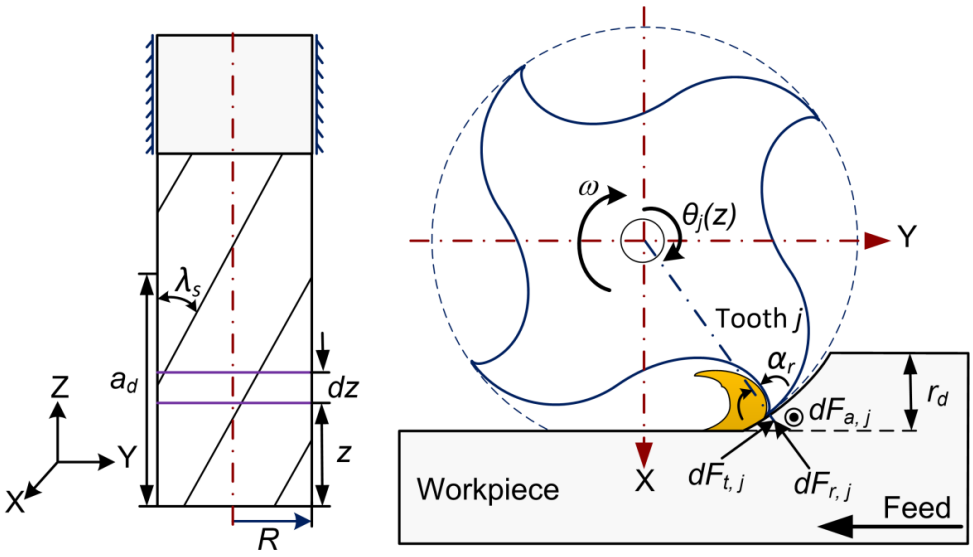

Figure 4.4 Helical end milling geometry with milling forces components

To account for intermittent cutting phenomenon that occurs due to multiple cutting edges, cutting edge engagement and disengagement with the workpiece has been modeled by using immersion angle. Figure 4.5(a) illustrates the immersion angle for down milling process. The cutter immersion angle $\theta_j(z)$ at time t for a differential cutting edge element on j^{th} cutting tooth at the axial location z is expressed as:

$$\theta_j(z) = \omega t + j \cdot \frac{2\pi}{N_t} - \tan(\lambda_s) \cdot \frac{z}{R} \qquad (4.3)$$

where ω is the angular velocity (rad/sec), N_t the number of teeth, R the end mill radius and λ_s is the cutter helix angle.

Precise determination of instantaneous chip thickness is essential for calculating the milling forces. In milling operation, instantaneous chip thickness varies periodically as a function of time varying immersion. Therefore, by assuming the tool path to be circular as suggested by Martellotti (1941), the uncut chip thickness shown in Figure 4.5(b) was calculated. The uncut chip thickness $h(\theta, z)$ is dependent on immersion angle as well as feed per tooth (f_t) and is given by:

$$h(\theta, z) = f_t \cdot \sin\theta_j \qquad (4.4)$$

The relationship applies under the conditions that the axis of rotation of the spindle coincides with the rotational axis of the end mill and the radius of each tooth of the cutter is constant and removes equal amount of material.

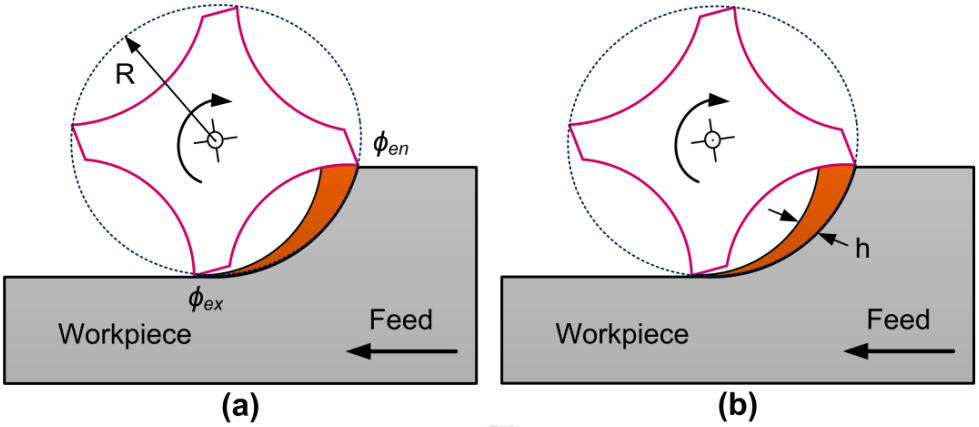

Figure 4.5 (a) Entry and exit angle, **(b)** Uncut chip thickness

The entry angle (θ_{en}) and the exit angle (θ_{ex}) are the key parameters required for the computation of milling forces. The angle at which the tool enters into the workpiece is termed as entry angle whereas the exit angle is the angle at which the tool exits the cut. These angles were computed by applying following equations.

$$\begin{aligned} &\theta_{st} = 0 \text{ and } \theta_{ex} = \arccos(1 - r_d / R) && \text{for up-milling} \\ &\theta_{st} = \pi - \arccos(1 - r_d / R) \text{ and } \theta_{ex} = 0 && \text{for down-milling} \end{aligned} \tag{4.5}$$

where r_d is the radial depth of cut. After the computation of uncut chip thickness, and entry and exit angles the cutting forces have been computed by using oblique cutting theory. The details are presented in the next section.

4.3.2 Oblique Cutting Model

The cutting phenomenon occurring at each element has been considered in the 'oblique' mode. Figure 4.6 illustrates the classical oblique cutting process. Geometric parameters were determined using the analytical models. As stated in Section 4.3, in the present work milling force coefficients have been computed by using the expressions given by Armarego (2000). These have been derived by using the oblique cutting model. To obtain these coefficients, it is essential to first obtain the necessary expressions for shear angle, rake angle, friction angle, shear strength, strain, strain rate and cutting velocity. These were obtained as follows.

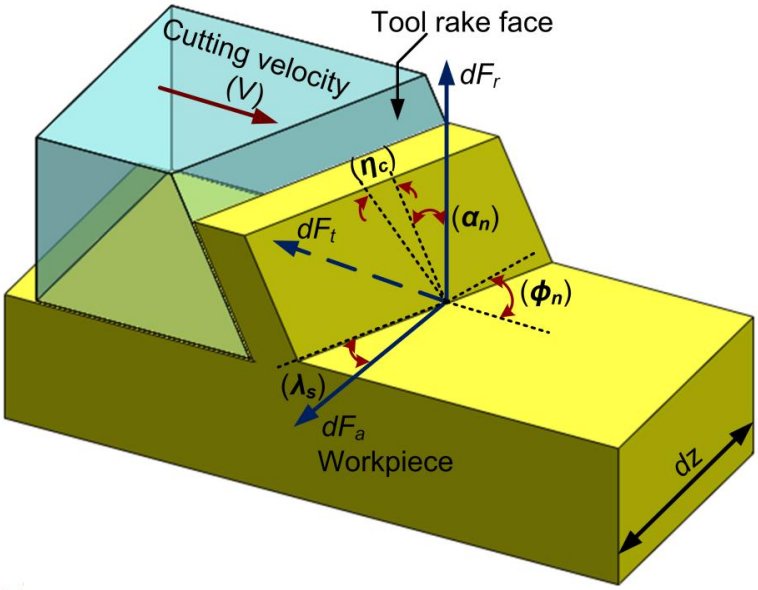

Figure 4.6 Schematic representation of oblique cutting process

The normal rake angle (α_n) has significant influence on the chip flow direction (Armarego and Brown (1969)). It can be computed by using the radial (specific) rake angle and helix angle and is expressed as:

$$\tan(\alpha_n) = \tan(\lambda_s) \cdot \tan(\alpha_r) \tag{4.6}$$

The mean friction angle on the tool rake face is a function of friction coefficient (μ) and can be obtained by using orthogonal cutting tests and is defined as:

$$\tan(\beta) = \mu \tag{4.7}$$

In this work it is assumed that the shear velocity is collinear with shear force (Armarego (2000)). Based on the oblique cutting deformation geometry, the normal friction angle can be expressed as a component of mean friction angle in the normal plane and is given as:

$$\tan(\beta_n) = \tan(\beta) \cdot \cos(\eta_c) \tag{4.8}$$

The normal shear angle (ϕ_n) is calculated using Merchant's theory (Merchant 1945). It is based on minimal principle energy principle and is a function of mean friction angle (β) and normal rake angle (α_n). The normal shear angle (ϕ_n) is given by:

$$\phi_n = \frac{\pi}{4} + \frac{1}{2}(\alpha_n - \beta) \tag{4.9}$$

The oblique machining process is then modelled by using thermo-mechanical approach which takes into account the stress, strain and temperature generated during the metal cutting operation. The details are presented in the next section.

4.3.3 Computation of Shear Stress

Metal cutting is a thermo-mechanical phenomenon in which the high strain rates, shear strain and temperature are essentially required to model the thermo-mechanical behavior of the process. In the present work, these aspects have been considered by using the law suggested by Johnson and Cook (1983). It is called as Johnson-Cook (J-C) constitutive law and it assumes that the workpiece material is isotropic and viscoplastic. According to the J-C model, the material shear flow stress can be expressed as:

$$\tau_s = \frac{1}{\sqrt{3}}\left[A - B\left(\frac{\gamma}{\sqrt{3}}\right)^n\right]\left[1 - c\ln\left(\frac{\dot{\gamma}}{\dot{\gamma}_o}\right)\right]\left[1 - \left(\frac{T_c - T_{room}}{T_{melt} - T_{room}}\right)^m\right] \tag{4.10}$$

where $\tau_s, \gamma, \dot{\gamma}, \dot{\gamma}_o$ and T_c represent the shear stress, shear strain, shear strain rate, reference strain rate and cutting temperature respectively. Here A (MPa) is the initial yield stress of material, B (MPa) the hardening modulus, c the strain rate dependency coefficient, n the work-hardening exponent, m the thermal softening coefficient for the material. J-C material parameter values for aluminum alloy 2024-T351are listed in Table 4.1.

Table 4.1 Johnson-Cook material parameters values for A2024-T351 (Mabrouki et al. (2008))

***A* (MPa)**	***B* (MPa)**	***n***	***c***	***m***
352	440	0.42	0.0083	1

To determine the flow stress, shear stress, shear strain, shear strain rate and the cutting temperature need to be calculated. The shearing strain in oblique cutting is given by:

$$\gamma = \frac{\left(\tan(\phi_n - \alpha_n) + \cot(\phi_n)\right)}{\cos(\eta_{sh})} \tag{4.11}$$

.

The shear stain rate is calculated as:

$$\dot{\gamma} = \frac{\tan(\phi_n - \alpha_n) + \cot(\phi_n)}{\cos(\eta_{sh})} \cdot \frac{V_s}{\Delta y} \tag{4.12}$$

To compute shear strain rate it is required to determine shear velocity (V_s), shear band spacing (Δy) and shear flow angle (η_{sh}). These are obtained as follows.

A. The shear velocity is a function of cutting speed (V_c) and is expressed as:

$$V_s = V \cdot \cos(\lambda_s) \cdot \sin(\phi_n) \cdot \gamma \tag{4.13}$$

B. The shear band (Δy) is a narrow zone developed due to severe plastic deformation in the shear deformation area. The shear bands are depicted in Figure 4.7. It was observed (Pawade et al. 2009) that shear band spacing is a function of workpiece material properties, cutting tool geometry, heat effect, and machining conditions. Based on the experimental work carried out by Kececioglu (1958), shear band spacing is approximated as a function of uncut chip thickness (h) and it is given by:

$$\Delta y = \frac{1}{4}h \tag{4.14}$$

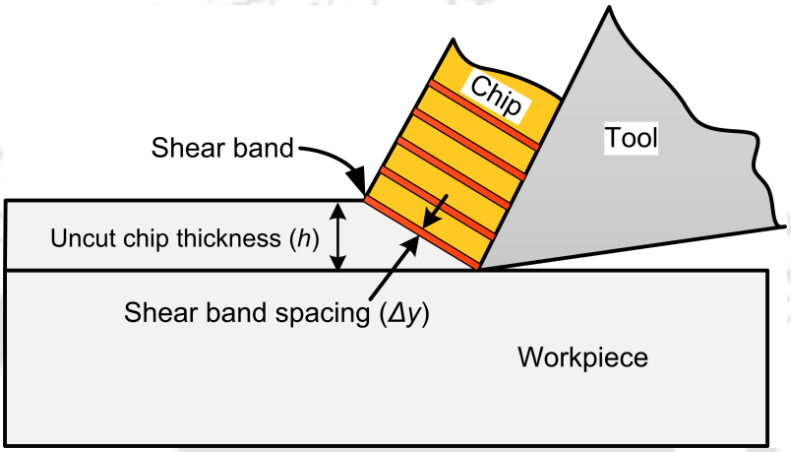

Figure 4.7 Schematic diagram of chip formation with shear band zone

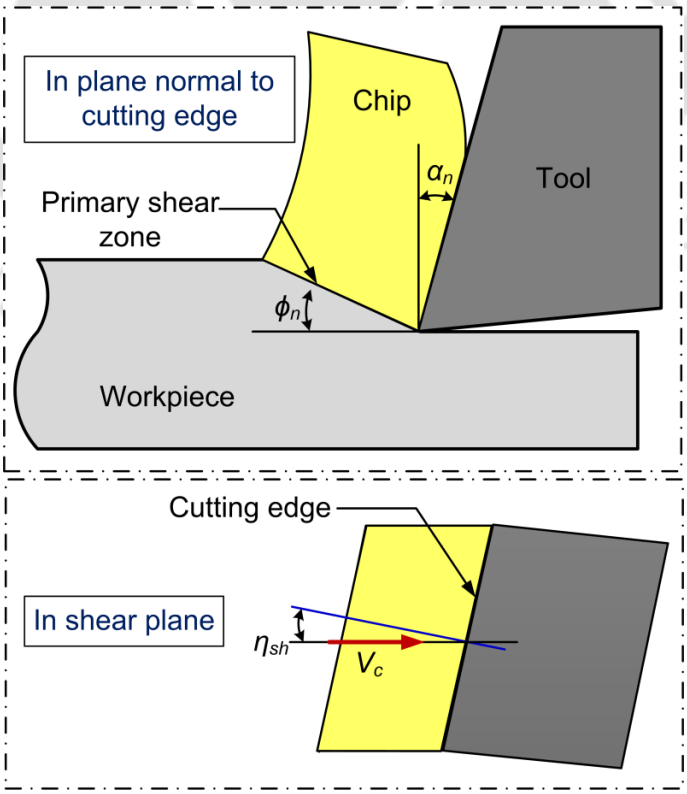

Figure 4.8 Schematic diagram of shear flow angle in oblique cutting

C. The shear flow angle (η_{sh}) takes into account the shear direction in the primary shear zone (see Figure 4.8). The shear flow angle can be determined as a function of chip flow angle (η_c), normal shear angle (ϕ_n), normal rake angle (α_n) and the inclination/helix angle (λ_s).

As per Moukfi et al. (2004), the shear flow angle is determined by analyzing the geometric relationship between chip flow angle, shear angle, normal rake angle and the inclination angle. It is given by using the following correlation:

$$\tan(\eta_{sh}) = \left[\frac{\tan(\eta_c) \cdot \sin(\phi_n) - \tan(\lambda_s) \cdot \cos(\phi_n - \alpha_n)}{\cos(\alpha_n)} \right] \tag{4.15}$$

where η_c is chip flow angle. Alternatively, the chip flow angle can be related to the shear flow angle by:

$$\tan(\eta_{sh}) = \left[\frac{\tan(\lambda) \cdot \sin(\eta_c)}{\tan(\lambda) \cdot \cos(\eta_c) \cdot \sin(\phi_n - \alpha_n) - \cos(\phi_n - \alpha_n)} \right] \tag{4.16}$$

Thus Equations (4.15) and (4.16) can be solved simultaneously to determine the chip flow angle.

D. During the metal cutting operation, a considerable amount of heat is generated. It is mainly due to the plastic deformation that occurs along the shear plane and the friction between the tool and the workpiece. Excessive heat affects tool life, part surface quality, and chip morphology. Increase in the temperature softens the work material and helps in smoother material removal. However excessive rise in temperature deforms the workpiece and the tool which affects the machining accuracy. Cutting temperature also reduces the tool hardness and makes the tool susceptible to wear and damage. It also significantly influences the morphology of the cut chips. Therefore, incorporation of cutting temperature in the milling force model is important to make it more realistic. Moreover, a study on the distribution of cutting temperature into the workpiece, cutting tool and chips helps in proper selection of milling parameters.

E. In a typical metal cutting operation, three regions of heat source can be distinguished. These are shown in Figure 4.9. The first heat source region (S1) occurs at the shear plane which is due to intense plastic deformation. The shear plane temperature influences the flow stress of workpiece material and temperature on the tool rake face. The frictional heat at the tool-chip interface generates the

second heat source (S2). Since the chip is in contact with the rake face, maximum temperature is experienced by the rake face which leads to tool wear and in turn damages the cutting tool. The third heat source (S3) is due to the contact between the workpiece and tool flank face. Literature reports research works by Hahn (1951), Loewen and Shaw (1954), Trigger and Chao (1951), Boothroyd and Knight (1989), Kronenberg (1996), Komanduri and Hou (2001) on the determination of cutting temperature during metal cutting process.

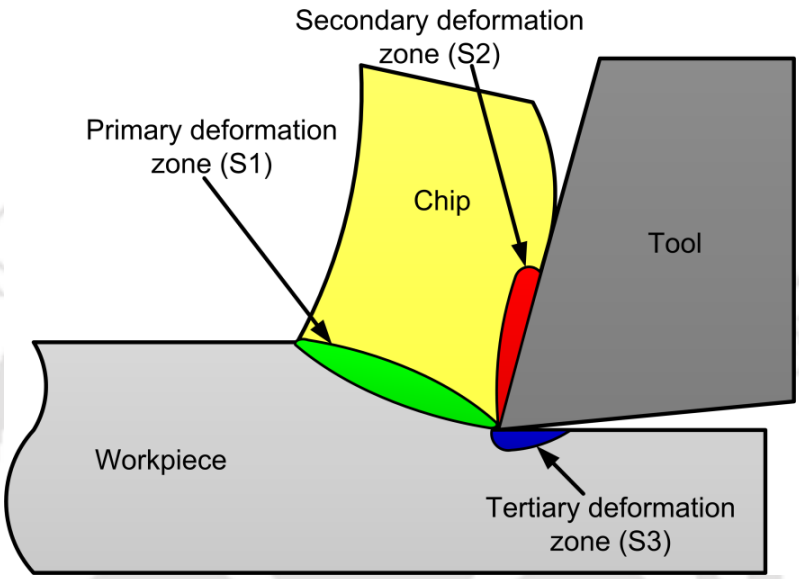

Figure 4.9 Locations of heat sources in metal cutting

Some of these formulations assume that entire plastic deformation takes place at the shear plane and the heat generated is consumed at the shear plane. But in reality, a portion of the heat generated due to the cutting action in the primary deformation zone is conducted into the workpiece whilst the remaining portion is conducted into and convected along the sheared chip. To accurately model the heat flow, the heat generated has to be partitioned carefully between the workpiece and chip. The heat partition is influenced by various factors viz. cutting parameters, material parameter and tool geometry parameters such as shear angle, normal rake angle, cutting speed, density of workpiece, thermal conductivity, uncut chip thickness and heat capacity (Artozoul et al. (2015), Puls et al. (2016)).

In the present work, the average cutting temperature in the primary shear zone is determined based on Oxley's energy partition function (Altintas, 2000).

$$T_c = T_{room} + \frac{\lambda_h \cdot (1-\lambda_s) \cdot \tau_s \cdot \cos(\alpha_n)}{\rho \cdot c_p \cdot \sin(\phi_n) \cdot \cos(\phi_n - \alpha_n)} \tag{4.17}$$

where λ_h is a factor which considers the plastic work done outside the thin shear zone and λ_w is the heat conducted into the work material. The fraction of heat conducted into the work material λ_s, is evaluated using:

$$\begin{cases} \lambda_w = 0.5 - 0.35\log(R_T \cdot \tan(\phi_n) \text{ for } 0.04 \le R_T \cdot \tan(\phi_n) \le 10 \\ \lambda_w = 0.3 - 0.15\log(R_T \cdot \tan(\phi_n) \text{ for } R_T \cdot \tan(\phi_n) \ge 10 \end{cases} \tag{4.18}$$

where R_T is a non-dimensional thermal number which depends on the workpiece thermal properties like density (ρ_m), specific heat (C_p) and thermal conductivity (k_t) and cutting conditions like cutting speed (V_c) and uncut chip thickness (h).

$$R_T = \frac{\rho \cdot C_p \cdot V_c \cdot h}{k_t} \tag{4.19}$$

Based on the expressions from 4.10 to 4.19, shear flow stress has been computed and it was further used to compute the milling forces.

4.3.4 Determination of Milling Force Coefficients

After the determination of shear stress, the milling force coefficients were determined. As stated earlier (Section 4.3: Equations 4.1 and 4.2), the force components in oblique cutting can be divided into two parts. The first component considers the shearing mechanism and the second takes into account the rubbing and ploughing effects. Collectively K_{tc}, K_{rc}, K_{ac}, K_{te}, K_{re}, and K_{ae} are called the milling force coefficients. The coefficients based on the shearing mechanism are termed as shearing coefficients and the coefficients based on rubbing and ploughing effects called as edge coefficients. The force components which account for the shearing at primary deformation zone are represented by tangential (K_{tc}), radial (K_{rc}), and axial (K_{ac}) shearing force coefficients. The second force components account for shearing action in tertiary deformation zone at the flank of the cutting edge due to ploughing, friction or rubbing actions. These are represented by tangential (K_{te}), radial (K_{re}), and axial (K_{ae}) edge force coefficients respectively.

Based on the transformation proposed by Armarego (2000) for an oblique cutting geometry, the total force components can be expressed in the form:

$$F_t = f_t \cdot h \cdot \left[\frac{\tau_s}{\sin(\phi_n)} \cdot \frac{\cos(\beta_n - \alpha_n) + \tan(\lambda_s) \cdot \tan(\eta_c) \cdot \sin(\beta_n)}{\sqrt{\cos^2(\phi_n + \beta_n - \alpha_n) + \tan^2(\eta_c) \cdot \sin^2(\beta_n)}} \right] + F_{te}$$

$$F_r = f_t \cdot h \cdot \left[\frac{\tau_s}{\sin(\phi_n) \cdot cos(\lambda_s)} \cdot \frac{\sin(\beta_n - \alpha_n)}{\sqrt{\cos^2(\phi_n + \beta_n - \alpha_n) + \tan^2(\eta_c) \cdot \sin^2(\beta_n)}} \right] + F_{re} \qquad (4.20)$$

$$F_a = f_t \cdot h \cdot \left[\frac{\tau_s}{\sin(\phi_n)} \cdot \frac{\cos(\beta_n - \alpha_n) \cdot \tan(\lambda_s) - \tan(\eta_c) \cdot \sin(\beta_n)}{\sqrt{\cos^2(\phi_n + \beta_n - \alpha_n) + \tan^2(\eta_c) \cdot \sin^2(\beta_n)}} \right] + F_{ae}$$

Then the three shearing force coefficients can be expressed as:

$$K_{tc} = \frac{\tau_s}{\sin(\phi_n)} \cdot \frac{\cos(\beta_n - \alpha_n) + \tan(\lambda_s) \cdot \tan(\eta_c) \cdot \sin(\beta_n)}{\sqrt{\cos^2(\phi_n + \beta_n - \alpha_n) + \tan^2(\eta_c) \cdot \sin^2(\beta_n)}}$$

$$K_{rc} = \frac{\tau_s}{\sin(\phi_n) \cdot cos(\lambda_s)} \cdot \frac{\sin(\beta_n - \alpha_n)}{\sqrt{\cos^2(\phi_n + \beta_n - \alpha_n) + \tan^2(\eta_c) \cdot \sin^2(\beta_n)}} \qquad (4.21)$$

$$K_{ac} = \frac{\tau_s}{\sin(\phi_n)} \cdot \frac{\cos(\beta_n - \alpha_n) \cdot \tan(\lambda_s) - \tan(\eta_c) \cdot \sin(\beta_n)}{\sqrt{\cos^2(\phi_n + \beta_n - \alpha_n) + \tan^2(\eta_c) \cdot \sin^2(\beta_n)}}$$

Thus in this research work by utilizing the Equation 4.21, shearing force components were determined.

Literature depicts that no single straightforward relationship exists to determine edge force coefficients. Researchers determined the force coefficients by carrying out orthogonal cutting experiments (Budak et al. (1996)), slot milling tests (Altintas (2000), Wang and Zheng (2002)) or arbitrary radial immersion tests (Gradisek et al. (2004)). It was noticed that to employ these approaches it is essential to conduct a number of cutting tests which may be time consuming and tedious. Thus it was thought appropriate to develop a simple way to determine the edge force coefficients. In view of this, in the present work, a finite element method (FEM) based simulation was carried out to determine the three edge force coefficients. In general, two-dimensional (2-D) or three-dimensional (3-D) mode of FEM simulation can be used to determine the edge coefficients. However, in view of better computational efficiency, in the present work, 2-D mode of FEM simulation was used to compute the edge force coefficients. The FEM based procedure to obtain these coefficients is presented as below.

Figure 4.10 shows the meshed models of the cutting tool, workpiece and the applied boundary conditions. Arbitrary Lagrangian-Eulerian (ALE) based FEM formulation was developed to simulate the orthogonal cutting. The workpiece was fully constrained at its bottom edge. The tool was modeled as a rigid body due to its relatively

high stiffness. The tool was constrained in the Y-direction, while the translational motion was allowed in negative X-direction. Details about the material properties and material flow are already provided in Section 3.6. The entire workpiece was defined as an adaptive mesh domain. The chip-tool interaction was defined using modified Coulomb friction model. (For more details see Section 3.9). The 2-D domain was meshed using four-node bilinear iso-parametric quadrilateral elements (CPE4R) under plane strain assumption. The workpiece was meshed with 9000 elements while the tool was meshed with 984 elements. Extensive simulations were carried out by varying the feed and then cutting force components were recorded.

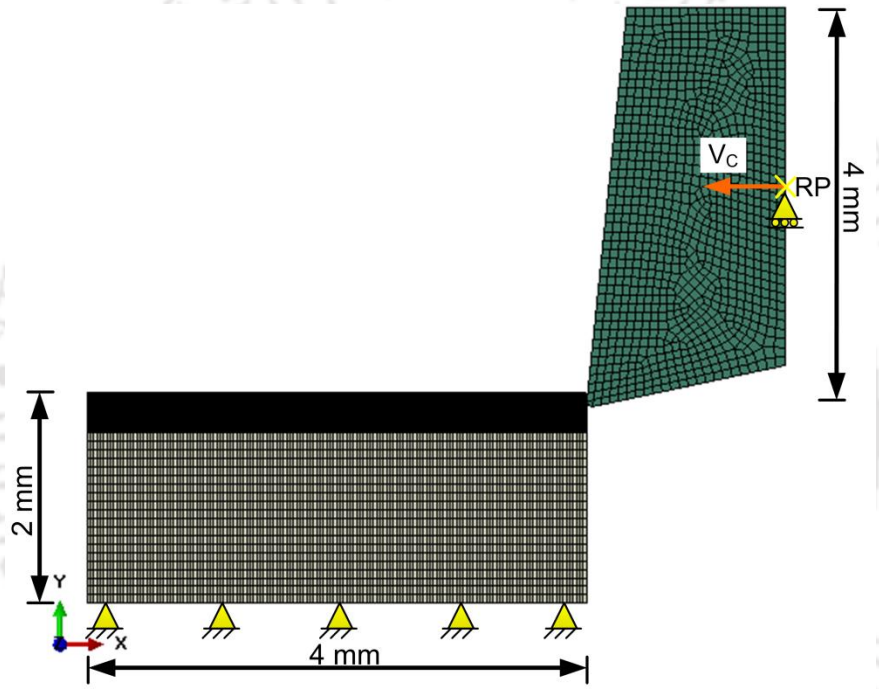

Figure 4.10 2-D FEM simulation model to determine edge coefficients

The simulated force components (F_t and F_r) were plotted against the feed values. The force components were linearly fitted to obtain the edge forces F_{te} and F_{re} by extrapolating the fit to zero feed (Altintas 2000). Based on the edge forces determined, the edge force coefficients are calculated using the relationships given by Equation 4.22 for unit cut width (in Z-direction).

$$K_{te} = \frac{F_{te}}{b_w}$$
$$K_{re} = \frac{F_{re}}{b_w} \qquad (4.22)$$

The value of axial edge coefficient K_{ae} is usually very small and is generally considered

to be zero (Armerego and Whitefield (1985)).

4.3.5 Determination of Milling Forces

After the determination of force coefficients obtained by employing the equations 4.21 and 4.22, the force components were derived. The forces acting along tangential, radial and axial directions acting on a differential flute element with height *dz* are given by Equation 4.23 (Altintas (2000)).

$$\begin{aligned} dF_t(\theta,z) &= [K_{te} + K_{tc}\cdot h(\theta,z)]\cdot dz \\ dF_r(\theta,z) &= [K_{re} + K_{rc}\cdot h(\theta,z)]\cdot dz \\ dF_a(\theta,z) &= [K_{ae} + K_{ac}\cdot h(\theta,z)]\cdot dz \end{aligned} \tag{4.23}$$

The elemental force components can be calculated by using the six force coefficients along with the values of uncut chip thickness *h(θ, z)* and elemental thickness *dz* for the chosen process conditions and tool-work material pair.

By using Equation 4.24, elemental oblique forces in the local co-ordinate system were transformed to the global co-ordinate system (X-Y-Z). Finally, the total force along the normal (X), feed (Y) and axial (Z) directions acting on the tool was obtained by integrating the elementary force components (dF_x, dF_y and dF_z) along the axial direction *z*. For this developed analytical model a computer code has been written in MATLAB R2013b.

$$\begin{bmatrix} dF_x \\ dF_y \\ dF_z \end{bmatrix} = \begin{bmatrix} \sin\theta & -\cos\theta & 0 \\ \cos\theta & \sin\theta & 0 \\ 0 & 0 & 1 \end{bmatrix} \begin{bmatrix} dF_t(\theta,z) \\ dF_r(\theta,z) \\ dF_a(\theta,z) \end{bmatrix} \tag{4.24}$$

A case study on the computation of milling forces based on the developed methodology is presented in a later section. The computations are duly validated with the experimental results. These milling forces are useful in the estimation of energy requirement during a metal cutting operation. Moreover, the forces can be employed in prediction of deflection of thin-wall during helical end milling operation. For this purpose, 3-D finite element based simulations were carried out. The forces computed by using proposed analytical-numerical modeling were employed to compute in-situ wall deflection. Details about the same are presented in the next section.

4.4 Prediction of In-situ Wall Deflection during End Milling of Thin-Wall Parts using 3-D FEM based Simulations

In this work, three-dimensional FEM based simulations were carried out to predict in-situ deflection of a thin-wall during metal cutting operation. Figure 4.11 gives an overview of wall deflection prediction methodology. Initially, the milling force values have been calculated by employing the methodology described in the previous section (Section 4.3) for chosen set of process parameters such as feed rate, cutting speed, axial and radial depth of cut and tool geometry parameters. These forces were then inputted into the 3-D simulation model to compute the deflection.

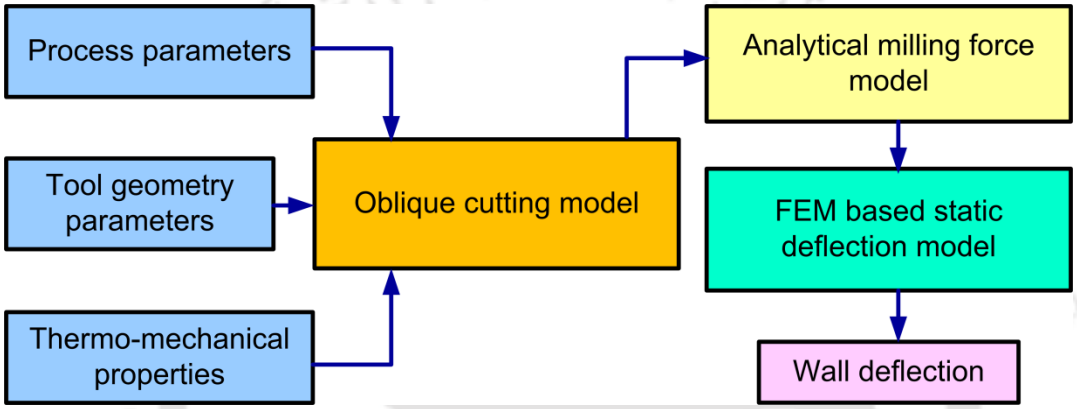

Figure 4.11 Deflection prediction methodology

A solid CAD model of the thin-wall workpiece was developed and imported into the FEM solver Abaqus/Explicit. The workpiece geometry was meshed by using C3-D8R type finite element. Figure 4.12 shows the meshed workpiece geometry and applied boundary constraints. It is to be noted that the 3-D solid model has been developed by considering the cut portion of the wall due to the previous location of cutting tool with respect to the wall. That means the geometry of process continuum has been developed by considering the already cut portion of the wall. The cutter contact zone has been modeled in such a way that the wall thickness is gradually reduced by considering the radial depth of cut. In this way, the wall deflections have been computed at various intermediate points along the tool path, by modeling the realistic geometries of the work parts. Then necessary material properties were provided as input to the model (see Section 3.6). During the complete machining simulation run, the cantilever thin-wall base was encastred while other surfaces were free to move.

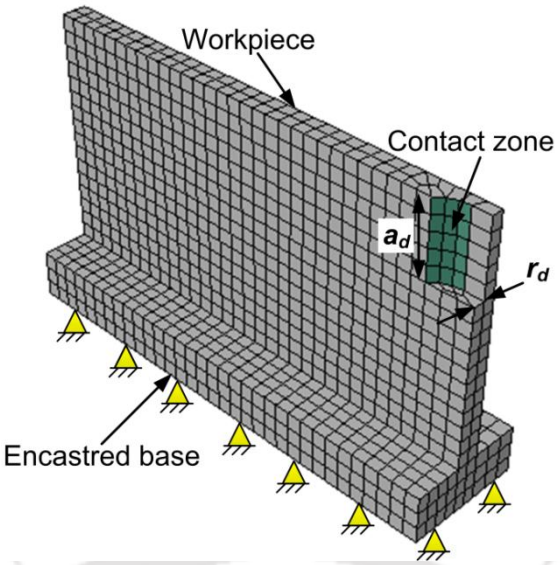

Figure 4.12 Meshed wall structure clamped at bottom end

During the simulation, the tool path along the feed direction was divided into a number of steps. Each step represents the position of the tool along the feed direction. The load is applied on the transition region. Transition region is a contact zone between the cutting tool and the workpiece. Its area varies according to the cutter geometry and feed (radial, axial) parameters. The milling forces computed from the analytical model were applied in the direction normal to the curved transition region (green color Figure 4.12). Based on the requirement, one can compute the thin-wall deflection at various transition regions/contact zones. However, in the present 3-D simulation, the deflections have been computed at five transition zones along the length of the wall. These locations are equidistant to each other and are at the top of the wall. Milling parameters were set and then the wall deflection was predicted. This methodology has been demonstrated by considering a case study in the next section.

4.5 Case Studies on the Computation of Thin-Wall Deflection using the Developed Integrated Model

In this section, a demonstration on the computation of thin-wall deflection using the proposed approach has been presented. For this purpose, four different sets of process conditions were chosen. These are listed in Table 4.2. The tests were conducted in down-milling mode.

Table 4.2 Milling parameters for test cuts

Cutting parameters	Test No.			
	1	**2**	**3**	**4**
d_i **(mm)**	8	12	4	12
f_z **(mm/z)**	0.06	0.04	0.02	0.04
a_d **(mm)**	8	24	8	12
r_d **(mm)**	1.25	0.625	0.3125	1.25

For the chosen process conditions (Table 4.2), values of thin-wall deflection were computed by using the developed integrated analytical-numerical approach. The predicted results were validated by using our own experimental data. The deflections have been computed by following the below-mentioned procedure.

- Input the milling parameters.
- Determine the shear coefficients by using equation 4.21.
- Obtain the edge force coefficients by using 2-D FEM based numerical simulations. For this purpose, cutting simulations were carried to obtain the cutting force components under various feed per tooth (uncut chip thickness) conditions which are listed in Table 4.3. FEM simulations were carried out over a wide range of feed per tooth (uncut chip thickness).

Table 4.3 Feed values for 2-D FE simulation to determine edge coefficients

Run No.	**1**	**2**	**3**	**4**	**5**	**6**	**7**
f_z **(mm/z)**	0.03	0.05	0.07	0.09	0.11	0.13	0.15

Figure 4.13(a, b) show the formation of cut chip with von Mises stress plot and convergence of cutting forces for a chosen process condition with feed per tooth of 0.15 mm/z. Similarly, 2-D cutting simulations were carried out for various feed values as mentioned in Table 4.3 and the plots of cutting force components against the feed values were obtained. These plots are shown in Figure 4.14. It can be seen that a linear relationship exists between the forces and feed per tooth. The required edge force components were obtained by extrapolating the fit of edge forces F_{te} and F_{re} to zero feed. In other words, the edge force components F_{te} and F_{re} are the intercepts of the force-feed plot with y-axis; it means the value of the force at zero uncut chip thickness. The edge force coefficients were calculated based on Equation 4.24; where the width of cut was

considered as 1 mm.

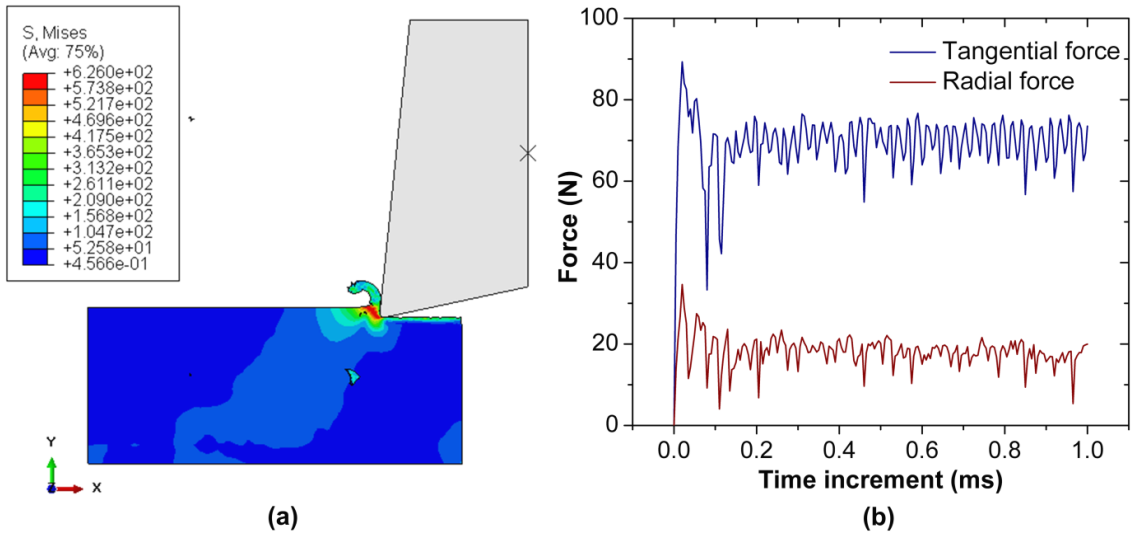

Figure 4.13 (a) 2-D FE simulation, **(b)** Tangential force and radial force components for V_c = 88 mm/min (3500 r/min) and f_z = 0.15 mm/z

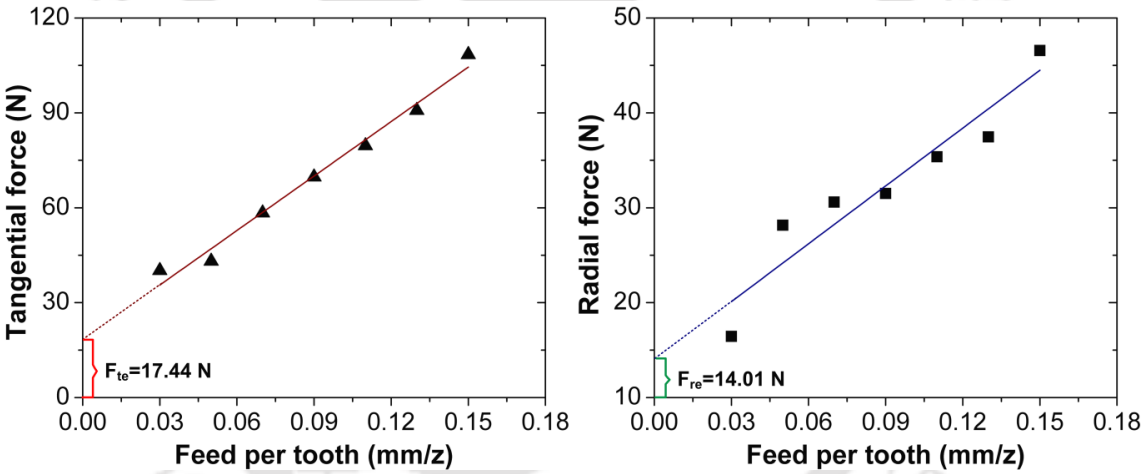

Figure 4.14 Cutting force components measured during orthogonal cutting simulations

Finally the milling forces were computed by using the shear force components and edge force components using Equations 4.21 to 4.24.

After the computations, the predicted force values were duly verified by conducting in-house cutting experiments. For each trial an unused (new) end mill with equal pitch was employed. The end milling cutter was having 8 mm diameter, 45° helix angle and 8° rake angle. A dynamometer fixed onto the table of the machining center (CNC-VMC) was used to measure the three force components. The experimental details are similar as stated in Chapter 3, Section 3.11.

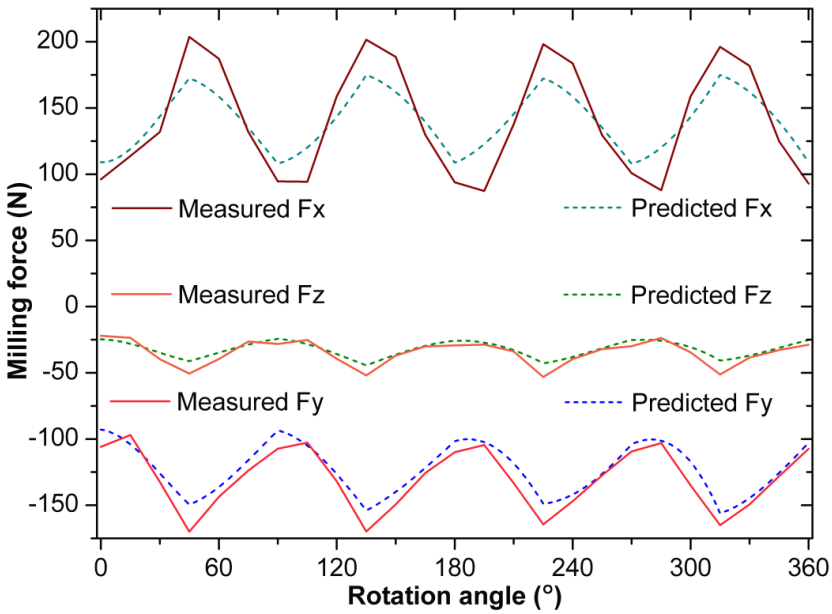

Figure 4.15 Comparison of measured and predicted milling forces for test case 1: n_s = 3500 r/min, d_i = 8 mm, f_z = 0.06 mm/z, a_d = 8 mm, r_d = 1.25 mm

Figure 4.15 shows the comparison of milling force components in X, Y and Z directions obtained by the proposed integrated analytical model and measured by conducting experiments. Force component F_x is normal to the workpiece and F_y is along the feed direction and F_z is along the tool axis. It can be seen that the magnitude of the force component *Fx* is higher in comparison to F_y. This is due to the increase in the frictional force between the tool flank and the workpiece. From the comparison, it was noted that the predicted force values are in good agreement with the experimental results with absolute errors of 5.36, 7.33 and 11.13% in F_x, F_y and F_z directions respectively. The trends of variation of the computed results were noted to be very well matching with the experimental results.

Similar to Case 1, the computed force components for case 2, 3 and 4 were verified with the experimental results. Table 4.4 shows the prediction errors of milling force components for all four test cases listed in Table 4.2. Moreover, comparison plots between the milling forces and respective experimental results are shown in Figure 4.16. It can be seen that the milling forces are in good agreement with the experimental results for all cases. The maximum absolute errors between the predicted and measured values were 13.12%, 9.51% and 29.9% for F_x, F_y and F_z components. This indicates that the proposed approach can be applied with confidence to compute the wall deflection using the 3-D FEM based simulation. Moreover, it is simple, quicker and cost effective in comparison with the FEM 3-D numerical model and experimental method of study.

Table 4.4 Comparison of the error between the predicted and measured average values of milling force components for four test cases listed in Table 4.2

Test case		Milling force components		
		F_x	F_y	F_z
1	**Predicted (N)**	139.62	121.35	32.10
	Measured (N)	147.53	130.96	36.12
	Absolute error (%)	5.36	7.33	11.13
2	**Predicted (N)**	212.3	180.53	22.33
	Measured (N)	184.43	163.36	31.86
	Absolute error (%)	13.12	9.51	29.9
3	**Predicted (N)**	82.65	73.72	9.67
	Measured (N)	88.78	67.89	13.27
	Absolute error (%)	6.90	7.90	27.12
4	**Predicted (N)**	154.93	134.50	21.42
	Measured (N)	177.8	141.63	25.98
	Absolute error (%)	12.86	5.03	17.55
	Mean error (%)	**9.56**	**7.44**	**21.48**

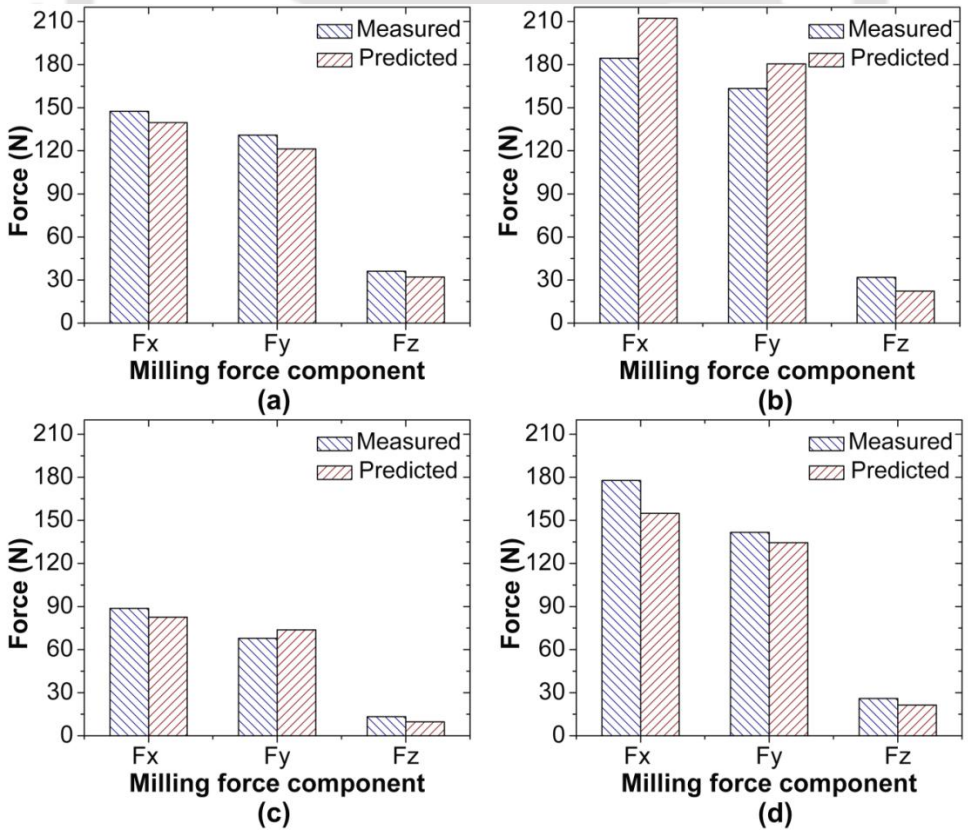

Figure 4.16 Comparison of experimental and simulated milling force components for cases listed in Table 4.2

Considering all test cases, the mean prediction errors F_x, F_y and F_z were noted to be 9.56%, 7.44% and 21.48% respectively.

After the computation of milling forces, 3-D numerical simulations were carried out to predict the in-situ wall deflection. The workpiece was modeled as a cantilever part with overall dimensions of length 50 mm, height 25 mm and thickness of 2.5 mm. To account for the cut portions due to previous full or partial cutting, the thickness of the wall was varied. Figure 4.17 shows three solid geometries those were considered to compute the deflections at the start, middle and end of a cutting pass for test case 1: spindle speed (n_s) of 3500 r/min, feed per tooth of 0.06 mm/z, axial and radial depth of 8 mm and 1.25 mm respectively. The computing milling force values by our analytical model were provided as input loads to the 3-D FE wall deflection model and wall deflections were computed by solving the problem using Abaqus/Explicit FEM solver. Figure 4.17 also shows the deflection contours of the workpiece at three tool positions.

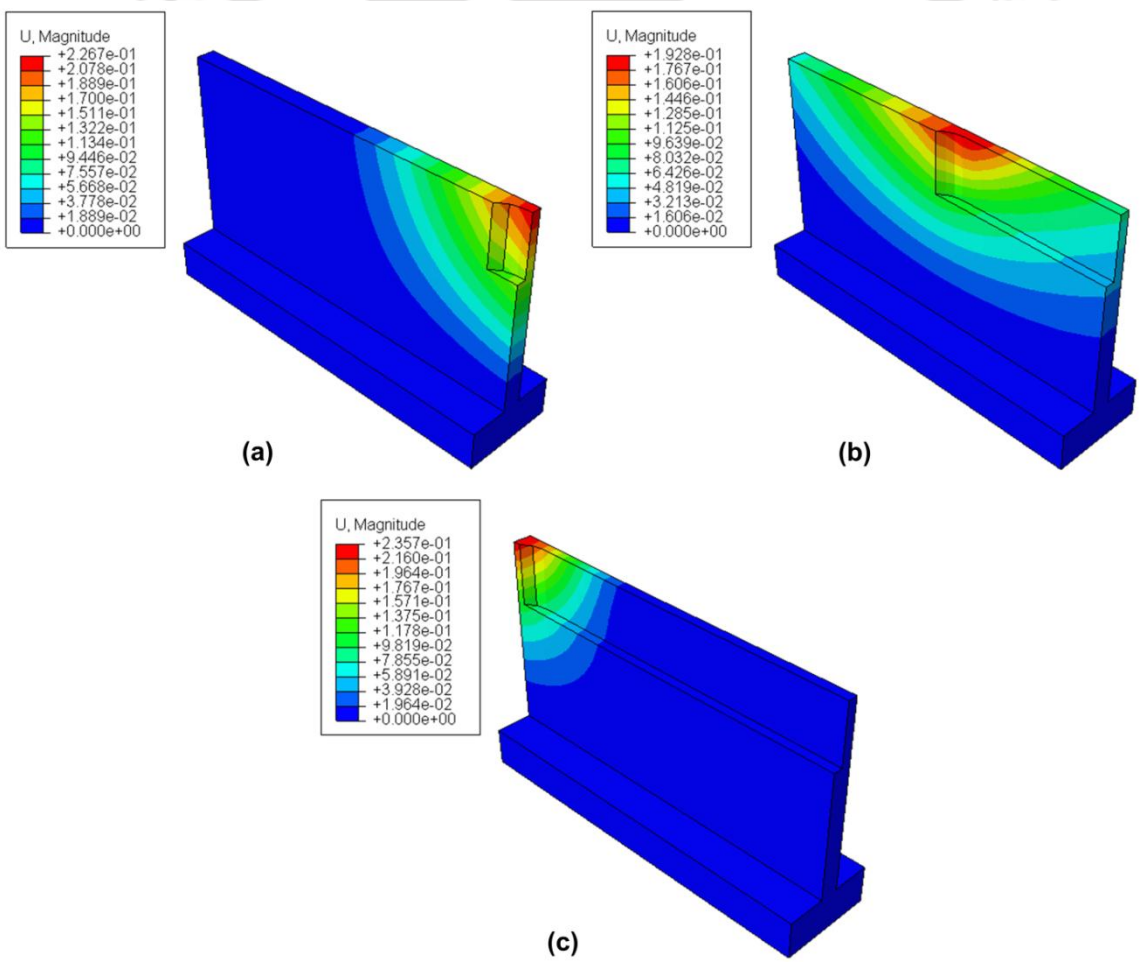

Figure 4.17 FE based deflection prediction for test case 1: **(a)** At the starting location of the wall, **(b)** At the middle of the wall, **(c)** At the end of the wall

Moreover, in the present case study, simulations have been performed to compute the deflections at two more intermediate locations along the tool path. Thus, in this work the deflections have been predicted at five equidistant locations along the cutting path. Then the obtained results were verified by conducting actual experiments. Experiments were carried out for all four test cases and the results in terms of wall deflection were recorded by employing linear variable differential transformer (LVDT).

Figure 4.18 shows the comparison of the wall deflection predicted by the developed model and measured by the experiment for test case 1. The maximum deflection was noted to be 0.2268 mm. As the cutting progresses till the middle portion of the wall, the magnitude of the wall deflection decreases (Figure 4.17(b)). It is mainly due to the higher stiffness of wall at the middle portion in comparison that at the free-end. Further, as the machining progresses and reaches to the end, the wall thickness reduces and the magnitude of the wall deflection increases as shown in Figure 4.17(c)). In conclusion, the deflection predicted was noted to be higher at the two free ends in comparison to that of the middle portion of the wall. This is found to be very well in line with the deflection values measured from actual experiments. This can be clearly seen in Figure 4.18. The trend of variation is also fairly matching.

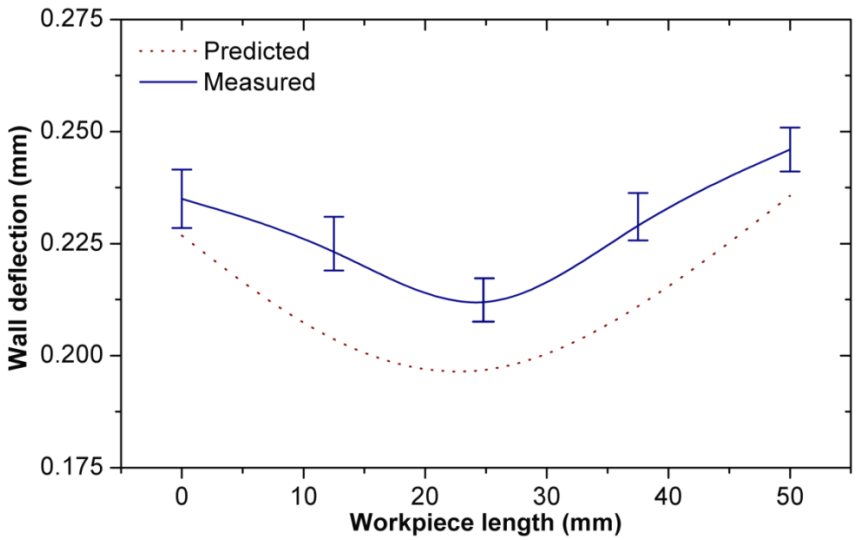

Figure 4.18 Comparison of predicted and measured wall deflection for test case 1

Figure 4.19 and Table 4.5 summarize the validation of our proposed integrated approach for all the cases. It can be seen that the deflection values predicted by our model are in good agreement with the one obtained in experiments for all test cases. Overall prediction error was found to be 9.315%. Thus it can be said that the developed

approach can be applied in practice with confidence to accurately predict the wall deflection prior to the actual thin-wall cutting. This will certainly help in enhancing the product quality by correcting the tool path, which could be an interesting and important area of research and development.

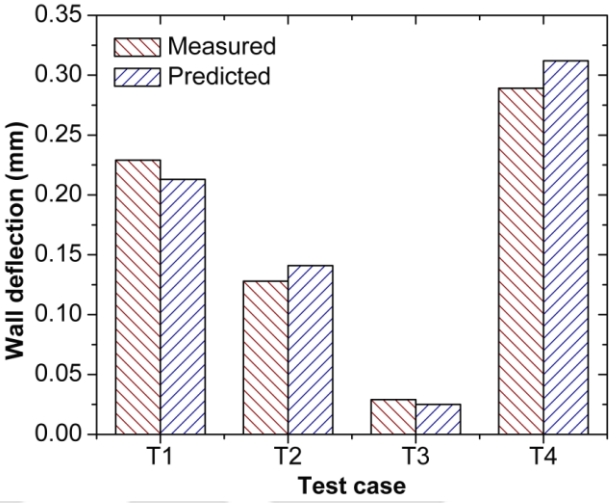

Figure 4.19 Comparison of the predicted and measured average values of wall deflection and error for four test cases listed in Table 4.2

Importantly, it is noted that the developed integrated model consumes approximately 40 minutes to predict the milling forces and instantaneous wall deflection, which otherwise might consume hundreds of hours by using 3-D FEM based numerical machining approach. Thus the integrated analytical-numerical force-deflection model has been found to be simple, efficient and realistic.

Table 4.5 Comparison of the error between the predicted and measured average values of wall deflection for four test cases listed in Table 4.2

Test case	Predicted (mm)	Measured (mm)	Absolute Error (%)	Prediction time (min)
1	0.213	0.229	6.89	40
2	0.141	0.128	9.21	40
3	0.025	0.029	13.79	40
4	0.312	0.289	7.37	40

4.6 Summary

This chapter presents the development of a simple and integrated force-deflection model for thin-wall milling process. The merits of this proposed approach lie in the utilization of unified mechanics based approach and three-dimensional finite element method based

simulation together to quickly and accurately predict the milling forces and in-situ wall deflection for chosen process condition. Unified mechanics based analytical equations have been thoroughly studied and then employed to compute the milling forces. Based on these forces, wall deflections have been computed using 3-D finite element method. The features of the proposed approach are as follows.

- The present approach considers realistic three-dimensional helical end mill geometry for the computation of milling forces.
- A thermo-mechanical oblique cutting model has been developed to determine the shear flow stress in the primary shear zone. It incorporates the modified Johnson-Cook law which is based on realistic material characteristics such as strain rate sensitivity, thermal softening and strain hardening. The model also considers the milling force coefficients.
- In this work, the shearing force coefficients those take care of primary shear deformation have been derived by using established empirical relations. The edge force coefficients those take into account the rubbing and ploughing effects have been derived by using simple and computationally inexpensive 2-D FEM model.
- The proposed methodology of employing 2-D FEM based simulation has been duly validated by using experimental results. The results in terms milling forces were found in good agreement with the experimental results. The merit of proposed approach lies in the ease of computing the milling force coefficients for chosen pair of cutting tool and workpiece material without conducting costly and time consuming experiments.
- The wall deflection has been predicted using 3-D FEM simulation model. The simulation considers the realistic geometry of the workpiece in terms of the curved transition region and cut portions due to previous tool passes. The model was able to predict the wall deflection with very good accuracy (about 9.315 % of prediction error). This error is attributed to various factors such as vibrations, friction, inhomogeneous structure of the workpiece, machining interruptions by generated chips, tool runout. These parameters are uncontrollable and it is very difficult to incorporate them into a numerical/analytical or mathematical model.
- The developed integrated model was found to be far more efficient than the 3-D FEM model which was developed initially (Chapter 3). The time duration for

prediction of the milling force and magnitude of wall deflection using the developed model reduced drastically from 344 hrs (3-D FEM model, Chapter 3) to 40 minutes.

Overall the present work provided a realistic, simple, efficient integrated approach for force-deflection prediction during helical end milling of thin-wall parts. Based on the results obtained it is felt that the developed model can be applied with confidence in practice for quick and accurate computation of in-situ wall deflection of thin-wall parts and prior estimation of energy required for machining by using the computed milling forces. However, the proposed model does not provide the information about the quality of surface machined, chip morphology which is vital in deciding the milling parameters to obtain the desired process performance. In view of this, it was thought appropriate to carry out comprehensive experimental studies on thin-wall milling operation. These are presented in the next two chapters. Then the optimal milling parameters have been obtained for efficient and quality thin-wall milling operation.

Chapter 5

Experimental Investigations into Thin-Wall Milling Process: Selection of Process Parameters and Tool Geometry Parameters

5.0 Scope

This chapter presents the results obtained during the experiments carried out on machining of thin-wall workpieces made of aluminum alloy 2024-T351. First, the need to carry out physical experiments is defined. The details of experimental procedure are elaborated in the following section. Then the response measurement methodologies are depicted. The rationale behind the selection of milling parameters, in particular the process parameters and tool geometry parameters are explained. Detailed discussions on the influence of process parameters such as spindle speed, feed per tooth, radial depth of cut, axial depth of cut on milling forces, surface roughness and magnitude of wall deflection have been presented. Moreover an investigation into the influence of tool geometry parameters on the process performance is carried out using grey relation analysis (GRA). Finally, the most influential parameters based on the experimental results are selected for further studies.

5.1 The Need

Economical and precise machining of thin-wall parts is the primary objective of present research work. As mentioned in the previous chapters, obtaining good quality surface, accurate part dimensions, efficient removal of large amount of (90-95%) of bulk material are the main challenges during thin-wall machining. Enhancement in productivity i.e. increase in material removal rate is generally achieved by employing maximum possible levels of process parameters viz. spindle speed, depth of cut and feed rate. However machining at these high levels often produces dimensionally inaccurate thin-wall parts with poorer surface quality. Aluminum alloys possess comparatively low modulus of elasticity which causes the workpiece to spring back. This spring back action often results in deflection and chatter. Chatter affects the material removal rate and leads to poor surface finish which again might lead to part rejection, increase in cost and loss of productivity. Therefore selection of proper levels of milling parameters is very crucial as they influence the milling forces, surface finish, dimensional accuracy and material removal rate. A need was thus identified to carry out systematic experimental study to

determine the influence of milling parameters on process response parameters, viz. milling force, wall deflection, surface quality, chip morphology and material removal rate during thin-wall machining of aluminum alloy 2024-T351.

As discussed in the previous chapters, analytical and numerical investigations into the thin-wall machining helped in understanding the complex interaction between cutting tool and workpiece. Also these studies can help in determining the milling forces and wall deflection during thin-wall machining process. However mathematical modeling of uncontrollable parameters such as imperfections in machine tool and cutting tool structures, errors in setting of cutting tools, deformations in the structure of machine tool such as spindle, workpiece fixtures, and material inhomogeneity is difficult. Moreover, requirement of huge computation time (in days) beset the application of numerical 3-D FEM based approaches in practice. In view of this, it was felt worth to carry out systematic and comprehensive experiments to determine proper levels of milling parameters to obtain desired process performance. Also, it was noted from the literature review that, very scant studies have been reported on obtaining optimal values of tool geometry parameters that influence the thin-wall machining process. These are presented in this and subsequent chapters in detail.

5.2 Experimental Procedure

In the present work, experimental studies have been carried out to determine the performance characteristics in thin-wall machining process. Figure 5.1 illustrates the step-by-step experimental procedure that followed in this study. Basically the experimental study was carried out in three phases.

1. In the first phase, a systematic study of published literature has been carried and based on this; the ranges of process parameters have been selected.
2. In the second phase, experiments were carried out to study the influence of tool geometry parameters on the responses.
3. Third phase involves extensive experiments to determine the influence of selected milling parameters on important responses on thin-wall machining. Once the experiments were carried out, the recorded response data were carefully analyzed to determine the proper levels of milling parameters. Further the data obtained during the third phase of experiments were used to develop mathematical models (more details are provided in Chapter 6).

In the coming sections, the details of experiments in terms of experimental setup, workpiece preparation, cutting tool selection, process responses measurement and experimental methodologies are presented one-by-one.

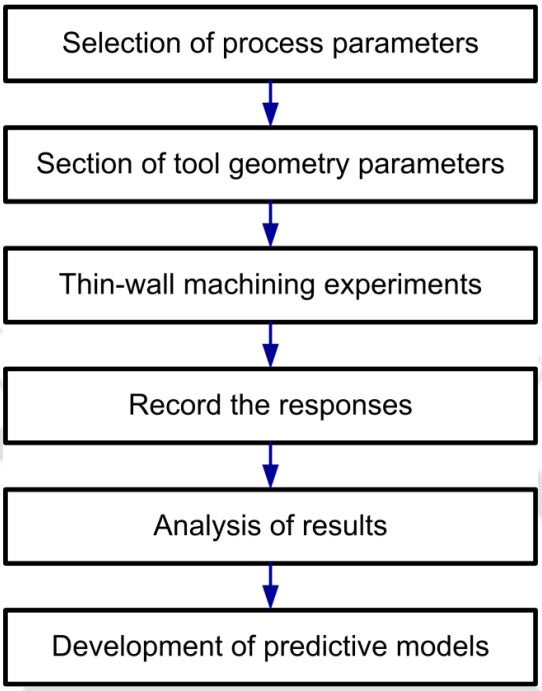

Figure 5.1 Detailed experimental procedure

5.3 Experimental Setup

Experiments were carried out on a three-axis CNC vertical machining center (VMC) *(PMK India make, Model: MC-3/400*) with spindle power of 5.5kW as seen in Figure 5.2. Specifications of the VMC are listed in Appendix A5.1. Figure 5.3 provides the details of the experimental setup. The work specimens were mounted on custom made work holder which was housed on a dynamometer. The dynamometer was screwed rigidly onto a base plate which was clamped to the machine work table.

Figure 5.2 CNC vertical machining center (VMC)

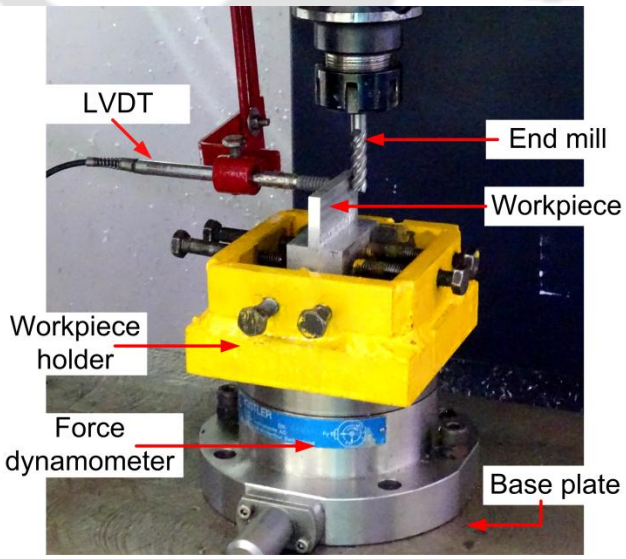

Figure 5.3 Experimental setup for thin-wall milling

5.4 Workpiece Material

Aluminum alloys are widely used in aerospace, automobile, electronics manufacturing industries to manufacture critical components such as aircraft wings structures, pan engine blocks, steering components, instrument panels, Heat sinks, housings for electronic equipments, etc. (Starke and Staley (1996), Miller et al. (2000)). In this work, aluminum alloy 2024-T351 an aerospace grade commercial alloy has been used for conducting the experiments. It is an Al–Cu–Mg alloy and it is solution heat-treated, control stretched and naturally aged. The alloy possesses high strength, low density and good fatigue resistance and is widely used in aircraft wings and fuselage structures. The chemical composition of the alloy is listed in Table 5.1

Table 5.1 Chemical composition of A2024-T351 (Bussu and Irving (2003))

Element	Si	Fe	Cu	Mn	Mg	Cr	Zn	Ti	Others	Al
Composition	0.5	0.5	3.8-4.9	0.3-0.9	1.2-1.8	0.1	0.2	0.5	0.15	Rem.

Specimens prepared for conducting the experiments are shown in Figure 5.4. Initially the blocks cut from the raw material were milled to the desired dimensions and then the experiments were carried out to reduce the thickness of the wall from 2.5 mm to the desired dimension of 1.25 mm. The present study mainly focuses on an experimental analysis of finishing operation. The roughing operation has been performed by applying regular cutting parameters. These process conditions are provided in Appendix A5.2.

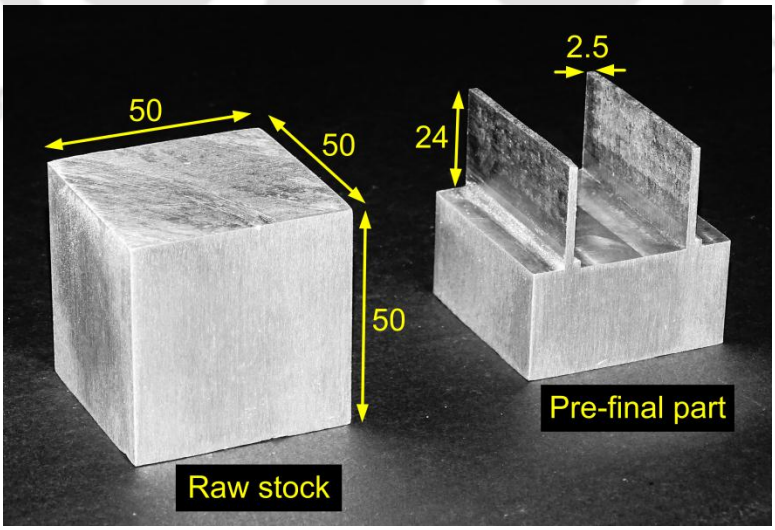

Figure 5.4 Initial and pre-final specimen geometry

5.5 Cutting Tools

The experiments were conducted using solid carbide flat-bottom end mills. Tungsten carbide is a cemented carbide material that composes of tungsten carbide powder (70-97%) cemented with a binder material namely cobalt or nickel. It is resistant to abrasion, erosion, wear, compression, and heat; and it exhibits longevity where other materials like high speed steel (HSS) fail. Selection of cutting tool geometry parameters for carrying out the experiments is explained in Section 5.9.

5.6 Measurement of Process Responses

The performance factors considered for the present investigation were surface quality, milling force, wall deflection and material removal rate. Details about the measurement methodologies of these responses are provided in the following sections.

5.6.1 Milling Force Measurement

Figure 5.5(a) depicts the three stages involved in the measurement of milling forces.

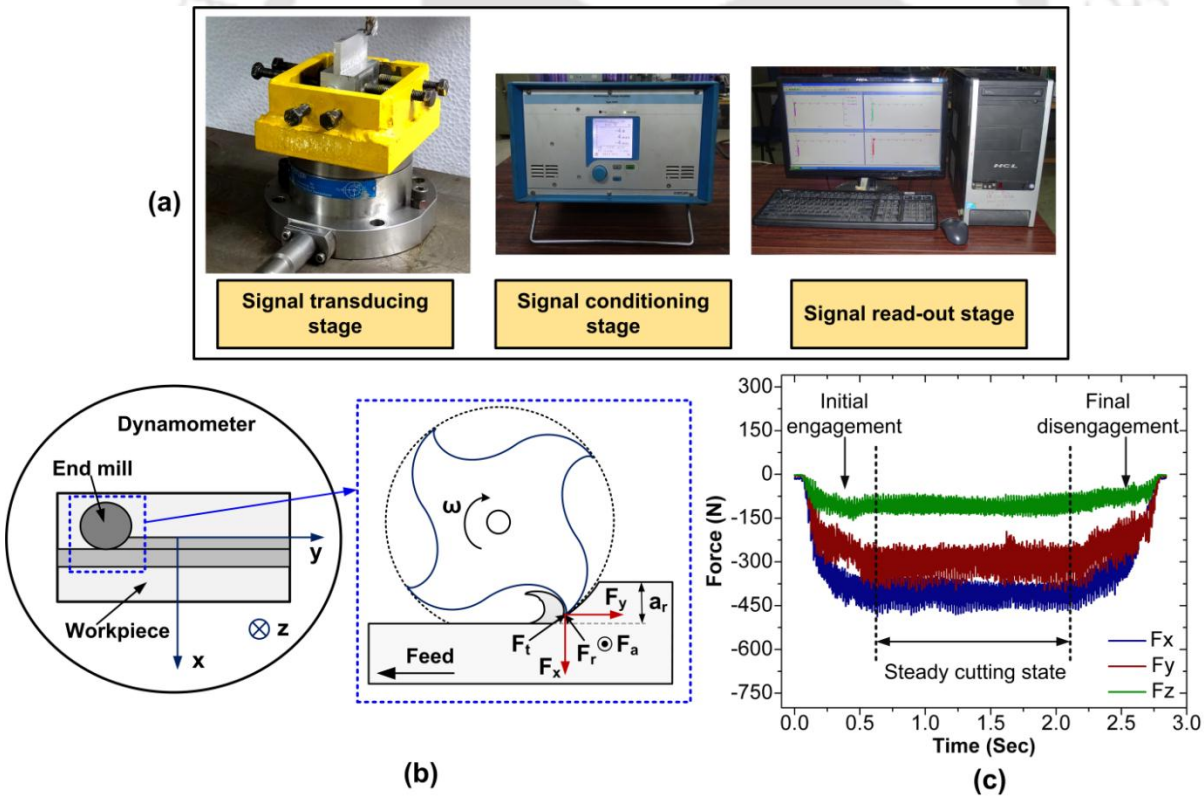

Figure 5.5 (a) Milling force measurement system, **(b)** Milling force components**, (c)** Typical milling force signal

These stages are: signal transducing, signal conditioning and signal readout. To measure the milling force components, a four-component piezoelectric based dynamometer

(*Kistler make, Model: 9272B*) having a measurement range of -5 to +5 kN was used. During the signal conditioning step, the signals of measurands were conditioned by using a multi-channel charge amplifier (*Kistler make, Model: 5070A*) which converts the electrical charge produced by piezoelectric sensors into a proportional voltage signal. The data sampling rate was set at 2000 Hz/Channel. For signal readout, an USB type data acquisition and analysis software (*DynoWare: 2825A*) which facilitates continuous recording and graphical visualization of the force data was used. The force signals were measured for a cutting time of 15 s. The specifications of the force dynamometer are listed in Appendix A5.3.

Three milling force components viz. F_x (cutting force), F_y (feed force) and F_z (thrust force) were measured based on the dynamometer specified reference system as shown in Figure 5.5(b). In this work, the resultant milling force (F_c) obtained by using the three measured quantities of force components (F_x, F_y and F_z) was considered to study the influence of input milling parameters. The data were processed through the data acquisition system and stored in a computer. During the data evaluation step, signal drift compensation was carried out to take care of any undue changes in ambient temperature. The inferences were obtained by studying the average values of the milling forces recorded in the steady cutting state (see Figure. 5.5(c)).

5.6.2 Surface Roughness Measurement

Surface roughness (R_a) of the machined components was measured in offline mode i.e. after the completion of machining operation. It was measured along the feed direction using an optical profilometer. It is a non-contact type, high precision white light interference microscope (*Taylor–Hobson*) with an objective lens of 20× magnification and focal distance of 4.7 mm. The specifications of the optical profilometer are listed in Appendix A5.4. Figure 5.6(a-c) shows various stages of measurement methodology of surface roughness by using optical profilometer. During the process of measurement, the objective lens unit was moved along the z-axis and focused onto the workpiece surface. Measurements were carried out at seven different zones as shown in Figure 5.6(d) and the average of these measurements was considered for further analysis. The data was collected and analyzed using the 3-D analysis software *TalyMap*.

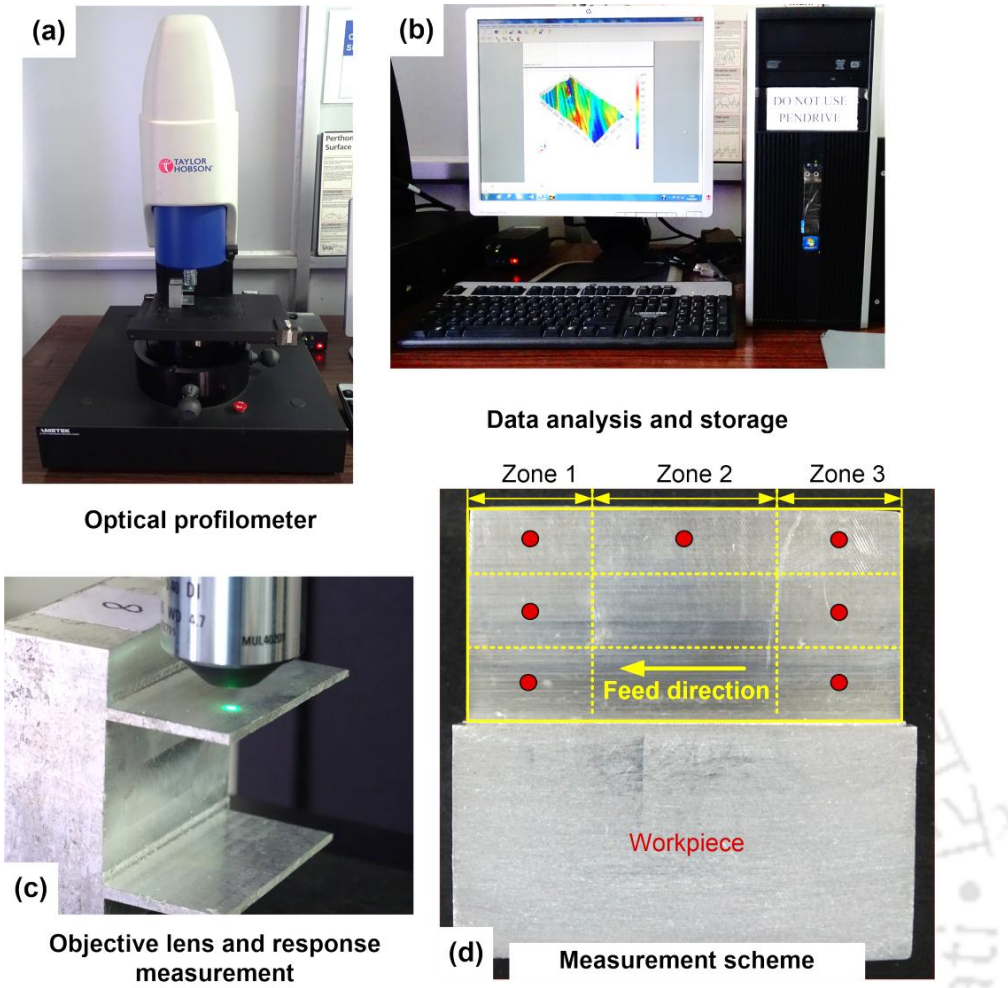

Figure 5.6 Surface roughness measurements using optical profilometer

5.6.3 In-situ Measurement of Wall Deflection

Due to low rigidity, the thin-wall workpiece deflects during the machining operation. To measure the instantaneous deflection (D_f) of the thin-wall during the actual machining, a linear variable differential transformer (LVDT) was used (see Figure 5.7(a)). The LVDT (*Solartron*) was mounted on a holder attached to the machine tool spindle. It records the instantaneous wall deflection when the work table moves with respect to the tool spindle.

Readings were noted using a digital display (*Solartron C55*) as shown in Figure 5.7(b). The deflection occurring at the free end of the cantilever wall was measured as per the scheme depicted by Figure 5.7(c). The specifications of the optical profilometer and display unit are listed in Appendix A5.5 and A5.6.

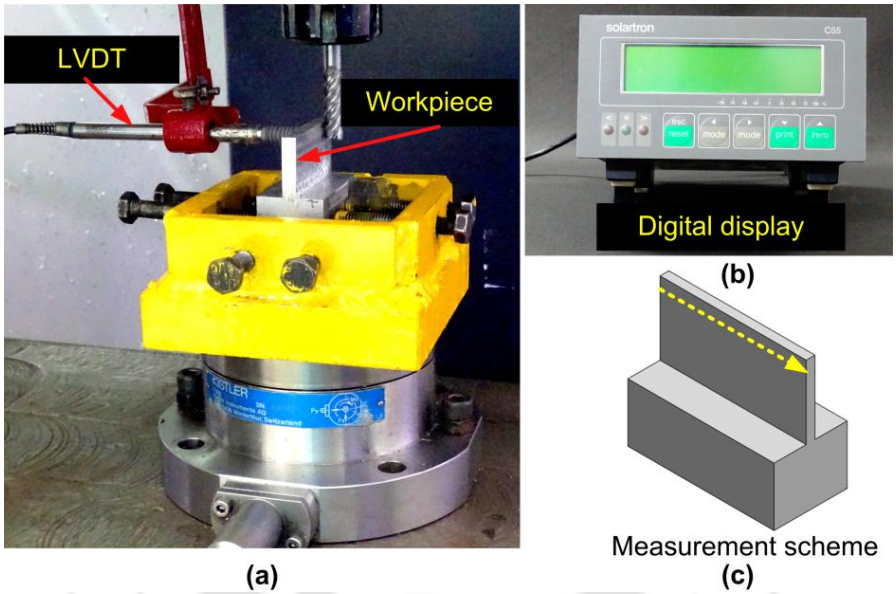

Figure 5.7 Wall deflection measurements using LVDT

5.7 Experimental Design

In this research work, experiments were carried out in three phases.

1. In the first phase, experiments were conducted to choose the proper ranges of process parameters. In this stage, initial ranges of process parameters were identified based on the available literature data in terms of research papers and machining handbooks. Then systematic experiments were conducted on the CNC-VMC located in Advanced Manufacturing Laboratory of Department of Mechanical Engineering, IIT Guwahati, Guwahati, India.
2. In the second part, extensive experiments were carried out to study the influence of end mill tool geometry parameters on the responses. The experiments were designed based on Taguchi orthogonal array scheme.
3. In the third phase of the experiments, comprehensive experiments were carried out for a detail parametric study of thin-wall milling process. For this study the most influential milling parameters that are obtained in phase 1 and 2 were employed.

In this chapter, the results of first and second phases of the experimental study are presented while the results obtained in phase 3 are presented in the next chapter.

5.8 Phase 1: Selection of the Experimental Process Parameters

Selection of proper process parameters and their respective appropriate levels is important in view of an efficient and accurate thin-wall machining process. Therefore in

this work, initially experiments were carried out to select the process parameters and their respective broad ranges that can further be fine-tuned. Various process parameters such as feed per tooth (f_z), spindle speed (n_s), axial depth of cut (a_d) and radial depth of cut (r_d) were varied and their influence on performance measures viz. milling force (F_c), surface roughness (R_a) and magnitude of deflection (D_f) was studied. In this phase, an end milling tool having a diameter of 8 mm and a helix of 35º was used to conduct the experiments. Taguchi's technique was used as it provides the quality characteristics of the process by employing minimal number of experiments (Tsao CC. (2009)). Figure 5.8 depicts the overview of the experimental work carried during the first phase to determine the influential process parameters. Experiments were designed based on L8 Taguchi orthogonal array where four parameters at two levels were chosen (see Table 5.2)

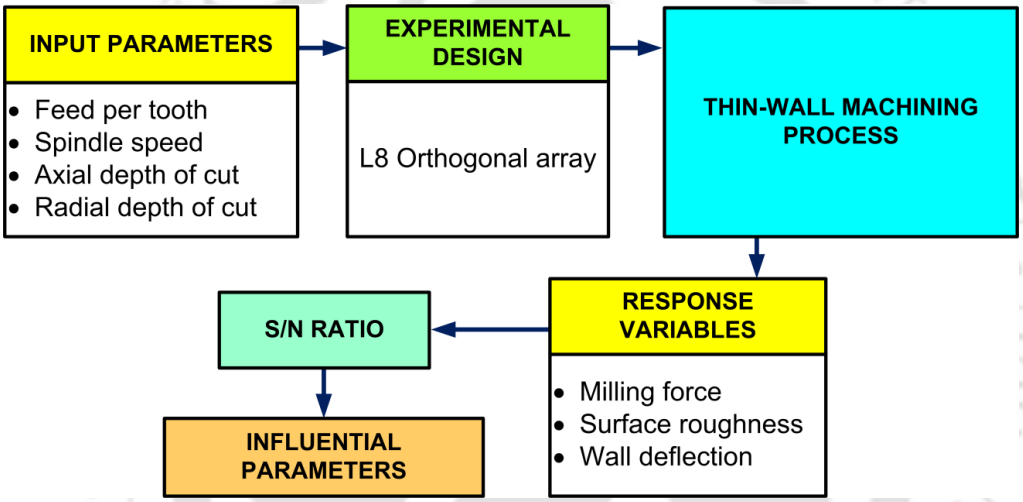

Figure 5.8 Flow of work for determination of range of process parameters

Table 5.2 L8 array and response data

Run	Factors				Results		
No.	f_z (mm/z)	n_s (r/min)	a_d (mm)	r_d (mm)	F_c (N)	R_a (µm)	D_f (mm)
1	0.06	3500	12	0.625	140.92	0.95	0.135
2	0.06	3500	24	1.25	409.69	1.37	0.628
3	0.06	4500	12	1.25	310.87	1.22	0.376
4	0.06	4500	24	0.625	247.59	1.08	0.164
5	0.1	3500	12	1.25	329.81	1.29	0.397
6	0.1	3500	24	0.625	293.43	1.27	0.251
7	0.1	4500	12	0.625	265.76	1.21	0.189
8	0.1	4500	24	1.25	440.1	1.51	0.714

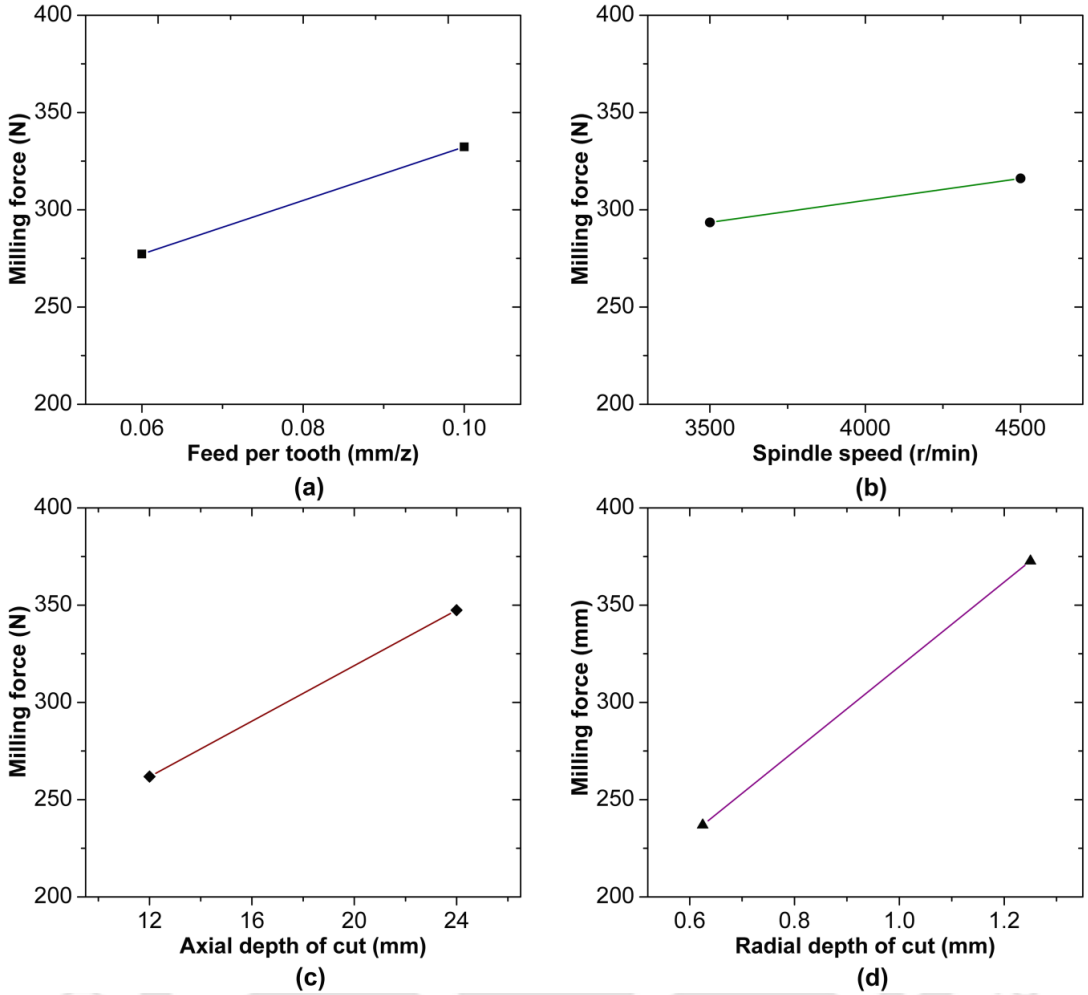

Figure 5.9 Main effect plots for milling force

Figure 5.9 shows the influence of process parameters on milling force. The plot suggests that the milling force (F_c) increases with the increase in feed per tooth, spindle speed, axial and radial depth of cut. To determine the influential factors, the experimental results were transformed into a signal-to-noise (S/N) ratio. To achieve the objective of minimum milling force, the "smaller is better" method was employed. The S/N ratio for minimum milling force under 'smaller-the-better' characteristic was calculated by using Equation 5.1, where n is the number of measurements, and y_i the measured characteristic value.

$$\eta = -10\log\left[\frac{1}{n}\sum_{i=1}^{n} y_i^2\right] \tag{5.1}$$

Table 5.3 presents the computed S/N ratio values for milling force. Higher the delta value, more influential is the factor. It can be observed from table that the influencing parameters are radial depth of cut (r_d) and axial depth of cut (a_d), respectively. Feed per

tooth (f_t) also influences the milling force; however spindle speed (n_s) has comparatively minimal influence on milling force.

Table 5.3 S/N ratios for milling force

Level	Factors			
	f_z (mm/z)	n_s (r/min)	a_d (mm)	r_d (mm)
1	-48.24	-48.74	-47.92	-47.17
2	-50.27	-49.77	-50.59	-51.33
Delta	2.03	1.04	2.66	4.16
Rank	3	4	2	1

Figure 5.10 shows the influence of process parameters on surface roughness (R_a). The plot shows that the surface roughness increases with the increase in feed per tooth, spindle speed, axial and radial depth of cut. The experimental results were transformed into a signal-to-noise (S/N) ratio to determine the influential factors.

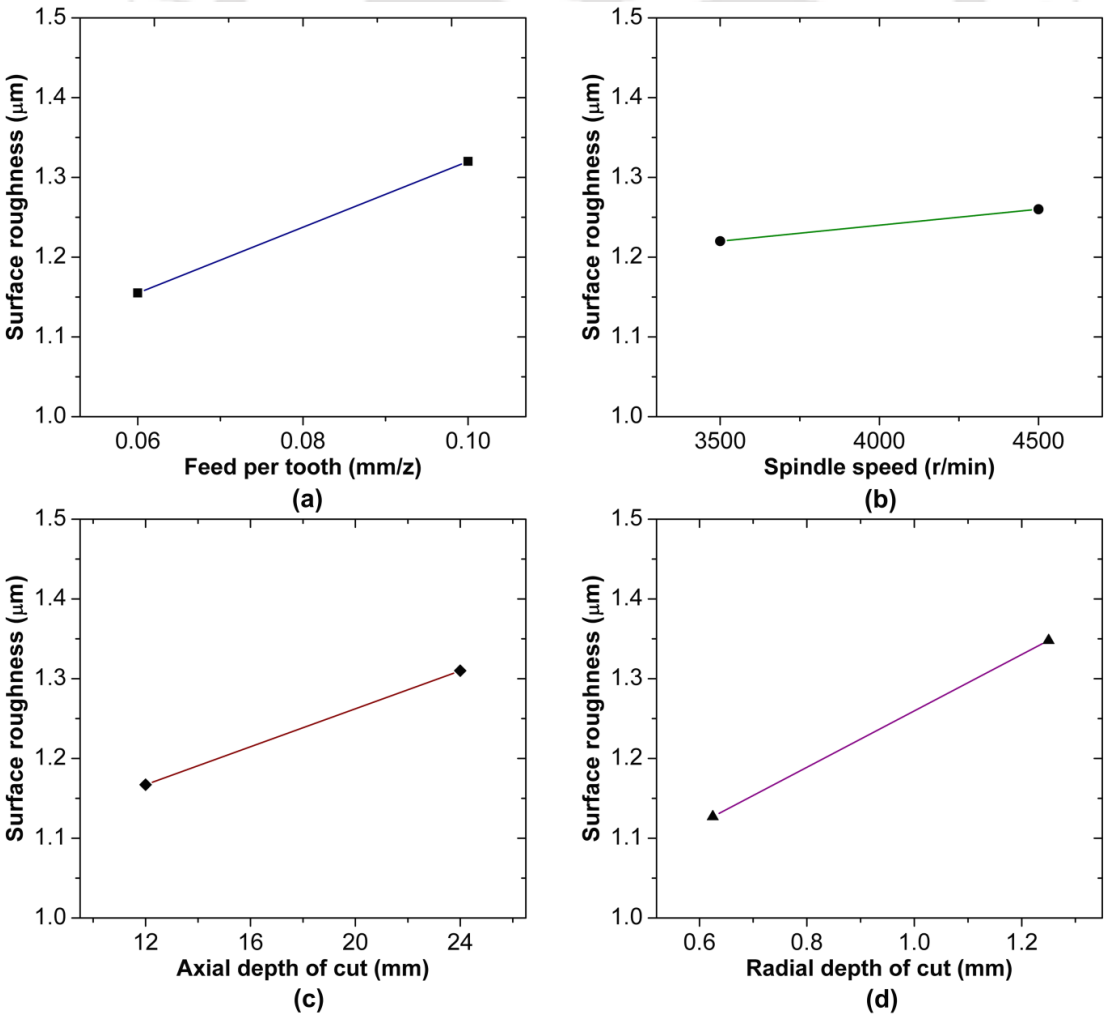

Figure 5.10 Main effect plots for surface roughness

Table 5.4 presents the computed S/N ratio values for surface roughness. It can be observed that the strongest influence was exerted by radial depth of cut (r_d) and feed per tooth (f_t), followed by axial depth of cut (a_d). Again spindle speed (n_s) was found to have minimal influence on surface roughness.

Table 5.4 S/N ratios for surface roughness

Level	Factors			
	f_z (mm/z)	n_s (r/min)	a_d (mm)	r_d (mm)
1	-1.1711	-1.6442	-1.2873	-0.9887
2	-2.3808	-1.9077	-2.2646	-2.5632
Delta	1.2096	0.2635	0.9773	1.5746
Rank	2	4	3	1

Figure 5.11 shows the influence of process parameters on wall deflection (D_f).

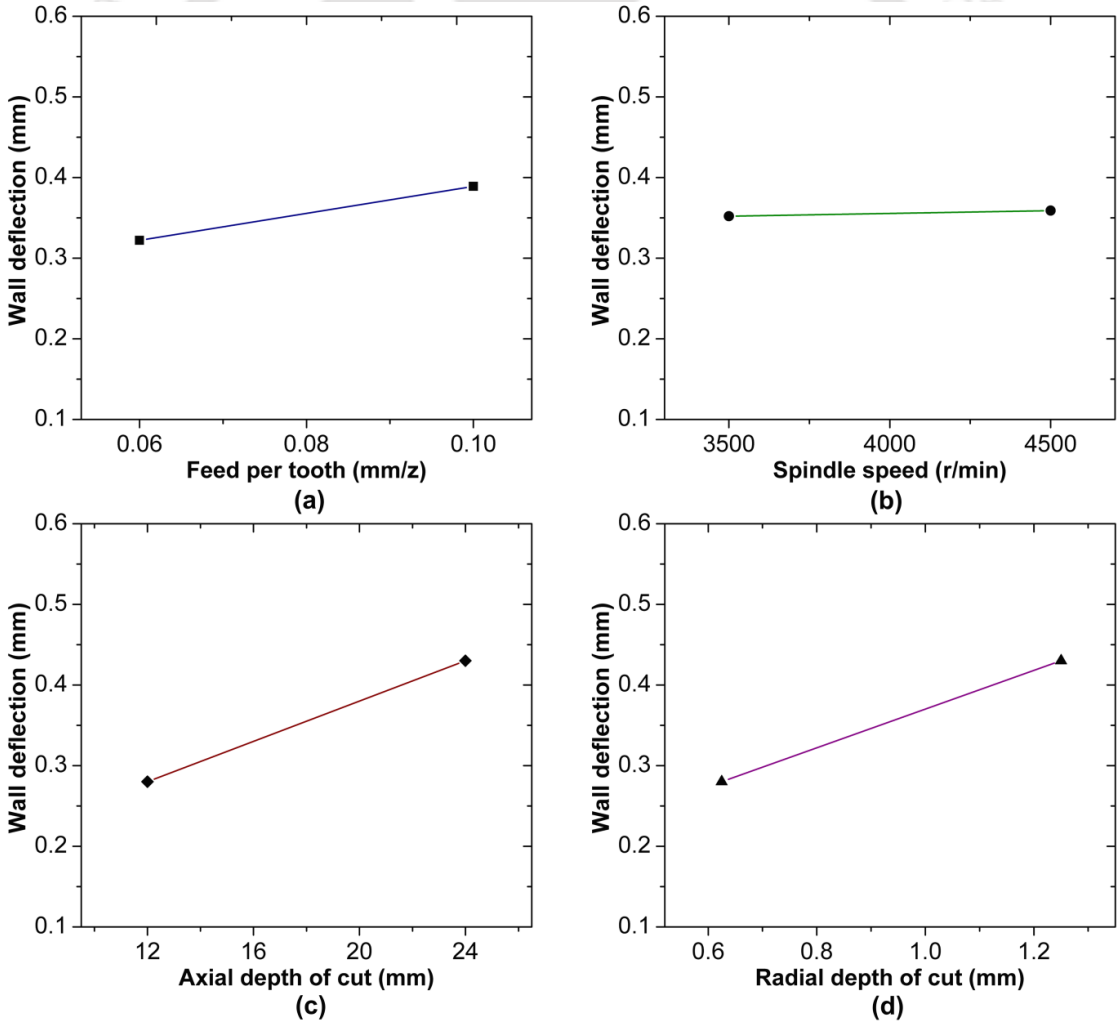

Figure 5.11 Main effect plots for wall deflection

The plot shows that the magnitude of wall deflection increases as the values of feed per tooth, spindle speed, axial and radial depth of cut increase. The experimental results were transformed into signal-to-noise (S/N) ratio to determine the influential factors. Table 5.5 presents the computed S/N ratio values for wall deflection. It can be seen that, similar to the cases of surface roughness and milling force, in case of deflection, the strongest influence was exerted by radial depth of cut (r_d) followed by axial depth of cut (a_d) and feed per tooth (f_t). Spindle speed (n_s) was found to have minimal influence on wall deflection magnitude.

Table 5.5 S/N ratios for wall deflection

Level	Factors			
	f_z (mm/z)	n_s (r/min)	a_d (mm)	r_d (mm)
1	11.703	10.617	12.072	15.169
2	9.250	10.337	8.882	5.785
Delta	2.453	0.280	3.190	9.384
Rank	3	4	2	1

5.8.1 Observations made during Phase 1 of Experiments

To determine the influential process parameters, initial experiments were carried out. Following are the observations made during this study.

- Radial depth of cut was found to influence all the three responses viz. milling force, surface roughness and wall deflection. It was found to be the most influential parameter. As it can be seen from previous section (Section 5.8), as the radial depth increases, the magnitude of milling force increases. This leads to the increase in magnitude of wall deflection. Surface roughness was also found to be influenced by radial depth of cut. Surface roughness increases with the increase in radial depth of cut. Literature reports a scant research on the influence of radial depth of cut on thin-wall deflection, milling force and surface quality. Therefore, it was decided to carry out further detail investigation to understand the influence of radial depth of cut on the process responses.
- Sandvik-Coromant and Boeing Research and Technology group reported that selection of proper machining strategies is a key for efficient thin-wall machining. A machining strategy mainly comprises of order of cutting passes and setting of appropriate values of process parameters viz. radial depth of cut and axial depth of

cut. The number of axial passes is based on the wall height and cutter contact length (axial depth of cut). From the initial experiments it was noted that axial depth of cut has a major influence on all three response parameters. Therefore, it was decided to study the influence of axial depth of cut on the process performance.

- It was noticed that, feed per tooth influences the milling force, wall deflection and surface roughness to some extent. In the present work, end milling cutters with sharp cutting edges were employed to carry out the experiments. But during the machining process, formation of built-up-edges (BUEs) was observed when high feed per tooth (0.1 mm/z) and axial depth of cut values (24 mm) conditions was employed (see Figure 5.12(a)). Also the surface quality was found to be deteriorated due to the persistent BUE formation. Therefore, it was thought worth to conduct further investigations to study the influence of feed on the response parameters while maintaining the feed value below 0.06 mm/z.
- Results from the initial experiments clearly suggested that spindle speed has minimal influence on milling force, part deflection and surface finish as compared to other three process parameters. But at a process condition of higher levels of spindle speed, radial and axial depth, formation of chatter marks (Figure 5.12(b)) was observed. Also, it was noted that machine tool structure vibrates at high spindle speed of 4500 r/min. Based on all the observations; it was decided to employ a spindle speed of 3500 r/min in the further experimental investigations.

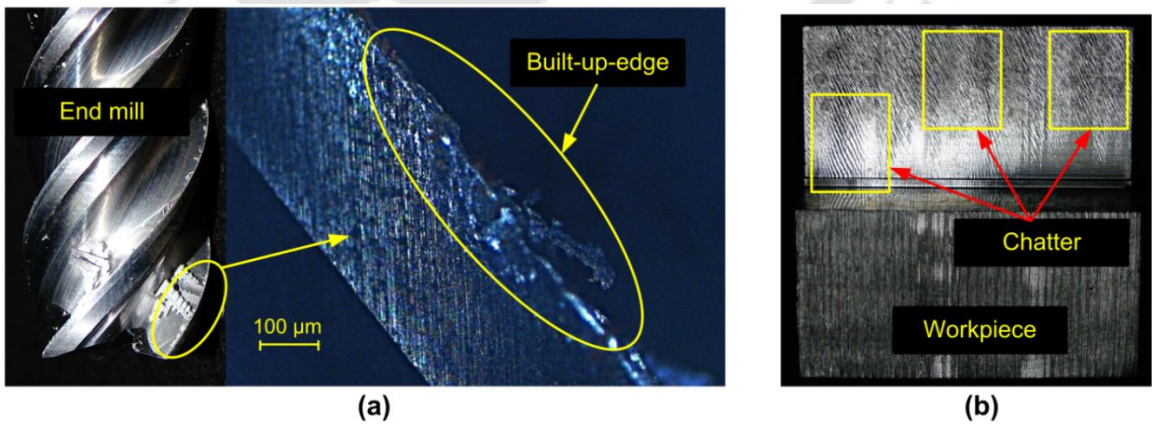

Figure 5.12 (a) Built-up-edge formation (BUE), **(b)** Chatter marks in the finished workpiece

After the completion of initial experiments, an experimental investigation was planned to study the influence of tool geometry parameters viz. tool diameter, tool path, helix angle, number of flutes on the process responses. The experimental details and results obtained are presented in the next section.

5.9 Phase 2: Selection of Cutting Tool Geometry Parameters

End milling of thin-wall parts is a tool-based manufacturing process. However, literature reports a scant work on the influence of tool geometry parameters on the surface finish and wall deflection. Therefore, in this work, experiments were carried out to study the influence of cutting tool geometry parameters on the surface quality and dimensional accuracy of the machined thin-wall parts.

Figure 5.13 depicts the overview of the experimental work carried out during the second phase of research work. Three tool geometry parameters viz., tool diameter, helix angle and number of flutes were selected to study their influence on performance parameters namely milling force, surface roughness and wall deflection. Grey relational analysis, a statistical analysis technique was used to determine the optimal milling parameters. Finally, confirmatory experiments were conducted to verify the validity of the computed optimal tool geometry parameters.

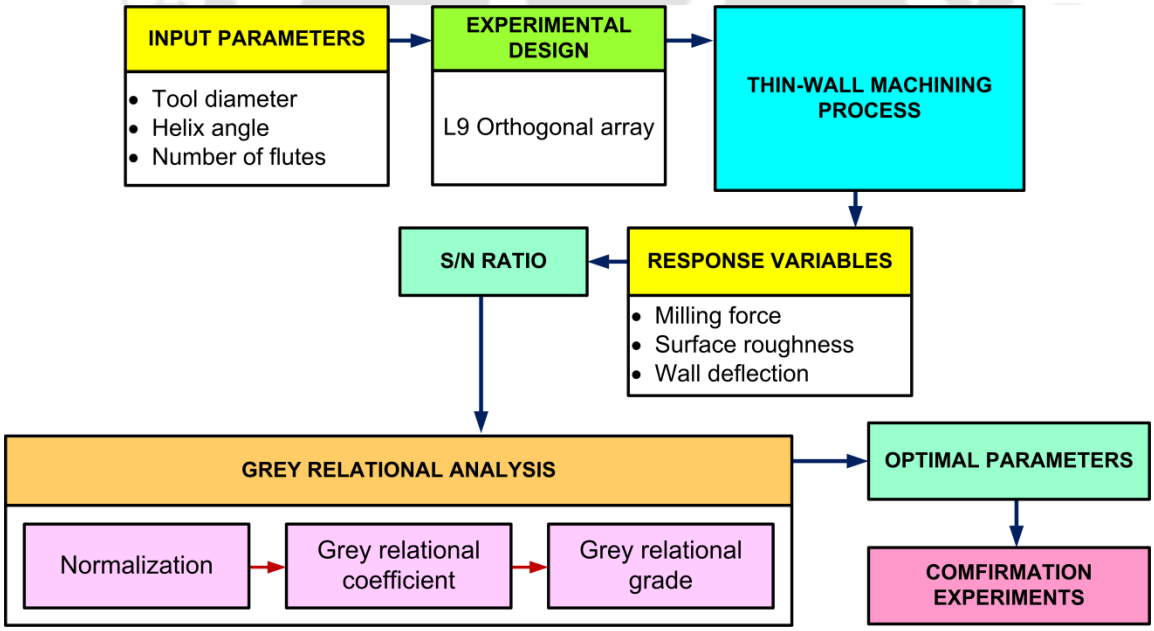

Figure 5.13 Flow of work for determination of tool geometry parameters

Figure 5.14 shows the solid carbide flat end mills with different geometrical characteristics those were used for conducting the experiments. The experiments were

carried out by incorporating down milling approach and the process parameters were selected based on the experimental results obtained in phase 1. For phase 2 of the experiments, the process parameters were fixed at spindle speed = 3500 r/min, axial depth of cut = 24 mm, radial depth of cut = 0.625 mm and feed value = 0.02 mm/z.

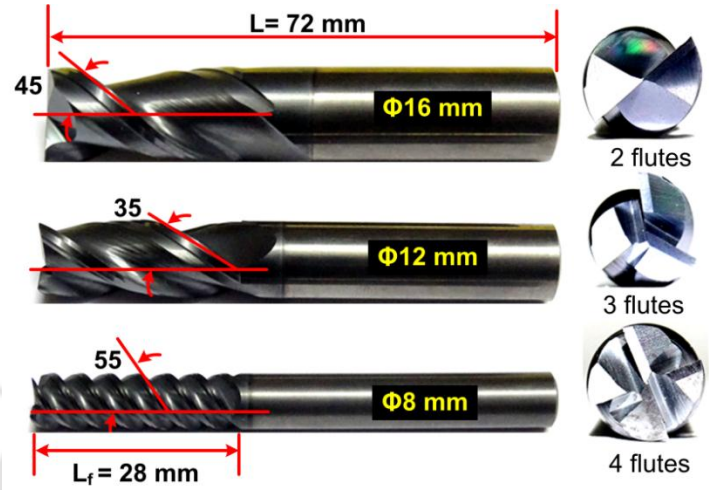

Figure 5.14 End milling cutters and tool geometry parameters

This study mainly focusses on the influence of three parameters viz. end mill diameter (d_i), helix angle (λ_s) and number of flutes (f_n) on the process performance measures viz. surface roughness, wall deflection and milling force. The selected factors and their levels are listed in Table 5.6.

Table 5.6 Tool geometry parameters and their levels

Design factors	Levels		
	1	**2**	**3**
Tool diameter, d_i (mm)	8	12	16
Tool helix angle, λ_s (°)	35	45	55
Number of flutes f_n (Nos.)	2	3	4

L9 Taguchi orthogonal array was adopted for designing the experiments. The values of the responses were converted to a quality characteristic evaluation index known as S/N ratio. S/N ratio is a statistical performance measure that was employed to analyze the resultant data. In Taguchi method, the effect of selected factors on the average responses are indicated by signals whereas the noises reveal the sensitivity of the experiment output to noise factors. To achieve the minimum values of surface roughness, part deflection and milling force, "smaller-is-better" method was used.

5.9.1 Grey Relational Analysis

During thin-wall machining process, it is desired to manufacture the thin-wall parts with superior surface finish and dimensional accuracy. Also it is envisaged that chosen tool geometry parameters should provide highest possible productivity. In these circumstances of multiple objectives, methodology based on Grey relational analysis was employed to obtain the optimal processing parameters for three responses viz. surface roughness, milling force and wall deflection. The multiple objective criteria were converted into the optimization of a single relational grade. The steps adopted in the Grey relational analysis are listed as follows.

Step 1: Grey relational generation

Generally the data values and units of each response are different; hence it is necessary to normalize the S/N ratio so that the different responses are comparable to each other. In the first step, the calculated S/N ratio is normalized between the ranges of 0 to 1. The process is known as grey relational generation and can be categorized into three types namely, Smaller-the-Better (*SB*), Larger-the-Better (*LB*) or Nominal-is-better (*NB*) criteria. The normalized data for the response variables viz. part deflection; surface roughness and milling force correspond to smaller the better (*SB*) criterion is expressed by:

$$x_i(J) = \frac{\max y_i(J) - y_i(J)}{\max y_i(J) - \min y_i(J)} \quad (i=1, 2,...., m; j=1, 2,...., n) \tag{5.2}$$

where m is the number of experimental data values; n the number of factors; $y_i(J)$ is the original sequence; $x_i(J)$ is the value obtained after grey relation generation.

Step 2: Grey relational coefficient

The grey relational coefficient is a parameter used to express the relationship between the reference data and actual normalized experimental data. The grey relation coefficient was calculated as:

$$\varepsilon_i(J) = \frac{\Delta\min + \phi \cdot \Delta\max}{\Delta_{oi}(J) + \phi \cdot \Delta\max} \tag{5.3}$$

where $\varepsilon_i(J)$ is the grey relation coefficient; $\Delta_{oi} = ||y_o(J)-y_i(J)||$; $y_o(J)$ is the ideal sequence; Δmin is the least value of $\Delta_{oi}(J)$ and Δmax is highest value of $\Delta_{oi}(J)$.

Step 3: Gray relational grade

The average of the grey relational coefficient related to every observation is computed to

determine the grey relational grades (GRG). It is given by

$$\beta_i = \sum_{J=1}^{n} w_J \cdot \varepsilon_i(J) \tag{5.4}$$

where w_J is the weighting value for each grey relational coefficient ranging from 0 to 1 (Tosun and Pihtili (2010)).

5.9.2 Experimental Results and Discussion

Based on the selected tool geometry parameters and their levels, Taguchi based L9 array was formulated, Table 5.7 shows the experimental array. The table also presents the experimental results obtained in terms of milling force, surface roughness, and wall deflection.

Table 5.7 L9 array with response data

Run No.	Factors			Performance parameters		
	d_i mm)	λ_s (°)	f_n (Nos.)	F_c (N)	R_a (µm)	D_f (mm)
1	8	35	2	127.33	0.719	0.088
2	8	45	3	118.38	0.573	0.074
3	8	55	4	106.89	0.441	0.079
4	12	35	3	204.77	1.164	0.127
5	12	45	4	194.18	0.661	0.109
6	12	55	2	211.16	0.879	0.115
7	16	35	4	236.05	1.284	0.136
8	16	45	2	229.29	1.602	0.147
9	16	55	3	225.45	1.428	0.127

To carry out Grey relational analysis (GRA), the experimental data need to be converted S/N ratio values. To calculate the S/N ratios, the smaller-the-better criterion was used. The three responses in the form of S/N ratio are listed in Table 5.8. The mean S/N ratios were calculated according to the Taguchi's method by averaging the S/N ratio obtained for each tool geometry parameter. In what follows is the GRA of the process responses which is discussed one by one.

Table 5.8 Response data in S/N ratio

Run No.	S/N Ratio		
	F_c (dB)	R_a (dB)	D_f (dB)
1	-42.0988	2.86542	-38.8897
2	-41.4656	4.83691	-37.3846
3	-40.5791	7.11123	-37.9525
4	-46.2254	-1.31906	-42.0761
5	-45.7640	3.59597	-40.7485
6	-46.4920	1.12022	-41.2140
7	-47.4602	-2.17130	-42.6708
8	-47.2076	-4.09325	-43.3463
9	-47.0610	-3.09456	-42.0761

5.9.2.1 Milling Force

Figure 5.15 displays the main effect plot of mean S/N ratios for milling force.

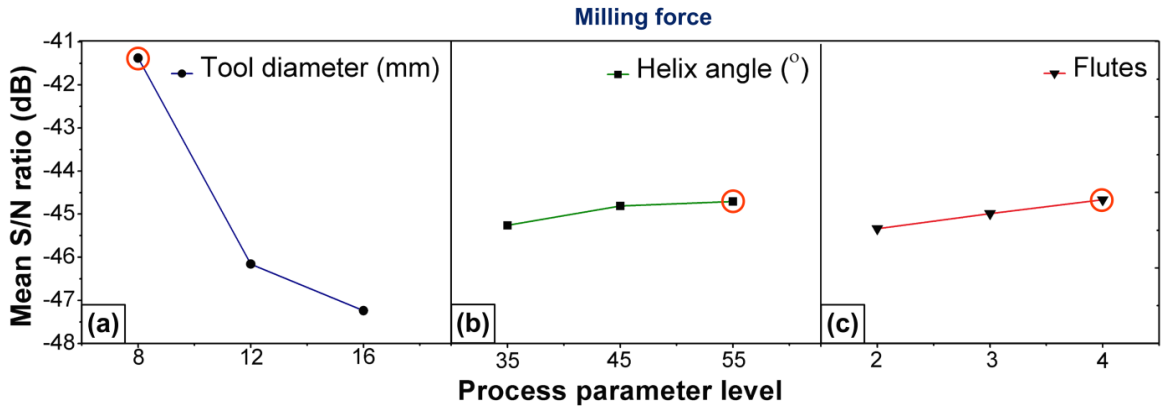

Figure 5.15 Main effect graph of S/N ratio for milling force

From Figure 5.15(a) it can be observed that milling force increase with the increase in tool diameter. Lower value of milling force was recorded when end mill having a diameter of 8 mm was used. Figure 5.15(b) shows that milling force decrease as the helix angle increases, whereas slight reduction in force value was noted when the cutting tool with 4 flutes was used (see Figure 5.15(c)). Figure 5.16 demonstrates the influence of tool diameter on the workpiece-tool contact points. It can be seen that during machining using a smaller diameter tool, the length of contact of cutting tooth with the work material is lesser in comparison with that of larger diameter tools. This reduces the milling force acting on the workpiece. The thin-wall parts possess low rigidity, thus the larger diameter tools which are more rigid causes the flexible wall to deflect during the

cutting operation. This induces the vibrations that leads to the chatter and causes the milling force value to increase significantly.

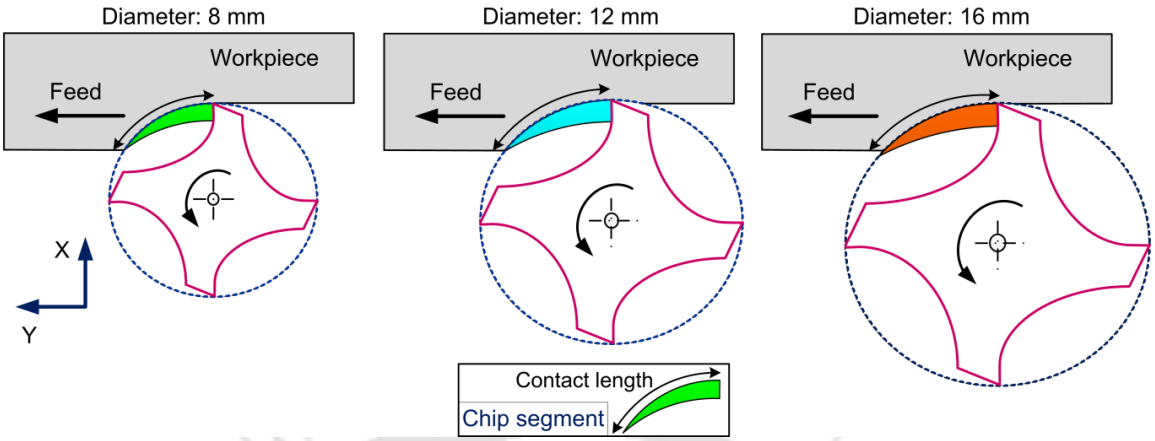

Fig. 5.16 Influence of tool diameter on work-tool contact length

During thin-wall machining operation, lower milling force is always favorable as it lowers the wall deflection. In case of variation in helix angle, it was observed that with the increase in helix angle from 35° to 55°, the milling force decreases. End mill having higher helix angle generated lower force due to sharper cutting edge which results in smoother cutting action. From Figure 5.17 it can be seen that with the increase in helix angle the value of force component F_x (X-direction) decreases, while the value of force component F_y (Y-direction) increases. However it is noted that there is reduction in the resultant milling force as helix angle increases.

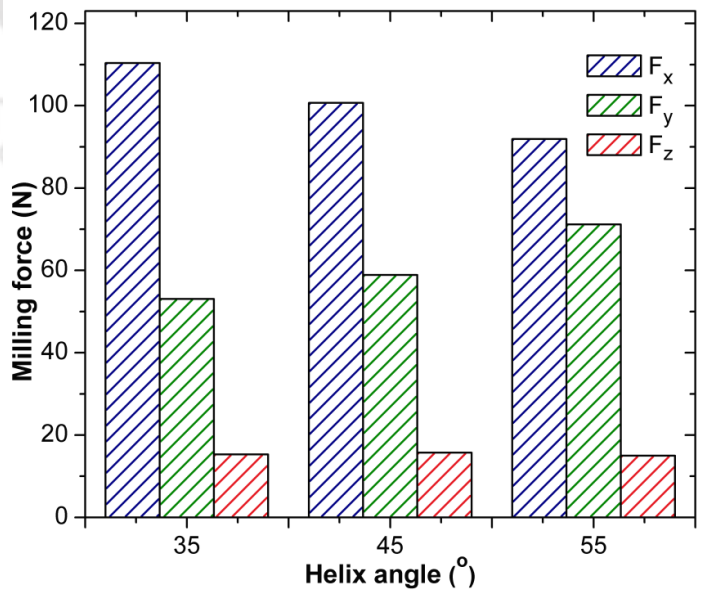

Figure 5.17 Variation of force components with tool helix angle

Influence of variation in helix angle on milling force can be understood by using Figure 5.18. The figure shows the contact between the end mill and the workpiece during machining. It can be noted that for a constant axial depth of cut, as the helix angle increases, the number of contact points between the tool and workpiece increases. It can clearly be seen that the number of contact points for a 35º helix tool is two whereas the contact points between the tool-work increases to five for 55º helix tool. Increase in number of contact points reduces the work volume to be machined by each helical tooth which lowers the milling force per tooth.

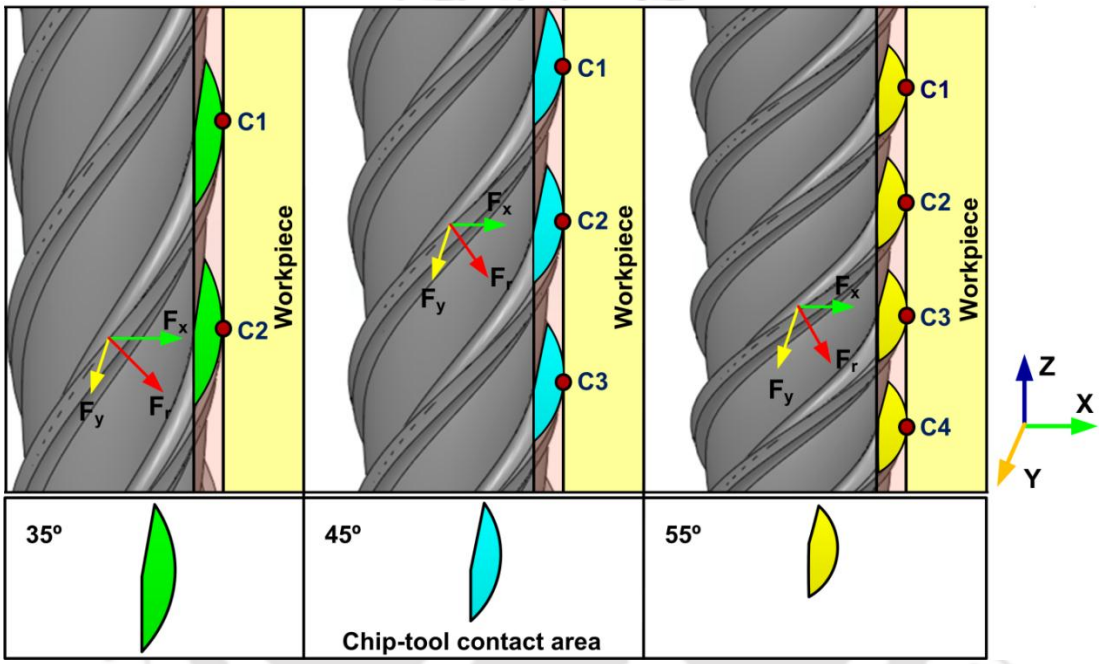

Figure 5.18 Influence of helix angle on milling force

Cutting flute is an important geometric parameter of an end mill cutter. Number of flutes in an end mill influences the rigidity of the cutter. As the number of flutes increases, the core diameter of the tool decreases thereby lowering the cutter rigidity. But increase in the number of flutes reduces the space available for chip to flow freely thus affecting the machining process. Figure 5.19 exhibits the influence of number of flutes during end milling process. Position 1 represents the location of the first cutting edge in a typical end milling operation. As the cutter traverses and rotates, for a fixed set of cutting conditions (fixed feed, speed and tool diameter), time taken by the second cutting flute (position 2) to engage with the workpiece is higher for a two fluted cutter in comparison to a three or four fluted cutter. As a result, availability of material to be machined at each cutting edge will be higher in case of a two flute cutter. For tool with higher number of flutes, the engagement time of each cutting edge with the workpiece

reduces thereby reducing the chip load and milling force. Therefore, it is essential to be careful during the selection of number of flutes for a particular cutting operation i.e. roughing or finishing. For roughing operation, in view of faster production, higher values of depth of cuts (radial as well as axial) are employed. These higher levels of process parameters generate large milling force. Hence it is recommended to employ a cutting tool with lesser number of flutes. In the case of finishing operation, it is always desirable to use tools with more number of flutes since they generate lower milling force.

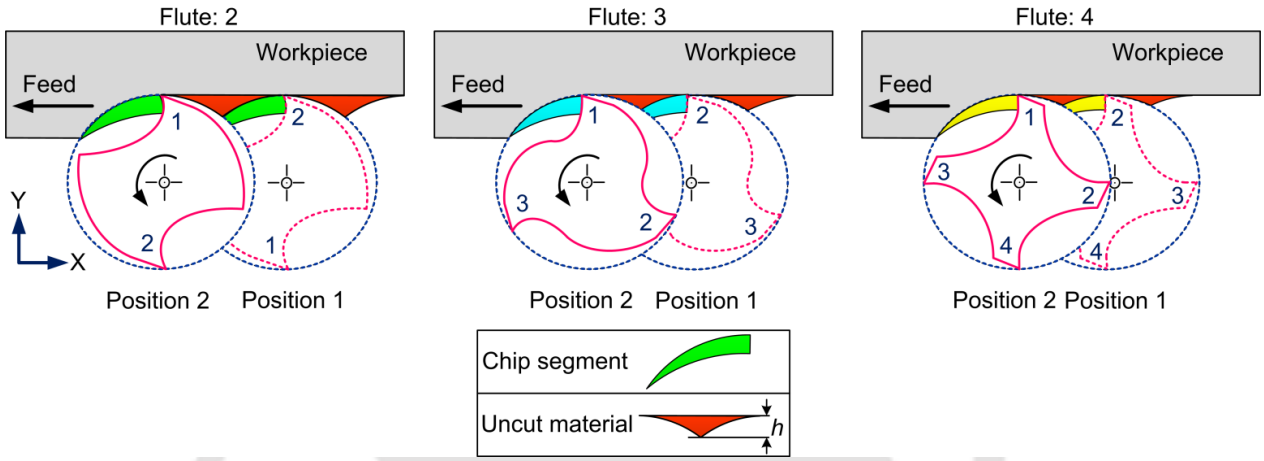

Figure 5.19 Influence of number of flutes on milling force and surface roughness

From the data provided in Table 5.9 the tool geometry parameters for minimal milling force are: a tool having diameter of 8 mm (Level 1), a helix angle of 55° (Level 3) and 4 cutting flutes (Level 3).

Table 5.9 Mean S/N ratios for milling force of each factor at their levels

Process parameter	Mean S/N ratio			Max-Min
	Level 1	Level 2	Level 3	
d_i	-41.38	-46.16	-47.24	5.86
λ_s	-45.26	-44.81	-44.71	0.55
f_n	-45.27	-44.92	-44.60	0.67

5.9.2.2 Surface Roughness

In the present work, the effect of variation in cutting tool geometry parameters on the surface roughness during thin-wall machining was investigated. Figure 5.20 depicts the variation of the mean S/N ratio of surface roughness with the change in tool geometry parameters. Figure 5.20(a) shows that the surface roughness is sensitive to the variation in tool diameter. Surface quality of thin-wall deteriorates as the diameter of the tool

increases. From Figure 5.20(b, c) it is observed that the surface finish of the machined workpiece improves with the increase in tool helix angle and number of flutes.

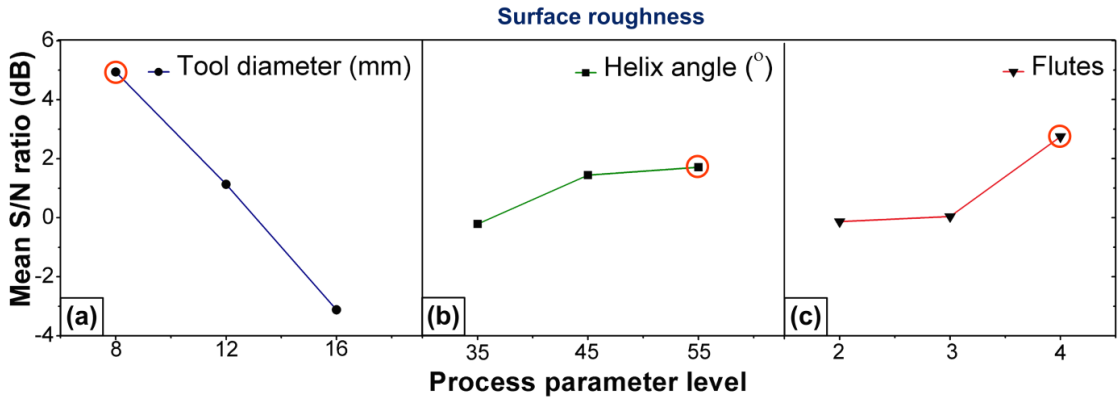

Figure 5.20 Main effect graph of S/N ratio for surface roughness

Figure 5.21 shows the 3-D surface of thin-wall parts generated by the cutters having different diameters. Figure 5.21(a) shows the topography of the surface machined using 8 mm dimeter tool (Test run No. 2). The surface generated after milling showed typical feed marks. Figure 5.21(b-c) shows the surface topography of machined thin-wall part when larger diameter tools were employed. It can clearly be seen that severe chatter occurred while machining the thin-wall workpieces with cutting tool of diameter 12 and 16 mm.

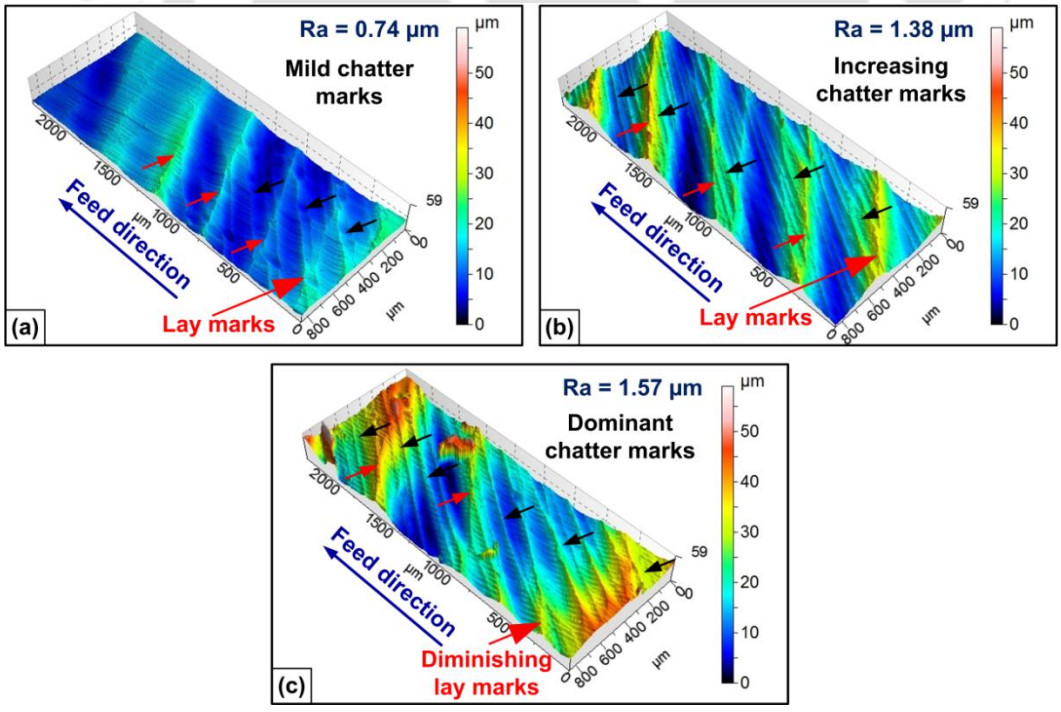

Figure 5.21 Topography of the machined surface obtained at the free end of the thin-wall using: **(a)** 8 mm tool diameter, **(b)** 12 mm tool diameter, **(c)** 16 mm tool diameter

The severity of the chatter was noted to increase when the tool diameter increased from 12 mm to 16 mm. Therefore, it can be perceived that, surface roughness produced by using 8 mm diameter cutting tools were comparatively better than those generated by using larger diameter tools. Increase in the surface roughness with larger tool diameters can be explained using Figure 5.22. Figure 5.22(a) shows the work-tool contact and the desired surface to be generated during an ideal machining condition. Under ideal machining conditions, the tool and the workpiece can be considered as rigid bodies and the surface produced is devoid of any chatter marks. But in practical application, chatter exists and can be attributed to either the tool or the workpiece. In case of tool chatter, the machine and cutting tool vibrate whereas in case of workpiece chatter the thin-wall vibrates.

During machining of low rigidity thin-wall workpieces, the rigidity of the tools can be considered higher in comparison to that of flexible thin-walls. Thus during machining, due to the increase in work-tool contact area, the low rigidity thin-wall workpiece vibrates and the relative movement between the workpiece and tool leads to non-uniformity of the uncut chip thickness (see Figure 5.22(b)). This change in the uncut chip generates dynamic cutting force that causes vibration and chatter. Thus it can be concluded that application of end mills with higher diameters is to be avoided.

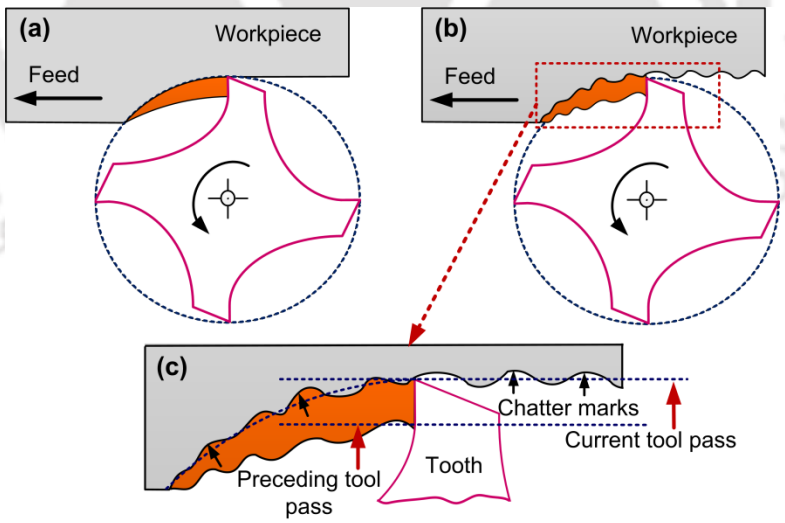

Figure 5.22 Influence of tool diameter on surface finish: **(a)** Ideal machining condition without chatter, **(b)** Machining with chatter

From Figure 5.20(b), it can be seen that the surface finish improves with the increase in tool helix angle. Increase in the helix angle enhances the effective shearing action which results in lower surface roughness. With higher helix angle, number of

cutting tool-workpiece contact points increases (see Figure 5.18). This reduces the volume of material to be machined by each cutting edge thereby lowering the chip load and milling force. This reduction in milling force helps in providing better surface finish. In the present work, end mill with four flutes provided better surface finish in comparison to two/three fluted cutters. This is attributed to the fact that more number of cutting points reduces the availability of the material to be machined per tooth as well as the engagement time of each cutting edge with the workpiece (see Figure 5.19). This reduction in the chip load and milling force improves the surface finish of the machined workpiece.

Table 5.10 presents the computed mean S/N ratio values for surface roughness. The best combination of tool geometry parameters that provides the superior surface finish is: cutter diameter of 8 mm (Level 1), helix angle of 55° (Level 3) and four cutting flutes (Level 3).

Table 5.10 Mean S/N ratios for surface roughness of each factor at their levels

Process parameter	Mean S/N ratio			Max-Min
	Level 1	Level 2	Level 3	
d_i	4.94	1.13	-3.12	8.06
λ_s	-0.21	1.45	1.71	1.92
f_n	-0.04	0.14	2.85	2.89

5.9.2.3 Wall Deflection

Figure 5.23 displays the main effect plot of S/N ratios for the wall deflection. From Fig. 5.23(a) it can be noted that part deflection is sensitive to the variation in cutter diameter. The deflection increases with the increase in tool diameter. As discussed in the earlier section (Section 5.9.2.1), with the increase in tool diameter, the contact between the workpiece and the tool cutting edge increases which increase the milling force. From Figure 5.24(a) it can be noted that average milling force components F_x and F_y increase with the increase in tool diameter. Increase in the force component F_x results in the increase in magnitude of wall deflection. Thus, as the cutting tool traverses along the Y-direction, the workpiece deflects along the X-direction (Fig. 5.24(b)).

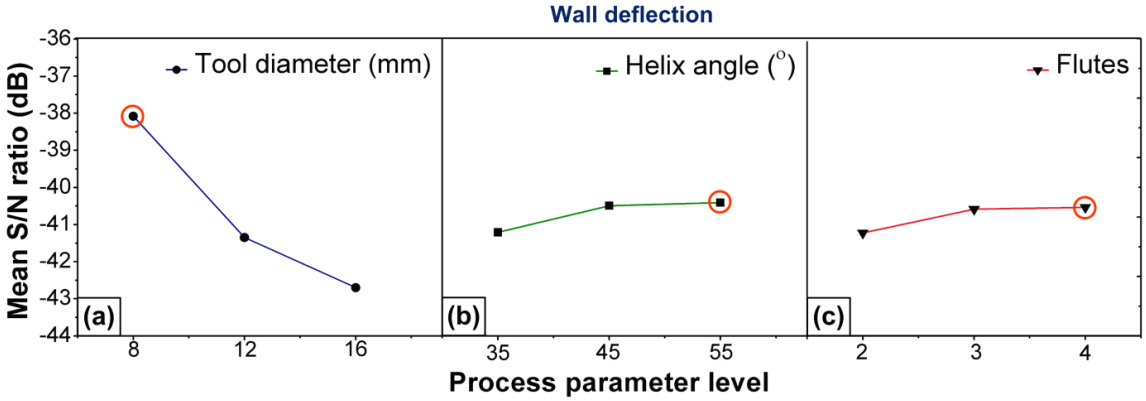

Figure 5.23 Main effect graph of S/N ratio for wall deflection

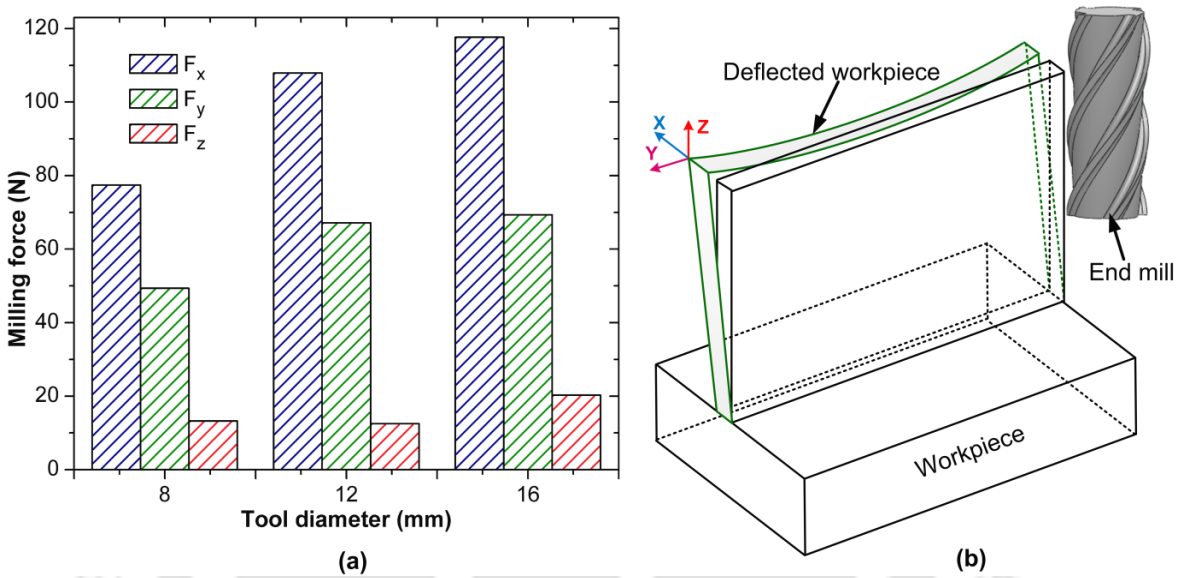

Figure 5.24 (a) Variation of force components with tool diameter **(b)** Thin-wall part deflection

From Figure 5.23 (b, c), it can be noted that wall deflection minimizes with the increase in helix angle and number of flutes. It is due to the fact that the end mill cutters with lower helix angle and smaller number of flutes develop higher milling force which deflect the thin-wall and induce chatter (see Figure 5.17). Thus it is recommended to use a tool with high helix angle as the sharper cutting edges provide smoother cutting action and help in reducing the milling force and wall deflection. Four fluted cutter generates comparatively lower cutting force which is helpful in reducing the wall deflection. Higher number of cutting teeth reduces the chip load per tooth which helps in reduction of milling force.

The best combination of tool geometry parameters to obtain lower wall deflection is: an end mill cutter of diameter 8 mm (Level 1), helix angle of 55° (Level 3) and 4

cutting flutes (Level 3) (see Table 5.11).

Table 5.11 Mean S/N ratios for wall deflection of each factor at their levels

Process parameter	Mean S/N ratio			Max-Min
	Level 1	Level 2	Level 3	
d_i	-38.08	-41.35	-42.70	4.62
λ_s	-41.21	-40.49	-40.51	0.80
f_n	-41.15	-40.51	-40.46	0.69

5.9.3 Selection of Optimum Tool Geometry Parameters using GRA

After the experiments, optimum tool geometry parameters were chosen by using Grey Relational Analysis (GRA). The objectives were set to obtain the desired process performance in terms of minimum part deflection, surface roughness and milling force. For this, all the performance parameters were equally weighted i.e. weight of 0.333 is assigned for each process responses. In GRA, grey relational generation, grey relational coefficient and the grey relational grade (GRG) were calculated by using Equations (5.2 to 5.4). The results are tabulated in Table 5.12 and Table 5.13.

Table 5.12 Normalized values and calculated Grey relational coefficient

Run No.	Grey relational generation			Grey relational coefficient		
	F_c	R_a	D_f	F_c	R_a	D_f
1	0.842	0.761	0.808	0.76	0.677	0.382
2	0.911	0.886	1	0.849	0.814	0.333
3	1	1	0.932	1	1	0.349
4	0.242	0.377	0.274	0.397	0.445	0.646
5	0.324	0.811	0.521	0.425	0.726	0.49
6	0.193	0.623	0.438	0.383	0.57	0.533
7	0	0.274	0.151	0.333	0.408	0.768
8	0.053	0	0	0.346	0.333	1
9	0.082	0.15	0.274	0.353	0.37	0.646

Table 5.13 Grey relational grade and rank

Run No.	Grey relational grade	Rank
1	0.606	3
2	0.665	2
3	0.783*	1*
4	0.496	9
5	0.547	5
6	0.495	8
7	0.503	6
8	0.56	4
9	0.456	7

In GRA, higher GRG corresponds to the combination of process parameters that comes closer to the preferred level. In other words, within the scope of the experiments, a higher GRG results in better response characteristics. In the present work, experiment 3 possesses the highest GRG (rank 1). Thus it can be concluded that the combination of tool geometry parameters in experiment 3 ($d_i1\lambda_s3f_n3$) provides the best performance characteristics that will be helpful in obtaining desired quality thin-wall parts.

As per the GRA methodology, the mean values of the GRG for all tool geometry parameters were calculated and are listed in Table 5.14. Figure 5.25 shows the plots of variation of mean GRG values for all levels of tool geometry parameters. From the table and the figure, it can be seen that the preferred combination of tool geometry parameters to achieve the best quality thin-walls components is $d_i1\lambda_s2f_n3$. It is interesting to note that the analysis based on mean GRG suggested altogether different combination of optimum tool geometry parameters. The suggested combination was: end mill diameter 8 mm with four flutes and helix angle of 45°. Table 5.14 also shows the respective differences between the maximum and minimum values of the mean GRG for the tool geometry parameters. These differences reflect the effect of tool geometry parameters on the response characteristics. More influential parameter possesses higher difference, which means the tool diameter is the most influential parameter on the multiple performance characteristics among all the tool geometry parameters.

Table 5.14 Main effects of tool geometry parameters on the Grey relational grade

Process parameter	Grey relational grade			Max-Min	Optimum level	Rank
	Level 1	Level 2	Level 3			
d_i	0.685*	0.513	0.506	0.179	1	1
λ_s	0.535	0.591*	0.578	0.043	2	3
f_n	0.554	0.539	0.611*	0.057	3	2

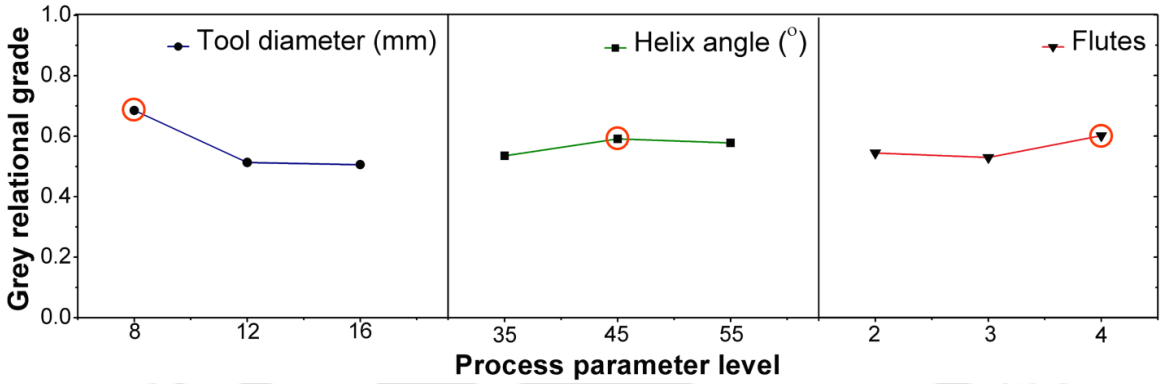

Figure 5.25 Effects of each process parameter on the Grey relational grade

5.9.4 Confirmation Experiments

After obtaining the optimum levels of tool geometry parameters, the GRG was computed as 0.751 by using a co-relation:

$$Y_{predict} = Y_{mean} + \sum_{i=1}^{n} (Y_i - Y_{mean}) \quad (5.5)$$

where, Y_{mean} is the total mean of the GRG, Y_i is the mean GRG at the preferred level, and i is the number of tool geometry parameters that significantly affect the multiple performance characteristics. After that, to verify the performance characteristic with the optimal combination of tool geometry parameters, actual experiment was carried out by using cutting tool of diameter 8 mm with helix angle of 45° and 4 flutes. The responses were recorded and are tabulated in Table 5.15.

Table 5.15 shows the comparison between the process performances obtained by employing the sets of tool geometry parameters suggested by GRG (See Table 5.13) and the optimal combination suggested by mean GRG (see Table 5.14). The combination suggests by GRG was $d_i1\lambda_s3f_n3$.The optimal combination suggested by mean GRG was $d_i1\lambda_s2f_n3$. The GRG computed for the suggested optimal combination by mean GRG was noted to be 0.715 (as per Equation (5.5)). Confirmatory experiments was carried out

verify the validity of the optimal combination. The results of the experiments are tabulated in Table 5.15. The GRG value computed for experimental verification was 0.788, which shows an improvement over the GRG value obtained using initial tool parameters.

Table 5.15 Results of confirmation experiment for the Grey relational grade

Performance characteristic	Initial tool parameters	Confirmed by experiment	% Improvement (Absolute)
Level	$d_i 1 \lambda_s 3 f_n 3$	$d_i 1 \lambda_s 2 f_n 3$	
F_c **(N)**	106.89	102.57	4.04
R_a **(µm)**	0.441	0.401	9.07
D_f **(mm)**	0.079	0.074	6.33
GRG	0.742	0.778	

From the table it can be seen that the optimum combination of tool geometry parameters provides considerable improvement in the surface finish of the machined part, whilst there is moderate reduction in milling force value and wall deflection. However, in the view of precision machining of thin-wall components this improvement can also be considered of a significant importance.

Figure 5.26 shows the comparison between the surface roughness topography and form error obtained by employing a typical tool geometry combination and the suggested optimal tool geometry parameters as per the present work. It can be seen the suggested tool geometry parameters produce an excellent surface finish with an average R_a value of 0.43 µm. Figure 5.26(b) shows comparison between the maximum error in thickness due to the deflection. It can also be noted there is significant reduction in the deflection of thin-wall (about 6.33%) when optimum parameters were used.

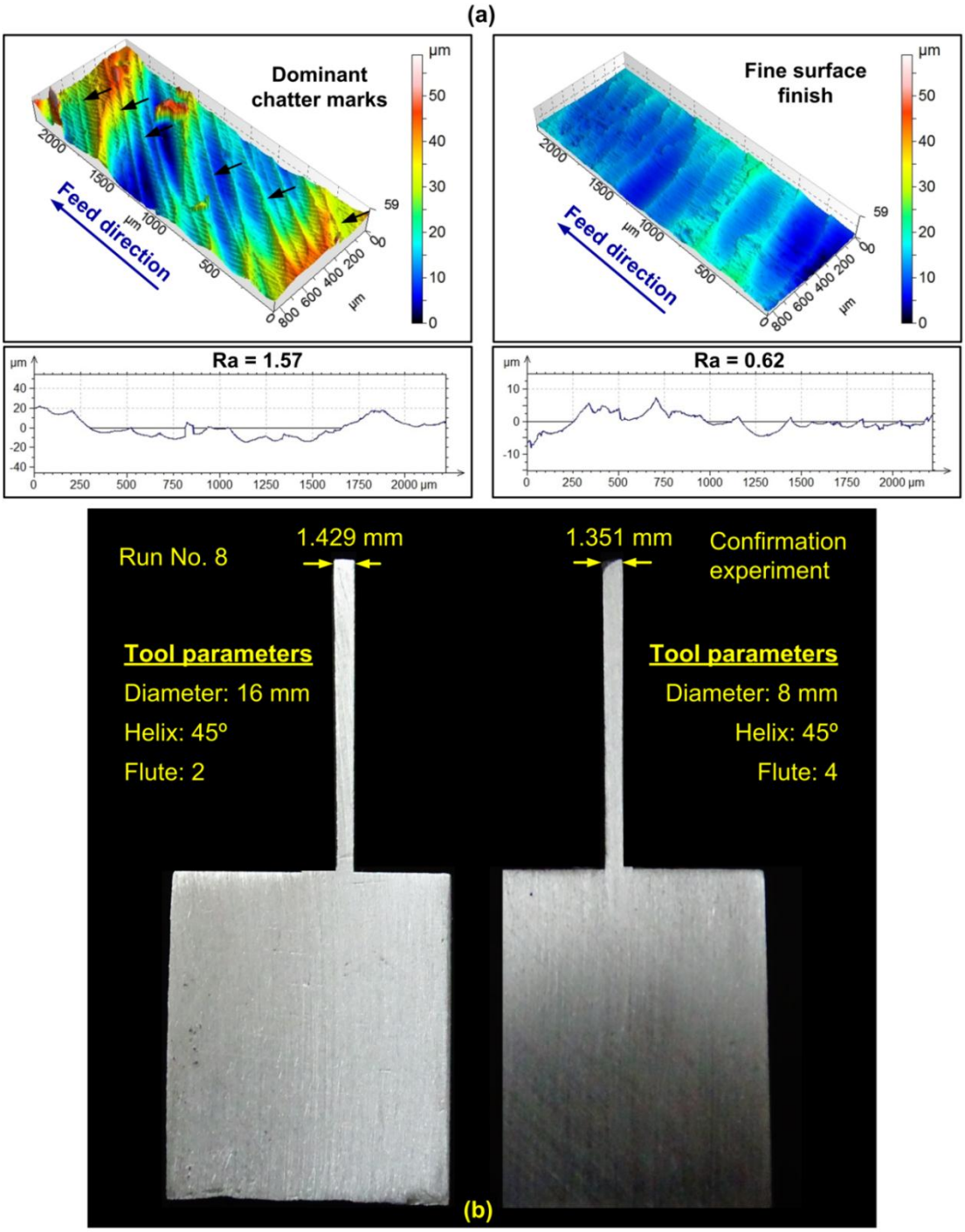

Figure 5.26 (a) 3-D surface topograph before and after optimization**, (b)** Form error before and after optimization

5.9.5 Study of Chip Morphology

After the optimization of tool geometry parameters, the effect of helix angle on the form and shape of the chips produced during machining was studied. Chip formation in machining process involves elastic-plastic deformation, work hardening due to plastic deformation and finally fracture of material. Peripheral end milling is a complex cutting

process due to the involvement of a geometrically complicated cutting tool. The helical cutting edges provide easy shearing of material and the flutes serve as passage for chip to flow during machining. Figure 5.27(a) shows a schematic view of chip formation in thin-wall milling where free and back surfaces are formed. Figure 5.27(b) exhibits the chips that were generated during thin-wall milling using end mills having different helix angles. It can be seen that the chips formed are continuous in nature and are of parabolic, semi-circular or nearly circular shape. The generation of typical shape of the chips can be attributed to the helix angle associated with the tool. The curl of the chip follows the helix angle of the tool (see Figure 5.27(b)). As the helix angle increases, the chip curl increases. At 35º helix, the flute i.e. chip flow path is quite straight while at 55º helix angle, the chip follows a curvilinear path. End mill having a helix of 35º produced chips of semi-parabolic form while tool with helix of 45º produced a semi-circular chip. End mill with helix of 55º produced chips of near circular shape.

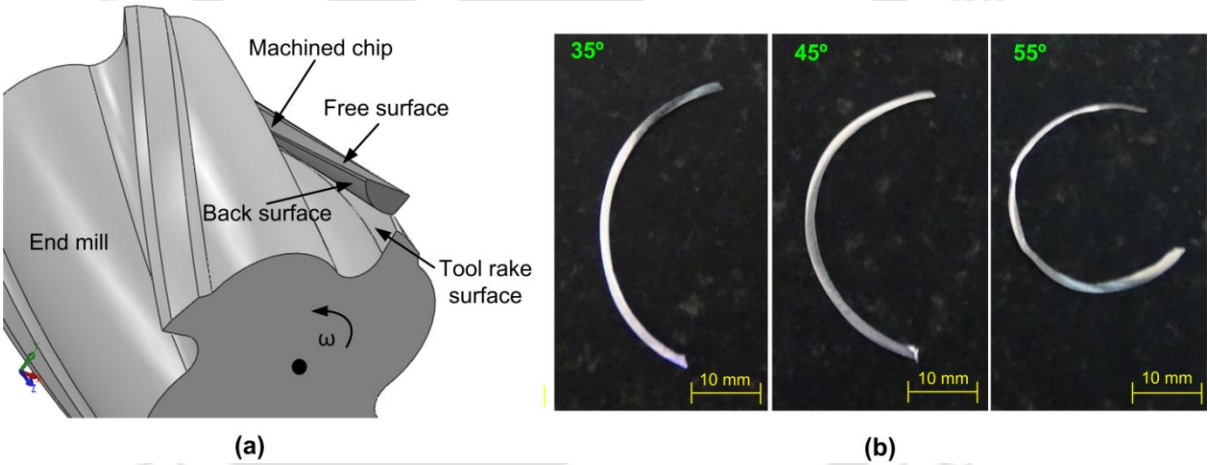

Figure 5.27 (a) A schematic of chip formation in peripheral end milling, **(b)** Chip geometry for various tool helix angles

The free surface of the chip was also observed under the optical microscope. Figure 5.28(a) shows that the free surface is not completely smooth but has many material folds. The fold-type chips occur due to low spindle speeds and it is a transitional morphology between the evolvement from continuous chip to the serrated chip. The formation of fold-type chip was also attributed to the reduction of strain and strain rate hardening and increase in thermal softening. Similar folds on the free surface were also observed when end mills with different helix angles were used.

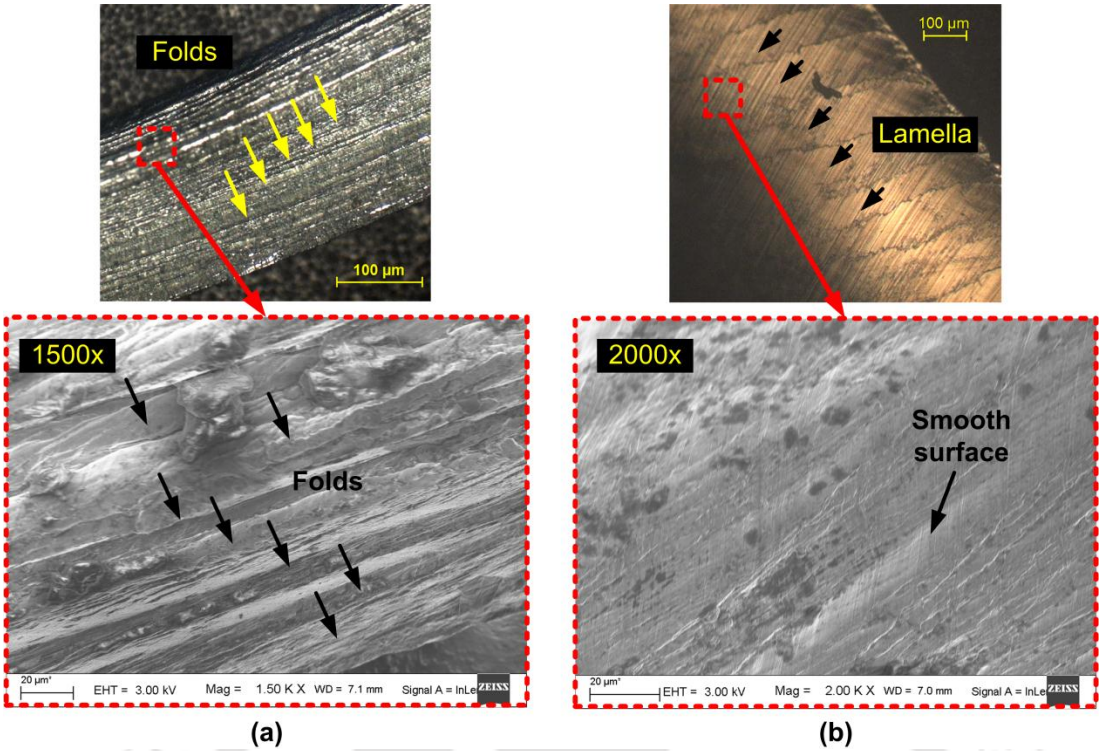

Figure 5.28 Chip morphology when using 35° helix tool: **(a)** Free surface, **(b)** Back surface

Figure 5.28(b) shows chip morphology on the back surface of the chips. The back surface is the surface of the chip which interacts with the rake face of the tool. In aluminum alloy machining, smooth and shiny back surfaces were observed due to high contact and shear stress that the chips experience on the rake face. However, it can also be seen that wavy stripes occur on the back surface of the chips. This is because the built-up-edges (BUEs) alter the tool geometry which causes uneven flow of chip over the rake surface that result in generation of wavy pattern on the back surface. It was noted that the stripes were more prominent when a tool with helix of 35º was employed than that of 55º helix tool. In case of machining with 55º helix tool, relatively fine and strip free surface was observed (see Figure 5.29). Thus it can be inferred that high helix angle produces better quality surface by helping in easy shearing of chips as compared to that by using a low helix tool. The width of chips produced during machining was measured. Figure 5.30 illustrates the variation of chip thickness with tool helix angle. Use of tool with lower helix angle resulted in wider chips as compared to that with higher helix angle. It is attributed to the fact that for a constant axial depth of cut, the number of contact points of a helical cutting tool with the workpiece will be higher in case of a high helix tool (see Figure 5.18). This reduces the amount of area to be machined, thereby producing chips with lower width.

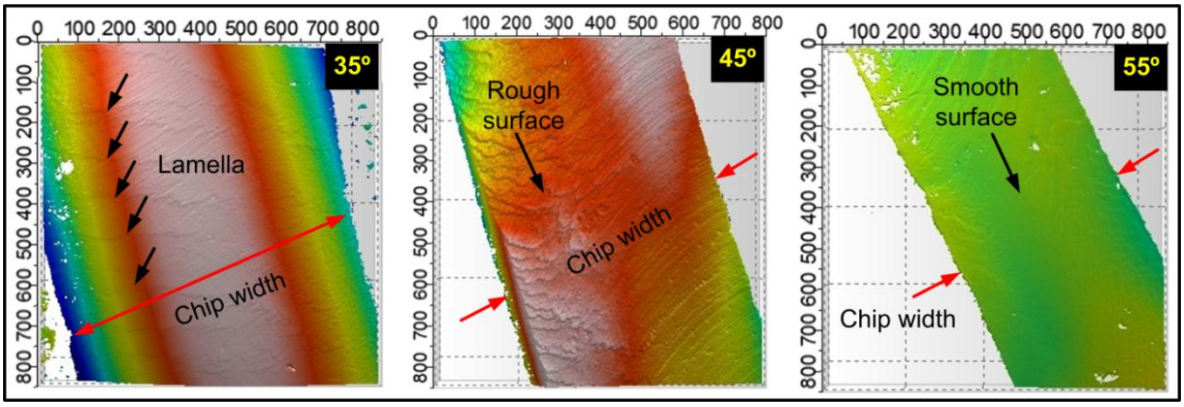

Figure 5.29 3-D profile of the back surface of the chip obtained by machining using different helix angles

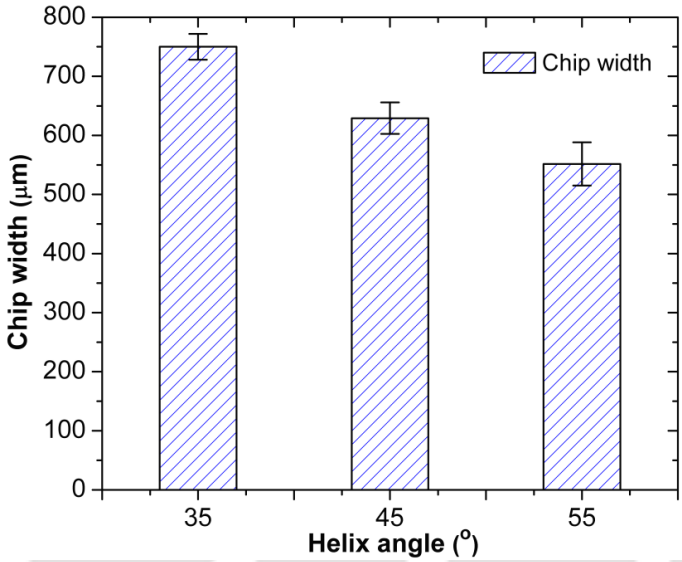

Figure 5.30 Influence of end mill helix angle on chip width

5.10 Summary

This chapter presents the results obtained during the systematic experiments carried out on thin-wall end milling operation. The experiments were conducted in two phases. At first, the experiments were carried out to determine the influential process parameters viz. feed per tooth, spindle speed, axial and radial depth of cut on the performance parameters such as milling force, surface roughness and wall deflection. Spindle speed was found to have relatively low effect on the responses. However, the radial depth of cut, axial cut depth and feed per tooth were found to have significant influence on the performance of thin-wall machining process. Based on the initial study, the levels of these process parameters were finalized. These were further used for detailed investigation.

In the second phase of the work, investigations into the influence of tool geometry parameters such as tool diameter, helix angle and number of flutes on the performance of the process were carried out. Grey relational analysis (GRA) methodology was utilized to obtain the optimal and influential tool geometry parameters. Based on the Grey relational rank, tool diameter was found be highly influencing on the process responses, viz. milling force, surface roughness and wall deflection. GRA suggested that an optimal combination of tool geometry parameters i.e. diameter 8 mm with helix angle of 45° and 4 flutes achieves the desired process performance. This optimal combination was verified by conducting actual experiment and it was found that the suggested tool geometry parameters produces a considerable improvement in the surface quality of machined part. An excellent surface finish of 0.401 µm *Ra* value was obtained. It was also noted that with the optimal tool geometry parameters, the average deflection of 0.074 mm was achieved. It can also be noted there is significant reduction in the deflection of thin-wall (about 6.33%) when optimum parameters were used.

In the present work, a study on the influence of tool helix angle on chip morphology was carried out. It was noted during thin-wall milling operation, continuous chips with semi-parabolic, semi-circular or near circular shape were formed. Material folds were observed on the free surface of chips. Lamella like structures was observed on the chip back surface, with lamella being prominent while tool having helix of 35º was used. Higher helix tools produced relatively lamella free surface. The back surface of the chip was shiny with abrasion marks from chip particles which adhered on the tool surface. High helix angle helped in easy shearing away of the chip as compared to a low helix tool and produces better surface quality.

Based on the studies carried out in this chapter, it was noted that feed per tooth, tool diameter, axial depth of cut and radial depth of cut are the most influential parameters. In view of this, a comprehensive full factorial experimental study was planned. The details of the experiments and the results obtained are elaborately presented in the next chapter.

Chapter 6

Comprehensive Full Factorial Experimental Investigations into Thin-Wall Milling Process using Response Surface Methodology (RSM)

6.0 Scope

This chapter presents the results obtained during full factorial experiments carried out on thin-wall machining of aluminum alloy 2024-T351. Experiments were conducted by considering the most influential milling parameters viz. axial depth of cut, radial depth of cut, feed per tooth, and tool diameter, those obtained from initial experiments as presented in Chapter 5. A systematic study has been presented on the influence of these milling parameters on the process performance measures such as cutting energy (milling force), productivity (material removal rate) and product quality (uniform wall thickness and surface quality). Based on the study, the recommendations for practical applications have been made. Finally, the predictive models for the process performance were developed.

6.1 The Need

During the thin-wall machining process, to meet the tight dimensional tolerance and obtain a superior surface quality of a workpiece, low feed and depth of cuts are generally employed. However, employing low levels of process parameters affects the process productivity, because, during the thin-wall milling process, a bulk of the material (approximately 90-95 %) is removed from the initial work volume. In order to increase the material removal rate (MRR), high feed and large depth of cut are to be employed which results in higher magnitude of milling force. As the thin-wall structures possess low stiffness they often deflect and deform under the action of milling force which generates form error and poor surface quality. Moreover, the aluminum alloys possess a comparatively low modulus of elasticity which causes the workpiece to spring back. This spring back action often results in deflection and chatter which reduces the material removal rate and leads to poor surface finish. Thus it can be summarized that the performance of machining of thin-wall parts has to be evaluated by using four parameters viz. milling force, material removal rate (MRR), wall deflection and surface roughness. Milling force determines the energy required the machine a workpiece; MRR presents the productivity of the process, whereas wall deflection and surface roughness

provide the information about the product quality. Literature reports various research works on the experimental analysis to achieve these criteria at individual level. (Chapter 2, Sections 2.3 and 2.6). There is hardly any attempt on an integrated and comprehensive study on the influence of critical milling parameters on all four performance measures. A need was thus identified to carry out a comprehensive experimental study to determine the influence of milling parameters on the process responses viz. milling force, wall deflection, surface roughness and material removal rate during thin-wall machining of aluminum alloy 2024-T351.

6.2 Experimental Details

The primary objective of the present experimental investigation is to analyze the influence of feed per tooth, axial depth of cut, radial depth of cut and tool diameter viz. on the performance parameters viz. milling force, material removal rate, surface roughness and wall deflection during thin-wall machining of aluminum alloy under dry cutting conditions. Figure 6.1 depicts the overview of the work carried out in the third phase of the work.

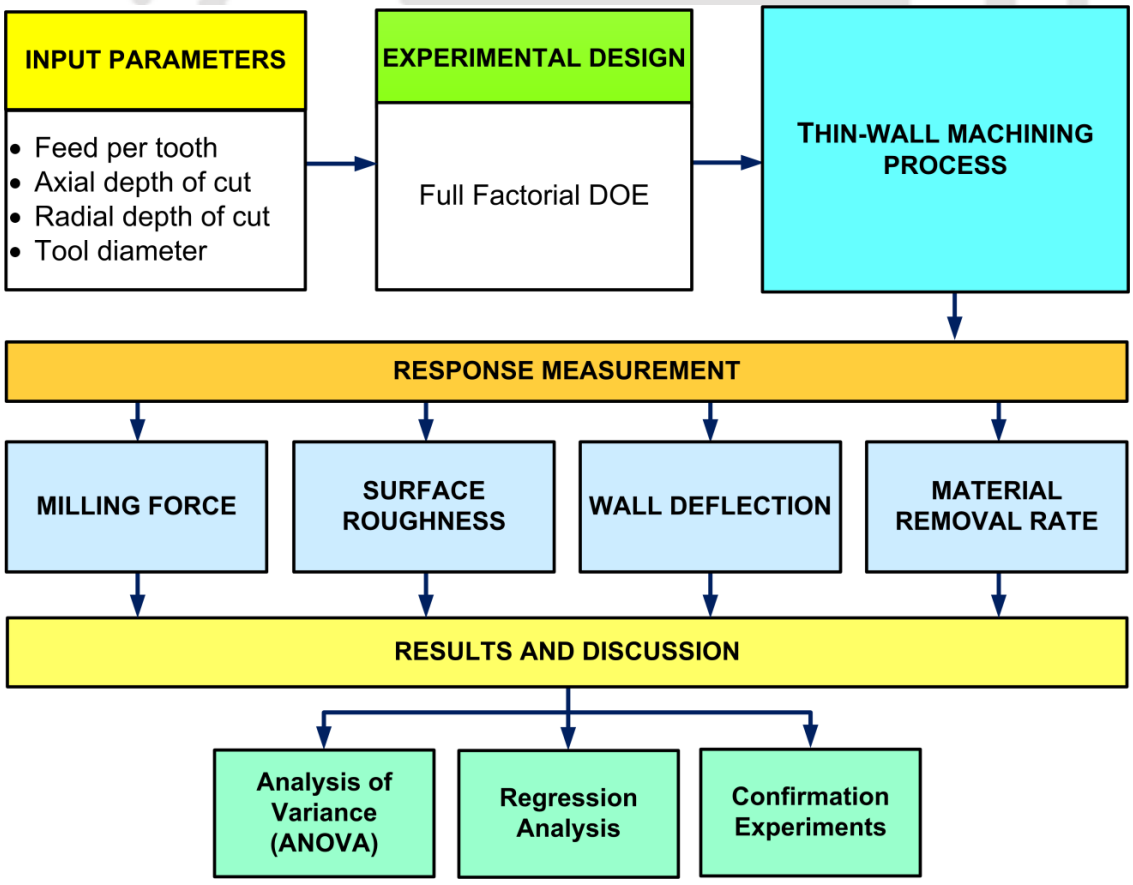

Figure 6.1 Overview of the work carried out in phase three

Based on the observations made during initial experiments (Chapter 5), four milling parameters were considered for the experimental study. Experiments were planned based on the full factorial experimental design. Initially, an experimental setup was developed and necessary fixtures for holding the workpiece and measurement system were designed and fabricated. Then experiments based on the full-factorial design (DoE) were planned and carried out. A total of 81 (3^4) experiments were executed. Table 6.1 shows the chosen milling parameters and their levels.

Table 6.1 Experimental milling parameters

Milling parameters	**Level 1**	**Level 2**	**Level 3**
f_z **(mm/z)**	0.02	0.04	0.06
d_i **(mm)**	4	8	12
a_d **(mm)**	8	12	24
r_d **(mm)**	0.3125	0.625	1.25

For each experiment, process responses i.e. milling force, material removal rate, surface roughness and wall deflection were measured. Details about the measurement procedure are presented in Chapter 5, Section 5.6. Finally, statistical analysis of the gathered data was carried out and guidelines for efficient and quality thin-wall machining were derived.

In the present work, the experimental results were analyzed by using the response surface methodology (RSM). RSM is a statistical tool developed for modeling and analysis of complex multivariate processes, where a response is influenced by several variables. It uses mathematical modeling and statistical procedure to determine the relationship between independent input process parameters and output data (response parameter) (Montgomery (2013), Asiltürk et al. (2016)). The first step in RSM analysis is to design the experiments based on the identified milling parameters. The models developed by RSM can be of first order or second order. The first-order models are termed as main effect models, as they consider only the main effects of the variables whereas, in the second order models, the interaction effects are also considered along with the main effects. Use of interaction terms introduces a curvature into the response function. For solving real-life complex problems, second-order models are generally used. They are flexible and can estimate the coefficients easily by the method of least squares. The generalized second-order polynomial model used in the response surface

analysis is given as:

$$y = \beta_0 + \sum_{i=1}^{k} \beta_i x_i + \sum_{i<j} \sum \beta_{ij} x_i x_j + \sum_{i=1}^{k} \beta_{ii} x_i^2 + \varepsilon \quad (6.1)$$

where, y is the predicted response, β_0 a constant, β_i, β_{ii} and β_{ij} are the first, second degree coded input parameters and parameter interactions respectively. The random error is denoted by ε.

6.3 Results and Discussion

Experiments on thin-wall machining operations were performed as per the designed array and the responses were measured using the instruments. The recorded values of process responses are tabulated in Table 6.2. Then a detailed analysis of process responses was carried out using analysis of variance (ANOVA). It examines the main effects of independent milling variables and their interaction effects. Plots pertaining to main effects and response surface corresponding to ANOVA analysis of all process responses were constructed, and then a systematic study was carried out to derive the useful conclusions. Statistical terms related to ANOVA are listed below:

- *P-value*: It denotes the probability that whether the results observed in the study could have occurred by chance. The *P-value* ranges from zero to one. If the *P-value* is greater than 0.1 for any parameter, then the parameter is deemed insignificant. If the *P-value* lies in between 0.05 to 0.1, then the parameter is considered as mildly significant, and if the value is less than 0.05, then the parameter considered as highly significant.
- R^2: It is called the coefficient of determination. It provides a measure of variability in the response values which are under observation and can be explained by controllable factors and their interactions. The predicted model is considered sensitive if the R^2 is greater than 75%, else the model is considered as insignificant. Usually, *adjusted-*R^2 is used in statistical methods to compare the models with different numbers of independent variables. This is because; *adjusted-*R^2 increases only if the new term improves the model more than would be expected. The value of *adjusted-*R^2 is always smaller than or equal to R^2. Another term used during the analysis is *predicted-*R^2. It determines how well the model can predict the responses for any new observation. Larger the value of predicted-R^2 greater is the predictive capability of the model.

Table 6.2 3^4 full factorial machining experiment results

Run No.	Milling parameters				Response parameters			
	d_i (mm)	f_z (mm/z)	a_d (mm)	r_d (mm)	R_a (µm)	F_c (N)	D_f (mm)	MRR (mm^3/min)
1	12	0.06	8	0.3125	0.585	84.39	0.077	1119.4
2	12	0.02	8	0.3125	0.407	64.08	0.021	426.231
3	12	0.04	12	0.625	0.687	136.9	0.077	2063.11
4	12	0.02	12	0.625	0.577	117.25	0.054	1093.8
5	8	0.06	24	0.3125	0.547	180.57	0.093	3692.09
6	8	0.06	8	1.25	0.705	176.27	0.222	4854.06
7	8	0.02	8	1.25	0.425	91.9	0.178	1855.67
8	4	0.06	8	0.3125	0.832	195.3	0.068	1340.69
9	4	0.02	8	1.25	0.797	124.45	0.098	2057.01
10	8	0.02	12	1.25	0.512	129.6	0.227	2785.87
11	12	0.04	8	0.3125	0.547	72.63	0.059	795.88
12	12	0.06	24	0.3125	0.685	327.87	0.141	3396.98
13	12	0.02	8	1.25	0.64	118.27	0.189	1693.04
14	12	0.04	12	1.25	0.75	204.81	0.276	4753.03
15	12	0.04	24	0.625	0.672	204.61	0.124	4148.59
16	8	0.02	24	1.25	0.442	183.41	0.394	5585.98
17	4	0.04	24	1.25	*	*	*	*
18	12	0.02	24	1.25	0.665	351.04	0.411	5101.7
19	12	0.02	12	0.3125	0.502	82.46	0.026	640.06
20	8	0.04	24	0.625	0.617	182.75	0.095	4690.37
21	4	0.06	8	0.625	0.945	222.25	0.112	2528.09
22	4	0.02	24	1.25	0.995	259.88	0.329	6181.82
23	8	0.04	24	0.3125	0.472	136.81	0.077	2623.46
24	4	0.06	24	0.3125	0.945	228.16	0.114	4039.07
25	4	0.06	12	0.3125	0.995	197.33	0.081	2013.16
26	4	0.02	8	0.625	0.625	135.24	0.069	964.691
27	4	0.02	12	1.25	0.962	165.65	0.139	3086.54
28	12	0.06	8	1.25	0.672	162.19	0.232	4447.67
29	4	0.04	8	0.3125	0.75	169.4	0.052	957.447
30	8	0.04	12	0.3125	0.507	81.86	0.047	1305.91
31	4	0.02	8	0.3125	0.557	112.67	0.026	515.429

32	8	0.02	24	0.625	0.437	113.25	0.075	2492.67
33	12	0.04	12	0.3125	0.67	110.26	0.072	1196.06
34	4	0.04	8	0.625	0.827	198.54	0.091	1799.15
35	8	0.06	8	0.625	0.69	90.16	0.08	2194.49
36	12	0.06	8	0.625	0.645	101.82	0.089	1946.57
37	12	0.06	24	0.625	0.707	373.64	0.168	5902.78
38	12	0.02	24	0.3125	0.487	158.19	0.071	1284.42
39	4	0.02	12	0.3125	0.655	130.2	0.056	773.509
40	4	0.06	12	0.625	1.125	235.58	0.221	3796.53
41	4	0.02	24	0.625	0.88	169.16	0.138	2898.83
42	4	0.04	12	0.625	1.062	209.54	0.171	2701.27
43	4	0.04	24	0.3125	0.822	209.12	0.081	2882.44
44	12	0.06	24	1.25	0.732	616.01	0.67	13515.9
45	12	0.02	8	0.625	0.497	79.58	0.041	728.571
46	8	0.02	12	0.3125	0.4	60.53	0.021	700.678
47	8	0.06	24	1.25	0.757	413.36	0.615	14683.3
48	8	0.02	8	0.625	0.385	51.83	0.0316	828.281
49	12	0.04	8	1.25	0.665	144.7	0.228	3161.81
50	4	0.04	8	1.25	0.872	178.16	0.138	3821.18
51	8	0.02	24	0.3125	0.335	86.87	0.046	1404.7
52	8	0.06	12	0.3125	0.592	109.83	0.065	1834.53
53	12	0.04	24	0.3125	0.64	255.6	0.097	2407.17
54	4	0.02	12	0.625	0.905	143.95	0.136	1447.77
55	8	0.04	24	1.25	0.625	315.59	0.547	10436.6
56	4	0.02	24	0.3125	0.625	138.77	0.0588	1549.21
57	8	0.04	12	0.625	0.625	108.99	0.07	2334.45
58	4	0.06	24	0.625	1.105	272.6	0.226	7619.52
59	8	0.02	8	0.3125	0.32	34.75	0.013	466.691
60	4	0.04	24	0.625	1.027	261.25	0.174	5414.01
61	4	0.06	8	1.25	1.107	212.27	0.186	5351.52
62	8	0.06	24	0.625	0.702	249.3	0.115	6640.63
63	12	0.06	12	1.25	0.755	244.07	0.321	6692.91
64	8	0.06	8	0.3125	0.532	66.18	0.059	1220.1
65	12	0.02	12	1.25	0.697	164.6	0.242	2542.37
66	4	0.06	12	1.25	*	*	*	*

67	12	0.06	12	0.625	0.722	163.65	0.123	2927.67
68	4	0.04	12	0.3125	0.89	172.97	0.066	1437.43
69	12	0.04	8	0.625	0.637	96.83	0.064	1372.69
70	12	0.04	24	1.25	0.732	554.99	0.603	9568.48
71	8	0.04	8	0.3125	0.455	54.83	0.024	869.516
72	8	0.04	8	0.625	0.605	81.25	0.051	1553.93
73	4	0.04	12	1.25	1.01	232.63	0.155	5736.78
74	12	0.02	24	0.625	0.527	192.46	0.104	2193.86
75	8	0.02	12	0.625	0.455	80.027	0.057	1243.5
76	8	0.06	12	0.625	0.817	140.84	0.09	3298.84
77	8	0.06	12	1.25	0.907	252.5	0.34	7299.62
78	4	0.06	24	1.25	*	*	*	*
79	8	0.04	12	1.25	0.645	185.47	0.326	5193.48
80	8	0.04	8	1.25	0.615	135.55	0.202	3456.85
81	12	0.06	12	0.3125	0.71	117.17	0.09	1683.54

*****Unable to collect data due to tool failure

6.3.1 Analysis of Milling Force

Milling force is an important performance parameter in thin-wall machining operation. It controls the precision and quality of the machined thin-wall component. Milling force values are used to estimate the cutting power requirements. Also, analysis of milling forces is helpful in monitoring the machine tool health. Table 6.3 shows the ANOVA applied for milling force. The test for significance of regression and individual model coefficients were obtained. The terms which do not affect the model significantly were eliminated by backward elimination procedure. After the elimination, the linear terms feed per tooth (f_z), axial depth of cut (a_d) and radial depth of cut (r_d) were found to be significant. The quadratic effect of tool diameter (d_i) was found to be significant so the linear term was included in the model. Interaction effects, $d_i{*}a_d$, $d_i{*}r_d$, $f_z{*}a_d$, $f_z{*}r_d$ and $a_d{*}r_d$ were found significant (Table 6.3).

Table 6.3 ANOVA for milling force after back elimination

Source	Sum of Squares	DOF	Mean Square	F Value	P–value	Remarks
Model	7.549E+005	10	75491.19	97.31	<0.0001	Significant
d_i	218.71	1	218.71	0.28	0.5972	Significant
f_z	1.397E+005	1	1.397E+005	180.13	<0.0001	Significant
a_d	3.094E+005	1	3.094E+005	398.8	<0.0001	Significant
r_d	1.864E+005	1	1.864E+005	240.33	<0.0001	Significant
d_i*a_d	51409.21	1	51409.21	66.27	<0.0001	Significant
d_i*r_d	11101.96	1	11101.96	14.31	0.0003	Significant
f_z*a_d	26855.32	1	26855.32	34.62	<0.0001	Significant
f_z*r_d	8959.02	1	8959.02	11.255	0.0011	Significant
a_d*r_d	48585.52	1	48585.52	62.63	<0.0001	Significant
d_i^2	66749.9	1	66749.9	86.04	<0.0001	Significant
Residual	51976.42	67	757.77			
Total	8.069E+005	77				

The results of reduced model indicated that the model was significant (*P*–value less than 0.05). The R^2, adjusted R^2 and predicted R^2 values for the milling force were found to be 0.936, 0.926 and 0.905 respectively. It can be noted that the predicted R^2 is in good agreement with adjusted R^2 which shows that the model was able to explain 90.50% of the variability in new data. The adequate precision ratio of 48.980 indicates the adequate model discrimination. The correlation between the influential factors (d_i, f_z, a_d and r_d) and milling force was obtained by carrying out regression analysis. After eliminating the non-significant terms, the final response equation derived for milling force (F_c) in terms of actual factors is:

$$F_c = \begin{bmatrix} 535.25 - 88.42 * d_i - 1314.48 * f_z - 14.40 * a_d - 172.49 * r_d + 1.20 * d_i * a_d \\ +10.00 * d_i * r_d + 168.22 * f_z * a_d + 1736.93 * f_z * r_d + 9.89 * a_d * r_d + 3.87 * d_i^2 \end{bmatrix} \quad (6.2)$$

The developed model can be used to predict the milling force (F_c) during thin-wall machining process for chosen process conditions within the scope of this work. Figure 6.2(a) displays the normal probability plot of the residuals for milling force. It can be noticed that the residuals are falling in a straight line, which means that the errors are normally distributed. Figure 6.2(b) illustrates the relationship between the actual and predicted values of milling force. These plots indicate that the developed models are

adequate and are able to predict the results with reasonably good accuracy.

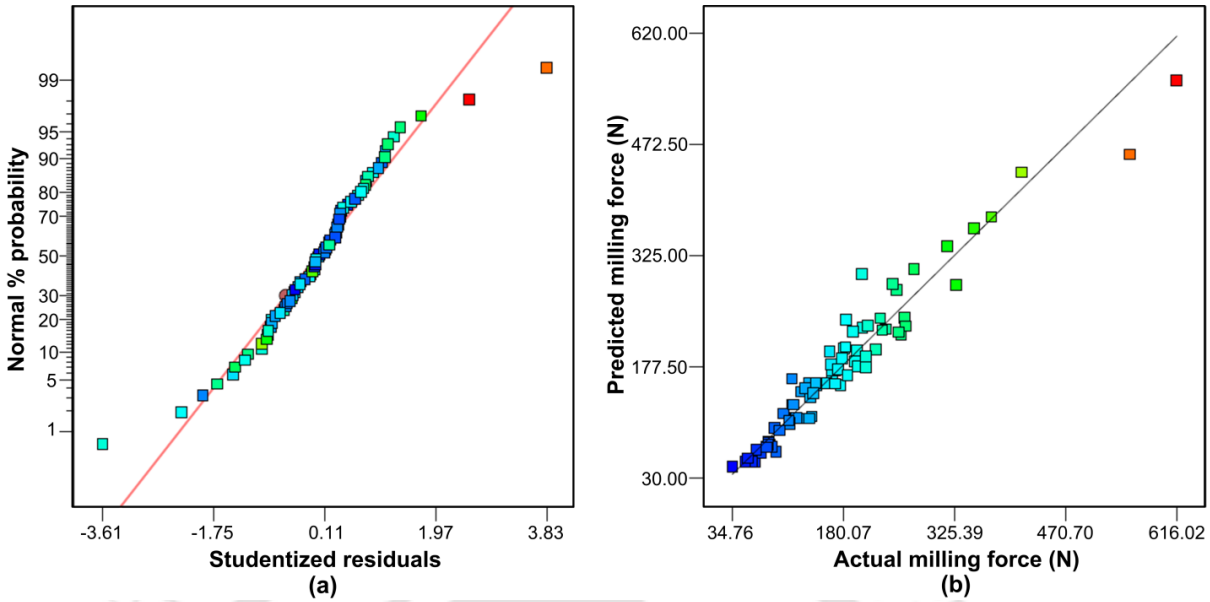

Figure 6.2 (a) Normal probability plot of studentized residuals, **(b)** Plot of actual vs. predicted response for milling force

Figure 6.3(a) shows the perturbation plot for variation in the milling force with respect to four milling parameters viz. feed per tooth, tool diameter, axial depth of cut and radial depth of cut. The steep positive slopes for input process parameters viz. feed per tooth, axial depth of cut and radial depth of cut show that the process response is sensitive to these process parameters. Figure 6.3(b) shows a 3-D surface response variation graph which illustrates the interaction effect between tool diameter and axial depth of cut on the milling force. It can be observed that the milling force increases considerably with the increase in axial depth of cut. The increase in tool diameter from 4 mm to 8 mm reduces the milling force but further increase in the tool diameter leads to increase in force values. From the interaction plot shown in Figure 6.3(c), a steep increase in milling force with the radial depth of cut was noted. From this figure, it is evident that minimum force can be obtained by employing lower radial depth of cut with a cutting tool of 8 mm diameter. From the interaction plot shown in Figure 6.3(d-f), it is observed that the milling force increases with feed per tooth, axial depth of cut and radial depth of cut. It can be noted that milling force is directly proportional to combination of the maximum levels of these parameters. High feed and depth values increase the material removal rate and in turn consume more energy. Primarily low values of milling force are desired for accurate and smoother machining of thin-walls.

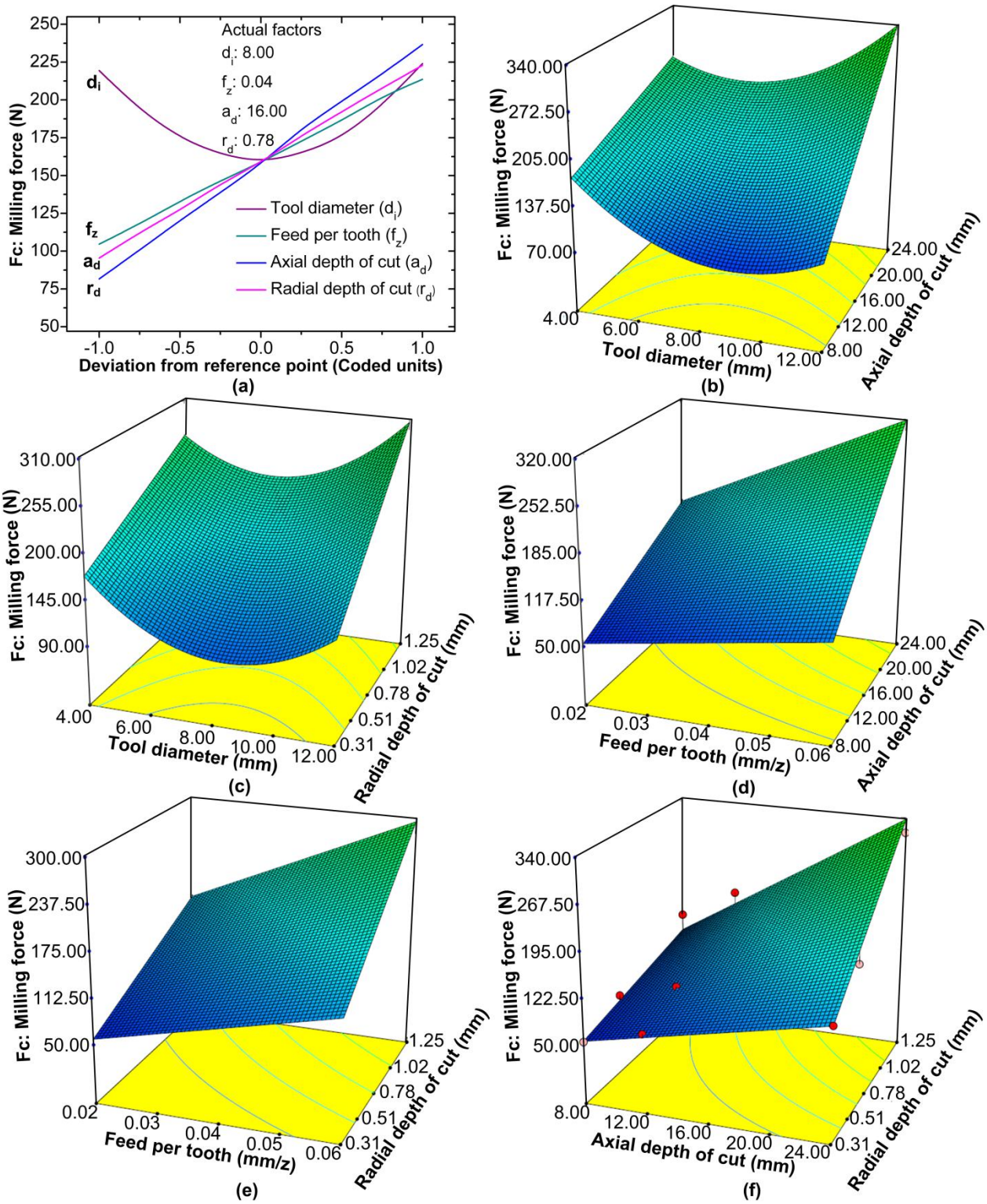

Figure 6.3 Analysis plots for milling force: **(a)** Perturbation plot, **(b)** Interaction of d_i and a_d, **(c)** Interaction of d_i and r_d, **(d)** Interaction of f_z and a_d, **(e)** Interaction of f_z and r_d, **(f)** Interaction of a_d and r_d

6.3.1.1 Influence of Variation in Milling Parameters on Milling Force

After the ANOVA analysis, the influence of various milling parameters on the milling force was studied. Figure 6.4(a) shows the effect of feed per tooth (f_z) on the milling

force. It can be seen that milling force increases with the increase in feed value. It is because an increase in feed value increases the cutter contact with the material thereby increasing the chip load which results in increase in the milling force. Figure 6.4(b) shows the variation of milling force with the increase in tool diameter. It can be noted that the milling force first decreases and then increases with the increase in tool diameter. For fixed values of feed per tooth, axial depth of cut and radial depth, 4 mm diameter tool produces higher force values. For conducting the experiments, end mills having sharp cutting edges were used. Therefore the increase in the milling force can be attributed to the low space availability along the cutter flutes which resists the chip flow over the cutting tool surfaces. This resulted in the formation of built-up edges (BUE) at the cutting edges (see Figure 6.5(a)). BUEs create a proxy blunt cutting edge. Also during the machining operation, it was observed that the cut chips swirl around the cutting tool (see Figure 6.5(b)).

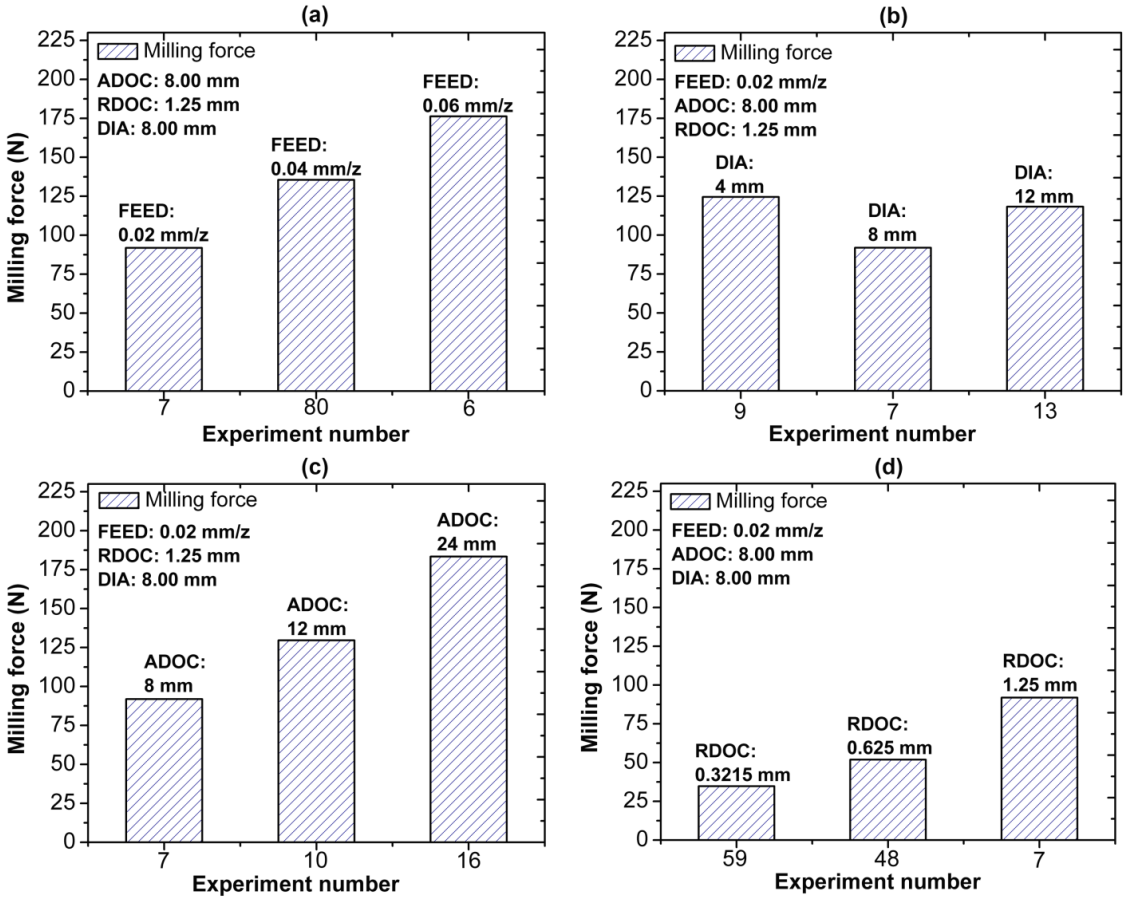

Figure 6.4 Variation of milling force with milling parameters: **(a)** Feed per tooth, **(b)** Tool diameter, **(c)** Axial depth of cut, **(d)** Radial depth of cut

Due to the blunt edge and swirled cut-chips, friction at tool-work contact area increases which results in the increase in milling force. Further, it can be seen that the milling

force reduced for 8 mm tools, as these tools provide sufficient space for chip flow along the cutter flutes. However, further increase in tool diameter to 12 mm increases the milling force values. It is because the larger diameter tool is more rigid and applies more pressure on thin-wall workpiece.

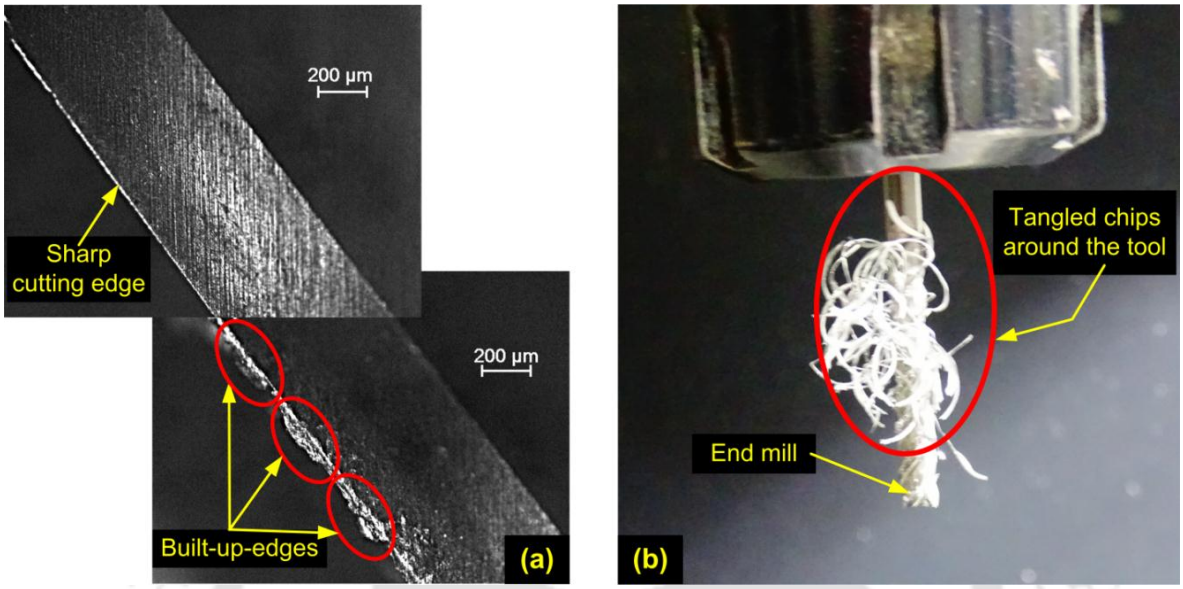

Figure 6.5 (a) Built-up-edge (BUE) formation, **(b)** Chips entangled around the cutting tool

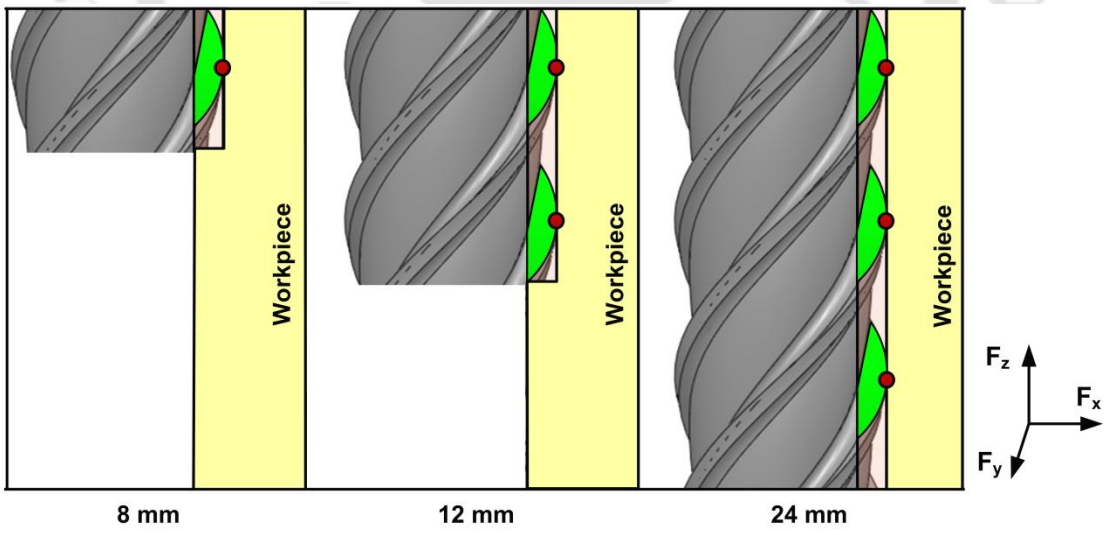

Figure 6.6 Influence of axial depth of cut on milling force

Axial depth of cut, (a_d) is an important process parameter in view of higher process productivity. For higher productivity, generally higher values of axial depth of cut are preferred. Figure 6.4(c) shows the influence of axial depth of cut on the milling force. It can be observed that increase in axial depth of cut increases the milling force and thereby increasing the power consumption. It is because with an increase in axial depth of cut,

engagement length of the flute with the workpiece increases. This is depicted in Figure 6.6. It can be seen that for a fixed radial depth of cut value (r_d), when the axial depth of cut (a_d) increases from ADOC1 (8 mm) to ADOC3 (24 mm), contact area increases in the axial direction which result in high milling force values.

In a similar fashion, for a fixed axial depth of cut (a_d), an increase in radial depth of cut increases the force values due to increase in width of the cut (see Figure 6.4(d)). At a high depth of cut condition, adhesion of chip material on the flute surface of 4 mm tool was observed and due to the low flute space available in slender end mills which resulted in clogging of the flutes (see Figure 6.7). This resulted in a drastic rise in the milling force causing catastrophic failure of tools at higher feed and depth of cut conditions. Therefore, it is recommended to avoid smaller diameter tool when high process conditions are needed. If the use of small diameter tool is inevitable, employment of lower levels of process conditions is recommended along with application of lubricants to keep the cutting edge free from BUEs.

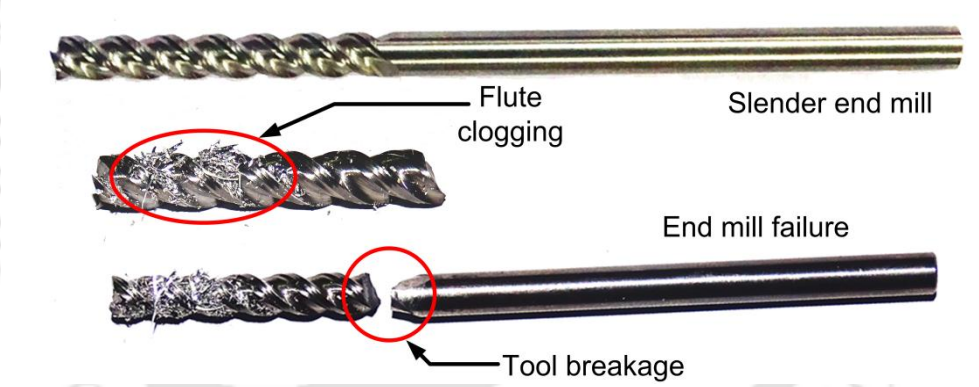

Figure 6.7 Tool flute clogging with chips and tool failure due to breakage

6.3.2 Analysis of Surface Quality

Excellent surface quality is an important requirement for components to be used in automobile and aerospace industry. Poor surface finish results in development of residual stresses which may lead to failure of work part when subjected to severe fatigue loading conditions such as the wing structures of an aircraft. For analysis of surface roughness, backward elimination procedure was used to eliminate the insignificant terms. The data after the ANOVA is given in Table 6.4. From the table, it can be seen that the individual and quadratic effects of all the parameters are significant. The *P*-value is noted to be less than 0.05. It indicates that the model is significant. Computed values of R^2, adjusted R^2 and predicted R^2 0.8899, 0.8715 and 0.845 indicate that the mode is adequate for the

prediction of process responses. The value of adequate precision ratio as 29.548 indicates adequate model discrimination.

The correlation between the influential factors (d_i, f_z, a_d and r_d) and surface roughness was obtained by using regression analysis. After eliminating the non-significant terms, the final response equation derived for surface roughness (R_a) in terms of actual factors is given as:

$$R_a = \begin{bmatrix} 0.46 - 0.21 * d_i + 14.27 * f_z + 0.06 * a_d + 0.62 * r_d - 0.27 * d_i * f_z - 6.65e^{-4} * d_i * a_d \\ -0.014 * d_i * r_d + 0.013 * d_i^2 - 85.05 * f_z^2 - 1.56e^{-3} * a_d^2 - 0.21 * r_d^2 \end{bmatrix} \quad (6.3)$$

The developed model can be used to predict the surface roughness (R_a) during thin-wall machining process for chosen process conditions.

Table 6.4 ANOVA for surface roughness after back elimination

Source	Sum of Squares	DOF	Mean Square	F Value	P–value	Remarks
Model	2.35	11	0.21	48.48	<0.0001	Significant
d_i	0.84	1	0.84	191.37	<0.0001	Significant
f_z	0.58	1	0.58	130.99	<0.0001	Significant
a_d	0.077	1	0.077	17.38	<0.0001	Significant
r_d	0.36	1	0.36	82.29	<0.0001	Significant
$di_* f_z$	0.015	1	0.015	3.52	0.0652	Significant
$d_{i*}a_d$	0.016	1	0.016	3.64	0.0609	Significant
$d_{i*}r_d$	0.023	1	0.023	5.12	0.0270	Significant
d_i^2	0.76	1	0.76	172.85	<0.0001	Significant
f_z^2	0.020	1	0.020	4.54	0.0368	Significant
a_d^2	0.091	1	0.091	20.69	<0.0001	Significant
r_d^2	0.029	1	0.029	6.51	0.0131	Significant
Residual	0.29	66	4.406E–003			
Total	2.64	77				

Figure 6.8(a) displays the normal probability plot of the residuals for surface roughness. It can be noticed that the residuals are falling in a straight line, which means that the errors are normally distributed. Figure 6.8(b) illustrates the relationship between the actual and predicted values of surface roughness. These figures indicate that the developed models are adequate and are able to predict the results with reasonably good

accuracy.

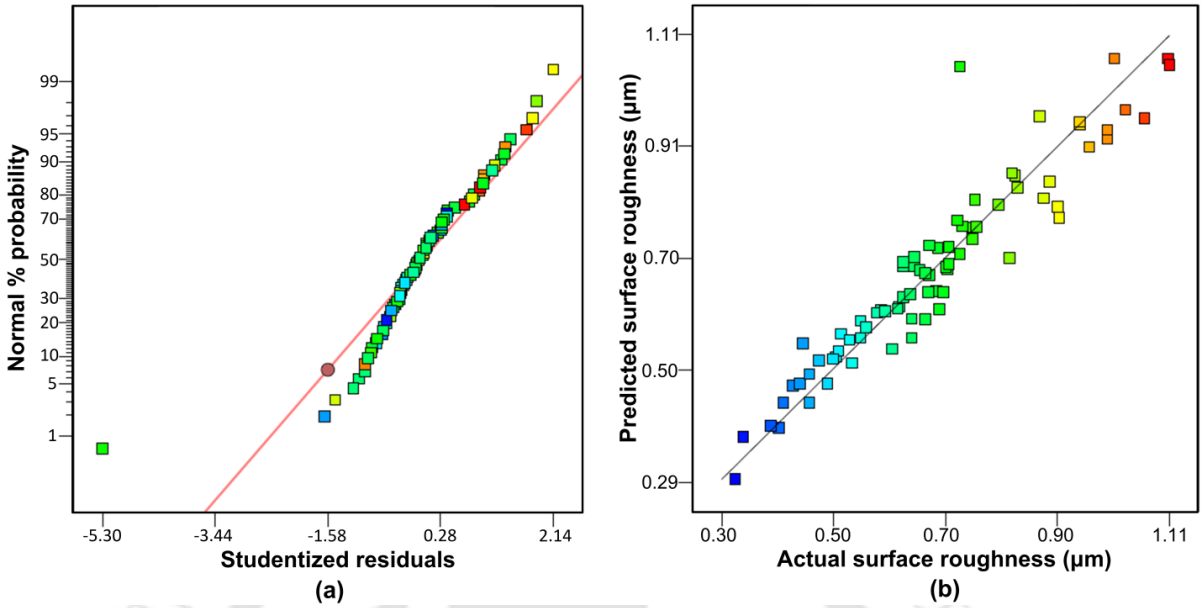

Figure 6.8 (a) Normal probability plot of studentized residuals, **(b)** Plot of actual vs. predicted response for surface roughness

Figure 6.9(a) illustrates the perturbation plot for variation of surface roughness with respect to the input parameters. It can be seen that increase in feed per tooth (f_z) and radial depth of cut (r_d) increase the surface roughness. In case of axial depth of cut (a_d), a non-linear trend was noted where the surface roughness decreases at high level of axial depth of cut. Tool diameter (d_i) is found to be an influential parameter for which the surface roughness is found to be higher on both the sides of the reference point. Figure 6.9(b) demonstrates the interaction effect of tool diameter and axial depth of cut on the surface finish. It can be inferred that, better quality finish can be achieved with a combination of low axial depth of cut and moderate tool diameter. Use of end mills having a diameter of 4 mm is to be avoided since it generates higher roughness due to flute clogging and deflection. Interaction effects of tool diameter and feed on the surface roughness are depicted in Figure 6.9(c). It can be observed that surface roughness increases with the increase in feed values. Therefore, it was concluded that use of end mill with 8 mm diameter at low feed values provides better finish during thin-wall milling. Figure 6.9(d) shows the estimated response surface plot for surface roughness in relation to tool diameter and radial depth of cut. The lower radial depth of cut in combination with moderate tool diameter is preferred when a good surface finish is desired.

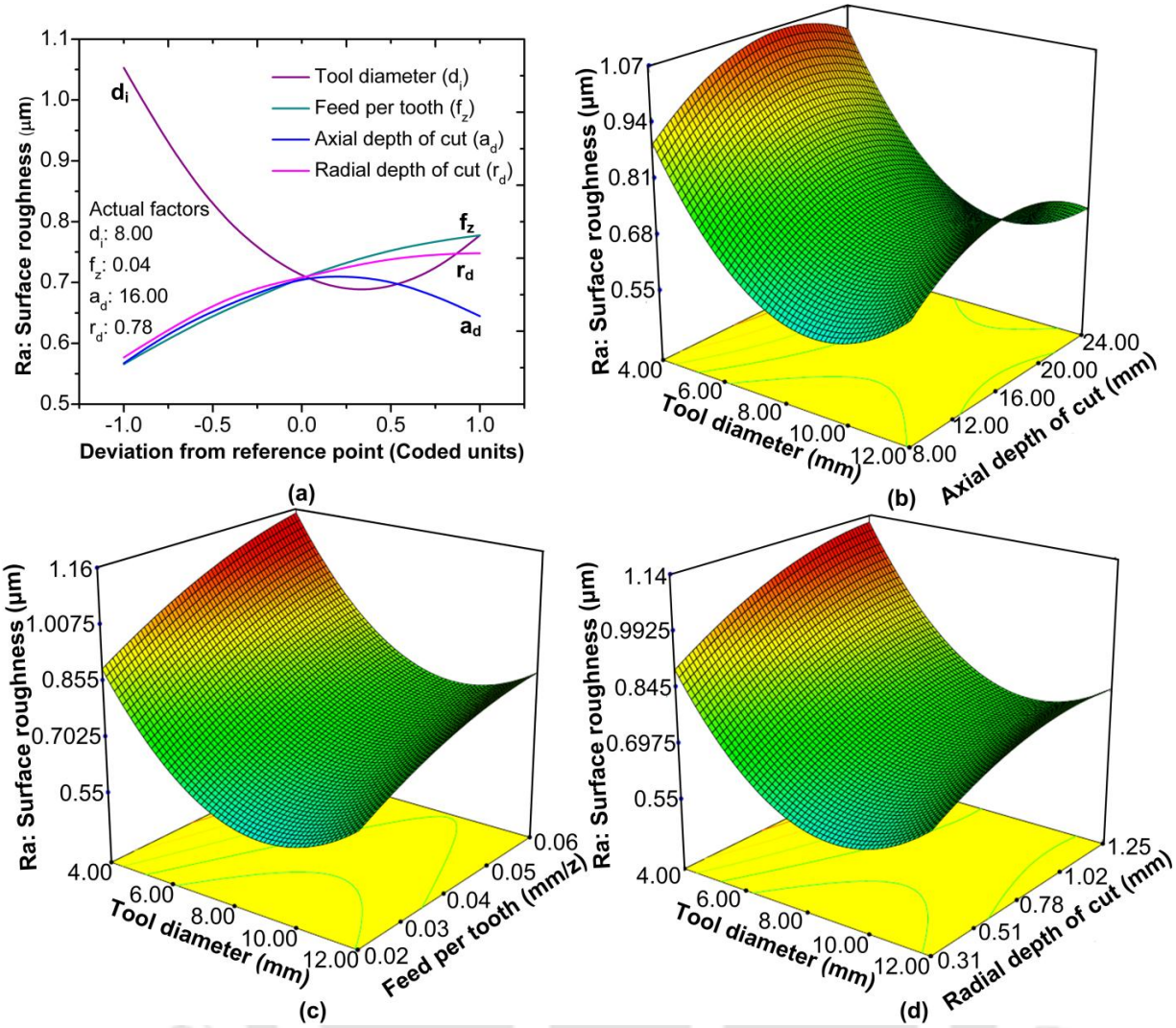

Figure 6.9 Analysis plots for surface roughness: **(a)** Perturbation plot, **(b)** Interaction of d_i and a_d, **(c)** Interaction of d_i and f_z, **(d)** Interaction of d_i and r_d

6.3.2.1 Influence of Variation in Milling Parameters on Surface Roughness

Figure 6.10 shows the effects milling parameters, viz. feed per tooth (f_z), tool diameter (d_i), axial depth of cut (a_d) and radial depth of cut (r_d) on the surface roughness. Figure 6.10(a) shows the variation of surface roughness with the increase in feed per tooth. It is noted that increase in the feed value increases the surface roughness. This can be attributed to the increase in chip load with the increased feed which further scales up the milling force values and in turn affects the surface quality. This can be understood as follows.

Chip thickness during milling was described by Martelotti (1941) as $t = f_z * sin\psi$, where f_z represents the feed per tooth and ψ the cutter angular position which in turn depends on the depth of cut and radius of the cutter (Borneman C.H. (1938)).

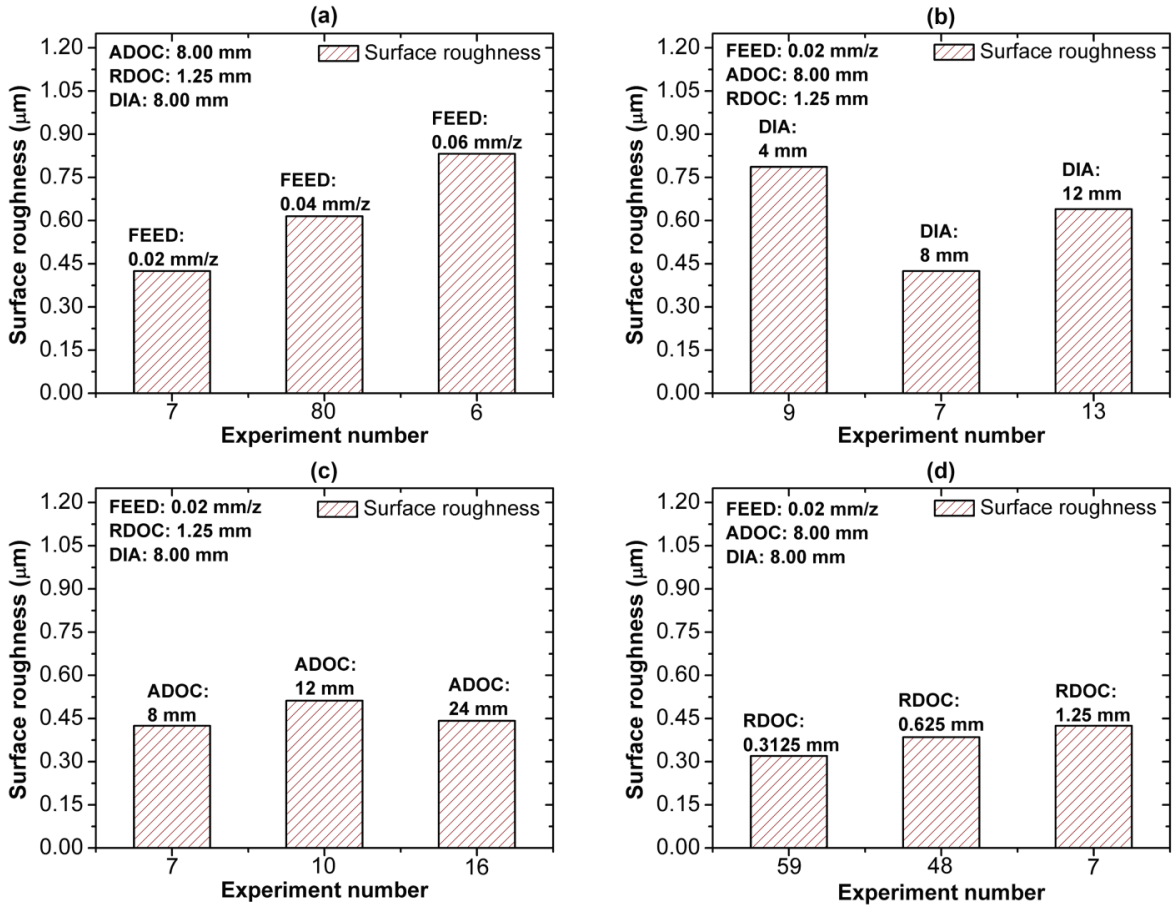

Fig. 6.10 Variation of surface roughness with milling parameters: **(a)** Feed per tooth **(b)** Tool diameter, **(c)** Axial depth of cut, **(d)** Radial depth of cut

Figure 6.11 shows the height of the tooth mark in milling and is expressed as:

$$hz = \frac{f_z^{\,2}}{8\left[R + \left(\frac{f_z \cdot f_n}{\pi}\right)\right]} \tag{6.4}$$

where, hz is the height of tooth mark above point of lowest level, R the radius of cutter and f_n the number of flutes. Thus as the feed per tooth increases, the surface roughness also increases.

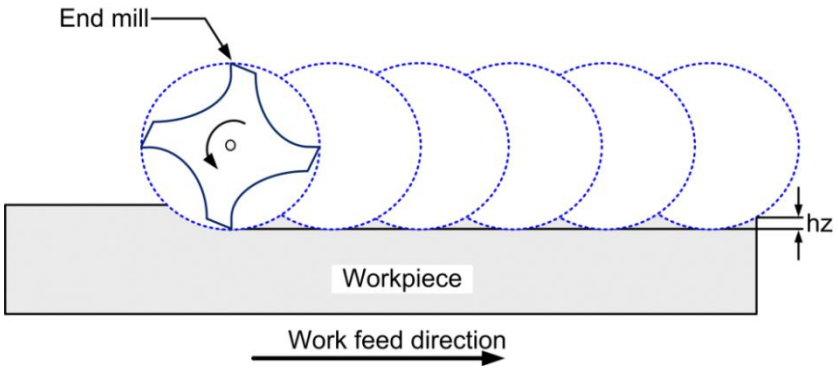

Figure 6.11 End milling surface generation

Figure 6.12(a-c) shows the 3-D surface profiles obtained by employing various levels of feed by keeping other milling parameters unchanged. It can be seen that lower feed produces superior surface quality with few lay marks (see Figure 6.12(a)). With the increase in feed value, the workpiece surface finish deteriorates (see Figure 6.12(c)) as the tool shears the work material very violently leading to more prominent feed marks. Similar trend of variation in surface roughness with the feed was observed in case of 4 mm and 12 mm diameter tools.

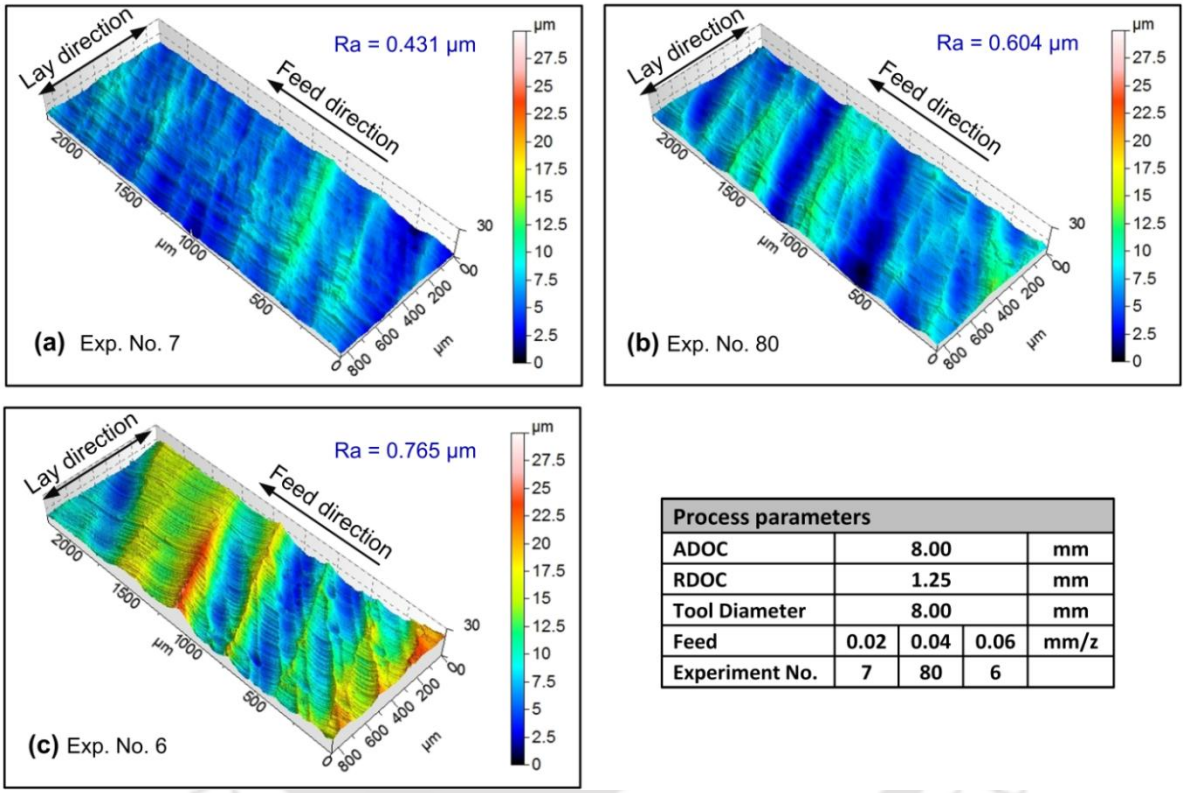

Process parameters				
ADOC	8.00			mm
RDOC	1.25			mm
Tool Diameter	8.00			mm
Feed	0.02	0.04	0.06	mm/z
Experiment No.	7	80	6	

Figure 6.12 3-D profiles of workpiece surfaces using 8 mm diameter tool at different feed values: **(a)** For experiment 7, **(b)** For experiment 80, (**c**) For experiment 6

From Figure 6.10(b), it can be observed that the surface roughness first decreases and then increases as the tool diameter increases. It is because the smaller diameter tool (4 mm) possesses low rigidity that generates chatter at tool-work contact and thus deteriorates surface quality. Moreover, to understand the problem of poor surface finish when using 4 mm tool further investigation was carried out. Figure 6.13 shows the 3-D surface profiles generated while machining with a 4 mm diameter tool. It can be observed that the surface roughness generated is higher in comparison with that obtained with 8 mm tool (Figure 6.12). To investigate this anomaly, the cutting edges of the all end mill cutters (4 mm, 8 mm and 12 mm) were examined under an optical microscope.

Cutter with a diameter of 4 mm showed the formation of built-up edges (BUEs) (see Figure 6.5(a)); however, the end milling cutters with the diameter of 8 mm and 12 mm were free from any BUEs. It may be due to the fact that, larger diameter tools (8 mm and 12 mm) dissipate more heat due to larger surface areas, which is not favorable to the formation of BUEs. Cutting edges with BUEs deteriorates the surface quality.

From Figure 6.10(b) it can also be noted that the surface roughness increases with the increase in tool diameter from 8 mm to 12 mm. This is because the larger tool applies higher intermittent milling forces that generate deep valleys on the work surface. Thus from this study, it is recommended to employ a medium diameter tool of 8 mm in practice that produces a superior quality surface finish.

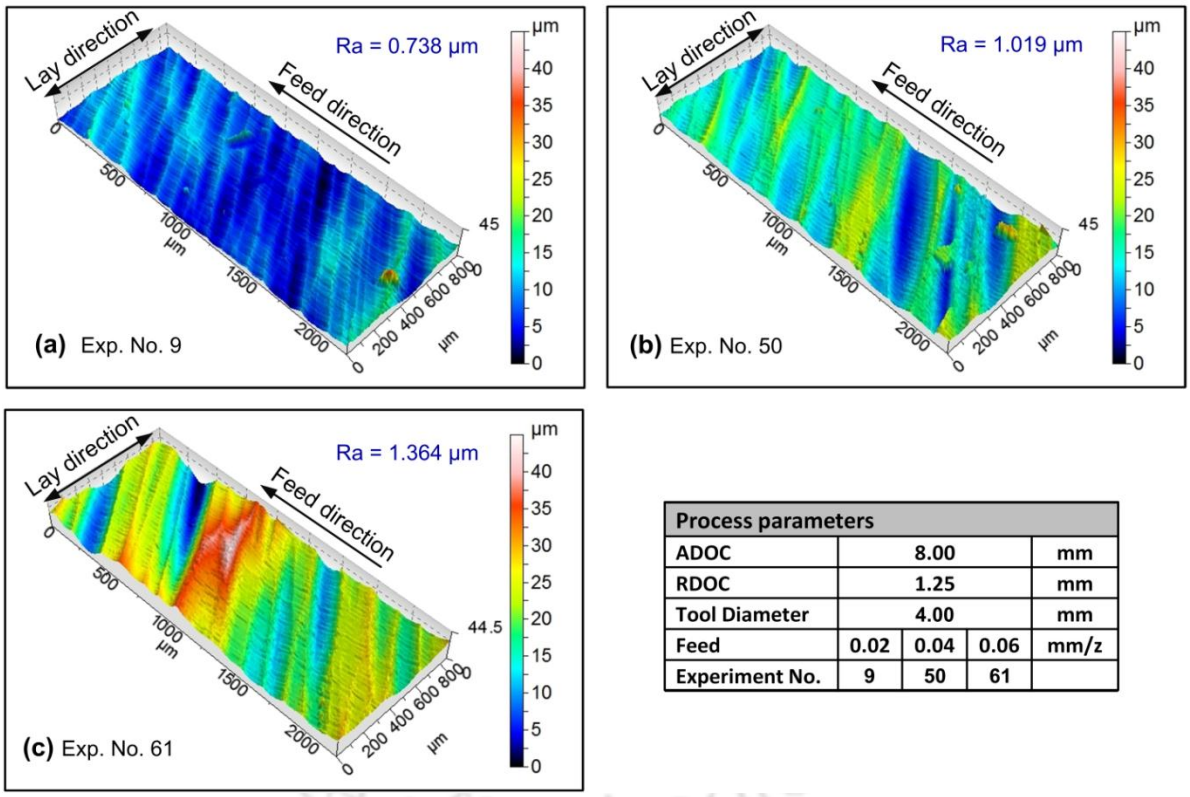

Process parameters				
ADOC	8.00			mm
RDOC	1.25			mm
Tool Diameter	4.00			mm
Feed	0.02	0.04	0.06	mm/z
Experiment No.	9	50	61	

Figure 6.13 3-D profiles of workpiece surfaces using 4 mm diameter tool at different feed values: **(a)** For experiment 9, **(b)** For experiment 50, **(c)** For experiment 61

From Figure 6.10(c), it is observed that surface roughness increases with the increase in ADOC. It is attributed to the fact that with the increase in ADOC (a_d), the contact area between the tool and work increases. This results in increase in the value of milling force; which in turn produces more deflection and poor surface finish of thin-wall. However, it is noted that the roughness value decreases with further increase in a_d to 24 mm. This is due to the fact that 24 mm ADOC eliminates the smearing of already

machined top surface which otherwise occurs in multiple passes cutting with lesser ADOCs (8 and 12 mm).

Figure 6.10(d) indicates that increase in radial depth of cut increases the surface roughness. This is because with the increase in radial depth of cut, the width of cut increases which produces larger milling force. Application of large and intermittent milling force during multi-teeth cutting of low rigidity components results in regular deflections of thin-wall during the cutting operation. This causes the material removal in an uneven fashion. This is can be observed in Figure 6.14(a-c) which shows the 3-D profiles of the machined surfaces obtained at three different locations of the sample (Experiment 9 (see Table 6.2)). It can be noted that the quality of the surface finish improves significantly from the free end of the wall towards its fixed end. It is attributed to the low rigidity of the free-end (top) of the wall. Due to low rigidity, the wall deflects more at the free end which causes higher surface roughness in comparison to that of the base of the wall. Moreover, the intermittent nature of cutting engagement with workpiece also affects the quality of the surface.

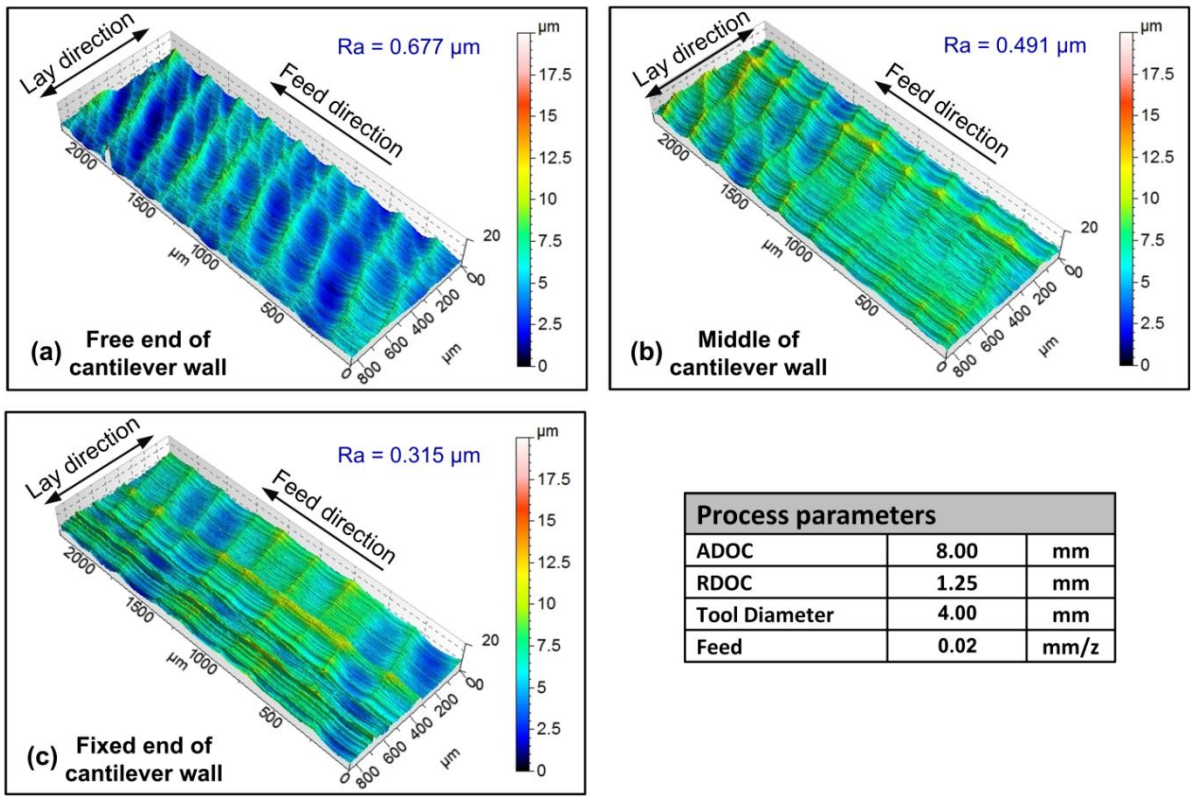

Process parameters		
ADOC	8.00	mm
RDOC	1.25	mm
Tool Diameter	4.00	mm
Feed	0.02	mm/z

Figure 6.14 Variation in surface roughness along the height of the wall: **(a)** At the free end of the cantilever, **(b)** At the middle of the cantilever, **(c)** At the fixed end of the cantilever

From further observations of the machined specimen, it was noted that many of them were having chatter marks. Chatter deteriorates the surface finish, reduces the geometrical accuracy and adversely affects the tool life. In end milling process, chatter can be associated with either tool or the workpiece. During the course of the investigation, chatter marks in the form of localized rough patches on the machined surface were observed. Figure 6.15 shows the 3-D surface profiles which were generated while machining thin-wall surface workpieces at high depth of cut conditions for three levels of tool diameter. Figure 6.15(a-c) shows the surface profiles indicating chatter at high feed (0.06 mm/z), axial depth (24 mm) and radial depth of cut (1.25 mm) condition. It can be seen that with 4 mm tool diameter, prominent chatter marks occurred. The occurrence of chatter can be attributed to the low flexural stiffness of cutting tool and high levels of axial and radial depth of cut i.e. 24 mm and 1.25 mm respectively. Due to low rigidity of the cutting tool, the tool deflects continuously with the cyclic milling forces which are generated during machining. This results in vibration. These vibrations were transmitted to the workpiece thereby generating chatter marks. Due to excessive vibrations, high cutting loads, the tool failure (breakage) was observed during the machining of thin-wall part using a 4 mm tool at high depth of cut conditions (Run Nos. 17, 66 and 78 (Table 6.2)).

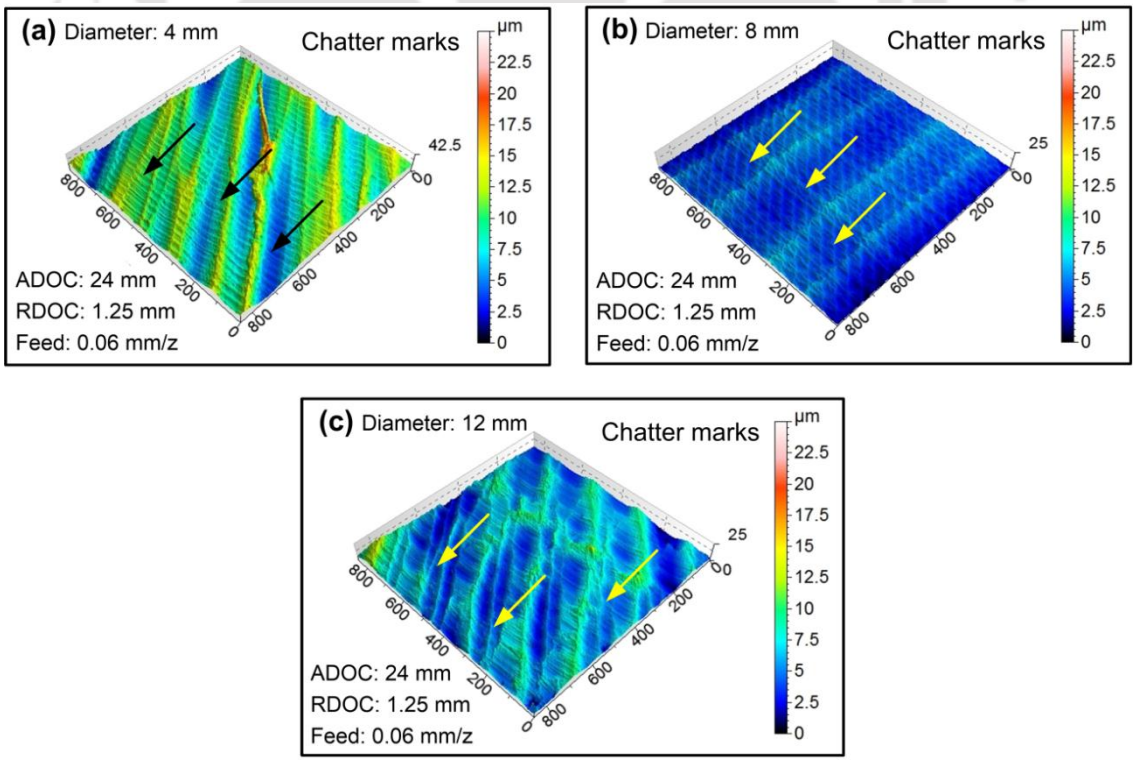

Figure 6.15 3-D optical profiles of part surface showing chatter mark for: **(a)** 4 mm diameter tool, **(b)** 8 mm diameter tool, **(c)** 12 mm diameter tool

Chatter marks were also observed while using 8 mm tool at high depth of cut condition (Figure 6.15(b)). However, the severity of the chatter was lower in comparison to that of a 4 mm tool. Figure 6.15(c) shows the surface topography of a machined specimen with a 12 mm tool. In spite of having sufficient rigidity, prominent chatter marks were observed. It may be due to the fact that the rigidity of 12 mm diameter tool was too high in comparison to the 1.25 mm thin-wall. As the cutting progresses, the thin-wall becomes flexible and eventually, the tooth passing frequency excites a resonant vibration in the thin-wall (Tlusty and Polacek (1963). The resonant vibration increases at the high axial depth of cut condition leading to an increase occurrence of interrupted and non-uniform contact between tool and the work surface thereby causing chatter which adversely affects the surface finish.

6.3.2.2 Analysis of Surface Defects

The machined parts were also examined to study the defects occurring on the machined surface. Figure 6.16 shows the 3-D profiles of the surfaces generated by a variety of process conditions. The surface profiles indicate the presence of surface defects such as material plucking, material adhesion, material smearing, and deformed layer formation.

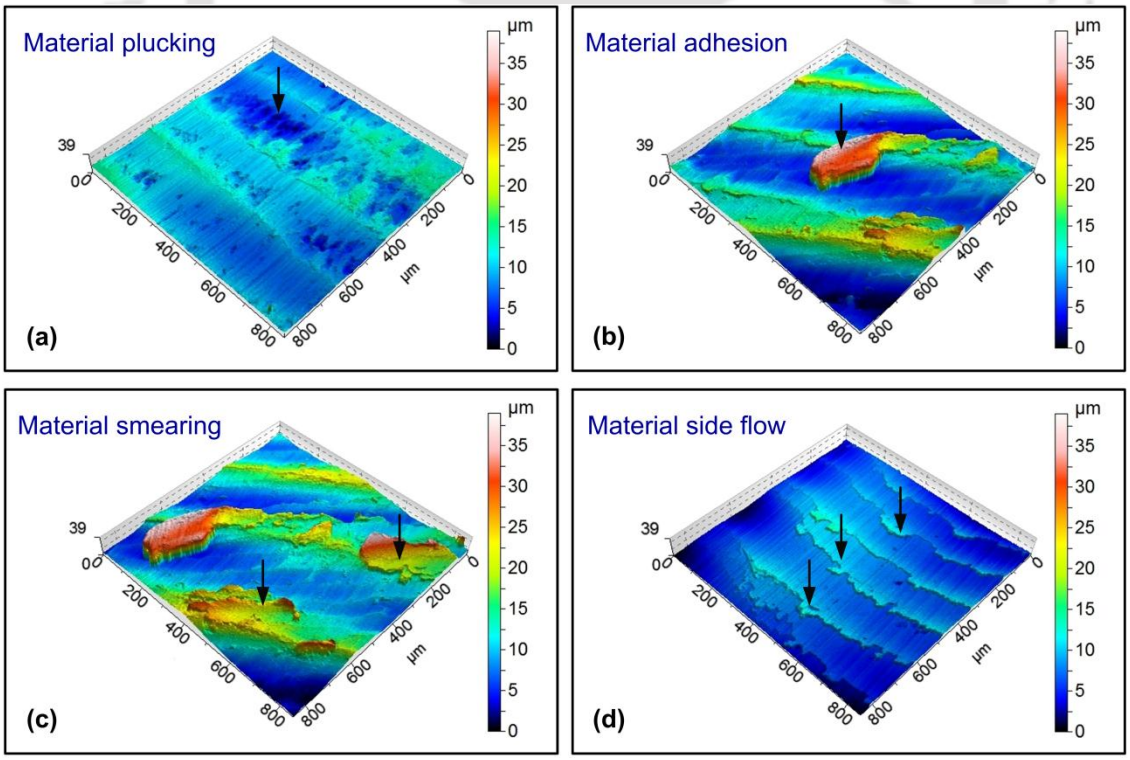

Figure 6.16 Surface defects: **(a)** Material plucking, **(b)** Material adhesion, **(c)** Material smearing, **(d)** Material side flow

Figure 6.16(a) shows the cavity formed while machining the aluminum alloy using 4 mm diameter tools. The cavities generally occur when fragments of the workpiece are removed from the general level of the machined surface. Formation of cavities due to material plucking can be attributed to built-up-edges (BUEs). However, as the cutting progresses, the BUEs get sheared from the machined surface causing the material pullout from the base material surface which results in cavities on the surface. Similar observations were reported by Elkhabeery and Bailey (1984) during machining of aluminum 2024 alloy at low cutting speed condition.

Figure 6.16(b) shows the material adhered to the machined surface. Material adhesion was observed when the machining was carried out at high feed conditions (0.04 and 0.06 mm/z). The small fragments of chips formed during the cutting operation are left behind at the workpiece surface. During engagement of the next cutting tooth, these chip debris gets entrapped between the tool and workpiece, causing the adhered material to smear onto the machined surface (see Figure 6.16(c)). Due to higher ductility of aluminum alloy, removal of the smeared material was difficult as the debris were firmly embedded in the machined surface. Figure 6.16(d) shows the step-like features that formed during the machining of aluminum using a 4 mm tool at high feed and depth values. These features were noted to be inclined in the direction of relative work-tool motion and indicate severe plastic flow of the work material. A similar observation was made by El-Wardany et al. (1996). They reported that rise in temperature due to the higher depth of cut was a crucial factor in inducing side flow as it increases the material plastification. These lamellas like structures worsen the surface quality.

6.3.3 Analysis of Wall Deflection

One of the important quality parameters in thin-wall machining is the dimensional accuracy. In situ wall deflection, significantly affects the dimensional accuracy. To analyze this, a systematic investigation has been carried out using analysis of variance. To investigate the effect of input parameters on the wall deflection, the test for significance of regression and individual model coefficients was conducted. The insignificant terms have been eliminated by using the backward elimination process to improve the adequacy of the model. Table 6.5 shows the results of ANOVA for wall deflection.

From the table, it can be seen that the individual of all the parameters and quadratic effect of radial depth of cut are significant. The *P*-value is noted to be less than 0.0001. It

indicates that the model is significant. Computed values of predicted and adjusted R^2 are 0.9076 and 0.9211, which indicate that the model is adequate for the prediction of process responses. The value of adequate precision ratio as 42.978 indicates adequate model discrimination and the model can predict the response with good accuracy.

Table 6.5 ANOVA table for wall deflection after back elimination

Source	Sum of Squares	DOF	Mean Square	F Value	P–value	Remarks
Model	1.41	9	0.16	100.81	<0.0001	Significant
d_i	4.905E-003	1	4.905E-003	3.16	0.0800	Significant
f_z	0.098	1	0.098	62.83	<0.0001	Significant
a_d	0.33	1	0.33	211.01	<0.0001	Significant
r_d	0.90	1	0.90	579.88	<0.0001	Significant
$d_i * r_d$	0.023	1	0.023	14.56	0.0003	Significant
$f_z * a_d$	9.771E-003	1	9.771E-003	6.29	0.0145	Significant
$f_z * r_d$	0.017	1	0.017	10.84	0.0016	Significant
$a_d * r_d$	0.20	1	0.20	130.54	<0.0001	Significant
r_d^2	0.031	1	0.031	19.71	<0.0001	Significant
Residual	0.11	68	1.553E-003			
Total	1.51	77				

The correlations between the influential factors (d_i, f_z, a_d and r_d) and magnitude of wall deflection was obtained by carrying out regression analysis. After eliminating the non-significant terms, the final response equations derived for wall deflection (D_f) in terms of actual factors is as:

$$D_f = \begin{bmatrix} 0.26388 - 8.53065e^{-3} * d_i - 1.19733 * f_z - 9.82837e^{-3} * a_d - 0.56974 * r_d \\ +0.014188 * d_i * r_d + 0.10129 * f_z * a_d + 2.37590 * f_z * r_d + 0.020055 * a_d * r_d \\ +0.21644 * r_d^2 \end{bmatrix} \quad (6.5)$$

The developed model can be used to predict the wall deflection (D_f) during thin-wall machining process for chosen process conditions. Figure 6.17(a) displays the normal probability plot of the residuals for wall deflection. It can be noticed that the residuals are falling in a straight line, which means that the errors are normally distributed. Figure 6.17(b) illustrates the relationship between the actual and predicted values of wall deflection. These figures indicate that the developed models are adequate and are able to predict the results with reasonably good accuracy.

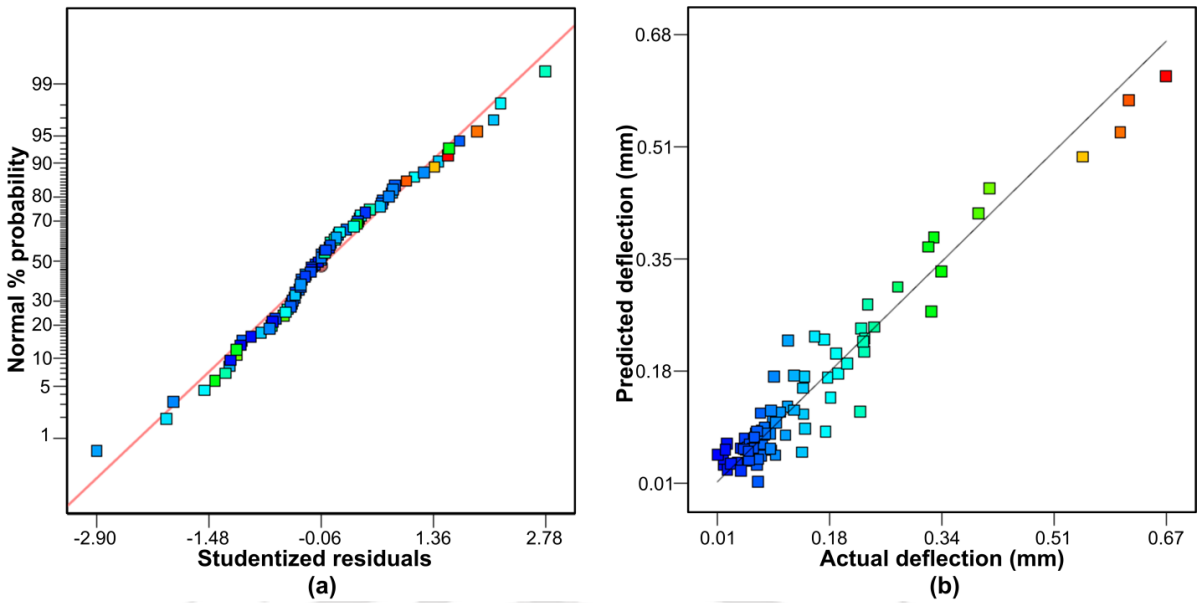

Figure 6.17 (a) Normal probability plot of studentized residuals, **(b)** Plot of actual vs. predicted response for wall deflection

Figure 6.18(a) illustrates the perturbation plot for variation of wall deflection with respect to the input parameters. It confirms the fact that increase in feed per tooth (f_z), axial depth of cut (a_d) and radial depth of cut (r_d) evidently increases the magnitude of wall deflection. Tool diameter (d_i) was found to have low influence in which a move towards the right side from the reference point results in a slight increment in the magnitude of wall deflection.

Figure 6.18(b) demonstrates the interaction effect of tool diameter and radial depth of cut on the wall deflection. It can be observed that as the radial depth of cut increases, the deflection increases with the increase in tool diameter. From Figure 6.18(c-e), it is observed that the wall deflection increases with the increase in feed per tooth, axial and radial depth of cut whereas it reduces with the increase in tool diameter. It is always desired to maintain the magnitude of wall deflection at low levels to prevent any dimensional inaccuracy. From the plots it is evident that lower wall deflection can be obtained by maintaining the feed per tooth (f_z), axial depth of cut (a_d) and radial depth of cut (r_d) at lower levels with 8 mm diameter tool.

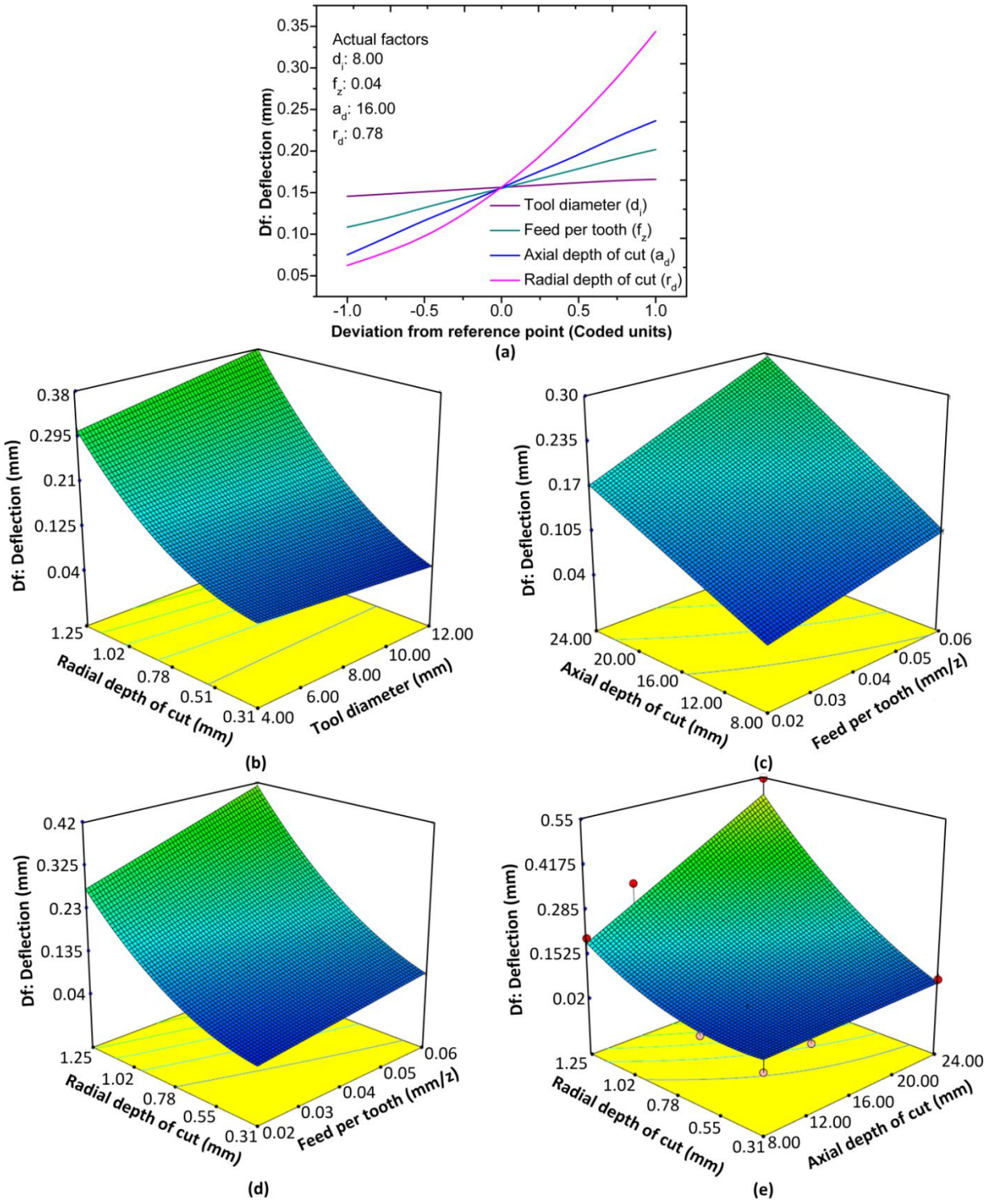

Figure 6.18 Analysis plots for wall deflection: **(a)** Perturbation plot, **(b)** Interaction of d_i and r_d, **(c)** Interaction of d_i and a_d, **(d)** Interaction of f_z and r_d, **(e)** Interaction of a_d and r_d

6.3.3.1 Influence of Variation in Milling Parameters on Wall Deflection

Figure 6.19 shows the effects milling parameters, viz. feed per tooth ($f_{z)}$, tool diameter (d_i), axial depth of cut (a_d) and radial depth of cut (r_d) on the magnitude of wall deflection. Figure 6.19(a) shows the variation of surface roughness with the increase in

feed per tooth when the other parameters were kept unchanged. It was noted that magnitude of wall deflection increases with the increase in the feed value. With the increase in feed value, the chip load increases that results in an increase in the force value. Higher force results in increase in the magnitude of wall deflection.

Figure 6.19(b) shows the effect of increase in tool diameter on the wall deflection. From the figure, it can be observed that deflection of thin-wall workpiece increases with the increase in tool diameter. However, from Figure 6.4(b), it can be noted that milling force was higher is case of 4 mm tool in comparison to 8 mm tool. But as per Figure 6.19(b) the magnitude of wall deflection was noted to be higher in case of 8 mm tool. This is attributed to the deflection of the 4 mm tool in addition to the wall deflection.

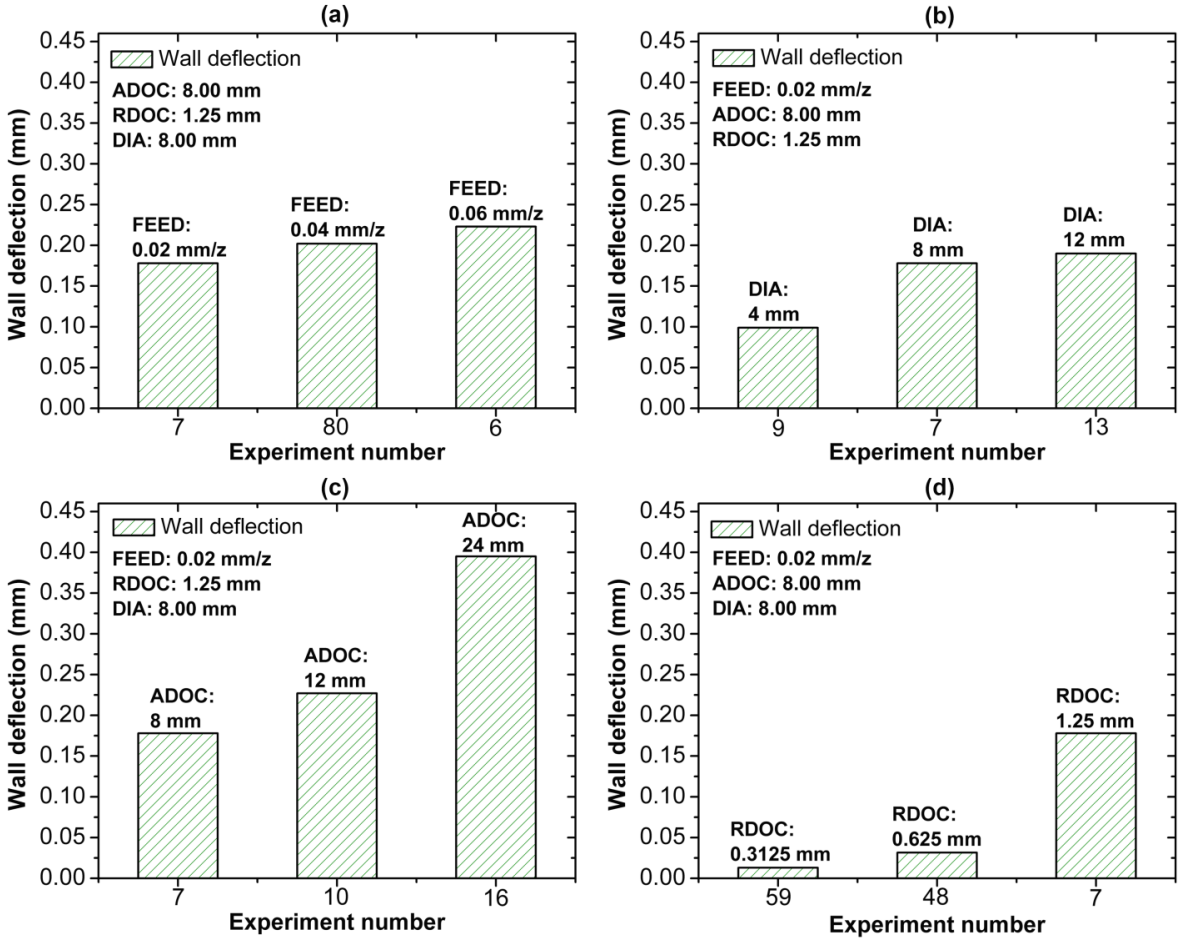

Fig. 6.19 Variation of wall deflection with milling parameters: **(a)** Feed per tooth **(b)** Tool diameter, **(c)** Axial depth of cut, **(d)** Radial depth of cut

Thin-walls were rigid enough to resist the force exerted by the 4 mm cutting tool causing the low rigidity end mill to deflect as compared to larger diameter tools where the thin-walls readily deflected during the machining process. This resulted in the deflection of

the wall to be marginally lower as compared to when tools with larger diameters were used. Figure 6.19(c) shows the variation of wall deflection with the increase in axial depth of cut. It can be observed that the wall deflection increases with the increase in axial cut depth (a_d). It is due to the fact that with the increase in axial depth, the length of the work-tool contact increases which increases the milling force values (Figure 6.4(c)). This in turn, enhances the wall deflection. Similar observations were made when the radial depth of cut was increased (r_d) (see Figure 6.19(d)).

Figure 6.20 shows the side views of thin-wall specimens those machined by using 8 mm diameter tool when the axial depth of cut was varied from 12 mm to 24 mm. It can be observed that due to the deflection, the material remains uncut at the top as compared to that at the base. It can be noted that magnitude of thickness at the free end of the thin-wall machined with an axial cut depth of 12 mm (see Figure 6.20(a)) was lower as compared to obtained with 24 mm (Figure 6.20(b)).

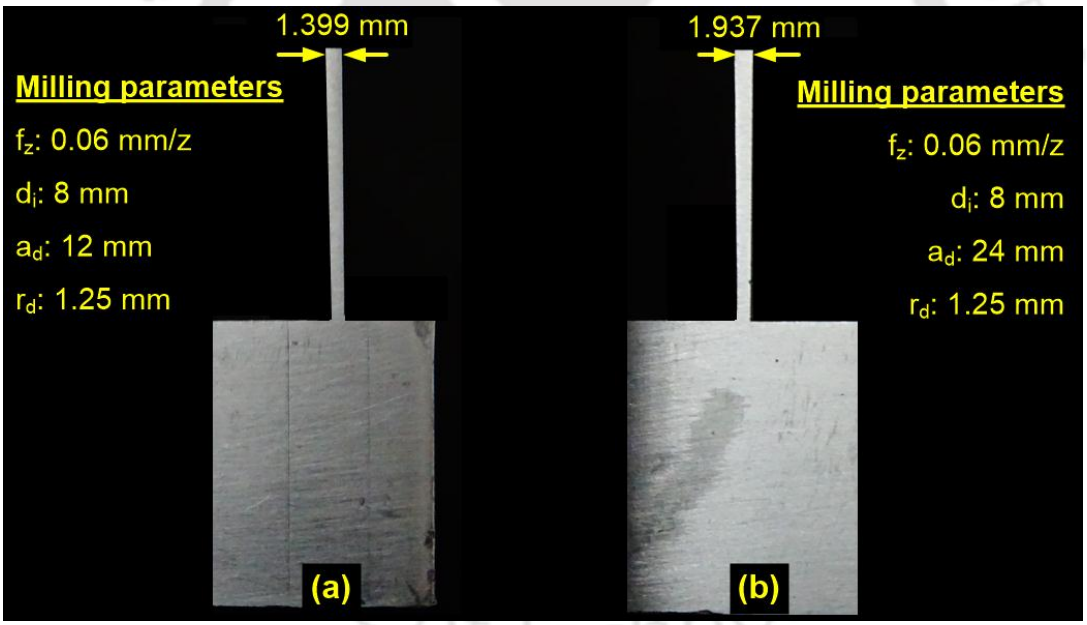

Figure 6.20 Side profile of a thin-wall after machining a 1.25 mm wall with: **(a)** 12 mm axial cut depth, **(b)** 24 mm axial cut depth

Figure 6.21 shows the side view of thin-wall workpieces machined using 12 mm diameter tools where the axial depth of cut was maintained at 24 mm and the radial depth of cut was varied from 0.625mm to 1.25 mm.

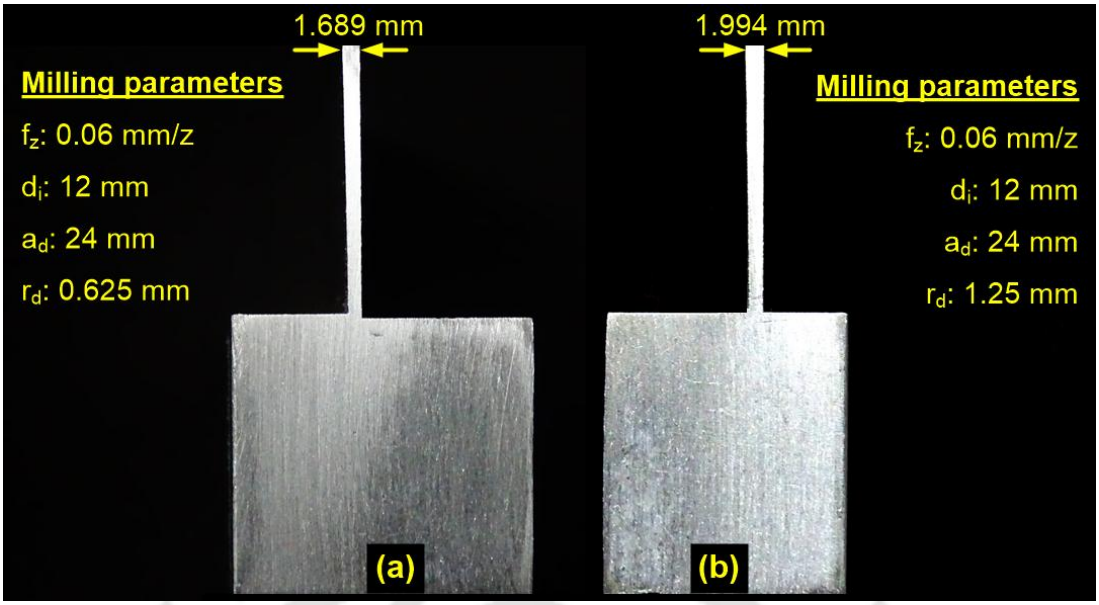

Figure 6.21 Side profile of a thin-wall after machining a 1.25 mm wall with: **(a)** 0.625 mm radial cut depth, **(b)** 1.25 mm radial cut depth

From Figure 6.21(a, b), it can be seen that there is a substantial rise in the magnitude of wall deflection with the increase in radial depth of cut (r_d). It is because, as the radial depth of cut increases the tool immersion into the workpiece increases which results in excessive wall deflection. It can be observed that due to the deflection, the material remains uncut at the top as compared to that at the base. The magnitude of thickness at the free end of the thin-wall was observed to be lower when the radial cut depth was maintained at 0.625 mm but was noted to increase when the depth of cut was raised to 1.25 mm.

6.3.4 Analysis of Material Removal Rate

In thin-wall machining process, achieving high productivity is of equal importance in addition to good surface quality and dimensional accuracy. In general, material removal rate (MRR) is used to describe the process productivity. In this section influence of milling parameters on the material removal rate has been studied.

For analysis of material removal rate, backward elimination procedure was used to eliminate the insignificant terms. The data after the ANOVA is given in Table 6.6. From the table, it can be seen that the individual and quadratic effects of all the parameters are significant. The *P*-value is noted to be less than 0.05. It indicates that the model is significant. Computed values of R^2, adjusted R^2 and predicted R^2 0.9853, 0.9831 and 0.9755 indicate that the mode is adequate for the prediction of process responses. The

value of adequate precision ratio as 95.49 indicates adequate model discrimination. The correlation between the influential factors (d_i, f_z, a_d and r_d) and material removal rate was obtained by using regression analysis. After eliminating the non-significant terms, the final response equation derived for material removal rate (*MRR*) in terms of actual factors is given as:

$$MRR = \begin{bmatrix} 3393.67863 + 16.21418 * d_i - 74428.7303 * f_z - 175.70881 * a_d \\ -5666.55524 * r_d - 3.33219 * d_i * a_d - 60.33996 * d_i * r_d \\ +5095.45512 * f_z * a_d + 1.05541e^{+5} * f_z * r_d + 323.38005 * a_d * r_d \\ +1326.75494 * r_d{}^2 \end{bmatrix} \quad (6.6)$$

The developed model can be used to predict the material removal rate (*MRR*) during thin-wall machining process for chosen process conditions. Figure 6.22(a) displays the normal probability plot of the residuals for wall deflection.

Table 6.6 ANOVA table for material removal rate after back elimination

Source	Sum of Squares	DOF	Mean Square	F Value	P–value	Remarks
Model	5.85E+08	10	5.85E+07	448.01	< 0.0001	Significant
d_i	4.94E+06	1	4.94E+06	37.82	< 0.0001	Significant
f_z	1.50E+08	1	1.50E+08	1149.95	< 0.0001	Significant
a_d	2.14E+08	1	2.14E+08	1639.32	< 0.0001	Significant
r_d	2.84E+08	1	2.84E+08	2179.17	< 0.0001	Significant
$d_i * a_d$	3.96E+05	1	3.96E+05	3.03	0.0863	Significant
$d_i * r_d$	4.05E+05	1	4.05E+05	3.1	0.0828	Significant
$f_z * a_d$	2.47E+07	1	2.47E+07	188.82	< 0.0001	Significant
$f_z * r_d$	3.31E+07	1	3.31E+07	253.77	< 0.0001	Significant
$a_d * r_d$	5.20E+07	1	5.20E+07	398.4	< 0.0001	Significant
r_d^2	1.15E+06	1	1.15E+06	8.8	0.0042	Significant
Residual	8.75E+06	67	1.31E+05			
Total	5.94E+08	77				

It can be noticed that the residuals are falling in a straight line, which means that the errors are normally distributed. Figure 6.22(b) illustrates the relationship between the actual and predicted values of wall deflection. These figures indicate that the developed models are adequate and are able to predict the results with reasonably good accuracy. Figure 6.23 illustrates the perturbation plot for variation of material removal rate with

respect to the input parameters and also depicts the interaction plots of input parameters. It can be clearly seen that the increase in feed per tooth (f_z), axial depth of cut (a_d) and radial depth of cut (r_d) increases the material removal rate linearly; however, the increase in tool diameter (d_i) decreases the MRR marginally.

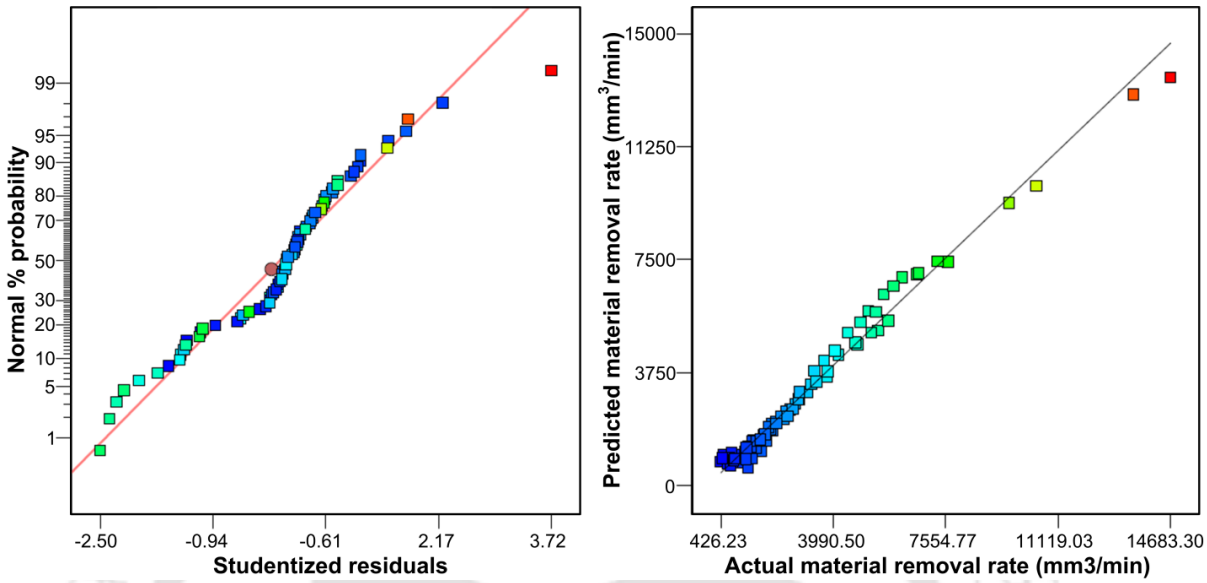

Figure 6.22 (a) Normal probability plot of studentized residuals, **(b)** Plot of actual vs. predicted response for material removal rate

It can be seen that MRR increases with the increase in feed value. This is due to the fact that at higher feed value (0.06 mm/z); the distance traversed by the tool per unit time will be higher in comparison to that at low feed condition (0.02 mm/z); which increases the amount of material removal. Theoretically, the MRR increases with increase in tool diameter. But in the present experimental study, it was noted that MRR decreases with the increase in tool diameter. This is attributed to the fact that in the present study the MRR is computed based the time duration that a tool takes to completely machine the thin-wall part as per the desired dimension. In practice of CNC milling, it is essential to provide sufficient ramp-on (tool approach to work part) and ramp-off (tool disengagement from work part). Ramp-on and ramp-off distances are directly proportional to the tool diameter. Thus with the higher diameter tool, the tool travel time increases and it eventually reduces the MRR. It can be observed that, material removal rate increases with the increase of axial cut depth. This is attributed to the fact that the amount of material removed from the workpiece mainly depends on the work-tool contact.

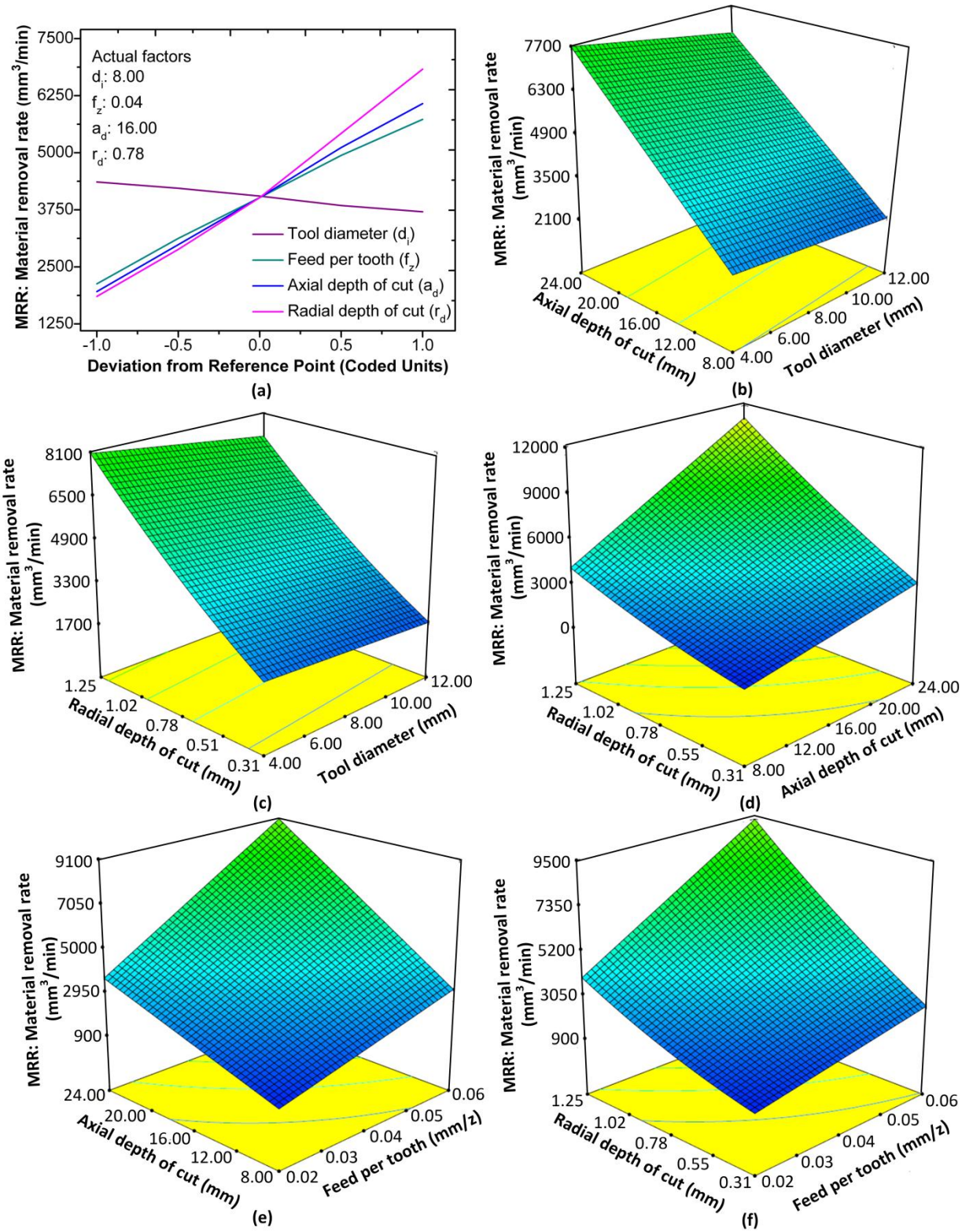

Figure 6.23 Analysis plots for material removal rate: **(a)** Perturbation plot, **(b)** Interaction of d_i and a_d, **(c)** Interaction of d_i and r_d, **(d)** Interaction of a_d and r_d, **(e)** Interaction of f_z and a_d, **(f)** Interaction of f_z and r_d

As contact length increases, the amount of material machined increases and thus enhances the productivity. Similarly, it can be noted that MRR increases with the

increase in radial depth of cut. As the radial depth of cut increases, the amount of cutter immersion increases which further improve the material removal. Thus it can be concluded that the rate of material removal can be maximized using high depth of cut and feed values. But higher values of feed per tooth, axial depth of cut, and radial depth of cut adversely affect the wall dimensional accuracy and surface quality. Therefore a trade-off must be obtained to have optimum levels of milling parameters that will produce quality thin-wall parts at maximum possible productivity. This has been addressed in the next chapter.

6.4 Confirmation Experiments

After the development of mathematical models from quadratic regression fit; five confirmation tests were performed to verify the adequacy of the model. Process conditions for these conformation tests were randomly chosen from the domain of the present experimental study. Systematic experiments were carried out as per the details provided earlier and the responses were recorded carefully. The predicted responses and their respective experimental values are summarized in Table 6.7.

Table 6.7 Confirmation experiments

		Sl. No.	1	2	3	4	5	Mean error
Milling parameters		**d_i (mm)**	4	12	8	8	12	
		f_z (mm/z)	0.06	0.02	0.04	0.03	0.05	
		a_d (mm)	24	12	8	24	15	
		r_d (mm)	0.3125	1.25	0.625	1	0.75	
Response parameters	**F_c (N)**	**Experiment**	228.16	164.6	81.25	239.03	243.10	
		Predicted	241.79	171.73	73.49	249.43	228.96	
		Absolute error (%)	5.97	4.15	9.55	4.02	5.82	**5.9**
	R_a (µm)	**Experiment**	0.945	0.697	0.605	0.6391	0.8276	
		Predicted	0.95	0.638	0.534	0.614	0.803	
		Absolute error (%)	0.53	8.46	11.73	3.92	2.97	**5.5**
	D_f (mm)	**Experiment**	0.114	0.242	0.051	0.337	0.155	
		Predicted	0.123	0.243	0.061	0.309	0.166	
		Absolute error (%)	7.31	0.41	16.39	8.3	7.23	**7.9**
	***MRR* (mm^3/ min)**	**Experiment**	4039.07	2542.37	1553.93	6581.28	4460.49	
		Predicted	4480.89	2307.17	1487.99	6206.62	4001.73	
		Absolute error (%)	9.84	9.24	4.25	5.67	10.29	**7.8**

It can be noted that the developed mathematical models predict the responses with good accuracy. The prediction errors (absolute) vary between 0.41 to 16.39%. The mean predictions error for milling force, surface roughness, wall deflection and material removal rate were noted to be 5.9%, 5.5%, 7.9% and 7.8%. Thus it can be said the mathematical models are robust and can be applied in practice.

6.5 Summary

This chapter presented a comprehensive experimental study on thin-wall machining of aluminum alloy 2024-T351. Full factorial experiments were carried out by varying feed per tooth, axial depth of cut, radial depth of cut and tool diameter at three levels. Total 81 experiments were conducted and the process performance in terms of milling force, surface roughness, wall deflection and material removal rate (MRR) was recorded for each experiment. Then based on the response surface methodology (RSM), systematic studies have been carried out on the perturbation and interaction effects of input milling parameters for individual performance parameters. Results were studied and the findings were presented with suitable scientific justifications. Based on the RSM, mathematical models for the prediction of individual responses were derived. Further, the predictions by the models were verified by conducting confirmatory experiments. All the models were found to have good prediction capabilities. The important findings of the present investigation are presented below.

- Tool diameter was found to have a profound influence on milling force. Milling force varied nonlinearly with tool diameter. Formation of built-up-edges (BUEs) and swirling of the machined chips interrupted the cutting process which resulted in an increase in milling force. Tool breakage was noticed in cases of 4 mm diameter tool with high feed and depth of cut. Machining with larger rigid tools (12 mm) increased the milling force value as larger diameter tools apply more pressure on the thin-wall workpiece. Use of 8 mm tool produced moderate milling force. Thus it was concluded that use of end mill of 4 mm diameter is to be avoided as they generate high force values due to chip clogging and formation of built-up edges.
- The cutting feed was found to have a negative impact on the surface finish. The low value of cutting feed is recommended to obtain good surface quality. Use of 4 mm tools deteriorated the surface finish. It was noted that the chips generated during the machining process deposited between tool and workpiece which resulted

in interrupted cutting which adversely affected the surface finish. It was noted that high axial and radial depth of cut conditions cause low rigidity wall to defect, which results in uneven material cutting and poor surface finish.

- Formation of chatter marks was noted when machining was carried out at high depth of cut conditions. Two types of chatter phenomenon were observed. The first type of chatter observed was associated with the tool. Due to lower flexural stiffness, a small variation in the milling force caused the tool to deflect easily. This resulted in dynamic instability causing the tool to vibrate. As the tool was in contact with the workpiece, the vibration was transmitted to the workpiece which resulted in generating chatter marks. The second type of chatter was due to workpiece vibration. During machining using a 12 mm diameter tool, at high axial depth of cut condition, the tooth passing frequency excites the resonant vibrations in the low rigidity thin-wall. These resonant vibrations increase the frequency of occurrence of interrupted and non-uniform contact between tool and the work surface. This causes the chatter and results in poor surface finish. Studies revealed that use of 8 mm tool helps in chatter-free machining and produces quality surface finish. It was also noted that deflection of the wall significantly affects the surface finish. Surface roughness was noted to be higher near to the free end due to more deflection of the free end as compared to the base of the wall.
- Detailed investigation of the machined surface indicated the presence of surface defects such as material plucking, material adhesion, material shearing, and deformed layer formation. These defects resulted in deterioration of surface finish.
- Wall deflection was found to be influenced by tool diameter, feed per tooth, axial and radial depth of cut. The higher force generated at high feed resulted in an unfavorable increase in the magnitude of wall deflection. Measured deflections were higher when thin-walls were machined with 12 mm diameter tool. Axial depth of cut was found to be the most dominating factor in terms of its influence on wall deflation. Also, a substantial rise in the magnitude of wall deflection was observed with a larger radial depth of cut.
- Material removal rate was found to increase with the increase in feed, axial and radial depth of cut. However, it was noted that material removal rate decrease with the increase in tool diameter. This was due to the incorporation of increased ramp-

on and ramp-off distances associated with larger tool diameters in the calculation of machining time.

- The developed mathematical models for the performance parameters were found to be adequate in terms of accuracy. The validity of regression equations for prediction of milling force, surface roughness, wall deflection and material removal rate were 90.5% ,84.5%, 90.8% and 97.55% respectively. The values indicate that the models are able to predict the responses accurately. This was confirmed by conducting validation tests. The mean error for milling force, surface roughness, wall deflection and material removal rate were 5.9%, 5.5%, 7.9% and 7.8%. The prediction error (absolute) varied from 0.41% to 16.39% which confirmed the adequacy of the model for predicting the responses in thin-wall machining.

Overall it can be concluded that the productivity of thin-wall operation can be maximized using high depth of cut and feed values at 8 mm tool diameter. But higher values of feed per tooth, axial depth of cut, and radial depth of cut adversely affect the wall dimensional accuracy and surface quality. Therefore, a trade-off must be obtained to have optimum levels of milling parameters that will produce quality thin-wall parts at maximum possible productivity. This has been addressed in the next chapter.

Chapter 7

Optimum Selection of End Milling Parameters using Non-Dominated Genetic Algorithm - II

7.0 Scope

This chapter presents a methodology for the optimum selection of end milling parameters using Non-Dominated Genetic Algorithm - II (NSGA-II) for thin-wall machining process. An overview of the formulation of the objective function for the optimization of milling parameter using Genetic Algorithm (GA) is initially presented. Details of the NSGA-II algorithm and the respective results are presented. Based on these studies, optimum milling parameters for roughing and finishing operations are recommended. Finally, case studies are presented to demonstrate the capability of employing the suggested optimum levels of milling parameters in practice.

7.1 The Need

Achieving tight dimensional tolerance and superior surface quality are the main challenges in machining of thin-wall parts. Moreover, it is essential to enhance the process productivity because approximately 90-95 % of the material from the initial work material volume gets removed during the operation. The increase in material removal rate is generally achieved by maximizing the process parameters viz. depth of cut and feed rate. Employing higher levels of these process parameters lead to inferior dimensional accuracy and surface quality due to the low rigidity of thin-wall parts. To improve process efficiency and product quality, the most favorable end milling process parameters are chosen on shop floor based on experience, thumb rules and handbook values, which often lead to suboptimal and inconsistent machining process performance. Due to the complex and nonlinear relationship between the process parameters and the performance measures, it is quite difficult to select the optimum process parameters for specific (roughing or finishing) application of the end milling process. A need thus exists, to develop a systematic methodology to select optimal input milling parameters for efficient performance of the end milling process in the manufacture of thin-wall parts.

Literature reports that Genetic Algorithm (GA) is a better optimization methodology over the classical optimization techniques due to its robustness (Phatak and Pande et al. (2012), Li et al. (2015), Qu et al. (2017)). Genetic algorithm is an evolutionary technique, which mimics the natural evolutionary principles to constitute

search and optimization procedures in a complex multi-modal solution space. In the real-world optimization problems, the nonlinear and complex interactions among the problem variables often exist. The search space has several solutions than a single optimal solution. Many such local optimal solutions are undesired, as they have inferior objective function values. Classical optimization methods viz. direct methods and gradient methods follow point-by-point approach, where one solution gets updated to a new solution after each iteration. They have a tendency to get attracted towards and trapped into local optimal solution, and in turn, provide an inferior solution to the problem (Li et al. (2015)). Evolutionary algorithms solve this problem by searching the space in parallel to achieve the global optimal solution. It was therefore thought that GA technique will be more suitable to solve our complex optimization problem.

Determination of optimum levels of parameters for efficient and quality bulk machining process has always been a key research problem and is still a subject of study for the manufacturing researchers and engineers. Literature reports significant work on optimization of bulk machining operations such as face milling and end milling. However, few attempts have been reported on optimization of thin-wall machining process to improve its productivity and product quality. Most of these works have limited applicability as they consider either wall deflection or surface roughness or material removal rate (Ghoddisian et al. (2011), Qu et al. (2017)). Nowadays researchers worldwide are focusing their attention on minimizing the carbon footprint of manufacturing processes. Energy saving has become a priority for the manufacturing industry. Therefore, reducing the power consumption during machining process has become an integral part of sustainable manufacturing (Zhang et al. (2015), Singh at al. (2015)). Thus it is imperative to consider the requirement of low power consumption in addition to the objectives of high surface quality and productivity. To the best of our knowledge, there is no published work that deals with the multi-objective optimization of thin-wall machining process for improving the productivity, product quality and power consumption.

7.2 The Proposed Approach

A comprehensive integrated approach has been developed to find out the optimum levels of milling parameters for an energy efficient, superior quality and high productivity thin-wall machining process. This can be achieved by maximizing the material removal rate,

minimizing the surface roughness, wall deflection and milling force. In view of this three objective functions have been defined. They are presented as below.

A. Power consumption: Machining forces are generally used to estimate the power consumption. In end milling, the power consumption P_c can be resolved into three parts viz. machining power of spindle P_m, power of feed motion P_f, and power consumed by auxiliary systems P_u. Machining power of spindle and power of feed motion are dependent upon the milling parameters and workpiece material. Therefore in order to minimize the power consumption, milling parameters need to be optimized. In the present work, the force components F_x and F_y acting on the milling cutter have been determined by using experimental results (Chapter 6). The machining power of spindle P_m as a function of main cutting force F_x is given by:

$$P_m = \frac{F_x \cdot \pi \cdot n_s \cdot d_i}{1000 \cdot 60} (\mathrm{W}) \tag{7.1}$$

The power consumption of feed motion P_f is calculated by:

$$P_f = \frac{F_y \cdot n_s \cdot f_z}{1000 \cdot 60} (\mathrm{W}) \tag{7.2}$$

where, F_x is the cutting force component, F_y the feed force, f_z is the feed per tooth (mm/z), n_s is the spindle speed (r/min), d_i is the diameter of the milling cutter (mm). In this work, only the cutting power and feed power have been considered. Therefore milling power consumption P_c is given by:

$$P_c = P_m + P_f \ (\mathrm{W}) \tag{7.3}$$

The calculated machining powers (spindle and feed power) are tabulated in Appendix A7.1. The correlations between the influential factors (d_i, f_z, a_d and r_d) and milling power (P_c) was obtained by carrying out the regression analysis. After eliminating the non-significant terms, the final response equations derived for milling power in terms of actual factors is given by:

$$P_c = \begin{bmatrix} 789.28 - 113.02 \cdot d_i - 4762.86 \cdot f_z - 28.16 \cdot a_d - 557.60 \cdot r_d \\ +262.74 \cdot d_i \cdot f_z + 2.47 \cdot d_i \cdot a_d + 29.02 \cdot d_i \cdot r_d + 236.05 \cdot f_z \cdot a_d \\ +2659.27 \cdot f_z \cdot r_d + 15.24 \cdot a_d \cdot r_d + 4.37 \cdot d_i^2 + 114.24 \cdot r_d^2 \end{bmatrix} \tag{7.4}$$

B. Product quality: Surface roughness and magnitude of wall deflection were considered as quality parameters in the thin-wall manufacturing process. A product quality parameter Q_1 has been defined by using the weighted function of surface

roughness and wall deflection. The product quality parameter Q_1 is given by:

$$Q_I = \left(\frac{D_{f\,max} - D_f}{D_{f\,max} - D_{f\,min}} \cdot w_1 \right) + \left(\frac{R_{a\,max} - R_a}{R_{a\,max} - R_{a\,min}} \cdot w_2 \right) \tag{7.5}$$

where Q_I is the quality index which varies in between, $0 \leq Q_I \leq 1$. A higher value of quality index specifies that the surface roughness and wall deflection are at minimum level and indicates better performance in terms of product quality. The variables D_{fmin}, D_{fmax} R_{amin}, and R_{amax} represent minimum and maximum values of deflection and surface roughness respectively. w_1 and w_2 represent the weights applied to quality parameters: surface roughness and wall deflection respectively. In thin-wall machining operation, both the surface roughness and wall deflection have been considered equally important, therefore the weights w_1 and w_2 were considered as 0.5.

C. Productivity (MRR): In this work, the productivity of thin-wall milling process has been computed based on the material removal rate (MRR) and is designated as P_y.

Above stated objectives are conflicting in nature. However, their importance is subjective and varies according to the desired application of the process (roughing or finishing). To achieve these objectives, multi-objective optimization has been carried out by using NSGA-II. Figure 7.1 outlines the framework of the optimization problem, objectives and milling parameters for the thin-wall machining operation. Its features are as follows.

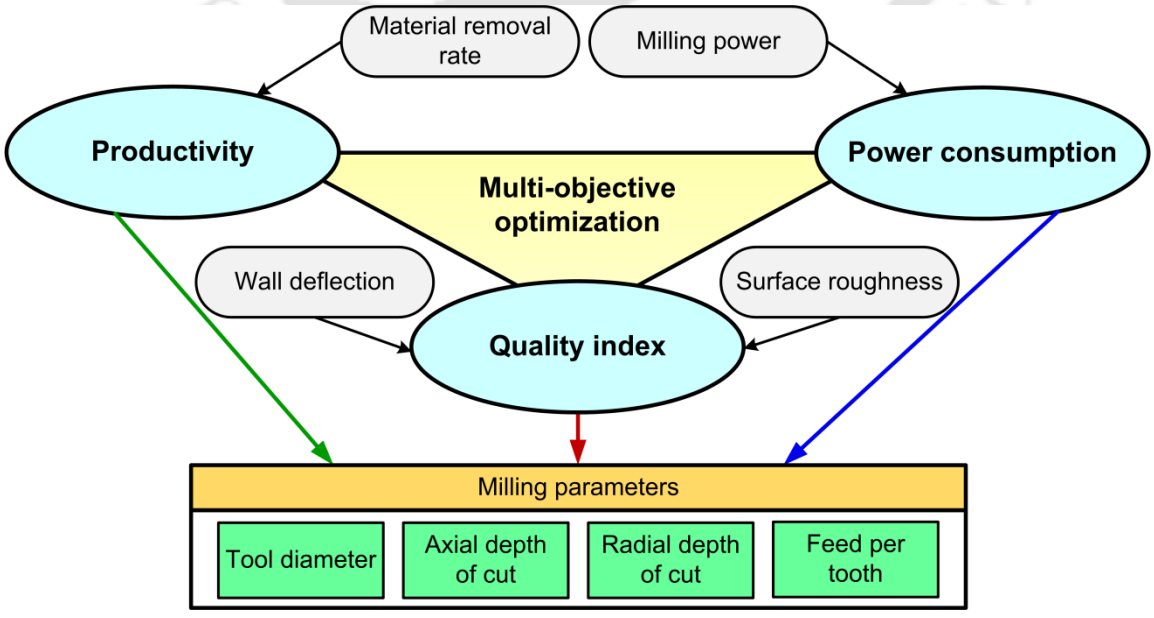

Figure 7.1 Framework of the optimization problem, objectives and milling parameters

- Systematic and exhaustive experiments have been carried out and the process responses were recorded for the chosen process input milling parameters (conditions).
- Based on the expected application of the process (roughing or finishing), objective criteria are defined for the optimization of the process.
- NSGA-II based optimization strategy is applied to obtain a set of input milling parameters to optimize the multiple objective criteria.

These can be used singly or in combination for the process optimization. Typical optimization strategies are presented in the sections to follow.

7.3 GA based Optimization Strategies

As discussed in the previous sections, in thin-wall end milling process, it is difficult to find a single optimal combination of parameters for higher MRR, lower surface roughness, wall deflection and lower milling force as the trends of variations of parameters are different. Hence, there is a need for a multi-objective optimization method to arrive at the solutions to this problem. Various classical methods of obtaining the solutions to multi-objective problems are available. Some examples are Min–Max, Weighted Sum and Distance Function methods (Deb (2001)). These methods change the multi-objective problem into a single objective, with the corresponding weights based on their relative importance. These methods suffer from a drawback that the decision maker must have a thorough knowledge of the ranking of the associated objective functions. Also, these methods fail when the objective functions become discontinuous. Genetic algorithm (GA) possesses advantages that it does not require any gradient information and has inherent parallelism in searching the design space, thus making it a robust adaptive optimization technique (Deb (2001)).

For multi-objective optimization methods, some modification to simple GA is necessary. Literature reports some of the popular GA based multi-objective solution methods such as multi-objective genetic algorithm (MOGA) with weighted sum method, vector evaluated genetic algorithm (VEGA) and non-dominated sorting genetic algorithm II (NSGA-II) (Joshi and Pande (2011)). In this work, NSGA-II (Deb (2001)) has been used to obtain the optimal machining conditions for thin-wall end milling process by following the methodology presented in Figure 7.1. NSGA-II provides Pareto

optimal solutions. These are the trade-off solutions which satisfy one or more objective criteria at a time. They provide a very useful tool to the process engineer to choose the optimum process conditions for the expected application of the process i.e. roughing or finishing. GA based optimization strategy with NSGA-II is presented in details in the next section.

7.4 NSGA-II: An Evolutionary Algorithm for Multi-Objective Optimization

NSGA-II is an Evolutionary Algorithm (EA). EAs are generic population-based metaheuristic optimization algorithms. They mimic the nature of evolution in driving the search towards optimality by incorporating the concepts of genetic recombination and survival-of-the-fittest. EAs are considered as general purpose optimization tools. EAs are population-based search techniques, as they maintain the data of potential solutions populations during searches. These algorithms do not take into account any background information of the problems when performing optimization and don't require any directional information in exploring the search space. Instead, the heuristic nature of the genetic searches allows them to efficiently perform the searching task in any fitness landscape. EAs are capable of approximating the Pareto-optimal set using a single run by evolving a population of solutions and are able to approximate the whole Pareto-front of a multi-objective optimization problem (Tsang (2009), Zhoua, et al. (2011)). They can evaluate all the objectives simultaneously and exploit similar solutions quickly to provide a group of uniformly distributed trade-off solutions close to the optimal Pareto set (Tsang (2009)). Therefore, EA has become one of the most popular approaches to solve multi-objective problems. NSGA-II is commonly being used (Coello et al. (2007)). It has been developed by Deb et al. (2002). The NSGA-II algorithm is capable of handling two or more objectives and is implemented using elitism-preserving approach. Elitism is established by storing all the non-dominated solutions determined so far including the initial population. Elitism helps in enhancement of convergence properties towards the Pareto-optimal front. It adapts a parameter-less diversity preservation mechanism which guarantees the result diversity and spread of solutions. Figure 7.2 shows the basic steps that are involved in EA.

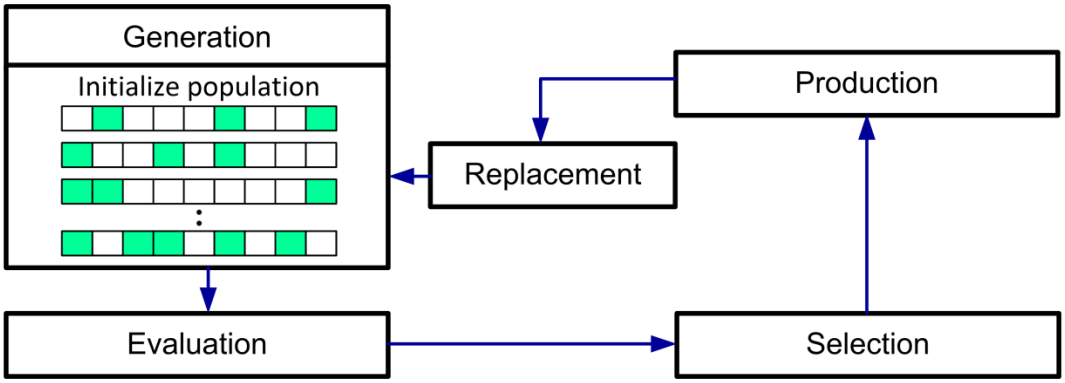

Figure 7.2 Basic steps in Evolutionary Algorithm

A. Define the objective function, number of variables and respective constraints.

B. Generation: In EA, the search for optimum solutions is started with an initial population (candidate solutions to a problem) comprising of a fixed number of individual solutions. The search procedure is carried out in a number of iterations which are called generations. Generally, the initial population is generated randomly. However one can use an already existing population obtained from the previous run. Population size specifies how many individuals there are in each generation. With a large population size, the EA searches the solution space more thoroughly, thereby reducing the chance that the algorithm will return to a local minimum. However, a large population size also causes the algorithm to run more slowly.

C. Evaluation: This is the most important part of an EA. The evaluation function determines the fitness of an individual solution. It measures the performance of an individual solution by using the objective function(s). Based on the performance, fitness of the individual solution in the existing population is evaluated.

D. Production and replacement: A new population is generated by retaining the best fitted individuals of the previous generation, while the remaining individuals are replaced by new off-springs which are produced by selected parents.

To generate a new population, various GA operators viz. selection, crossover and mutation can be utilized. In the context of NSGA-II, these are presented as the next section.

The steps followed in the NSGA-II based optimization of helical end milling of thin-wall components are as follows.

Initially, a random population *P* of size *N* is created by using the results of the mathematical models developed by using the experimental data gathered in Chapter 6. It is sorted into different non-domination levels by checking whether the solution under consideration satisfies the rules given below.

$$\text{Obj. } 1[i] > \text{Obj. } 1[j] \text{ and Obj. } 2[i] \geq \text{Obj. } 2[j]$$
$$\text{or} \qquad (7.6)$$
$$\text{Obj. } 1[i] \geq \text{Obj. } 1[j] \text{ and Obj. } 2[i] > \text{Obj. } 2[j], \; i \neq j$$

where, *i* and *j* are the solution numbers. If the above rules are satisfied then the selected solution is marked as non-dominated. Otherwise, the selected solution is marked as dominated. In the first sorting, all non-dominated solutions (N1) are assigned rank 1. From the remaining ($N - N_1$) dominated solutions, candidate solutions are again sorted. The non-dominated solutions after the second sorting are ranked 2. Each solution is assigned a fitness equal to its non-domination level (1 is the best level). The procedure shown in Figure 7.3 will be repeated till the Pareto optimal front is obtained. The steps are described as follows:

Step 1: Parents are selected from the population by using the Tournament selection based method and then sorted using crowding distance algorithm (Deb K (2001)) (from the previous generation). The algorithm is presented at length in Step 4.

Step 2: The selected population generates offspring using the crossover and mutation operators. Intermediate operator for crossover and constraint dependent mutation scheme is used in the present study.

Step 3: Combine parent and offspring populations and perform a non-dominated sorting. If a solution is strictly better than any other solutions for all objectives then it is called non-dominant solution i.e. it is not dominated by any other solution and a set of such solutions is called non-dominated set. The first front being completely non-dominant set in such sorted population and the second front being dominated by the individuals in the first front only and the front goes so on. Each individual in each front is assigned rank (fitness) values based on the front in which they belong to. Individuals in the first front are given a fitness value of 1 and individuals in second are assigned fitness value of 2 and so on.

Step 4: Once the non-dominated sort is complete, the crowding distance is assigned. The crowding distance of a solution is a measure of the search space around the solution which is not occupied by any other solution in the population. It expresses the Euclidian

distance between each individual in a front based on their *m* objectives in the *m* dimensional hyperspace. Crowding distance is assigned front wise (Deb K (2001)). Comparing the crowding distance between two individuals in different fronts is meaningless. Large average crowding distance will result in better diversity in the population. The individuals in the boundary are always selected since they have infinite distance assignment.

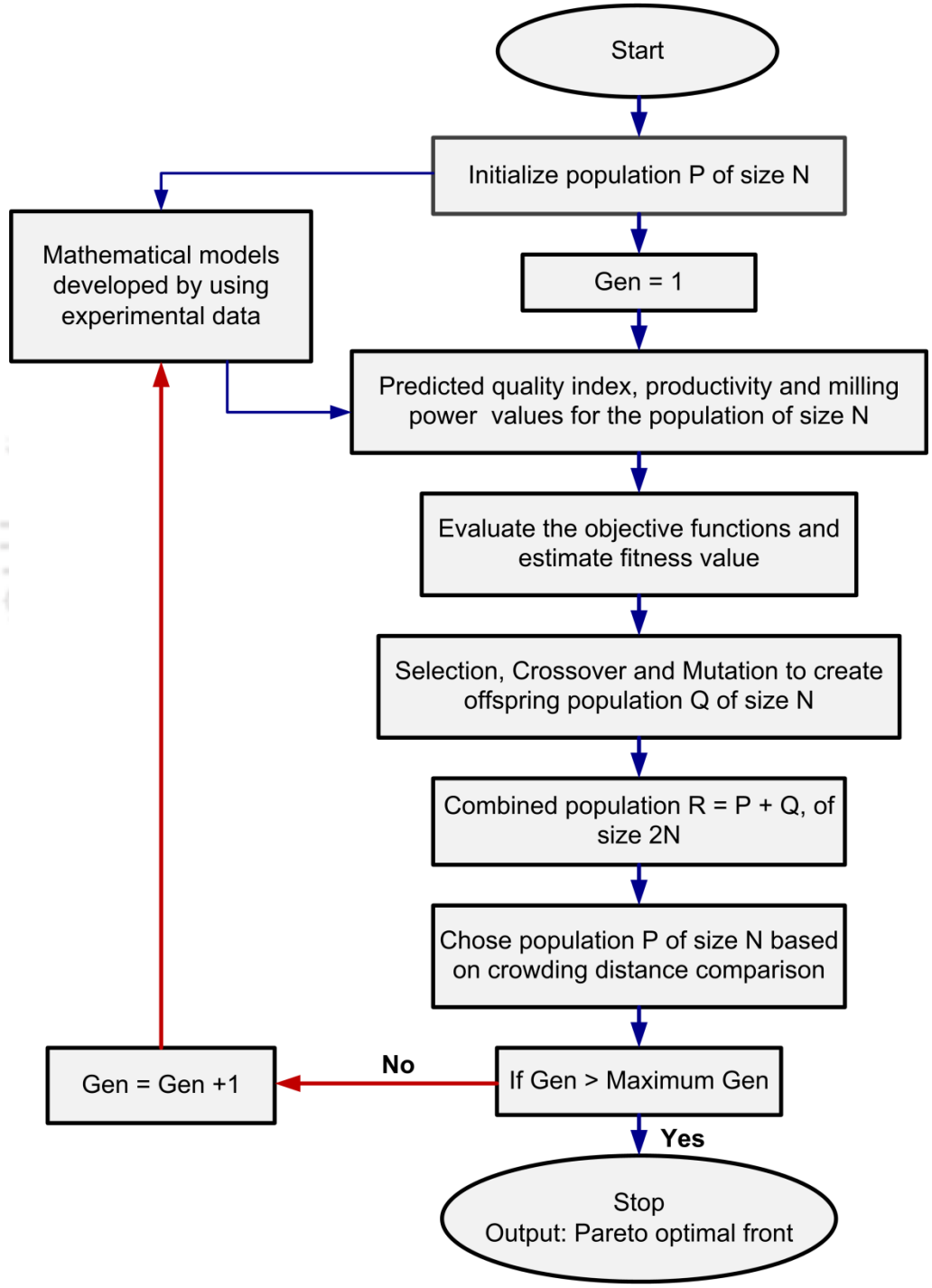

Figure 7.3 Flow chart of NSGA-II approach for optimization of thin-wall machining process

The stepwise crowding distance (CD) assignment procedure is specified below.

Step 4.1: Say the number of elements in a Front is equal to p

Step 4.2: For each objective function ($m=1, 2,..., M$), sort the elements in the ascending order of objective function value (f_m) i.e. find sorted indices vector (I_m).

Step 4.3: Assign the large CD values to boundary elements in sorted elements in step 4.2 or $d_{I_1^m} = d_{I_p^m} = \infty$, and for other solutions j=2 to (p-1), the CD is calculated using:

$$d_{I_j^m} = d_{I_j^{m-1}} + \frac{f_m^{I_{j+1}^m} - f_m^{I_{j-1}^m}}{f_m^{\max} - f_m^{\min}} \qquad (7.7)$$

where I_j^m denotes the solution index of j^{th} member in the sorted list based on m^{th} objective function,

$d_{I_j^{m-1}}$ is the CD value from the previous objective function,

$f_{\mathrm{m}}^{\max}$ and $f_{\mathrm{m}}^{\min}$ are the maximum and minimum values of m^{th} objective function,

$f_m^{I_{j+1}^m}$ and $f_m^{I_{j-1}^m}$ are the objective function values of the neighboring elements in the sorted list from Step 4.2.

Step 5: The new generation is filled by each front subsequently until the population size exceeds the current population size from non-dominated sorted population from step 3. If by adding all the individuals in a front, the population exceeds maximum population size, and then the individuals in the front are selected based on their crowding distance in the descending order until the population size reached its maximum size.

Reproduction or selection operator

The primary objective of the reproduction operator is to make duplicates of good solutions and eliminate bad solutions in a population while keeping the population size constant (Deb (2001)). This is achieved by performing the following tasks:

- Identify good solutions in a population
- Make multiple copies of good solutions
- Eliminate bad solutions from the population so that multiple copies of good solution can be placed in the population

The selection mechanism improves the quality of the population by passing high quality chromosomes to the next generation. Selection process involves choosing the parents for mating to generate offspring's. In this work tournament selection is used to select good solutions for the next generation (Deb et al. (2000)). In the tournament selection, tournaments are played between two solutions and the better solution is chosen and placed in the mating pool. Two other solutions are picked again and another slot in the mating pool is filled with the better solution. Out of the two solutions in mating pool better solution is picked. The best solution in the population will win both the times, thereby making two copies of it in the new population. The worst solution will lose in both tournaments and will be eliminated from the population. In this way, each solution of a population will have zero, one or two copies in the new population.

Crossover operator

A crossover operator creates new solutions in the population. Crossover specifies how the genetic algorithm combines two parents, to form a crossover child for the next generation. In this work, intermediate crossover operator has been used. The operator is used when there are linear constraints and children are created by taking a weighted average of the parents.

Mutation operator

After crossover operation, mutation takes place. Mutation is an important operator in NSGA-II. The mutation operator produces new population by modifying the single solutions (individuals). It improves the overall performance of chromosomes and to avoid the premature convergence in the searching process. The mutation also helps in maintaining diversity in the population. Like the crossover point, the mutation point is also randomly chosen. Mutation is done by slightly changing the value of genome in the chromosome.

Once the offspring's (new parents) are generated then they replace the previous generation (parents). Figure 7.4 shows the process of generating offspring's (new parents). The offspring's can replace entire parent population or a fraction of parent population. The offspring's undergo selection procedure to determine the fitness to generate new population.

The NSGA-II algorithm terminates when either of the following conditions satisfies.

- Maximum number of generation is achieved.

- Fitness value for the best solution has finally met the desired fitness.

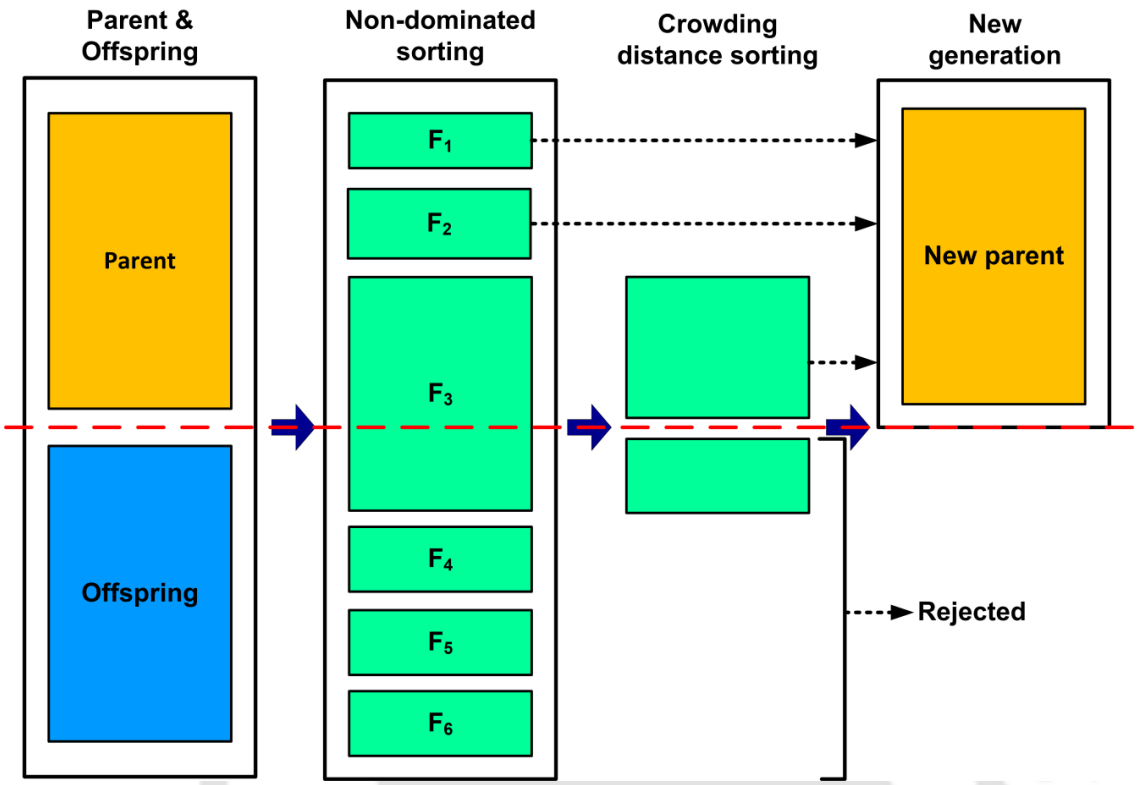

Figure 7.4 Offspring (new parent) generation in NSGA-II

7.5 Optimum Parameters for End Milling of Thin-Wall Parts using NSGA-II

Using the above discussed NSGA-II procedure, an extensive analysis was carried out to select optimum milling parameters for roughing and finishing operations for helical end milling of thin-wall parts of aluminum alloy 2024-T351. Extensive studies using the NSGA-II have been carried out to identify the range of milling parameters for optimal performance of end milling process. An initial random binary population of 100 individuals was taken and fed it into the empirical correlations obtained by using experiments. Four milling parameters namely tool diameter, feed per tooth, axial depth of cut and radial depth of cut were considered as the input variables. According to the framework of the optimization problem, objectives and cutting parameters, the multi-objective optimization problem is described as:

$$\begin{cases} \text{Maximization of } \textit{Quality index, } Q_I \\ \text{Maximization of } \textit{Productivity, } P_y \\ \text{Mimimization of } \textit{Power consumption, } P_c \end{cases} \qquad \begin{cases} f_{z\,min} \le f_z \le f_{z\,max} \\ d_{i\,min} \le d_i \le d_{i\,max} \\ a_{d\,min} \le a_d \le a_{d\,max} \\ r_{d\,min} \le r_d \le r_{d\,max} \end{cases} \tag{7.8}$$

where f_z is feed per tooth, d_i is the tool diameter, a_d is the depth of cut, and r_d is the

radial depth of cut.

7.5.1 Implementation

A computer utility available in MATLAB R2013b was used to obtain the optimum levels of parameters using NSGA-II. It typically took about 5 minutes on an Intel i7 machine with 4 GB RAM. The parameters used during the NSGA-II are listed in Table 7.1.

Table 7.1 NSGA-II parameters

Sl. No.	Attribute		Value/condition
1	Population size		100
2	Tournament		Binary Tournament selection
3	Reproduction		0.8
4	Mutation		Constraint dependent
5	Crossover		Intermediate
6	Number of iteration		200
7	Mutation	Fraction	0.2
		Interval	20

7.5.2 Results and Discussion

As outlined in the previous section, three objective criteria were thought of viz. low power consumption, high product quality and high productivity. Table 7.2 shows the results of NSGA-II for optimization of thin-wall milling problem. It shows 100 optimal milling parameters (decision variables) of the non-dominated solution set (optimal Pareto front) and the corresponding process responses (objective function values). These solutions suggest the milling parameters are in fraction or real numbers. However, it is to be noted that, the comparative analysis, feasibility analysis and experimental verification of these Pareto solutions have been carried out by considering nearest integer values of milling parameters. Also, the feasibility of applying the suggested value has also been considered. For example, suggested value of 6.6 mm cutter diameter is difficult to manufacture and unavailable in the market. Therefore such values are rounded off to their nearest feasible levels.

Table 7.2 Optimum combinations of milling parameters based on Pareto front

Sl. No.	Milling parameters				Response parameters		
	d_i (mm)	f_z (mm/z)	a_d (mm)	r_d (mm)	Q_I	P_c (W)	P_r (mm^3/min)
1	4	0.0594	23.99	1.2442	0.093	372.96	13919.17
2	8.9	0.06	23.85	1.234	0.303	634.89	13162.62
3	8.9	0.0202	8.25	0.4887	0.941	47.29	820.2631
4	4.8	0.0201	23.43	0.3181	0.803	24.98	1208.125
5	8.9	0.02	8.22	0.3158	0.965	51.95	878.2777
6	8.5	0.0585	23.7	1.0493	0.409	505.83	10903.63
7	8.9	0.06	23.85	1.1605	0.345	598.34	12352.77
8	6.6	0.0278	23.42	0.3741	0.825	75.6	1966.671
9	7.9	0.0413	23.64	0.642	0.68	232.44	4955.815
10	8.5	0.0573	23.65	0.9194	0.484	442.24	9378.151
11	8.4	0.0265	9.07	0.4243	0.905	55.62	985.3546
12	4	0.06	24	1.25	0.087	378.41	14098.5
13	4.9	0.0567	23.8	1.0731	0.264	326.23	11369.09
14	4.9	0.0237	23.48	0.7094	0.635	83.4	3634.621
15	7.8	0.0299	22.82	0.5498	0.775	147.98	2987.732
16	7.6	0.0267	23.02	0.3766	0.859	96.03	1779.879
17	7.9	0.0584	23.71	1.195	0.318	532.36	12521.86
18	8.6	0.0584	23.76	1.1253	0.369	548.03	11702.82
19	7.4	0.0555	23.06	0.7306	0.562	295.13	7253.4
20	7.6	0.0418	23.63	0.4327	0.763	167.98	3501.749
21	8.9	0.0201	8.22	0.3158	0.965	51.98	878.3563
22	6.9	0.0309	23.4	0.4303	0.796	103.03	2528.036
23	4.5	0.0569	23.99	1.0785	0.233	318.23	11594.71
24	8.7	0.059	23.84	1.24	0.302	616.28	13074.04
25	8.2	0.0595	23.95	1.2447	0.289	588.8	13339.6
26	8.6	0.0581	23.81	1.2267	0.313	595.88	12767.72
27	6.7	0.0597	23.53	0.7106	0.531	284.54	7797.372
28	6.9	0.0309	23.41	0.446	0.79	105.91	2621.822
29	6.3	0.0555	23.57	0.6729	0.549	240.49	6996.663
30	8.9	0.0314	8.24	0.4887	0.889	56.42	1034.027
31	6.4	0.0542	23.98	0.4329	0.671	179.46	4822.888

32	7.5	0.0567	23.72	0.9958	0.425	413.01	10207.19
33	8.2	0.0552	23.71	0.7605	0.568	353.47	7616.376
34	7.4	0.0349	23.66	0.6063	0.718	174.03	4036.407
35	8.9	0.0593	23.84	1.0186	0.427	526.89	10717.33
36	6.6	0.051	23.75	0.5332	0.645	196.04	5289.861
37	5	0.0468	23.94	1.1368	0.29	302.63	10440.74
38	6.8	0.0348	23.43	0.4348	0.77	115.83	2920.649
39	7.9	0.0303	23.35	0.4763	0.808	140.34	2648.792
40	7.9	0.0355	23.6	0.6521	0.706	208.14	4358.619
41	7.3	0.0521	23.65	0.9411	0.468	355.61	8981.969
42	4.9	0.0435	23.75	0.8734	0.435	202.91	7461.296
43	7.4	0.0492	23.94	0.4219	0.733	189.88	4170.709
44	8	0.058	23.66	1.0672	0.393	478.02	11057.55
45	6.7	0.0391	23.51	0.431	0.746	128.69	3305.577
46	8.6	0.0582	23.7	1.1466	0.358	555.33	11868.91
47	5.4	0.0598	23.99	1.2389	0.187	427.9	13736.23
48	4.9	0.0587	23.97	1.238	0.163	399.65	13588.75
49	8	0.0454	23.66	0.707	0.633	276.25	5942.347
50	9	0.06	23.86	1.2473	0.296	649.54	13301.88
51	8	0.0352	9.53	0.5001	0.842	65.13	1339.927
52	6.6	0.0257	23.8	0.8139	0.659	156.53	4413.779
53	7	0.0594	23.94	1.2381	0.263	507.61	13409.05
54	8.4	0.0592	23.75	1.0272	0.417	494.71	10815.79
55	7.7	0.05	22.74	0.7261	0.594	277.51	6430.355
56	7.4	0.0444	23.66	0.7371	0.609	253.47	6129.788
57	8.5	0.0586	23.83	0.9969	0.437	486.21	10429.41
58	5.5	0.0598	23.67	0.7346	0.461	251.45	8220.402
59	7.6	0.0585	23.77	1.1973	0.309	516.32	12633.68
60	7.8	0.0564	23.73	0.9472	0.459	408.9	9639.682
61	7.2	0.0569	23.73	0.9833	0.421	393.25	10150.95
62	6.4	0.0527	23.8	0.6599	0.571	230.73	6609.469
63	6.7	0.0596	23.98	1.1887	0.279	470.71	12953.44
64	7.8	0.0585	22.24	0.4261	0.7	224.52	4630.781
65	7.5	0.0584	23.94	0.8263	0.506	360.71	8827.433
66	7.4	0.0347	22.5	0.4984	0.758	140.77	3135.481

67	8.6	0.0588	23.7	1.1499	0.354	560.57	12004.73
68	8.5	0.0555	23.75	0.9952	0.451	465.98	9908.467
69	8.9	0.06	23.85	1.2379	0.301	636.87	13205.99
70	7.9	0.0427	23.64	0.6437	0.673	239.38	5128.228
71	6.8	0.0316	23.25	0.4019	0.799	97.75	2417.673
72	5	0.0494	23.89	1.189	0.247	333.75	11379.94
73	8.3	0.0581	23.7	1.1752	0.338	547.57	12198.04
74	8.4	0.0564	23.82	0.838	0.528	402.03	8527.095
75	6.6	0.0537	23.82	1.0129	0.399	359.24	10073.51
76	7.4	0.041	23.83	0.483	0.741	170.98	3834.753
77	5.6	0.056	23.98	1.1754	0.253	390.32	12335.22
78	8.2	0.0567	23.79	0.667	0.609	328.99	6953.06
79	5.8	0.0493	23.82	1.117	0.331	338.22	10507.38
80	7.9	0.0584	23.71	1.195	0.318	532.36	12521.86
81	8.5	0.0581	23.54	0.9582	0.46	460.54	9839.987
82	7.3	0.0269	23.28	0.3757	0.852	89.01	1831.928
83	6.4	0.0409	23.42	0.4598	0.712	132.91	3684.143
84	5.5	0.0597	23.95	1.2384	0.194	430.96	13678.43
85	8.1	0.0551	23.6	0.7609	0.566	345.95	7582.664
86	4.4	0.0586	23.82	1.0823	0.216	322.52	11845.81
87	6.1	0.0304	23.19	0.3895	0.781	77.24	2297.486
88	8.3	0.0495	23.22	0.5882	0.674	266.89	5299.567
89	7.9	0.0537	23.72	0.8745	0.511	371.79	8529.693
90	6.9	0.0589	23.58	0.7814	0.507	313.12	8386.018
91	7.9	0.0582	23.39	1.0787	0.385	472.19	11103.02
92	6.5	0.0483	23.62	0.6129	0.616	201.12	5646.246
93	7.7	0.0573	23.71	0.9537	0.45	410.37	9841.242
94	8.4	0.0552	23.62	0.8231	0.54	386.29	8153.447
95	8	0.0473	23.66	0.707	0.624	285.38	6171.767
96	8.5	0.0577	23.65	0.9175	0.483	443.65	9416.405
97	8.6	0.0589	23.86	1.2361	0.303	606.91	13036.97
98	6	0.0211	23.14	0.3887	0.834	44.71	1511.242
99	8.4	0.0555	23.31	0.9429	0.478	429	9232.157
100	5.8	0.0234	23.18	0.4445	0.789	56.34	2006.509

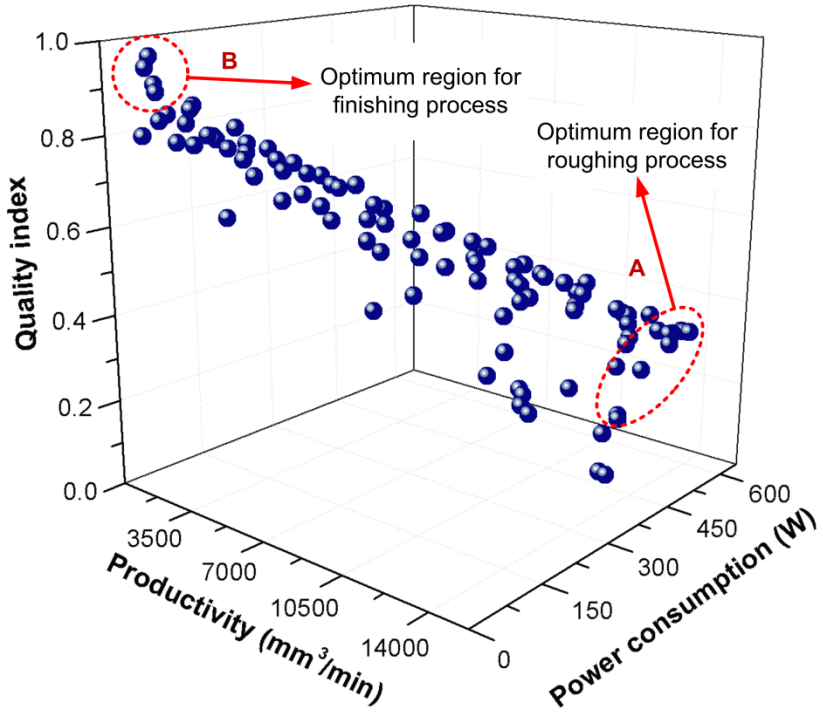

Figure 7.5 3-D plot of the Pareto-optimal solutions for quality index, productivity and power consumption

Figure 7.5 shows the surface generated by all the optimal solutions given by the NSGA-II. It is observed that NSGA-II provided all possible combinations of input milling parameters for best possible fitness values of the objective functions. The solutions encircled in red color suggested the best optimal solutions for roughing and finishing operation. The other solutions also provide process conditions but they are not suitable. From Figure 7.5, two regions '*A*' and '*B*' can be perceived to be appropriate for the machining criteria viz. roughing operation and finishing operation. Employing the solutions of region '*A*' may boost the productivity; however they consume considerable power and produce low quality work parts. Solutions in region '*B*' produce high quality work parts with energy efficient machining but at the expense of process productivity. These can be used for finishing operation of thin-wall parts where maintaining the accuracy of dimensions and surface quality are of prime importance. Therefore it is essential to carefully examine the proposed Pareto solutions and choose the appropriate ones for practical application.

Case 1: Optimum Parameters for Roughing Operation

Since none of the solutions in the non–dominated set is absolutely better than any other, any one of them is an acceptable solution. The choice of one solution over the other depends on the requirement of the process engineer. During the roughing operation of the thin-wall machining process, the material removal rate is to be given the utmost priority in view of maximization of the productivity. Therefore the solutions providing higher MRR can be considered for application in practice. From Table 7.2, it can be seen that of the process conditions of solution number (Sl. No.) 01, 47, 48 provide the maximum possible MRR; however, it is to be noted that these conditions are not suitable to employ in practice. This is because these solutions suggest the use of 4 mm diameter tool, which induces severe chatter at a higher depth of cut. Moreover, these low rigidity slender tools are susceptible to frequent breakages. After careful study of Pareto solutions, the process conditions suggested by Sl. No. 53 and 97 are recommended to be applied in practice. These solutions with rounded-off and adjusted values of milling parameters are shown in Table 7.3. The rounded-off values are according to the nearest possible levels of milling parameters which can be applied in practice with ease. For example the 8.9 mm tool is difficult to design and manufacture and therefore it is replaced by 8 mm tool which is readily available in the market. For this modified values of milling parameters, the value of process responses are computed by using the regression equation developed based on the entire experimental data.

Table 7.3 Recommended optimum conditions for roughing operation

Milling parameters			
d_i	f_z	a_d	r_d
(mm)	**(mm/z)**	**(mm)**	**(mm)**
8	0.06	24	1.25

To confirm the performance of these milling parameters, experiments was carried out and the MRR was recorded (Table 7.3). It can be seen that recommended process conditions produce the thin-wall part with a productivity of 14683.3 mm^3/min, which is more than that of predicted value by 8.42%. Moreover, these conditions provide product quality index of 0.28 and power consumption of 581.98 W, which are in acceptable ranges. It can thus, be seen that the NSGA based approach developed in this work can give the process engineer an efficient tool to choose a range of optimal milling

parameters for fast and economical roughing.

Case 2: Optimum Parameters for Finishing Operation

For finishing operation of thin-wall milling process, solutions that provide high Quality Index were considered as optimal solutions. From Table 7.2 it is noted that Sl. No. 5 and 30 provide high Quality index. Experiments were carried out to verify the performance of suggested optimum parameters. The results obtained during experiments are listed in Table 7.4. It can be clearly seen that both the sets of process condition provide excellent surface finish of 0.33 µm and 0.494µm and wall dimensions with very low magnitude of deflections 0.027 mm and 0.034 mm.

Table 7.4 Recommended optimum conditions for finishing operation

Sl. No.	Milling parameters				Performance parameters	
	d_i (mm)	f_z (mm/z)	a_d (mm)	r_d (mm)	R_a (µm)	D_f (mm)
5	8	0.03	8	0.5	0.484	0.034
30	8	0.02	8	0.3125	0.331	0.027

These encouraging results justify the employment of the optimal combination of milling parameters in practice. Moreover, a comparative assessment of product quality performance of the suggested optimum parameters with the regular parameters was carried out. Figure 7.6(a) shows the 3-D topography of the surface machined using regular milling conditions (Exp. No. 44, Chapter 6, Table 6.2) and Figure 7.6(b, c) shows the surface topography obtained using the optimal milling parameter combinations. It is clearly observed that the surface finish has significantly improved while machining with optimized combination of milling parameters.

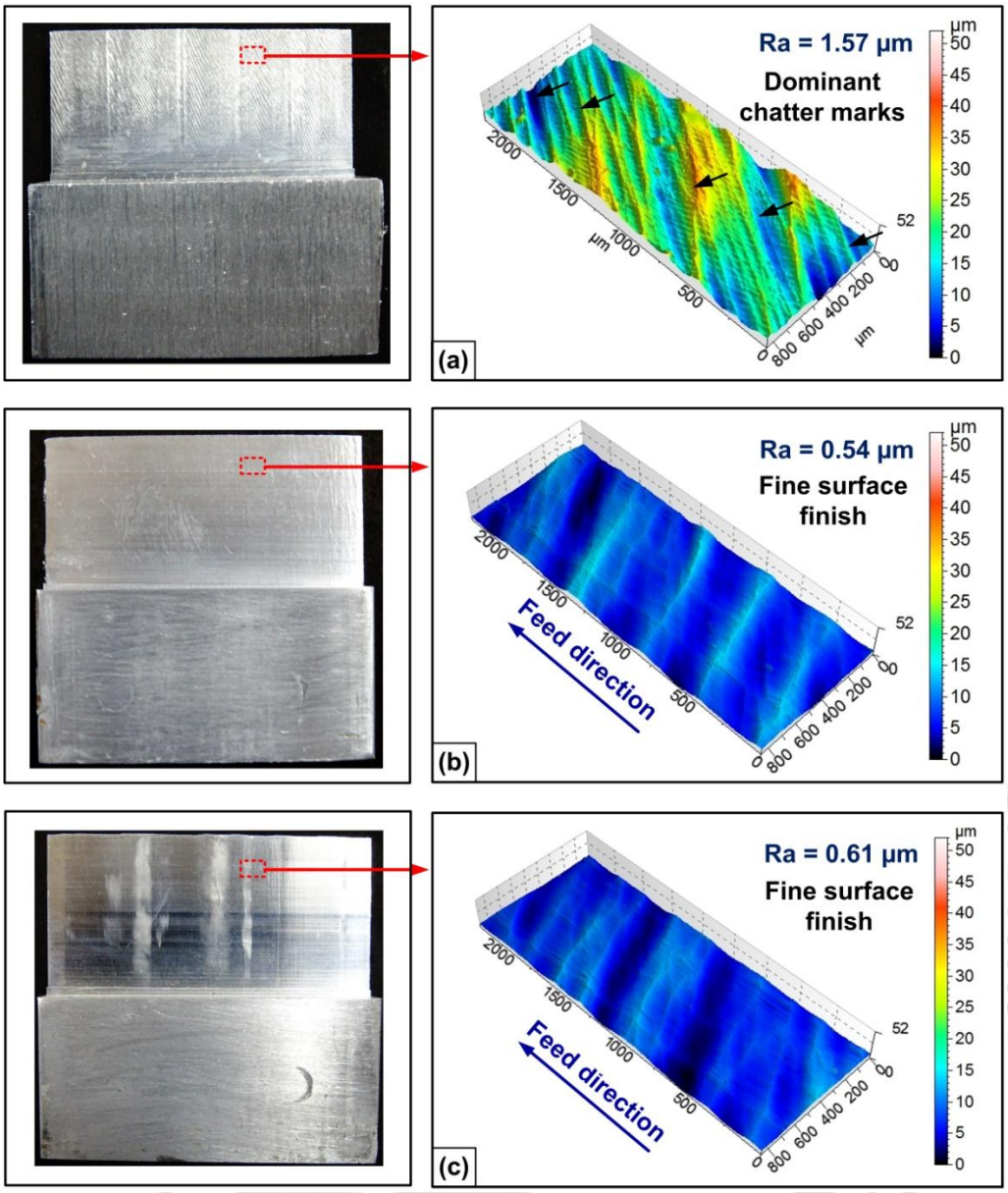

Figure 7.6 Machined surface and 3-D surface topography while machining thin-wall part using: **(a)** Conditions used in Exp. No. 44 (Chapter 6, Table 6.2), **(b)** Optimal condition 1 (Sl. No. 5, Table 7.2), **(c)** Optimal condition 2 (Sl. No. 30, Table No. 7.2)

Figure 7.7(a) shows the error due to the deflection of the thin-wall workpiece machined using regular cutting conditions (Exp No. 44, Chapter 6, Table 6.2) and Figure 7.7(b, c) shows the error due to the deflection of the thin-wall workpiece measured while machining using optimal milling parameter combinations. The experiments were carried out using the optimal milling conditions listed in Table 7.4 to machine thin-walls having a thickness of 1.25 mm.

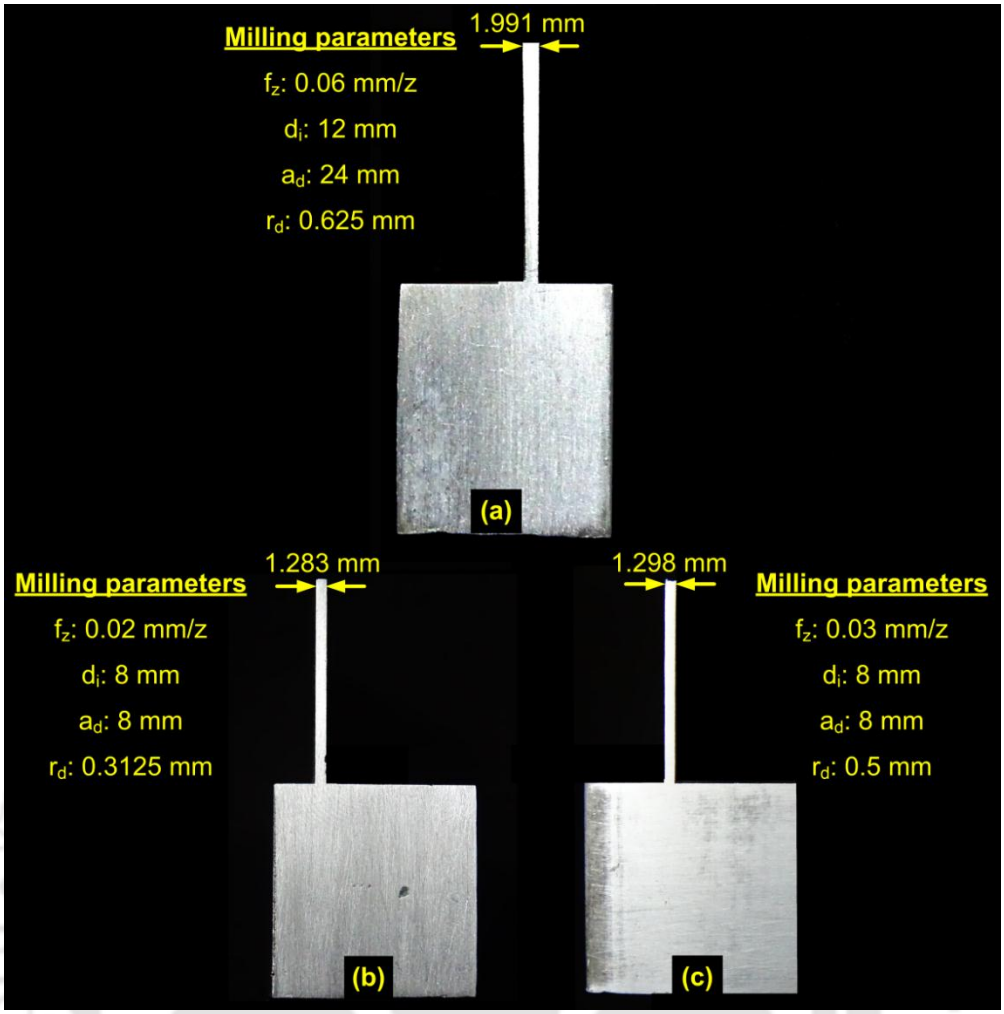

Figure 7.7 Maximum deflection error while machining thin-wall part using: **(a)** Conditions used in Exp. No. 44, **(b)** Optimal condition 1 (Sl. No. 5, Table 7.2), **(c)** Optimal condition 2 (Sl. No. 30, Table No. 7.2

It can be noticed that dimensional accuracy has also been improved significantly using the optimized set of milling parameters. The maximum error due to deflection using the conditions specified for experiment 44 (Chapter 6, Table 6.2) was 0.741 mm. By using the optimal conditions, the errors have been reduced to 0.033 mm and 0.048 mm respectively. Thus it can be concluded that suggested milling parameters can be applied practice with confidence to achieve good quality surface finish with minimal deflection.

7.6 Precision Machining of Ultra-Thin-Walls of 0.7 mm Thickness using Optimum Parameters

To verify the usefulness of optimal milling parameters, experiments were carried out to machine ultra-thin-walls of thickness of 0.7 mm. An experimental setup was developed similar to the one that was used for carrying out thin-wall milling operation (Chapter 5

and 6). Figure 7.8(a, b) shows the 3-D surface topography obtained after machining thin-wall workpiece having a thickness of 0.7 mm using the optimal combination of milling parameters. It is observed that optimum milling parameters produce excellent surface finish of 0.5–0.65 µm (Ra value) which is far improved in comparison with that of general milling parameters. Figure 7.8(a, b) also shows that the proposed optimal conditions could machine the ultra-thin-walls successfully. For the present cases, the maximum non-uniformity in the thickness was noted to be about 0.065 to 0.082 µm. These results prove that by employing optimal milling conditions suggested by the present study, one can easily manufacture precision ultra-thin-wall parts by commercially available low-medium duty CNC-VMC in real life shop floor conditions.

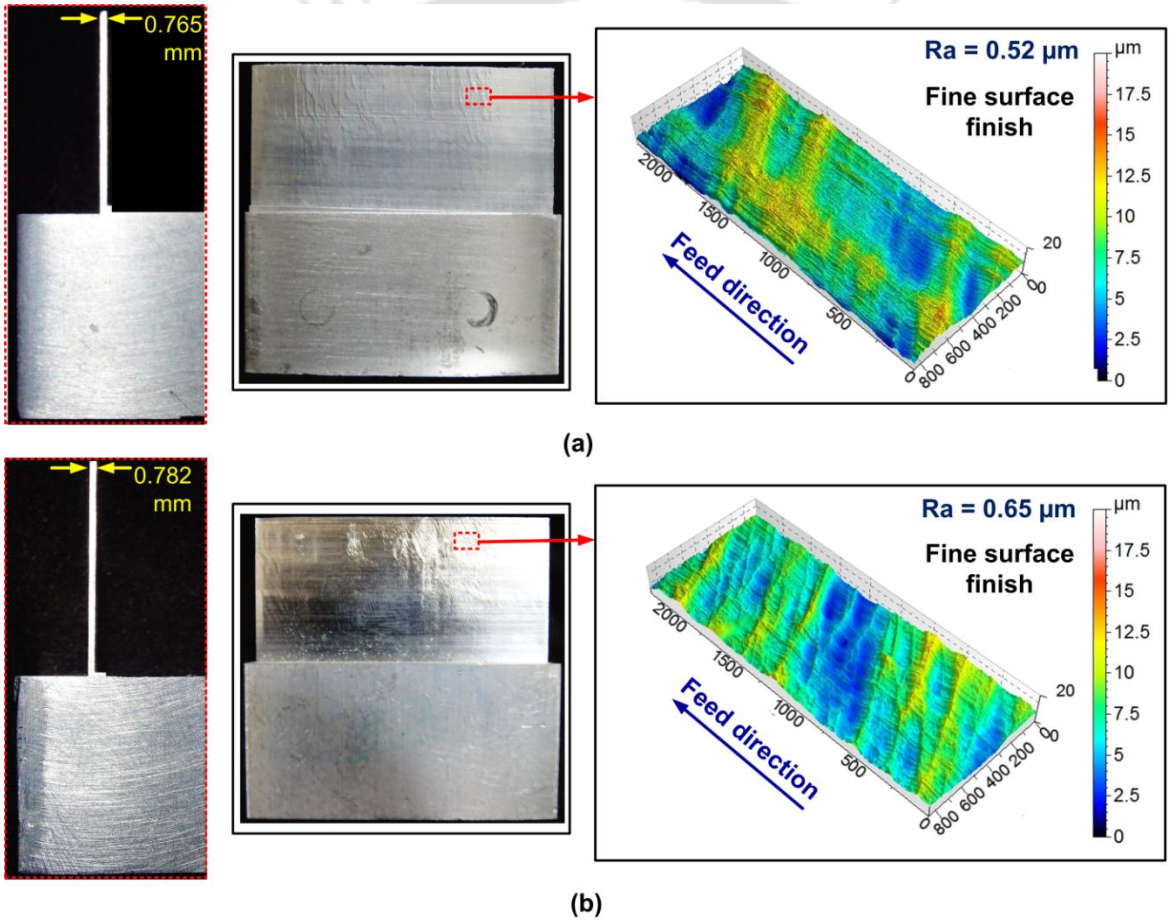

Figure 7.8 Surface finish and maximum deflection error while machining thin-wall part using: **(a)** Optimal condition 1 (Sl. No. 5, Table 7.2), **(b)** Optimal condition 2 (Sl. No. 30, Table No. 7.2)

7.7 Precision Machining of Curved Ultra-Thin-Wall using Optimum Parameters

From the literature, it has been prominently noted that reported research works mainly focused upon machining of straight walled workpieces. Very scant work has been

reported on machining of curved thin-walls. Thus it was thought worthy to carry out a study on machining curvilinear thin-walled part using optimum milling parameters. Thus, in the present work experiments were performed to manufacture 0.7 mm thick curvilinear ultra-thin-walls using a 8 mm diameter tool and the proposed optimum machining conditions of feed per tooth 0.02 mm/z, axial and radial depth of cut of 8 mm and 0.3125 respectively. Machining was carried out on the concave and convex sides of the work specimen.

Figure 7.9(a, b) shows the curvilinear ultra-thin-walls manufactured using optimum conditions and the respective 3-D surface topography images of machined surfaces. It can be noted that proposed conditions produce ultra-thin curvilinear walls with uniform thickness along the height and an excellent surface finish of 0.25 to 0.32 µm. The surface finish is improved in comparison with that of open straight ultra-thin-walls (Section 7.6).

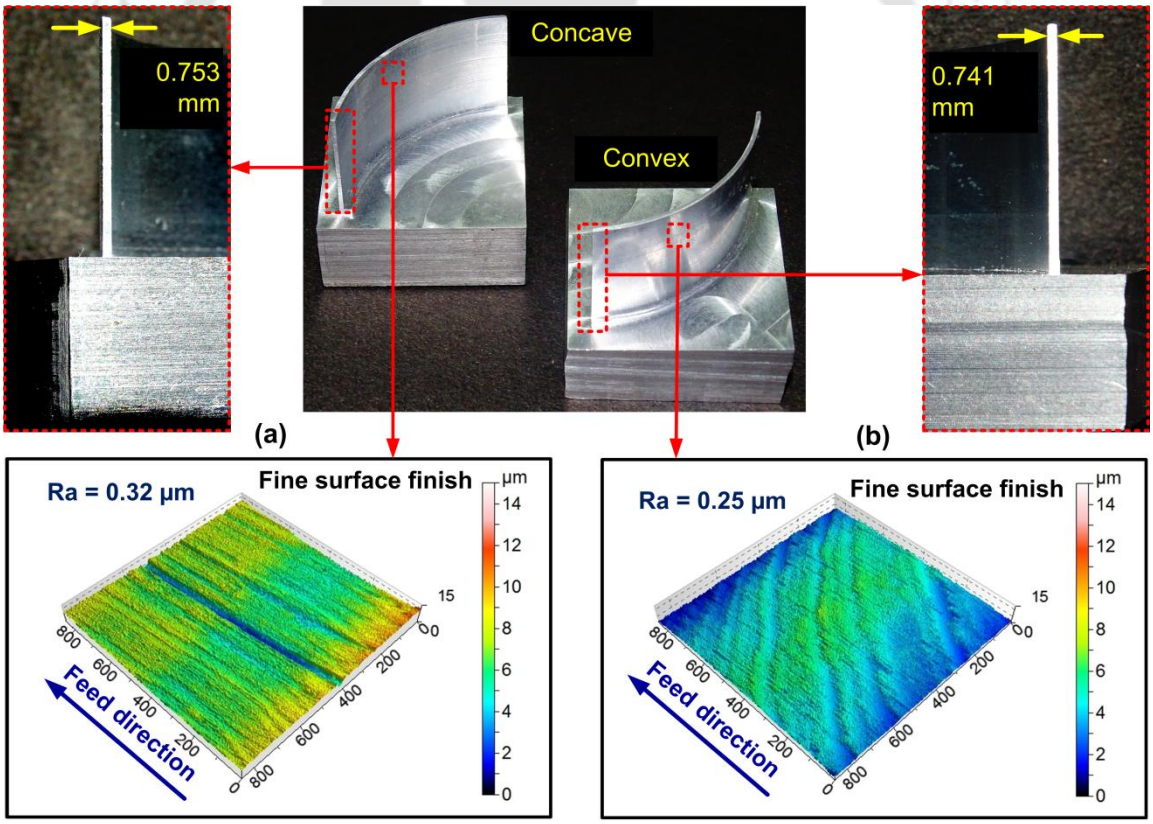

Figure 7.9 Surface finish and maximum deflection error while machining curvilinear thin-wall part: **(a)** Concave surface machining, **(b)** Convex surface machining

This is due to the fact that curvilinear wall possess higher rigidity due to their curved geometry. This helps in reducing the in-situ wall deflection which results in improved surface quality.

From Figure 7.9(a, b) it can also be observed that concave machining approach results in higher deflection error as compared to convex approach. Milling of concave side of the workpiece is considered as anticlastic machining while the convex side is described as synclastic machining. Since anticlastic structures are stiffer than synclastic type parts, the deflection while machining concave was expected to be lower. But it was noted that the deflection while machining a concave side was higher than the convex wall. This higher magnitude of deflection is attributed to the milling force. The recorded milling force during concave machining was higher as compared to the convex side as listed in Table 7.5. This higher magnitude of milling force resulted in higher deflection of the workpiece machined on its concave side. But overall, due to the geometry assisted rigidity of the wall, the magnitude of error was lower as compared to straight walls.

Table 7.5 Comparison of response parameters for concave and convex surface machining

Geometry	F_c (N)	R_a (µm)	D_f (mm)
Concave	65.40	0.32	0.041
Convex	47.51	0.25	0.032

Overall it is concluded the recommended milling parameters are able to produce regular as well as ultra-thin-walls of straight and curvilinear shapes with excellent surface finish and dimensional accuracy. The determined optimal milling parameters can be employed in practice at shop floor with confidence. The developed integrated comprehensive optimization approach provides a very useful tool to the process engineers to choose optimum process conditions.

7.8 Summary

This chapter presented an integrated comprehensive approach for the selection of optimal milling parameters of the helical end milling process to manufacture thin-wall parts. The approach has the peculiar merit that it takes into account productivity, process efficiency (power consumption) and product quality together. The milling parameters viz. tool diameter, feed per tooth, axial and radial depth of cut were considered as milling parameters. Based on a study of different GA based optimization strategies, non-dominated sorting GA - II (NSGA-II) was chosen to solve our optimization problem.

NSGA-II was employed to obtain the Pareto optimal fronts for the roughing and finishing operations. Independent sub–criteria were defined. Exhaustive NSGA-II runs

were carried out by varying the number of generations. The Pareto optimal fronts were studied and optimal milling parameters for roughing and finishing operations were suggested. These recommendations were further verified by conducting in-house experiments. The recommendations from the NSGA-II based optimization strategy were found to be very effective in producing quality thin-walled parts of straight as well as curvilinear shapes. It is concluded that good quality surface finish with minimal deflection can be obtained by using an end mill of diameter 8~9 mm and by maintaining the feed, axial and radial depth values at 0.02 mm/z, 8 mm and 0.3125 mm respectively. Thus it can be seen that the approach developed in this work provides a very effective tool to the process engineers to choose optimum helical end milling parameters for enhancing the product quality and process productivity.

Chapter 8 summarizes the research carried out in the present work. It also presents the conclusions and research contributions.

Chapter 8

Conclusions

8.1 Overview

The work presented in this thesis primarily focused on improving process productivity, product quality and power consumption by conducting systematic numerical, analytical and experimental studies on thin-wall machining of aluminum alloy 2024-T351. To the best of our knowledge, there is no published work that deals with quicker and accurate prediction of instantaneous wall deflection during thin-wall machining and multi-objective optimization of milling parameters for improving the productivity, product quality and energy consumption. The work reported herein was carried out in the following stages:

- Development of a finite element based three-dimensional thermo-mechanical numerical model of thin-wall machining by considering realistic assumptions followed by the experimental validation of developed numerical model.
- Development of an integrated analytical-finite element based model for quicker prediction of milling force and wall deflection during thin-wall machining.
- Experimental investigations into the influence of cutting tool geometry parameters and process parameters on performance parameters such as milling force, surface roughness, wall deflection and material removal rate.
- Multi-objective optimization of thin-wall machining process to derive optimum levels of milling parameters for obtaining desired process performance.

Important observations and research contributions from the present work are summarized in the section to follow.

8.2 Conclusions and Research Contributions

Specific contributions of the current research work are presented below.

8.2.1 Three-Dimensional Thermo-Mechanical Numerical Simulation of Thin-Wall Machining Process using Finite Element Method (FEM)

- A realistic three-dimensional thermo-mechanical finite element method (FEM) based model was developed to simulate the complex physical interaction of helical cutting tool and workpiece during thin-wall milling of an aerospace grade aluminum alloy.

Lagrangian formulation with explicit solution scheme was employed to simulate the interaction between helical milling cutter and the workpiece. The behavior of the material at high strain, strain rate and the temperature was defined by Johnson-Cook material constitutive model. Johnson-Cook damage law and friction law were used to account for chip separation and contact interaction.

- Experimental work was carried out to validate the results predicted by the developed 3-D numerical model. Total four case studies were conducted to test the capability of developed 3D numerical mode. It was noted that the milling force component values predicted by the developed model match well with the values that are obtained by experiments for all the test cases. Mean prediction errors for F_x, F_y , F_z , wall deflection and workpiece temperature were found to be 11.61%, 16.38%, 26.1%., 10.02% and 15.61% respectively. Overall a very good agreement between the simulated and experimentally measured responses has been noted which demonstrates the capability of the developed model to predict the process responses accurately.
- It was noted that maximum deflections were occurring at the free end of the wall as compared to that at the center. It was also observed that due to the deflection of the wall, some material at the base of the wall remained uncut that further leads to geometric form error in the workpiece.
- The simulated chip dimensions were in good agreement with experimental results while the computed cutting temperature varied by 17% with respect to the experimental value. Overall, it was found that the developed model predicts the process responses with fair and acceptable prediction accuracy. Predicted milling force can provide an approximate estimation of energy requirement during machining. The simulated cut-chip was noted to have a similar curl as that occurs in physical experiments.
- From this work, it can be seen that a 3-D numerical model and its successful simulation helps in understanding the complex physical interaction of the helical milling cutter with the thin-wall workpiece. It also helps in the prediction of important process performance parameters such as milling force, deformation, stresses, chip morphology and temperature quite accurately and easily. A prior knowledge about these parameters certainly assists the process engineers and

scientists to tune up the milling parameters to achieve the desired process performance as per the following points.

- Predicted milling force provides an approximate estimation of energy requirement.
- Deformation values forecast the quality of the product in terms of the dimensional accuracy.
- Stresses will help in the estimation of the strength of the machined workpiece, while the chip morphology predicts the surface quality of the machined workpiece.

- The FEM based numerical model developed in this work was found to be accurate but computationally very expensive at it consumes about 345 hours to simulate the single pass of machining of 50 mm long thin-wall part. This limits the applicability of the 3-D numerical model to carry out exhaustive parametric analysis to derive the optimum milling parameters.

8.2.2 An Integrated Analytical-FEM Based Force and Deflection Prediction Model

- In the present work, a simple and integrated force-deflection model for thin-wall milling process was developed. The merits of this proposed approach lie in the utilization of unified mechanics based approach and three-dimensional finite element method based simulation together for quicker and accurate prediction the milling force and in-situ wall deflection for chosen milling conditions. Unified mechanics based analytical equations have been thoroughly studied and employed to compute the milling force. Based on these forces, wall deflections have been computed using 3-D finite element method.
- The present approach considered realistic three-dimensional helical end mill geometry for the computation of milling force.
- A thermo-mechanical oblique cutting model was developed to determine the shear flow stress in the primary shear zone. It incorporated the modified Johnson-Cook law which is based on realistic material characteristics such as strain rate sensitivity, thermal softening and strain hardening. The model also considered the milling force coefficients.
- In this work, the shearing force coefficients those take care of primary shear

deformation were derived using established empirical relations. The edge force coefficients those consider the rubbing and ploughing effects were derived by using simple and computationally inexpensive 2-D FEM model.

- The proposed methodology of employing 2-D FEM based simulation was duly validated by using experimental results. The results in terms milling force were found in good agreement with the experimental results. The main advantage of the proposed model is its ability to predict the milling force coefficients for a chosen pair of cutter and workpiece material without carrying out costly and time consuming experiments.
- Based on the milling force computed by developed analytical model, 3-D FEM simulations were carried out to predict the wall deflection quickly. It is specifically to be noted that, the developed integrated analytical-numerical approach does not simulate the formation of chips during metal cutting operation. However, this 3-D FEM based simulation considers the realistic geometry of the workpiece in terms of the curved transition region and cut portions due to previous tool passes.
- To examine the capability of the proposed approach, four case studies were carried out. Considering all test cases, the mean prediction errors for milling force components F_x, F_y and F_z were noted to be 9.56%, 7.44% and 21.48% respectively. The model was able to predict the wall deflection with a very good accuracy (mean prediction error of 9.3 %). This error can be attributed to various factors such as vibrations, friction, inhomogeneous workpiece hardness, machining interruption by generated chips, tool runout. Some of these parameters are uncontrollable and it is very difficult to incorporate the effects of the same in the numerical or analytical modeling.
- The developed integrated model was found to be far more efficient than the 3-D FEM model which was developed initially (Chapter 3). The time duration for prediction of the milling force and magnitude of wall deflection using the developed integrated model was noted as 40 min in comparison of 344 hrs (average) consumed by the 3-D FEM based thermo-mechanical model.
- Overall the present work provided a novel, simple, efficient integrated approach for force-deflection prediction during helical end milling of thin-wall parts. Based on the results obtained it was felt that the developed model can be applied with confidence

in practice for quick and accurate computation of in-situ wall deflection of thin-wall parts and prior estimation of energy required for cutting. However, the proposed model does not provide the information about the quality of surface machined, chip morphology which is vital in deciding the milling parameters to obtain the desired process performance.

8.2.3 Experimental Studies on Thin-Wall Machining of Aluminum Alloy 2024-T351

- In this research work, systematic experiments have been carried out on thin-wall end milling operation. The experiments were conducted in three phases. Initially, the experiments were carried out to determine the most influential parameters among the milling parameters viz. feed per tooth, spindle speed, axial and radial depth. To carry out this exercise, the performance of milling process was measured in terms of milling force, surface roughness and wall deflection. Radial depth of cut, axial cut depth and feed rate were found to have a significant influence on the performance of thin-wall machining process. However, spindle speed was found to have comparatively less effect on the responses. The levels of these milling parameters were finalized, so that these can be further used to carry out detailed experimental investigation.
- In the second phase of experiments, investigations into the influence of tool geometry parameters such as tool diameter, helix angle and number of flutes on the performance of the process were carried out. Grey relational analysis (GRA) methodology was utilized to obtain the optimal and influential tool geometry parameters. Based on the Grey relational rank, tool diameter was found be highly influencing on the process responses, viz. milling force, surface roughness and wall deflection. GRA suggested that an optimal combination of tool geometry parameters i.e. diameter 8 mm with a helix angle of 45° and 4 flutes achieves the desired process performance. This optimal combination was verified by conducting experiments and it was found that the suggested tool geometry parameters produce a significant improvement in the surface quality of the machined part. An excellent surface finish of 0.401 µm *Ra* value was obtained. It was also noted that the optimal tool geometry parameters significantly reduces the wall deflection by 6.33%.
- During thin-wall milling operation, a study on the influence of tool helix angle on chip morphology was carried out. For chosen process conditions, continuous chips

with semi-parabolic, semi-circular or near circular shape were formed. Specific observations about the chip morphology are as follows:

- Material folds were observed on the free surface of chips.
- Lamella like structures was observed on the chip back surface, with lamella being prominent while tool having a helix of 35º was used.
- Higher helix tools produced relatively lamella free surface. The back surface of the chip was shiny with abrasion marks from chip particles which adhered on the tool surface.
- High helix angle helped in easy shearing away of the chip as compared to a low helix tool and produced better surface quality.

- In the third phase of work, full factorial experiments were carried out by varying feed per tooth, axial depth of cut, radial depth of cut and tool diameter at three levels. Total 81 experiments were conducted and the process performance in terms of milling force, surface roughness, wall deflection and material removal rate (MRR) were recorded for each experiment. Based on response surface methodology (RSM), systematic studies have been carried out on the perturbation and interaction effects of input milling parameters on the individual performance parameters. Results were studied and the findings were presented with suitable scientific justifications. Based on the RSM, mathematical models for the prediction of individual responses were derived. Further, the predictions by the models were verified by conducting confirmatory experiments. All the models were found to have good prediction capabilities. Some of the important conclusions are as follows.
  - Tool diameter was found to have significant influence on milling force. It was observed that formation of built-up-edges (BUEs) and swirling of the machined chips interrupted the cutting process which resulted in an increase in milling force.
  - Tool breakage was noticed when 4 mm diameter tool was employed with high feed and depth of cut conditions. Machining using larger rigid tools (12 mm) increased the milling force value as they apply more pressure on the thin-wall workpiece. Use of 8 mm tool produced moderate milling force. It was concluded that use of end mill of 4 mm diameter is to be avoided while 8 mm diameter tool

can be employed in practice for quality thin-wall machining.

- Formation of chatter marks was noted when machining was carried out at high depth of cut conditions. Two types of chatter phenomenon were observed. The first type of chatter observed was associated with the tool. Due to lower flexural stiffness, a small variation in the milling force caused the tool to deflect easily. This resulted in dynamic instability causing the tool to vibrate. As the tool was in contact with the workpiece, the vibration was transmitted to the workpiece which resulted in generating chatter marks. The second type of chatter was due to workpiece vibration. During machining using a 12 mm diameter tool, at high axial depth of cut condition, the tooth passing frequency excites the resonant vibrations in the low rigidity thin-wall. These resonant vibrations increase the frequency of occurrence of interrupted and non-uniform contact between tool and the work surface. This causes the chatter and results in poor surface finish. Studies revealed that use of 8 mm tool helps in chatter-free machining and produces quality surface finish. It was also noted that deflection of the wall significantly affects the surface finish. Surface roughness was noted to be higher near to the free end due to more deflection of the free end as compared to the base of the wall.
- Investigation of the machined surface indicated the presence of surface defects such as material plucking, material adhesion, material shearing, and deformed layer formation. These defects resulted in deterioration of surface finish.
- Wall deflection was found to be influenced significantly by tool diameter, feed per tooth, axial and radial depth of cut. Large values of milling force those generated due to high feed led to an unfavorable increase in the magnitude of wall deflection. Measured deflections were higher when thin-walls were machined with 12 mm diameter tool. Axial depth of cut was found to be the most influencing parameter on wall deflection. Also, a substantial rise in the magnitude of wall deflection was observed with a larger radial depth of cut.
- It was noted that material removal rate decrease with the increase in tool diameter. This was due to the incorporation of increased ramp-on and ramp-off distances associated with larger tool diameters in the calculation of machining time.

- Based on the extensive data generated during the experimental studies, mathematical predictive models were developed. For all performance parameters, these models were found to be adequate in terms of accuracy. The validity of regression equations for prediction of milling force, surface roughness, wall deflection and material removal rate were 90.5%, 84.5%, 90.8% and 97.55% respectively. The values indicated that the models were able to predict the responses accurately. This was confirmed by conducting validation tests. It was noted that the developed mathematical models predict the responses with good accuracy. The prediction errors (absolute) vary between 0.41 to 16.39%. The mean error for milling force, surface roughness, wall deflection and material removal rate were observed to be 5.9%, 5.5%, 7.9% and 7.8%.

- Overall it can be concluded that the productivity of thin-wall operation can be maximized using high values of depth of cut and feed with 8 mm tool diameter. But higher values of feed per tooth, axial depth of cut, and radial depth of cut adversely affect the wall dimensional accuracy and surface quality. Therefore, a trade-off must be obtained to have optimum levels of milling parameters that will produce quality thin-wall parts at maximum possible productivity.

- Extensive data was generated on the process performance for the chosen process conditions by carrying out physical experiments. This data was used to derive optimum process conditions by carrying out multi-objective optimization using the genetic algorithm (GA).

8.2.4 Optimum Selection of End Milling Parameters using Non-Dominated Genetic Algorithm - II

- An integrated comprehensive approach for the selection of optimal milling parameters of the helical end milling process to manufacture thin-wall parts was carried out. The approach has the peculiar merit that it takes into account productivity, process efficiency (power consumption) and product quality together. The milling parameters viz. tool diameter, feed per tooth, axial and radial depth of cut were considered in the study. Based on a study of different GA based optimization strategies, non-dominated sorting GA - II (NSGA-II) was selected to solve our optimization problem.

- NSGA-II was employed to obtain the Pareto optimal fronts for the roughing and

finishing operations. Independent objective sub-criteria were defined. Exhaustive NSGA-II runs were carried out by varying the number of generations. The Pareto optimal fronts were studied and optimal milling parameters for roughing and finishing operations were suggested. These recommendations were further verified by conducting in-house experiments. The recommendations from the NSGA-II based optimization strategy were found to be very effective in producing quality thin-wall parts of straight as well as curvilinear shapes. It is concluded that good quality surface finish with minimal deflection can be obtained by using an end mill of diameter 8~9 mm and by maintaining the feed, axial and radial depth values at 0.02 mm/z, 8 mm and 0.3125 mm respectively.

- The recommended optimum process conditions were applied to manufacture a 700 µm ultra-thin-wall of curvilinear shape. It was observed that the suggested process conditions produce an excellent surface finish of 0.25~0.32 µm (R_a values) and uniform thin-wall (deflection error of 32~41 µm). Thus it can be said that the approach developed in this work provided a very effective tool to the process engineers to choose optimum levels of end milling parameters for enhancing the product quality and process productivity.

In conclusion, the present research work has contributed by developing a realistic 3-D thermo-mechanical FEM based numerical model of thin-wall milling, an integrated simple and efficient analytical-numerical force-deflection prediction model, and exhaustive experimental studies on thin-wall machining process. Our integrated model quickly and accurately predicts the milling force and instantaneous wall deflection. The optimum milling parameters suggested by our multi-objective approach are found to give the desired performance of thin-wall machining process to a very good degree. Suggested optimum process parameters can be applied with confidence in practice to enhance the productivity and finishing capability of machining of thin as well as ultra-thin-wall parts.

8.3 Scope for Future work

The present research work can be extended on the following fronts.

- Improving the thermo-mechanical (FEM) model of metal cutting by incorporating the effects of material anisotropy, inhomogeneity, and pre-stresses in the work parts.

- Incorporating the phenomenon of recrystallization and grain growth in the model and study its influence on the responses
- Including the influence of tool path strategies during the numerical and analytical simulations of thin-wall machining process.
- Employing the analytical model for other work-tool material pairs.
- Carrying out investigations by using coated and uncoated carbide tools, green/environmental friendly cutting fluids during thin-wall machining of titanium and its alloys.

References

- Ab-Kadir, A. R., Osman, M. H., & Shamsuddin, K. A. (2013). A comparison of milling cutting path strategies for thin-walled aluminium alloys fabrication. *The Internal Journal of Engineering and Science*, *2*(3), 1-8.
- Adetoro, O. B., & Wen, P. H. (2010). Prediction of mechanistic cutting force coefficients using ALE formulation. *The International Journal of Advanced Manufacturing Technology*, *46*(1), 79-90.
- Agmell, M., Ahadi, A., & Ståhl, J. E. (2011). A fully coupled thermomechanical two-dimensional simulation model for orthogonal cutting: formulation and simulation. *Proceedings of the Institution of Mechanical Engineers, Part B: Journal of Engineering Manufacture*, *225*(10), 1735-1745.
- Aijun, T., & Zhanqiang, L. (2008). Deformations of thin-walled plate due to static end milling force. *Journal of Materials Processing Technology*, *206*(1), 345-351.
- Alauddin, M., El Baradie, M. A., & Hashmi, M. S. J. (1996). Optimization of surface finish in end milling Inconel 718. *Journal of Materials Processing Technology*, *56*(1-4), 54-65.
- Alrashdan, A., Bataineh, O., & Shbool, M. (2014). Multi-criteria end milling parameters optimization of AISI D2 steel using genetic algorithm. *The International Journal of Advanced Manufacturing Technology*, *73*(5-8), 1201-1212.
- Altintas, Y., & Montgomery, D. (1991). Mechanism of cutting force and surface generation in dynamic milling. *Journal of Engineering for Industry*, *113*(2), 160-168.
- Altintas, Y., Montgomery D., & Budak E., (1992). Dynamic peripheral milling of flexible structures. *J Eng Ind, Trans ASME*, *114*(2), 137-145.
- Altintas, Y., & Armarego, E. J. A. (1996). Prediction of milling force coefficients from orthogonal cutting data. *Trans. ASME J. Engng Ind*.
- Altintas, Y. (2000). *Manufacturing automation: metal cutting mechanics, machine tool vibrations, and CNC design*. Cambridge university press.
- Armarego, E. J. A., & Brown, R. H. (1969). The machining of metals. *Prentice-Hall Inc., Englewood Cliffs, N. J., 1969, 437 P*.
- Armarego, E. J. A., & Whitfield, R. C. (1985). Computer based modelling of popular machining operations for force and power prediction. *CIRP Annals-Manufacturing Technology*, *34*(1), 65-69.
- Armarego, E. J. A. (1998). A generic mechanics of cutting approach to predictive technological performance modeling of the wide spectrum of machining operations. *Machining Science and Technology*, *2*(2), 191-211.
- Armarego, E. J. A. (2000). The unified-generalized mechanics of cutting approach—a step towards a house of predictive performance models for machining operations. *Machining science and technology*, *4*(3), 319-362.
- Arrazola, P. J., Ugarte, D., & Dominguez, X. (2008). A new approach for the friction identification during machining through the use of finite element modeling. *International Journal of Machine Tools and Manufacture*, *48*(2), 173-183.

- Arrazola, P. J., & Özel, T. (2010). Investigations on the effects of friction modeling in finite element simulation of machining. *International Journal of Mechanical Sciences*, *52*(1), 31-42.
- Artozoul, J., Lescalier, C., & Dudzinski, D. (2015). Experimental and analytical combined thermal approach for local tribological understanding in metal cutting. *Applied Thermal Engineering*, *89*, 394-404.
- Asad, M., Mabrouki, T., Memon, A. A., Shah, S. M. A., & Khan, M. A. (2013). Three-dimensional finite element modeling of rough to finish down-cut milling of an aluminum alloy. *Proceedings of the Institution of Mechanical Engineers, Part B: Journal of Engineering Manufacture*, *227*(1), 75-83
- Asiltürk, I., Neşeli, S., & Ince, M. A. (2016). Optimisation of parameters affecting surface roughness of Co28Cr6Mo medical material during CNC lathe machining by using the Taguchi and RSM methods. *Measurement*, *78*, 120-128.
- Bacaria, J. L., Dalverny, O., & Caperaa, S. (2001). A three-dimensional transient numerical model of milling. *Proceedings of the Institution of Mechanical Engineers, Part B: Journal of Engineering Manufacture*, *215*(8), 1147-1150.
- Barge, M., Hamdi, H., Rech, J., & Bergheau, J. M. (2005). Numerical modelling of orthogonal cutting: influence of numerical parameters. *Journal of Materials Processing Technology*, *164*, 1148-1153.
- Becze, C. E., & Elbestawi, M. A. (2002). A chip formation based analytic force model for oblique cutting. *International Journal of Machine Tools and Manufacture*, *42*(4), 529-538.
- Boothroyd, G., & Knight, W. A. (1989). Fundamentals of Machining and Machine Tools, Marcel-Dekker. *New York*.
- Borneman, C. H. (1938). Chip thickness in milling. *Am. Mach. Ref. Book Sheet*, *82*, 189-190.
- Budak, E., & Altintas, Y. (1994). Peripheral milling conditions for improved dimensional accuracy. *International Journal of Machine Tools and Manufacture*, *34*(7), 907-918.
- Budak, E., & Altintas, Y. (1995). Modeling and avoidance of static form errors in peripheral milling of plates. *International Journal of Machine Tools and Manufacture*, *35*(3), 459-476.
- Budak, E. (2006). Analytical models for high performance milling. Part I: Cutting forces, structural deformations and tolerance integrity. *International Journal of Machine Tools and Manufacture*, *46*(12), 1478-1488.
- Bussu, G., & Irving, P. E. (2003). The role of residual stress and heat affected zone properties on fatigue crack propagation in friction stir welded 2024-T351 aluminium joints. *International Journal of Fatigue*, *25*(1), 77-88.
- Campatelli, G., Lorenzini, L., & Scippa, A. (2014). Optimization of process parameters using a response surface method for minimizing power consumption in the milling of carbon steel. *Journal of cleaner production*, *66*, 309-316.
- Campbell Jr, F. C. (2011). *Manufacturing technology for aerospace structural materials*. Elsevier.

- Cao, Y., Bai, Y., He, Y., & Li, Y. (2010, May). NC milling deformation analysis of aluminum alloy thin-walled components based on orthogonal cutting experiments on a vertical machining center. In *2nd International Conference on Industrial Mechatronics and Automation (ICIMA).*
- Ceretti, E., Fallböhmer, P., Wu, W. T., & Altan, T. (1996). Application of 2D FEM to chip formation in orthogonal cutting. *Journal of Materials Processing Technology*, *59*(1-2), 169-180.
- Chandrasekaran, M., Muralidhar, M., Krishna, C. M., & Dixit, U. S. (2010). Application of soft computing techniques in machining performance prediction and optimization: a literature review. *The International Journal of Advanced Manufacturing Technology*, *46*(5-8), 445-464.
- Chao, B. T. (1955). Temperature distribution at the tool-chip interface in metal cutting. *Trans. ASME*, *77*, 1107.
- Chen, X. X., Zhao, J., Li, Y. E., Han, S. G., Cao, Q. Y., & Li, A. H. (2012). Numerical modelling of high-speed ball end milling with cutter inclination angle. *Proceedings of the Institution of Mechanical Engineers, Part B: Journal of Engineering Manufacture*, *226*(4), 606-616.
- Cheng, Y., Zuo, D., Wu, M., Feng, X., & Zhang, Y. (2015). Study on simulation of machining deformation and experiments for thin-walled parts of titanium alloy. *International Journal of Control and Automation*, *8*(1), 401-410.
- Coello, C. A. C., Lamont, G. B., & Van Veldhuizen, D. A. (2007). *Evolutionary algorithms for solving multi-objective problems* (Vol. 5). New York: Springer.
- Conradie, P., Dimitrov, D., & Saxer, M. (2012). An approach for evaluation of cutting strategies for milling of Ti6Al4V. In *Computers and Industrial Engineering 42*, 123(1)-123(15).
- Datron Dynamics Inc., http//www.datrondynamics.com/Thin_Wall_Machining (2017)
- Davim, J. P., Maranhão, C., Jackson, M. J., Cabral, G., & Gracio, J. (2008). FEM analysis in high speed machining of aluminium alloy (Al7075-0) using polycrystalline diamond (PCD) and cemented carbide (K10) cutting tools. *The International Journal of Advanced Manufacturing Technology*, *39*(11), 1093-1100.
- Deb, K. (2000). An efficient constraint handling method for genetic algorithms. *Computer methods in applied mechanics and engineering*, *186*(2), 311-338.
- Deb, K. (2001). *Multi-objective optimization using evolutionary algorithms* (Vol. 16). John Wiley & Sons.
- Deb, K., Pratap, A., Agarwal, S., & Meyarivan, T. A. M. T. (2002). A fast and elitist multiobjective genetic algorithm: NSGA-II. *IEEE transactions on evolutionary computation*, *6*(2), 182-197.
- Denkena, B., & Schmidt, C. (2007). Experimental investigation and simulation of machining thin-walled workpieces. *Production engineering*, *1*(4), 343-350.
- DeVor, R. E., & Kline, W. (1980). A mechanistic model for the force system in end milling with application to machining airframe structures. In *8th Manufacturing Engineering Transactions and North American Manufacturing Research Conference.*

- DeVor, R. E., Sutherland, J. W., & Kline, W. A. (1983). Control of surface error in end milling. *Manufacturing Engineering Transactions*, *11*, 356.
- Du, S., Chen, M., Xie, L., Zhu, Z., & Wang, X. (2016). Optimization of process parameters in the high-speed milling of titanium alloy TB17 for surface integrity by the Taguchi-Grey relational analysis method. *Advances in Mechanical Engineering*, *8*(10), 1-12. 1687814016671442.
- Du, Z., Zhang, D., Hou, H., & Liang, S. Y. (2017). Peripheral milling force induced error compensation using analytical force model and APDL deformation calculation. *The International Journal of Advanced Manufacturing Technology*, *88*(9-12), 3405-3417.
- Ee, K. C., Dillon, O. W., & Jawahir, I. S. (2005). Finite element modeling of residual stresses in machining induced by cutting using a tool with finite edge radius. *International Journal of Mechanical Sciences*, *47*(10), 1611-1628.
- Elkhabeery, M. M., & Bailey, J. A. (1984). Surface integrity in machining solution-treated and aged 2024-aluminum alloy, using natural and controlled contact length tools. Part I-Unlubricated conditions. *Journal of Engineering Materials and Technology*, *106*(2), 152-160.
- El-Wardany, T. I., Mohammed, E., & Elbestawi, M. A. (1996). Cutting temperature of ceramic tools in high speed machining of difficult-to-cut materials. *International Journal of Machine Tools and Manufacture*, *36*(5), 611-634.
- Fry, C., Fry, T., & Raman, S. (1999). Experimental verification of tool wear effects in alternate path traversal in milling. In *Proceeding of the ASME Energy Sources Technology Conference*.
- Fu, Z., Yang, W., Wang, X., & Leopold, J. (2015). Analytical modelling of milling forces for helical end milling based on a predictive machining theory. *Procedia CIRP*, *31*, 258-263.
- Gang, L. (2009). Study on deformation of titanium thin-walled part in milling process. *Journal of materials processing technology*, *209*(6), 2788-2793.
- Geng, Z., Ridgway, K., Turner, S., & Morgan, G. (2011). Application of thin-walled dynamics for advanced manufacturing solutions. *IOP Conference Series: Materials Science and Engineering*, 26(1), 012011
- Ghoddosian A., Pour M., & Eskandar H. (2011). Identification optimization cutting parameters based on ICA method in peripheral milling of thin wall. *World Applied Science Journal*, 13(8), 1886-1894.
- Ginting, A., & Nouari, M. (2006). Experimental and numerical studies on the performance of alloyed carbide tool in dry milling of aerospace material. *International Journal of Machine Tools and Manufacture*, *46*(7), 758-768.
- Ginting, A., & Nouari, M. (2007). Optimal cutting conditions when dry end milling the aeroengine material Ti–6242S. *Journal of Materials Processing Technology*, *184*(1), 319-324.
- Gologlu, C., & Sakarya, N. (2008). The effects of cutter path strategies on surface roughness of pocket milling of 1.2738 steel based on Taguchi method. *Journal of materials processing technology*, *206*(1), 7-15.

- Gradišek, J., Kalveram, M., & Weinert, K. (2004). Mechanistic identification of specific force coefficients for a general end mill. *International Journal of Machine Tools and Manufacture*, *44*(4), 401-414.
- Guo, Y., Zhong, H., He, W., & Tao, G. (2016). Experiment Study on Efficient Flank Milling of Ti6AL4V Thin-walled Components. *International Journal of Multimedia and Ubiquitous Engineering*, *11*(7), 79-86.
- Haddag, B., Atlati, S., Nouari, M., & Znasni, M. (2010). Finite element formulation effect in three-dimensional modeling of a chip formation during machining. *International Journal of Material Forming*, *3*, 527-530.
- Haglund, A. J., Kishawy, H. A., & Rogers, R. J. (2008). An exploration of friction models for the chip–tool interface using an Arbitrary Lagrangian–Eulerian finite element model. *Wear*, *265*(3), 452-460.
- Hahn, R. S. (1951, January). On the temperature developed at the shear plane in the metalcutting process. In *Journal of Applied Mechanics-Transactions of the ASME*, 18(3), 323-323.
- Herranz, S., Campa, F. J., De Lacalle, L. L., Rivero, A., Lamikiz, A., Ukar, E., Sánchez, A., & Bravo, U. (2005). The milling of airframe components with low rigidity: a general approach to avoid static and dynamic problems. *Proceedings of the Institution of Mechanical Engineers, Part B: Journal of Engineering Manufacture*, *219*(11), 789-801.
- Houjun, Q., Dawei, Z., Bing, Y., & Yujun, C. (2009). Effect of part-cutter deflection on flexible milling force in high speed peripheral milling process. In *International Technology and Innovation Conference*.
- Huang, P. L., Li, J. F., Sun, J., & Zhou, J. (2014). Study on performance in dry milling aeronautical titanium alloy thin-wall components with two types of tools. *Journal of Cleaner Production*, *67*, 258-264.
- Huang, P. L., Li, J. F., Sun, J., & Jia, X. M. (2016). Cutting signals analysis in milling titanium alloy thin-part components and non-thin-wall components. *The International Journal of Advanced Manufacturing Technology*, *84*(9-12), 2461-2469.
- Izamshah, R. A. R., Mo, J. P., & Ding, S. (2011). Deflection Prediction on Machining Thin-Walled Monolithic Aerospace Component. *Journal of Mechanical Engineering and Technology*, *3*(1). 23-44.
- Izamshah, R. A., Mo, J., & Ding, S. L. (2011). Finite element analysis of machining thin-wall parts. In *Key Engineering Materials*, *458*, 283-288.
- Izamshah, R., Mo, J. P. T., & Ding, S. (2012). Hybrid deflection prediction on machining thin-wall monolithic aerospace components. *Proceedings of the Institution of Mechanical Engineers, Part B: Journal of Engineering Manufacture*, *226*(4), 592-605.
- Izamshah, R., Yuhazri, M. Y., Hadzley, M., Ali, M. A., & Subramonian, S. (2013). Effects of end mill helix angle on accuracy for machining thin-rib aerospace component. *Applied Mechanics and Materials*, *315*. 773-777

- Izamshah, R. A. J. A., Zulhairy, M., Kasim, M. S., Hadzley, M., Amran, M., & Amri, M. (2014). Cutter path strategies for shoulder milling of thin deflecting walls. In *Advanced Materials Research*, *903*, 175-180.
- Jabbaripour, B., Sadeghi, M. H., & Faridvand, S. (2010). A study of the effects of cutter path strategies and cutting speed variations in milling of thin-walled parts. In *The 7th Jordanian International Mechanical Engineering Conference*.
- Ji, C., Li, Y., Qin, X., Zhao, Q., Sun, D., & Jin, Y. (2015). 3D FEM simulation of helical milling hole process for titanium alloy Ti-6Al-4V. *The International Journal of Advanced Manufacturing Technology*, *81*(9-12), 1733-1742.
- Jiang, X., Li, B., Yang, J., & Zuo, X. (2013). Effects of tool diameters on the residual stress and distortion induced by milling of thin-walled part. *International Journal of Advanced Manufacturing Technology*, *68*. 175–186.
- Jiao, L., Wang, X., Qian, Y., Liang, Z., & Liu, Z. (2015). Modelling and analysis for the temperature field of the machined surface in the face milling of aluminium alloy. *The International Journal of Advanced Manufacturing Technology*, *81*(9-12), 1797-1808.
- Johnson, G. R., & Cook, W. H. (1983, April). A constitutive model and data for metals subjected to large strains, high strain rates and high temperatures. In *Proceedings of the 7th International Symposium on Ballistics* (Vol. 21, No. 1, pp. 541-547).
- Johnson, G. R., & Cook, W. H. (1985). Fracture characteristics of three metals subjected to various strains, strain rates, temperatures and pressures. *Engineering fracture mechanics*, *21*(1), 31-48.
- Jomaa, W., Lévesque, J., Bocher, P., Divialle, A., & Gakwaya, A. (2017). Optimization study of dry peripheral milling process for improving aeronautical part integrity using Grey relational analysis. *The International Journal of Advanced Manufacturing Technology*, *91*(1-4), 931-942.
- Joshi, S. N., & Pande, S. S. (2011). Intelligent process modeling and optimization of die-sinking electric discharge machining. *Applied soft computing*, *11*(2), 2743-2755.
- Juneja, B. L. (2003). *Fundamentals of metal cutting and machine tools*. New Age International.
- Kazemi, M., Poor, B. J., Sadeghi, M. H., & Moetakef Imani, B. (2007, June). Surface Integrity of Thin-Walled Titanium Parts Machined by Peripheral Milling. In *4th International conference and exhibition on design and production of machines and dies/molds*.
- Kececioglu, D. (1958). Shear-strain rate in metal cutting and its effects on shear-flow stress. *Trans. ASME*, *80*(1), 158.
- Kennedy B., (2007). Wall smartcutting tool engineering magazine. 59
- Kılıçaslan, C. (2009). *Modelling and simulation of metal cutting by finite element method* (Master's thesis, İzmir Institute of Technology).
- Kline, W. A., DeVor, R. E., & Shareef, I. A. (1982). The prediction of surface accuracy in end milling. *Trans, of ASME Aug*, *104*(3), 272-278.
- Komanduri, R., & Hou, Z. B. (2001). Thermal modeling of the metal cutting process-Part III: temperature rise distribution due to the combined effects of shear plane heat source and the

tool–chip interface frictional heat source. *International Journal of Mechanical Sciences*, *43*(1), 89-107.

- Kondayya, D., & Krishna, A. G. (2012). An integrated evolutionary approach for modelling and optimisation of CNC end milling process. *International Journal of Computer Integrated Manufacturing*, *25*(11), 1069-1084.
- Kronenberg, M. (1966). *Machining science and application: theory and practice for operation and development of machining processes*. Pergamon Press.
- Kuram, E., Ozcelik, B., Bayramoglu, M., Demirbas, E., & Simsek, B. T. (2013). Optimization of cutting fluids and cutting parameters during end milling by using D-optimal design of experiments. *Journal of Cleaner Production*, *42*, 159-166.
- Li, B., Hu, Y., Wang, X., Li, C., & Li, X. (2011). An analytical model of oblique cutting with application to end milling. *Machining Science and Technology*, *15*(4), 453-484.
- Li, B., Jiang, X., Yang, J., & Liang, S. Y. (2015). Effects of depth of cut on the redistribution of residual stress and distortion during the milling of thin-walled part. *Journal of Materials Processing Technology*, *216*, 223-233.
- Li, H. Z., Zhang, W. B., & Li, X. P. (2001). Modelling of cutting forces in helical end milling using a predictive machining theory. *International Journal of Mechanical Sciences*, *43*(8), 1711-1730.
- Li, H. Z., & Wang, J. (2013). A cutting forces model for milling Inconel 718 alloy based on a material constitutive law. *Proceedings of the Institution of Mechanical Engineers, Part C: Journal of Mechanical Engineering Science*, *227*(8), 1761-1775.
- Li, J. L., Jing, L. L., & Chen, M. (2009). An FEM study on residual stresses induced by high-speed end-milling of hardened steel SKD11. *Journal of Materials Processing Technology*, *209*(9), 4515-4520.
- Li, J., Wang, Z. L., Xi, P., & Jiao, Y. (2015). Analysis of 45 Steel Rectangular Thin-Walled Parts Milling Deformation. *Key Engineering Materials*, *667*, 22-28.
- Li, J., Yang, X., Ren, C., Chen, G., & Wang, Y. (2015). Multiobjective optimization of cutting parameters in Ti-6Al-4V milling process using nondominated sorting genetic algorithm-II. *The International Journal of Advanced Manufacturing Technology*, *76*(5-8), 941-953.
- Li, K., Gao, X. L., & Sutherland, J. W. (2002). Finite element simulation of the orthogonal metal cutting process for qualitative understanding of the effects of crater wear on the chip formation process. *Journal of materials processing technology*, *127*(3), 309-324.
- Lin, B., Wang, L., Guo, Y., & Yao, J. (2016). Modeling of cutting forces in end milling based on oblique cutting analysis. *The International Journal of Advanced Manufacturing Technology*, *84*(1-4), 727-736.
- Liu, J. (1993) Fixture design for thin-walled parts*, Master's Thesis, University of Manitoba, Winnipeg, Canada.*
- Liu, J., Bai, Y., & Xu, C. (2014). Evaluation of ductile fracture models in finite element simulation of metal cutting processes. *Journal of Manufacturing Science and Engineering*, *136*(1), 011010.

- Loewen, E. G. (1954). On the analysis of cutting-tool temperatures. *Trans. ASME*, *76*, 217.
- Lu, J., Chen, J., Fang, Q., Liu, B., Liu, Y., & Jin, T. (2016). Finite element simulation for Ti-6Al-4V alloy deformation near the exit of orthogonal cutting. *The International Journal of Advanced Manufacturing Technology*, *85*(9-12), 2377-2388.
- Mabrouki, T., Girardin, F., Asad, M., & Rigal, J. F. (2008). Numerical and experimental study of dry cutting for an aeronautic aluminium alloy (A2024-T351). *International Journal of Machine Tools and Manufacture*, *48*(11), 1187-1197.
- Maranhão, C., & Davim, J. P. (2010). Finite element modelling of machining of AISI 316 steel: numerical simulation and experimental validation. *Simulation Modelling Practice and Theory*, *18*(2), 139-156.
- Martellotti, M. E. (1941). An analysis of the milling process. *trans. ASME*, *63*(8), 677-700.
- Martellotti, M. E. (1945). An analysis of the milling process, Part II - Down milling. *trans. ASME*, *67*, 233-251.
- Masmiati, N., Sarhan, A. A., Hassan, M. A. N., & Hamdi, M. (2016). Optimization of cutting conditions for minimum residual stress, cutting force and surface roughness in end milling of S50C medium carbon steel. *Measurement*, *86*, 253-265.
- Maurel-Pantel, A., Fontaine, M., Thibaud, S., & Gelin, J. C. (2012). 3D FEM simulations of shoulder milling operations on a 304L stainless steel. *Simulation Modelling Practice and Theory*, *22*, 13-27.
- Merchant, M. E. (1945). Mechanics of the metal cutting process. I. Orthogonal cutting and a type 2 chip. *Journal of applied physics*, *16*(5), 267-275.
- Michalik, P., Zajac, J., Hatala, M., Mital, D., & Fecova, V. (2014). Monitoring surface roughness of thin-walled components from steel C45 machining down and up milling. *Measurement*, *58*, 416-428.
- Miller, W. S., Zhuang, L., Bottema, J., Wittebrood, A., De Smet, P., Haszler, A., & Vieregge, A. (2000). Recent development in aluminium alloys for the automotive industry. *Materials Science and Engineering: A*, *280*(1), 37-49.
- Modern machine shop: wwwmmsonline.com/articles/how-to-machine-aircrafttitanium-the-8-to-1-rule-for-finishing-walls-and-ribs
- Montgomery, D. C. (2013). *Design and analysis of experiments*. John Wiley & Sons.
- Moufki, A., Dudzinski, D., Molinari, A., & Rausch, M. (2000). Thermoviscoplastic modelling of oblique cutting: forces and chip flow predictions. *International Journal of Mechanical Sciences*, *42*(6), 1205-1232.
- Moufki, A., Devillez, A., Dudzinski, D., & Molinari, A. (2004). Thermomechanical modelling of oblique cutting and experimental validation. *International Journal of Machine Tools and Manufacture*, *44*(9), 971-989.
- Moufki, A., Dudzinski, D., & Le Coz, G. (2015). Prediction of cutting forces from an analytical model of oblique cutting, application to peripheral milling of Ti-6Al-4V alloy. *The International Journal of Advanced Manufacturing Technology*, *81*(1-4), 615-626.

- Mundim, R. B., & Borille, A. V. (2017). An approach for reducing undesired vibrations in milling of low rigidity structures. *The International Journal of Advanced Manufacturing Technology*, *88*(1-4), 971-983.
- Ning, H., Zhigang, W., Chengyu, J., & Bing, Z. (2003). Finite element method analysis and control stratagem for machining deformation of thin-walled components. *Journal of materials processing technology*, *139*(1), 332-336.
- Okonkwo, U. C., Okokpujie, I. P., Sinebe, J. E., & Ezugwu, C. A. (2015). Comparative analysis of aluminium surface roughness in end-milling under dry and minimum quantity lubrication (MQL) conditions. *Manufacturing Review*, *2*, 30.
- Öktem, H., Erzurumlu, T., & Kurtaran, H. (2005). Application of response surface methodology in the optimization of cutting conditions for surface roughness. *Journal of materials processing technology*, *170*(1), 11-16.
- Özel, T., & Altan, T. (2000). Process simulation using finite element method-prediction of cutting forces, tool stresses and temperatures in high-speed flat end milling. *International Journal of Machine Tools and Manufacture*, *40*(5), 713-738.
- Özel, T. (2006). The influence of friction models on finite element simulations of machining. *International Journal of Machine Tools and Manufacture*, *46*(5), 518-530.
- Özel, T., & Zeren, E. (2007). Finite element modeling the influence of edge roundness on the stress and temperature fields induced by high-speed machining. *The International Journal of Advanced Manufacturing Technology*, *35*(3), 255-267.
- Özel, T., Sima, M., Srivastava, A. K., & Kaftanoglu, B. (2010). Investigations on the effects of multi-layered coated inserts in machining Ti–6Al–4V alloy with experiments and finite element simulations. *CIRP Annals-Manufacturing Technology*, *59*(1), 77-82.
- Özel, T., Llanos, I., Soriano, J., & Arrazola, P. J. (2011). 3D finite element modelling of chip formation process for machining Inconel 718: comparison of FE software predictions. *Machining Science and Technology*, *15*(1), 21-46.
- Özel, T., & Ulutan, D. (2012). Prediction of machining induced residual stresses in turning of titanium and nickel based alloys with experiments and finite element simulations. *CIRP Annals-Manufacturing Technology*, *61*(1), 547-550.
- Palanisamy, P., Rajendran, I., Shanmugasundaram, S., & Saravanan, R. (2006). Prediction of cutting force and temperature rise in the end-milling operation. *Proceedings of the Institution of Mechanical Engineers, Part B: Journal of Engineering Manufacture*, *220*(10), 1577-1587.
- Palanisamy, P., Rajendran, I., & Shanmugasundaram, S. (2007). Optimization of machining parameters using genetic algorithm and experimental validation for end-milling operations. *The International Journal of Advanced Manufacturing Technology*, *32*(7), 644-655.
- Patil, P., Polishetty, A., Goldberg, M., Littlefair, G., & Nomani, J. (2014). Slot machining of TI6AL4V with trochoidal milling technique. *Journal of Machine Engineering*, *14*(4), 42-54.
- Pawade, R. S., Sonawane, H. A., & Joshi, S. S. (2009). An analytical model to predict specific shear energy in high-speed turning of Inconel 718. *International Journal of Machine Tools and Manufacture*, *49*(12), 979-990.

- Pereira, R. B. D., Leite, R. R., Alvim, A. C., de Paiva, A. P., Ferreira, J. R., & Davim, J. P. (2017). Multi-objective robust optimization of the sustainable helical milling process of the aluminum alloy Al 7075 using the augmented-enhanced normalized normal constraint method. *Journal of Cleaner Production*, *152*, 474-496.
- Phatak, A. M., & Pande, S. S. (2012). Optimum part orientation in rapid prototyping using genetic algorithm. *Journal of manufacturing systems*, *31*(4), 395-402.
- Pittalà, G. M., & Monno, M. (2010). 3D finite element modeling of face milling of continuous chip material. *The International Journal of Advanced Manufacturing Technology*, *47*(5-8), 543-555.
- Polishetty, A., Goldberg, M., Littlefair, G., Puttaraju, M., Patil, P., & Kalra, A. (2014). A Preliminary Assessment of Machinability of Titanium Alloy Ti 6AL 4V During thin Wall Machining Using Trochoidal Milling. *Procedia Engineering*, *97*, 357-364.
- Pu, Z., Umbrello, D., Dillon, O. W., Lu, T., Puleo, D. A., & Jawahir, I. S. (2014). Finite element modeling of microstructural changes in dry and cryogenic machining of AZ31B magnesium alloy. *Journal of Manufacturing Processes*, *16*(2), 335-343.
- Puls, H., Klocke, F., & Veselovac, D. (2016). FEM-based prediction of heat partition in dry metal cutting of AISI 1045. *The International Journal of Advanced Manufacturing Technology*, *86*(1-4), 737-745.
- Puso, M. A., & Solberg, J. (2006). A stabilized nodally integrated tetrahedral. *International Journal for Numerical Methods in Engineering*, *67*(6), 841-867.
- Qasim, M., Lei He, L., & Xiao H. (2014, March) Deflection prediction of aluminum alloy 7075 of a thin walled component and optimization of parameters. In *2nd International Conference on Research in Science, Engineering and Technology*.
- Qu, S., Zhao, J., & Wang, T. (2017). Experimental study and machining parameter optimization in milling thin-walled plates based on NSGA-II. *The International Journal of Advanced Manufacturing Technology*, *89*(5-8), 2399-2409.
- Rai, J. K., & Xirouchakis, P. (2008). Finite element method based machining simulation environment for analyzing part errors induced during milling of thin-walled components. *International Journal of Machine Tools and Manufacture*, *48*(6), 629-643.
- Rai, J. K., & Xirouchakis, P. (2009). FEM-based prediction of workpiece transient temperature distribution and deformations during milling. *The International Journal of Advanced Manufacturing Technology*, *42*(5), 429-449.
- Ramaswami, R. (1974). Effect of built-up edge on surface finish, vibration and tool wear during orthogonal turning. *Microtecnic*, *28*(4), 221-227.
- Rao, B., Dandekar, C. R., & Shin, Y. C. (2011). An experimental and numerical study on the face milling of Ti–6Al–4V alloy: tool performance and surface integrity. *Journal of Materials Processing Technology*, *211*(2), 294-304.
- Ratchev, S., Govender, E., Nikov, S., Phuah, K., & Tsiklos, G. (2003). Force and deflection modelling in milling of low-rigidity complex parts. *Journal of Materials Processing Technology*, *143*, 796-801.

- Ratchev, S., Huang, W., Liu, S., & Becker, A. A. (2004). Modelling and simulation environment for machining of low-rigidity components. *Journal of Materials Processing Technology*, *153*, 67-73.
- Ratchev, S., Liu, S., Huang, W., & Becker, A. A. (2004). A flexible force model for end milling of low-rigidity parts. *Journal of Materials Processing Technology*, *153*, 134-138.
- Ratchev, S., Liu, S., Huang, W., & Becker, A. A. (2004). Milling error prediction and compensation in machining of low-rigidity parts. *International Journal of Machine Tools and Manufacture*, *44*(15), 1629-1641.
- Ratchev, S., Nikov, S., & Moualek, I. (2004). Material removal simulation of peripheral milling of thin wall low-rigidity structures using FEA. *Advances in Engineering Software*, *35*(8), 481-491.
- Ratchev, S., Liu, S., Huang, W., & Becker, A. A. (2006). An advanced FEA based force induced error compensation strategy in milling. *International Journal of Machine Tools and Manufacture*, *46*(5), 542-551.
- Rech, J., Yen, Y. C., Schaff, M. J., Hamdi, H., Altan, T., & Bouzakis, K. D. (2005). Influence of cutting edge radius on the wear resistance of PM-HSS milling inserts. *Wear*, *259*(7), 1168-1176.
- Rotella, G., & Umbrello, D. (2014). Finite element modeling of microstructural changes in dry and cryogenic cutting of Ti6Al4V alloy. *CIRP Annals-Manufacturing Technology*, *63*(1), 69-72.
- Sabberwal, A. J. P., & Koenigsberger, F. (1961). Chip section and cutting force during the milling operation. *Annals of the CIRP*, *10*(3), 197-203.
- Saffar, R. J., Razfar, M. R., Zarei, O., & Ghassemieh, E. (2008). Simulation of three-dimension cutting force and tool deflection in the end milling operation based on finite element method. *Simulation Modelling Practice and Theory*, *16*(10), 1677-1688.
- Saini, A., Chauhan, P., Pabla, B. S., & Dhami, S. S. (2016). Multi-process parameter optimization in face milling of Ti6Al4V alloy using response surface methodology. *Proceedings of the Institution of Mechanical Engineers, Part B: Journal of Engineering Manufacture*, 0954405416673682.
- SandvikCoromat.,http://www.sandvik.coromant.com/en-gb,industrysolutions/aerospace/alumi-inum /pages/wing-rib (2017)
- Sarikaya, M., Yılmaz, V., & Dilipak, H. (2016). Modeling and multi-response optimization of milling characteristics based on Taguchi and gray relational analysis. *Proceedings of the Institution of Mechanical Engineers, Part B: Journal of Engineering Manufacture*, *230*(6), 1049-1065.
- Scippa, A., Grossi, N., & Campatelli, G. (2014). FEM based cutting velocity selection for thin walled part machining. *Procedia CIRP*, *14*, 287-292.
- Seguy, S., Dessein, G., & Arnaud, L. (2008). Surface roughness variation of thin wall milling, related to modal interactions. *International Journal of Machine Tools and Manufacture*, *48*(3), 261-274.

- Shi, G., Deng, X., & Shet, C. (2002). A finite element study of the effect of friction in orthogonal metal cutting. *Finite Elements in Analysis and Design*, *38*(9), 863-883.
- Shoulder milling of thin deflecting walls., wwwsandvik.coromant.com/en-gb/knowledge/milling/application_overview/shoulder_milling/shoulder_milling_thin_walls (2017)
- Singh, A., Philip, D., Ramkumar, J., & Samanta, S. (September 2015) Simulation analysis for sustainable manufacturing: A green roadmap. In *Proceedings of the 2015 International Conference on Operations Excellence and Service Engineering.*
- Sivasakthivel, P. S., & Sudhakaran, R. (2013). Optimization of machining parameters on temperature rise in end milling of Al 6063 using response surface methodology and genetic algorithm. *The International Journal of Advanced Manufacturing Technology*, *67*(9-12), 2313-2323.
- Slusarczyk, L., & Matras, A. (2016). Influence of cutting data on the thin wall deformation in milling of difficult to cut materials. *Key Engineering Materials*, *686*, 86-91.
- Smith, S., & Dvorak, D. (1998). Tool path strategies for high speed milling aluminum workpieces with thin webs. *Mechatronics*, *8*(4), 291-300.
- Smith, S., Wilhelm, R., Dutterer, B., Cherukuri, H., & Goel, G. (2012). Sacrificial structure preforms for thin part machining. *CIRP Annals-Manufacturing Technology*, *61*(1), 379-382.
- Sonawane, H. A., & Joshi, S. S. (2015). Modeling of machined surface quality in high-speed ball-end milling of Inconel-718 thin cantilevers. *The International Journal of Advanced Manufacturing Technology*, *78*(9-12), 1751-1768.
- Song, G., Sui, S., & Tang, L. (2015). Precision prediction of cutting force in oblique cutting operation. *The International Journal of Advanced Manufacturing Technology*, *81*(1-4), 553-562.
- Song, Q., Liu, Z., & Ai, X. (2014). Influence of Chatter on Machining Distortion for Thin-Walled Component Peripheral Milling. *Advances in Mechanical Engineering*, *6*, 329564.
- Songmene, V., Khettabi, R., Zaghbani, I., Kouam, J., & Djebara, A. (2011). Machining and machinability of aluminum alloys. In *aluminium alloys, theory and applications*. InTech.
- Soo, S. L., Aspinwall, D. K., & Dewes, R. C. (2004). 3D FE modelling of the cutting of Inconel 718. *Journal of Materials Processing Technology*, *150*(1), 116-123.
- Soo, S. L., Aspinwall, D. K., & Dewes, R. C. (2004). Three-dimensional finite element modelling of high-speed milling of Inconel 718. *Proceedings of the Institution of Mechanical Engineers, Part B: Journal of Engineering Manufacture*, *218*(11), 1555-1561.
- Soo, S. L., Dewes, R. C., & Aspinwall, D. K. (2010). 3D FE modelling of high-speed ball nose end milling. *The International Journal of Advanced Manufacturing Technology*, *50*(9), 871-882.
- Starke, E. A., & Staley, J. T. (1996). Application of modern aluminum alloys to aircraft. *Progress in Aerospace Sciences*, *32*(2-3), 131-172.
- Suresh, P. V. S., Rao, P. V., & Deshmukh, S. G. (2002). A genetic algorithmic approach for optimization of surface roughness prediction model. *International Journal of Machine Tools and Manufacture*, *42*(6), 675-680.

- Tănase, I., Ghionea, A., & Ghionea, I. (2010). Measurement and analysis of cutting forces and deformation at milling thin parts. *Proceedings in Manufacturing Systems*, *5*(4), 243-248.
- Tang, L., Huang, J., & Xie, L. (2011). Finite element modeling and simulation in dry hard orthogonal cutting AISI D2 tool steel with CBN cutting tool. *The International Journal of Advanced Manufacturing Technology*, *53*(9), 1167-1181.
- Tlusty, J. & Polacek, M. (1963). The stability of machine tools against self-excited vibrations in machining. *International research in production engineering*. 465-474.
- Tosun, N., & Pihtili, H. (2010). Gray relational analysis of performance characteristics in MQL milling of 7075 Al alloy. *The International Journal of Advanced Manufacturing Technology*, *46*(5), 509-515.
- Tsang, W. P. (2009). Bio-inspired algorithms for single and multi-objective optimization. University of Hong Kong
- Tsao, C. C. (2009). Grey–Taguchi method to optimize the milling parameters of aluminum alloy. *The International Journal of Advanced Manufacturing Technology*, *40*(1), 41-48.
- Wang, F., Zhao, J., Li, A., Zhu, N., & Zhao, J. (2014). Three-dimensional finite element modeling of high-speed end milling operations of Ti-6Al-4V. *Proceedings of the Institution of Mechanical Engineers, Part B: Journal of Engineering Manufacture*, *228*(6), 893-902.
- Wang, J. J., & Zheng, C. M. (2002). Identification of shearing and ploughing cutting constants from average forces in ball-end milling. *International Journal of Machine Tools and Manufacture*, *42*(6), 695-705.
- Wan, M., Zhang, W., Qiu, K., Gao, T., & Yang, Y. (2005). Numerical prediction of static form errors in peripheral milling of thin-walled workpieces with irregular meshes. *Transactions-American Society of Mechanical Engineers Journal of Manufacturing Science and Engineering*, *127*(1), 13-22.
- Wan, M., & Zhang, W. H. (2006). Efficient algorithms for calculations of static form errors in peripheral milling. *Journal of Materials Processing Technology*, *171*(1), 156-165.
- Wan, M., Zhang, W. H., Tan, G., & Qin, G. H. (2008). Systematic simulation procedure of peripheral milling process of thin-walled workpiece. *Journal of materials processing technology*, *197*(1), 122-131.
- Wang, M. H., & Sun, Y. (2014). Error prediction and compensation based on interference-free tool paths in blade milling. *International Journal of Advanced Manufacturing Technology*, *71*, 1309-1318.
- Wu, H. B., & Zhang, S. J. (2014). 3D FEM simulation of milling process for titanium alloy Ti6Al4V. *The International Journal of Advanced Manufacturing Technology*, *71*(5-8), 1319-1326.
- Yang, G. (1980), *Elastic and plastic mechanics*, People Education Published Inc., PRC.
- Yang, W. A., Guo, Y., & Liao, W. (2011). Multi-objective optimization of multi-pass face milling using particle swarm intelligence. *The International Journal of Advanced Manufacturing Technology*, *56*(5), 429-443.

- Yildiz, A. R. (2013). Cuckoo search algorithm for the selection of optimal machining parameters in milling operations. *The International Journal of Advanced Manufacturing Technology*, *64*(1-4), 55-61.
- Young, H. T., Mathew, P., & Oxley, P. L. B. (1994). Predicting cutting forces in face milling. *International Journal of Machine Tools and Manufacture*, *34*(6), 771-783.
- Zain, A. M., Haron, H., & Sharif, S. (2010). Application of GA to optimize cutting conditions for minimizing surface roughness in end milling machining process. *Expert Systems with Applications*, *37*(6), 4650-4659.
- Zhang, H., Deng, Z., Fu, Y., Lv, L., & Yan, C. (2017). A process parameters optimization method of multi-pass dry milling for high efficiency, low energy and low carbon emissions. *Journal of Cleaner Production*, *148*, 174-184.
- Zhang, Y., Zou, P., Li, B., & Liang, S. (2015). Study on optimized principles of process parameters for environmentally friendly machining austenitic stainless steel with high efficiency and little energy consumption. *The International Journal of Advanced Manufacturing Technology*, *79*(1-4), 89-99.
- Zheng, H. Q., Li, X. P., Wong, Y. S., & Nee, A. Y. C. (1999). Theoretical modelling and simulation of cutting forces in face milling with cutter runout. *International Journal of Machine Tools and Manufacture*, *39*(12), 2003-2018.
- Zhou, A., Qu, B. Y., Li, H., Zhao, S. Z., Suganthan, P. N., & Zhang, Q. (2011). Multiobjective evolutionary algorithms: A survey of the state of the art. *Swarm and Evolutionary Computation*, *1*(1), 32-49.

Appendix

Appendix 2

Permission for Figure 2.3

This Agreement between Indian Institute of Technology Guwahati -- Gururaj Bolar ("You") and Elsevier ("Elsevier") consists of your license details and the terms and conditions provided by Elsevier and Copyright Clearance Center.

License Number	4153130006170
License date	Jul 20, 2017
Licensed Content Publisher	Elsevier
Licensed Content Publication	CIRP Annals - Manufacturing Technology
Licensed Content Title	Sacrificial structure preforms for thin part machining
Licensed Content Author	Scott Smith,Robert Wilhelm,Brian Dutterer,Harish Cherukuri,Gaurav Goel
Licensed Content Date	Jan 1, 2012
Licensed Content Volume	61
Licensed Content Issue	1
Licensed Content Pages	4
Start Page	379
End Page	382
Type of Use	reuse in a thesis/dissertation
Portion	figures/tables/illustrations
Number of figures/tables /illustrations	1
Format	both print and electronic
Are you the author of this Elsevier article?	No
Will you be translating?	No
Original figure numbers	figure 4
Title of your thesis/dissertation	Numerical and Experimental Studies on Thin-Wall Machining of Aerospace Grade Aluminum Alloy
Expected completion date	Jul 2017
Estimated size (number of pages)	230
Requestor Location	Indian Institute of Technology Guwahati Guwahati Guwahati, Assam 781039 India Attn: Indian Institute of Technology Guwahati

Permissions for Figures 2.4 and 2.7

This Agreement between Indian Institute of Technology Guwahati -- Gururaj Bolar ("You") and Elsevier ("Elsevier") consists of your license details and the terms and conditions provided by Elsevier and Copyright Clearance Center.

License Number	4153141037445
License date	Jul 20, 2017
Licensed Content Publisher	Elsevier
Licensed Content Publication	International Journal of Machine Tools and Manufacture
Licensed Content Title	Milling error prediction and compensation in machining of low-rigidity parts
Licensed Content Author	S. Ratchev,S. Liu,W. Huang,A.A. Becker
Licensed Content Date	Dec 1, 2004
Licensed Content Volume	44
Licensed Content Issue	15
Licensed Content Pages	13
Start Page	1629
End Page	1641
Type of Use	reuse in a thesis/dissertation
Intended publisher of new work	other
Portion	figures/tables/illustrations
Number of figures/tables /illustrations	2
Format	both print and electronic
Are you the author of this Elsevier article?	No
Will you be translating?	No
Original figure numbers	figure 2, figure 7
Title of your thesis/dissertation	Numerical and Experimental Studies on Thin-Wall Machining of Aerospace Grade Aluminum Alloy
Expected completion date	Jul 2017
Estimated size (number of pages)	230
Requestor Location	Indian Institute of Technology Guwahati Guwahati Guwahati, Assam 781039 India Attn: Indian Institute of Technology Guwahati

Permission for Figure 2.5

This Agreement between Indian Institute of Technology Guwahati -- Gururaj Bolar ("You" and Springer ("Springer") consists of your license details and the terms and conditions provided by Springer and Copyright Clearance Center.

License Number	4153131121770
License date	Jul 20, 2017
Licensed Content Publisher	Springer
Licensed Content Publication	The International Journal of Advanced Manufacturing Technology
Licensed Content Title	FEM-based prediction of workpiece transient temperature distribution and deformations during milling
Licensed Content Author	Jitender K. Rai
Licensed Content Date	Jan 1, 2008
Licensed Content Volume	42
Licensed Content Issue	5
Type of Use	Thesis/Dissertation
Portion	Figures/tables/illustrations
Number of figures/tables /illustrations	1
Author of this Springer article	No
Order reference number	
Original figure numbers	figure 9
Title of your thesis / dissertation	Numerical and Experimental Studies on Thin-Wall Machining of Aerospace Grade Aluminum Alloy
Expected completion date	Jul 2017
Estimated size(pages)	230
Requestor Location	Indian Institute of Technology Guwahati Guwahati Guwahati, Assam 781039 India Attn: Indian Institute of Technology Guwahati
Billing Type	Invoice
Billing Address	Indian Institute of Technology Guwahati Guwahati Guwahati, India 781039 Attn: Indian Institute of Technology Guwahati

Permission for Figure 2.6

This Agreement between Indian Institute of Technology Guwahati -- Gururaj Bolar ("You") and Elsevier ("Elsevier") consists of your license details and the terms and conditions provided by Elsevier and Copyright Clearance Center.

License Number	4152780099775
License date	Jul 19, 2017
Licensed Content Publisher	Elsevier
Licensed Content Publication	International Journal of Mechanical Sciences
Licensed Content Title	Modelling of cutting forces in helical end milling using a predictive machining theory
Licensed Content Author	H.Z. Li,W.B. Zhang,X.P. Li
Licensed Content Date	Aug 1, 2001
Licensed Content Volume	43
Licensed Content Issue	8
Licensed Content Pages	20
Start Page	1711
End Page	1730
Type of Use	reuse in a thesis/dissertation
Intended publisher of new work	other
Portion	figures/tables/illustrations
Number of figures/tables /illustrations	1
Format	both print and electronic
Are you the author of this Elsevier article?	No
Will you be translating?	No
Order reference number	
Original figure numbers	figure 2
Title of your thesis/dissertation	Numerical and Experimental Studies on Thin-Wall Machining of Aerospace Grade Aluminum Alloy
Expected completion date	Jul 2017
Estimated size (number of pages)	230
Elsevier VAT number	GB 494 6272 12
Requestor Location	Indian Institute of Technology Guwahati Guwahati

Permission for Figure 2.8

This Agreement between Indian Institute of Technology Guwahati -- Gururaj Bolar ("You") and Elsevier ("Elsevier") consists of your license details and the terms and conditions provided by Elsevier and Copyright Clearance Center.

License Number	4152781075187
License date	Jul 19, 2017
Licensed Content Publisher	Elsevier
Licensed Content Publication	Simulation Modelling Practice and Theory
Licensed Content Title	Finite element modelling of machining of AISI 316 steel: Numerical simulation and experimental validation
Licensed Content Author	C. Maranhão,J. Paulo Davim
Licensed Content Date	Feb 1, 2010
Licensed Content Volume	18
Licensed Content Issue	2
Licensed Content Pages	18
Start Page	139
End Page	156
Type of Use	reuse in a thesis/dissertation
Intended publisher of new work	other
Portion	figures/tables/illustrations
Number of figures/tables /illustrations	1
Format	both print and electronic
Are you the author of this Elsevier article?	No
Will you be translating?	No
Order reference number	
Original figure numbers	figure 16
Title of your thesis/dissertation	Numerical and Experimental Studies on Thin-Wall Machining of Aerospace Grade Aluminum Alloy
Expected completion date	Jul 2017
Estimated size (number of pages)	230
Elsevier VAT number	GB 494 6272 12
Requestor Location	Indian Institute of Technology Guwahati Guwahati

Permission for Figures 2.9

This Agreement between Indian Institute of Technology Guwahati -- Gururaj Bolar ("You") and Elsevier ("Elsevier") consists of your license details and the terms and conditions provided by Elsevier and Copyright Clearance Center.

License Number	4152781406453
License date	Jul 19, 2017
Licensed Content Publisher	Elsevier
Licensed Content Publication	International Journal of Mechanical Sciences
Licensed Content Title	Investigations on the effects of friction modeling in finite element simulation of machining
Licensed Content Author	Pedro J. Arrazola,Tug˘rul Özel
Licensed Content Date	Jan 1, 2010
Licensed Content Volume	52
Licensed Content Issue	1
Licensed Content Pages	12
Start Page	31
End Page	42
Type of Use	reuse in a thesis/dissertation
Intended publisher of new work	other
Portion	figures/tables/illustrations
Number of figures/tables /illustrations	1
Format	both print and electronic
Are you the author of this Elsevier article?	No
Will you be translating?	No
Order reference number	
Original figure numbers	figure 6
Title of your thesis/dissertation	Numerical and Experimental Studies on Thin-Wall Machining of Aerospace Grade Aluminum Alloy
Expected completion date	Jul 2017
Estimated size (number of pages)	230
Elsevier VAT number	GB 494 6272 12
Requestor Location	Indian Institute of Technology Guwahati Guwahati

Permission for Figure 2.10

This Agreement between Indian Institute of Technology Guwahati -- Gururaj Bolar ("You") and Elsevier ("Elsevier") consists of your license details and the terms and conditions provided by Elsevier and Copyright Clearance Center.

License Number	4152790186486
License date	Jul 19, 2017
Licensed Content Publisher	Elsevier
Licensed Content Publication	Simulation Modelling Practice and Theory
Licensed Content Title	3D FEM simulations of shoulder milling operations on a 304L stainless steel
Licensed Content Author	A. Maurel-Pantel,M. Fontaine,S. Thibaud,J.C. Gelin
Licensed Content Date	Mar 1, 2012
Licensed Content Volume	22
Licensed Content Issue	n/a
Licensed Content Pages	15
Start Page	13
End Page	27
Type of Use	reuse in a thesis/dissertation
Intended publisher of new work	other
Portion	figures/tables/illustrations
Number of figures/tables /illustrations	1
Format	both print and electronic
Are you the author of this Elsevier article?	No
Will you be translating?	No
Order reference number	
Original figure numbers	figure 7
Title of your thesis/dissertation	Numerical and Experimental Studies on Thin-Wall Machining of Aerospace Grade Aluminum Alloy
Expected completion date	Jul 2017
Estimated size (number of pages)	230
Elsevier VAT number	GB 494 6272 12
Requestor Location	Indian Institute of Technology Guwahati Guwahati

Permission for Figure 2.11

This Agreement between Indian Institute of Technology Guwahati -- Gururaj Bolar ("You") and Springer ("Springer") consists of your license details and the terms and conditions provided by Springer and Copyright Clearance Center.

License Number	4152790623667
License date	Jul 19, 2017
Licensed Content Publisher	Springer
Licensed Content Publication	The International Journal of Advanced Manufacturing Technology
Licensed Content Title	3D FEM simulation of milling process for titanium alloy Ti6Al4V
Licensed Content Author	H. B. Wu
Licensed Content Date	Jan 1, 2013
Licensed Content Volume	71
Licensed Content Issue	5
Type of Use	Thesis/Dissertation
Portion	Figures/tables/illustrations
Number of figures/tables /illustrations	1
Author of this Springer article	No
Order reference number	
Original figure numbers	figure 4
Title of your thesis / dissertation	Numerical and Experimental Studies on Thin-Wall Machining of Aerospace Grade Aluminum Alloy
Expected completion date	Jul 2017
Estimated size(pages)	230
Requestor Location	Indian Institute of Technology Guwahati Guwahati Guwahati, Assam 781039 India Attn: Indian Institute of Technology Guwahati
Billing Type	Invoice
Billing Address	Indian Institute of Technology Guwahati Guwahati Guwahati, India 781039 Attn: Indian Institute of Technology Guwahati

Appendix 3

Appendix A3.1

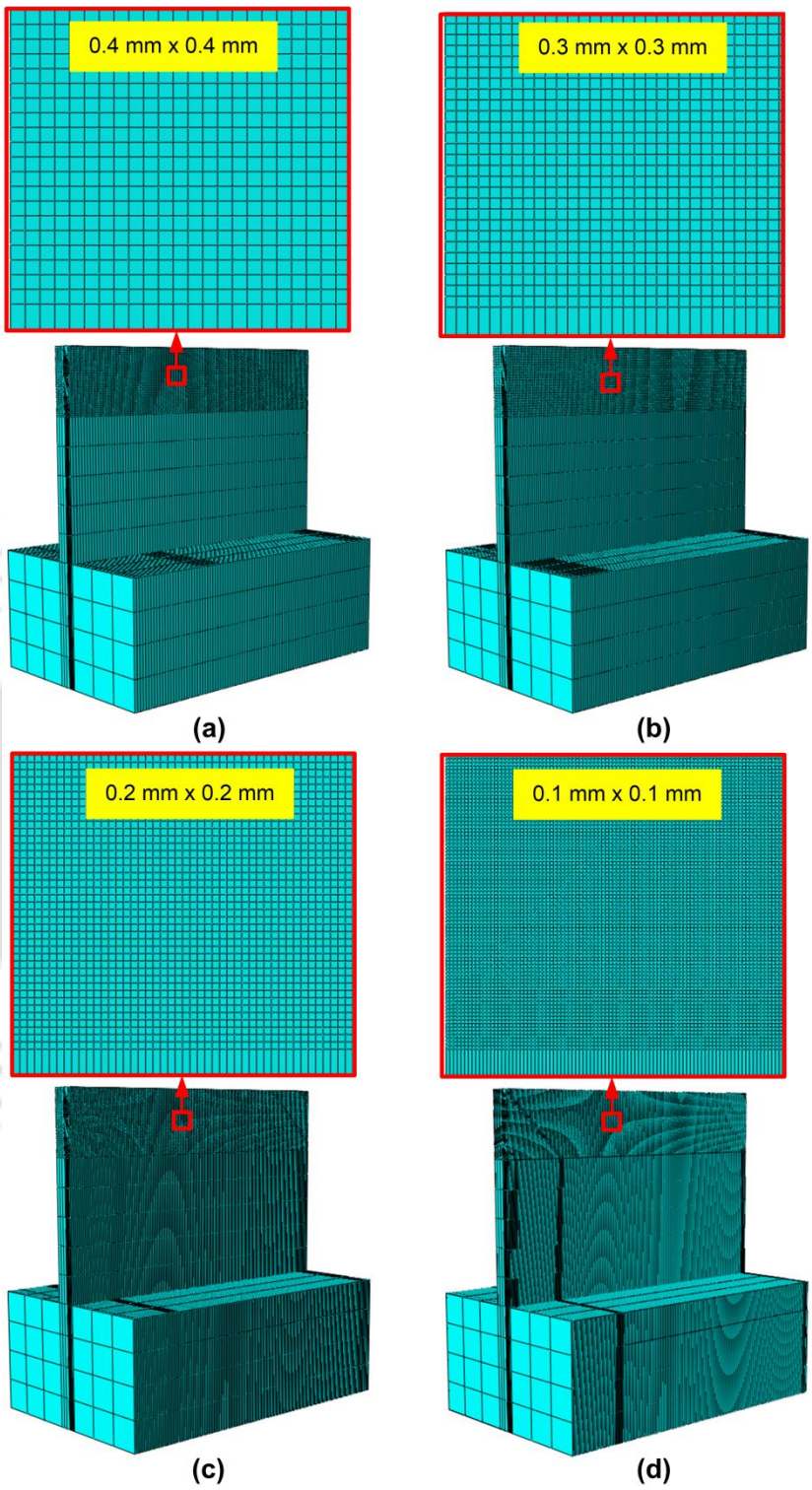

Figure A3.1 Mesh size for mesh refinement analysis (a) 0.4 mm x 0.4 mm, (b) 0.3 mm x 0.3 mm, (c) 0.2 mm x 0.2 mm, (d) 0.1 mm x 0.1 mm

Permissions for Table 3.2, Table 3.3 and Table 3.4

This Agreement between Indian Institute of Technology Guwahati -- Gururaj Bolar ("You") and Elsevier ("Elsevier") consists of your license details and the terms and conditions provided by Elsevier and Copyright Clearance Center.

License Number	4152770818762
License date	Jul 19, 2017
Licensed Content Publisher	Elsevier
Licensed Content Publication	International Journal of Machine Tools and Manufacture
Licensed Content Title	Numerical and experimental study of dry cutting for an aeronautic aluminium alloy (A2024-T351)
Licensed Content Author	Tarek Mabrouki,François Girardin,Muhammad Asad,Jean-François Rigal
Licensed Content Date	Sep 1, 2008
Licensed Content Volume	48
Licensed Content Issue	11
Licensed Content Pages	11
Start Page	1187
End Page	1197
Type of Use	reuse in a thesis/dissertation
Portion	figures/tables/illustrations
Number of figures/tables /illustrations	3
Format	both print and electronic
Are you the author of this Elsevier article?	No
Will you be translating?	No
Order reference number	
Original figure numbers	table 1, 2, 3
Title of your thesis/dissertation	Numerical and Experimental Studies on Thin-Wall Machining of Aerospace Grade Aluminum Alloy
Expected completion date	Jul 2017
Estimated size (number of pages)	230
Elsevier VAT number	GB 494 6272 12
Requestor Location	Indian Institute of Technology Guwahati Guwahati Guwahati, Assam 781039

Appendix 5

Permission for Table 5.1

This Agreement between Indian Institute of Technology Guwahati -- Gururaj Bolar ("You") and Elsevier ("Elsevier") consists of your license details and the terms and conditions provided by Elsevier and Copyright Clearance Center.

License Number	4152771314163
License date	Jul 19, 2017
Licensed Content Publisher	Elsevier
Licensed Content Publication	International Journal of Fatigue
Licensed Content Title	The role of residual stress and heat affected zone properties on fatigue crack propagation in friction stir welded 2024-T351 aluminium joints
Licensed Content Author	G Bussu,P.E Irving
Licensed Content Date	Jan 1, 2003
Licensed Content Volume	25
Licensed Content Issue	1
Licensed Content Pages	12
Start Page	77
End Page	88
Type of Use	reuse in a thesis/dissertation
Intended publisher of new work	other
Portion	figures/tables/illustrations
Number of figures/tables /illustrations	1
Format	both print and electronic
Are you the author of this Elsevier article?	No
Will you be translating?	No
Order reference number	
Original figure numbers	table 1
Title of your thesis/dissertation	Numerical and Experimental Studies on Thin-Wall Machining of Aerospace Grade Aluminum Alloy
Expected completion date	Jul 2017
Estimated size (number of pages)	230
Elsevier VAT number	GB 494 6272 12
Requestor Location	Indian Institute of Technology Guwahati Guwahati

Appendix A5.1: Specification of 3-Axis Vertical Milling Machine

Make	Precision Machinkraft	
Maximum spindle speed	10000 r/min	
Clamping area	300 mm*500 mm	
Distance from spindle face to table	150mm-550mm	
Maximum traverse	X-axis	400 mm
	Y-axis	300 mm
	Z-axis	350 mm
Axis	Rapid m/mm	36/36/34
	Feed m/mm	10000

Appendix A5.2: Milling parameters for roughing operation to obtain pre-final part

Spindle speed (r/min)	3000
Feed per tooth (mm/z)	0.03
Axial depth of cut (mm)	2
Tool diameter (mm)	16
Number of flutes	2

Appendix A5.3: Specification of 4 component dynamometer

Make		Kistler	
Measuring range		-5 KN to 5KN	
Maximum bending moment		-400 Nm to 400Nm	
Threshold	Fx, Fy	Fz	< 0,01
	Fz	N	< 0,2
	Mz	mN·m	< 0,02
Sensitivity	Fx, Fy	pC/N	≈ –7,8
	Fz	pC/N	≈ –3,5
	Mz	pC/N·m	≈ –160
Linearity, all ranges	%FSO		≤ ±1
Hysteresis, all ranges	% FSO		≤1
Operating temperature range	0°C -70°C		
Mass	4.2Kg		

Appendix A5.4: High precision non-contact computerized surface profilometer

Make	Tylor Hobson
precision	1 mega pixel
Lens magnification	20X
Field of view	0.825mm*0.825mm
Focal distance	4.7mm
Power supply	220V AC supply

Appendix A5.5: Specification of the LVDT

Make	Solartron
Measurement Range	±5 mm
Accuracy1 (% of reading or µm):	0.5, 5µm
Repeatability	0.15 µm
Pre-travel	0.15 mm
Post-travel	0.85 mm
Pre-travel Adjustment range	1.5 mm
Tip Force: Standard/Vacuum ±20%	0.7 N @ mid position
Tip Force: Feather Touch ±20%	0.3 N @ mid position

Appendix A5.6: Specification of the LVDT display unit

Make	**Solartron digital display C55**
Voltage	95 -264 VAC / 50 -60 Hz
Power	20 W max
Fuse Rating	Amp 20 mm, Time delay
Voltage	3 VAC rms
Frequency	2.5 kHz, 5 kHz, 10 kHz or 13 kHz factory set
Temperature Drift	<100 ppm/°C
Resolution	±32768 counts
Frequency of Acquisition	100 kHz max.
Input Impedance	2 kΩ, 10 kΩ, 100 kΩ factory set
Update Rate	<200 µs
Response	Output filter -3 dB @ 1 kHz

Appendix A7.1 Feed power (P_f), spindle power (P_m) and Milling power (P_c) based on Equation (7.1-7.3)

Run No.	P_f (W)	P_m (W)	P_c (W)
1	0.777	138.7	139.477
2	0.179	112.1	112.279
3	0.794	234.72	235.514
4	0.333	204.15	204.483
5	1.667	193.89	195.557
6	1.288	216.38	217.668
7	0.223	114.03	114.253
8	1.585	115.72	117.305
9	0.258	80.85	81.108
10	0.298	163.24	163.538
11	0.434	122.03	122.464
12	3.206	501.38	504.586
13	0.292	220.11	220.402
14	1.039	376.09	377.129
15	1.283	328.02	329.303
16	0.397	234.81	235.207
17	-	-	-
18	0.966	614.02	614.986
19	0.252	136.03	136.282
20	1.045	207.75	208.795
21	1.738	133.74	135.478
22	0.519	170.43	170.949
23	0.84	147.55	148.39
24	2.127	121.61	123.737
25	1.473	120.93	122.403
26	0.29	87.73	88.02
27	0.343	107.62	107.963
28	1.217	298.1	299.317
29	0.851	104.05	104.901
30	0.519	86.11	86.629
31	0.272	70.03	70.302
32	0.319	129.4	129.719
33	0.671	182.67	183.341
34	0.937	124.69	125.627
35	0.81	98.66	99.47
36	0.873	175.45	176.323
37	3.54	590.26	593.8
38	0.518	244.2	244.718
39	0.325	79.72	80.045

40	1.752	144.19	145.942
41	0.434	102.04	102.474
42	0.962	132.55	133.512
43	1.207	117.97	119.177
44	5.26	1043.9	1049.16
45	0.222	138.75	138.972
46	0.187	65.31	65.497
47	3.112	502.04	505.152
48	0.147	59.55	59.697
49	0.728	266.64	267.368
50	0.884	109.05	109.934
51	0.248	99.46	99.708
52	1.03	116.68	117.71
53	1.617	406.56	408.177
54	0.339	90.38	90.719
55	1.508	390.43	391.938
56	0.374	81.64	82.014
57	0.633	122.29	122.923
58	2.412	151.58	153.992
59	0.103	38.49	38.593
60	1.488	149.93	151.418
61	1.728	123.71	125.438
62	2.229	273.53	275.759
63	1.899	442.42	444.319
64	0.618	70.58	71.198
65	0.413	304.59	305.003
66	-	-	-
67	1.448	275.99	277.438
68	0.779	110.22	110.999
69	0.563	165.83	166.393
70	2.985	982.52	985.505
71	0.333	59.74	60.073
72	0.464	92.57	93.034
73	1.116	142.41	143.526
74	0.607	307.45	308.057
75	0.224	92.68	92.904
76	1.297	151.59	152.887
77	1.866	308.44	310.306
78	-	-	-
79	0.925	226.38	227.305
80	0.68	164.75	165.43
81	1.095	184.43	185.525

List of Publications

Book Chapter

- *G. Bolar, S.N. Joshi, End milling of low rigidity thin-wall parts: Numerical and experimental investigations*. Precision product, process design and optimization, Select papers from AIMTDR 2016 - 6th International & 27th All India Manufacturing Technology, Design and Research Conference (AIMTDR 2016), Editors: Prof. S. S. Pande and Prof. U. S. Dixit *(Accepted for publication)*

Journal Papers

- *S.N. Joshi, G. Bolar, (2017) Three-dimensional finite element based numerical simulation of machining of thin-wall components with varying wall constraints*. Journal of the Institution of Engineers (India): Series C, 9*8*(3), 343-352.
- *G. Bolar, S.N. Joshi, (2017) Three-dimensional numerical modeling, simulation and experimental validation of milling of a thin-wall component*. Proceedings of the Institution of Mechanical Engineers, Part B: Journal of Engineering Manufacture, 231(5), 792- 804.
- *G. Bolar, A. Das and S.N. Joshi, Measurement and analysis of cutting force and product surface quality during precision machining of thin–wall components*. Measurement *(Communicated)*
- *G. Bolar, S.N. Joshi, Experimental investigations into end milling of open straight and curved thin-walls. Materials and Manufacturing Process (Communicated)*
- *G. Bolar, S.N. Joshi, An evaluation of workpiece surface integrity and dimensional accuracy in machining of low-rigidity part (communicated)*
- *G. Bolar, S.N. Joshi, Analysis and optimization of cutter geometric parameters for improving the part quality during precision thin-wall machining (To be communicated)*
- *G. Bolar, S.N. Joshi, An investigation into product quality and productivity in end milling of low rigidity parts using response surface methodology (To be communicated)*
- *G. Bolar, A. Das and S.N. Joshi, Optimization of thin-wall machining process using Non-Dominated Genetic Algorithm - II (NSGA-II) (To be communicated)*
- *G. Bolar, S.N. Joshi, An integrated analytical -FEM based modeling of milling force and deflection in helical end-milling of thin-wall parts (To be communicated)*

Conference Papers

- *G. Bolar, S. N. Joshi, Three Dimensional Finite Element Modeling and Simulation of Curvilinear Thin-wall Machining of Aluminum 7075-T6 Alloy, In* Processing and Fabrication of Advanced Materials – XXIII *(PFAM 2014), December 5th –7th December 2014, Uttarakhand, India, pp. 906-915.*
- *G. Bolar, S. N. Joshi, 3D finite element modeling of thin-wall machining of aluminum 7075-T6 alloy, In* 5th International & 26th All India Manufacturing Technology, Design and Research Conference *(AIMTDR 2014), 12th –14th December 2014, Assam, India, pp. 135-1–135-6.*
- *A. Das, B Salunkhe, G. Bolar and S.N. Joshi, A comparative study on performance of approaches for machining of thin-wall components, In* 6th International & 27th All India Manufacturing Technology, Design and Research Conference (*AIMTDR 2016), 16th –18th December 2016, Maharashtra, India, pp. 553-556.*
- *G. Bolar, A. Das and S.N. Joshi, Analysis of Surface Integrity and Dimensional Accuracy during Thin-Wall Machining, In* International Conference on Advanced Technologies for Societal Applications *(Techno-Societal 2016), 20th –21st December 2016, Maharashtra, India, pp. 681-688.*
- *G. Bolar, M. Mekonen, A. Das, S. N. Joshi, Experimental Investigation on Surface Quality and Dimensional Accuracy during Curvilinear Thin-Wall Machining, In* 7th International Conference on Materials Processing and Characterization, *(ICMPC 2017), 17th –19th March 2017, Hyderabad, India.*